2010

Mechanistic Studies on the Electrochemistry of Proton Coupled Electron Transfer and the Influence of Hydrogen Bonding

Timothy Alligrant
Virginia Commonwealth University

College of Humanities and Sciences
Virginia Commonwealth University

This is to certify that the dissertation prepared by Timothy M. Alligrant entitled Mechanistic Studies on the Electrochemistry of Proton Coupled Electron Transfer and the Influence of Hydrogen Bonding has been approved by his committee as satisfactory completion of the dissertation requirement forthe degree of Doctor of Philosophy.

_____
Dr. Julio C. Alvarez, Director of Dissertation, Chemistry Department

_____
Dr. Fred M. Hawkridge, Committee Member, Chemistry Department

_____
Dr. Maryanne M. Collinson, Committee Member, Chemistry Department

_____
Dr. Ramana M. Pidaparti, Committee Member, Mechanical Engineering Department

_____
Dr. James Terner, Committee Member, Chemistry Department

_____
Dr. Scott Gronert, Chairman, Chemistry Department

_____
Dr. Robert D. Holsworth, Dean, College of Humanities and Sciences

_____
Dr. F. Douglas Boudinot, Dean, School of the Graduate Studies

_____
Date

Mechanistic Studies on the Electrochemistry of Proton Coupled Electron Transfer and the Influence of Hydrogen Bonding

A dissertation submitted in partial fulfillment of the requirements for the degree of Doctor of Philosophy at Virginia Commonwealth University

By

Timothy M. Alligrant

Director: Dr. Julio C. Alvarez
Professor of Chemistry

Virginia Commonwealth University
Richmond, Virginia
June 30, 2010

ACKNOWLEDGMENTS

The modest accomplishments of this dissertation must not in any way conceal the enormous debt of gratitude I owe to various people who have helped me bring this work to fruition. First and foremost, I would like to thank Dr. Julio Alvarez, who guided me through my work. I am also grateful to the members of my committee, Dr. Fred M. Hawkridge, Dr. Maryanne M. Collinson, Dr. James Terner and Dr. Ramana M. Pidaparti, all of whom have contributed to my success. I would also like to thank the following for their advice and assistance in getting started with diffusion NMR and computational chemistry work, Dr. Yun Qu, Dr. John C. Hackett (VCU Institute for Structural Biology and Drug Discovery), Dr. Paul Momoh, Dr. J. Neel Scarsdale (VCU Department of Biochemistry & Molecular Biology), Dr. Angel Kaifer and his group (University of Miami) and Dr. Ghirmai H. Meresi (Varian, Inc.). In addition, I would like to thank my friends, the members of Dr. Alvarez's group. I would also like to thank the Virginia Commonwealth University Graduate School and Philip Morris Inc. for sponsoring me for one academic year each in pursuit of this work.

I also wish to give my profound gratitude to my parents, Walter and Donna Hogwood, who supported me in my education. My heartfelt appreciation also goes to my wonderful wife, Jennifer A. N. Alligrant, for her support during the duration of this work and her understanding when she and I would not see each other for many days, because I needed to get this work done. I also appreciate the contributions given by my friends and other members of my family. I would especially like to thank my cousin, Jeremy Clark, a Chemistry teacher, who I could talk to about publication and experimental problems that I had during the pursuit of my degree.

In memory of my Grandmother, Shirley Brier, and Father, Walter Hogwood, who were both always there and proud of me.

TABLE OF CONTENTS

LIST OF TABLES

LIST OF FIGURES

Figure 14. Cyclic voltammograms of 5.0 mM 1,4-QH_2 without pyridine (thick black CV), with 5.0 mM pyridine (dashed black line) and 10.0 mM pyridine (thin gray line). Voltammetry measured with 0.2 M $TBAPF_6$ as supporting electrolyte in acetonitrile at a glassy carbon electrode (0.059 cm^2) with a scan rate of 0.1 V s^{-1}.

Figure 15. Cyclic voltammograms of 5.0 mM 1,4-Q alone (thick black CV) and 5.0 mM 1,4-Q with 13 mM pyridinium nitrate (thin gray CV) added. Voltammetry conducted at 27 ^oC in 0.2 M $TBAPF_6$ at 0.1 V s^{-1} in acetonitrile at a glassy carbon electrode (0.059 cm^2).

Figure 16. ^{1}H-NMR spectra of 1,4-QH_2 in the presence of 0, 3.0 and 10.0 mM pyridine.

Figure 17. Cyclic voltammogram (solid line) and simulation (circles) of 5.0 mM HQ with 0.2 M $TBAPF_6$ as supporting electrolyte in acetonitrile at a glassy carbon electrode (0.06 cm^2) at a scan rate of 0.1 V s^{-1}.

Figure 18. Voltammetry (solid line) and simulation (circles) of 5.0 mM 1,4-QH_2 with 10.0 mM pyridine. Voltammetry was recorded at 0.1 V s^{-1} in anhydrous acetonitrile with 0.2 M $TBAPF_6$ at a glassy carbon electrode (0.060 cm^2), under dry conditions.

Figure 19. Voltammetry (solid line) and simulation (circles) of 5.0 mM 1,4-Q with 13.0 mM pyridinium. Voltammetry was recorded at 0.1 V s^{-1} in anhydrous acetonitrile with 0.2 M $TBAPF_6$ at a glassy carbon electrode (0.059 cm^2), under dry conditions.

Figure 20. A.) ^{1}H-NMR spectra of 5.0 mM 1,4-QH_2 with 0, 10.0 and 30.0 mM trifluoroacetate. B.) ^{1}H-NMR spectra of 5.0 mM 1,4-QH_2 with 0, 10.0 and 30.0 mM pyridine. C.) Molar ratio plot from the ^{1}H-NMR titration of 1,4-QH_2 with trifluoroacetate (circle), pyridine (square) and DIPEA (triangle).

Figure 21. A.) Cyclic voltammetry of 5.0 mM 1,4-QH_2 alone (thin black line), with 10.0 mM trifluoroacetate (thick black line), with 30.0 mM trifluoroacetate (thick gray line) and simulations of 5.0 mM 1,4-QH_2 with 10.0 mM trifluoroacetate and with 30.0 mM trifluoroacetate (open and closed black circles, respectively). B.) Cyclic voltammetry of 5.0 mM 1,4-QH_2 alone (thin black line), with 10.0 mM pyridine (gray line) and the simulation (open circles). Voltammetry measured at a glassy carbon electrode in 0.2 M $TBAPF_6$ at 0.1 V s^{-1}.

Figure 22. Cyclic voltammetry of 5.0 mM 1,4-QH_2 with 10.0 mM trifluoroacetate (black CV) and 5.0 mM 1,4-Q with 30.0 mM trifluoroacetic acid (gray CV). All voltammetry recorded at 0.1 V s^{-1} at a glassy carbon electrode at 25 ^oC under dry conditions in anhydrous acetonitrile with 0.2 M tetrabutylammonium hexafluorophosphate.

Figure 23. Equilibrium concentrations of 1,4-QH_2 species as a function of the total trifluoroacetate concentration, where K_1 = 55 M^{-1} and K_2 = 5 M^{-1}: 1,4-QH_2 (solid black line), 1,4-QH_2(B) (dashed black line) and 1,4-$QH_2(B)_2$ (solid gray line).

Figure 24. (A.) ^{1}H-NMR spectra of 5.0 mM 1,4-QH_2 alone (top spectra), 5.0 mM 1,4-QH_2 with 10.0 mM trifluoroacetate (middle spectra) and 5.0 mM 1,4-QH_2 with 10.0 mM trifluoroacetate

and 5.0 mM trifluoroacetic acid in ACN-d_3. (B.) Change in the diffusion coefficient of 5.0 mM 1,4-QH_2 in the presence of 10.0 mM trifluoroacetate as trifluoroacetic acid is titrated.

Figure 25. Cyclic voltammetry of (A.) 5.0 mM 1,4-QH_2 with 10.0 mM trifluoroacetate alone (black CV) and 5.0 mM 1,4-QH_2 with 10.0 mM trifluoroacetate and 25.0 mM trifluoroacetic acid (blue CV). Cyclic voltammetry of (B.) 5.0 mM 1,4-QH_2 with 30.0 mM trifluoroacetate alone (black CV) and 5.0 mM 1,4-QH_2 with 30.0 mM trifluoroacetate and 50.0 mM trifluoroacetic acid. All voltammetry recorded at 0.1 V s^{-1} at a glassy carbon electrode at 25 ^oC under dry conditions in anhydrous acetonitrile with 0.2 M tetrabutylammonium hexafluorophosphate.

Figure 26. Equilibrium concentrations of 1,4-QH_2 (both A. and B.) and trifluoroacetic acid homoconjugate species (A. only) as a function of the total trifluoroacetic acid concentration for the addition of trifluoroacetic acid to 1,4-QH_2 solutions of (A.) 10.0 and (B.) 30.0 mM trifluoroacetate. In both A. and B. 1,4-QH_2 is represented by the thick black line, 1,4-QH_2(B) the thin blue line and 1,4-QH_2 the thin green line. In A. trifluoroacetate is represented by the thick gold line and its homoconjugate the thick red line.

Figure 27. A.) Anodic (circles) and cathodic (squares) peak potential (E_p) as a function of the total concentration of added protiated (closed shapes) and deuterated (open shapes) trifluoroacetic acid to a solution of 1,4-QH_2 or 1,4-QD_2, respectively. B.) Anodic (circles) and cathodic (squares) peak current (i_p) as a function of the total concentration of added protiated (closed shapes) and deuterated (open shapes) trifluoroacetic acid to a solution of 1,4-QH_2 or 1,4-QD_2, respectively.

Figure 28. Experimental (solid lines) and simulated (circles) CV's of 2.0 mM N-Methyl-4,4'-Bipyridyl Chloride ($NMBC^+$) in unbuffered solution with KCl (I = 0.5) at pH 3.35 (black), 4.01 (blue) and 7.00 (green). Experiments performed at a glassy carbon electrode (0.073 cm^2) at 0.2 V s^{-1} at 300 K. Inset: Simulations of the reduction of 2.0 mM of the theoretical compound, B, at pH 2 (black), 3 (blue) and 7 (green).

Figure 29. CV's of 2.0 mM N-Methyl-4,4'-Bipyridyl Chloride (NMBC) in 0.1 M phosphate buffer with KCl (I = 0.5) at pH 3.00 (black), 6.00 (blue) and 10.00 (green). Experiments performed at a glassy carbon electrode (0.073 cm^2) at 0.1 V s^{-1} at 300 K. Inset: Plot of $E_{1/2}$ versus pH for peaks I and IV (red circles) and peaks II and III (blue squares). Fitted black line represents the fitting of equation 60 to the $E_{1/2}$ versus pH data for peaks I and IV.

Figure 30. Simulated CV's of 2.0 mM B in a simulated 0.1 M phosphate buffer at pH 3 (black), 6 (blue) and 10 (green). Inset: (A.) Plot of $E_{1/2}$ versus pH for peaks I and II (red circles), fitted black line represents the fitting of equation 60 to the $E_{1/2}$ versus pH data for peaks I and II. (B.) Plot of ΔE_p versus pH for proton transfer rate constant values of 1 x 10^7 (black dots and line), 1 x 10^8 (blue squares and line) and 1 x 10^9 M^{-1} s^{-1} (green triangles and line).

Figure 31 – Plot of i_{pc} (peak I) versus citrate buffer concentration for 2.0 mM of $NMBC^+$. Inset: Plot of i_{pc} versus simulated citrate buffer concentration for the hypothetical model compound, B.

Figure 32. Experimental CV's of 1-(4-Pyridyl)pyridinium Chloride (PPC) in unbuffered solution with KCl (I = 0.5) at pH 2.87 (black), 3.65 (blue), 7.80 (gold) and 10.82 (green). Experiments performed at a glassy carbon electrode (0.073 cm^2) at 0.1 V s^{-1} at 300 K. Inset: Simulations of the reduction of 2.0 mM of the theoretical compound, B, at pH 2 (black), 3 (blue) and 7 (green).

Figure 33. CV's of 2.0 mM (4-Pyridyl)pyridinium Chloride (PPC) in 0.1 M phosphate buffer with KCl (I = 0.5) at pH 2 (black), 6 (blue) and 11 (green). Experiments performed at a glassy carbon electrode (0.073 cm^2) at 0.1 V s^{-1} at 300 K. Inset: Plot of $E_{1/2}$ versus pH for peak I (red circles). Fitted black line represents the fitting of equation 61 to the $E_{p,\ I}$ versus pH data for peaks I and IV.

Figure 34. Simulated CV's of 2.0 mM B in a simulated 0.1 M phosphate buffer at pH 2 (black), 4 (blue) and 11 (green). Inset: (A.) Plot of $E_{1/2}$ versus pH for peaks I and II (red circles), fitted black line represents the fitting of equation 60 to the $E_{1/2}$ versus pH data for peaks I and II. (B.) Plot of ΔE versus pH for proton transfer rate constant values of 1 x 10^6 (black dots and line), 1 x 10^7 (blue squares and line), 1 x 10^8 (gold diamonds and line) and 1 x 10^9 M^{-1} s^{-1} (green triangles and line).

Figure 35. Plot of i_{pc} (peak I) versus succinate buffer concentration for 2.0 mM of PPC^+. Inset: Plot of i_{pc} versus simulated succinate buffer concentration for the hypothetical model compound, B.

Figure 36. Overlaid voltammetry of 2.0 mM PPC^+ in I = 0.5, 0.1 M phosphate and KCl solution at pH = 2, at 300 K, at a glassy carbon electrode (0.060 cm^2) at two different potential window widths.

Figure 37. PPC^+ fence scheme structures determined using PCM/B3LYP/6-31G*.

Figure 38. $NMBC^+$ fence scheme structures determined using PCM/B3LYP/6-31G*.

Figure 39. (A.) Multiple overlaid voltammograms (first CV is the given by the thick black line) of 1.0 mM 4-nitrobenzenediazonium tetrafluoroborate ($NBDBF_4$) in acetonitrile with 0.1 M $TBABF_4$ as supporting electrolyte. (B.) Voltammograms of 1.0 mM 1,4-QH_2 in acetonitrile with 0.2 M $TBAPF_6$ before $NBDBF_4$ modification (black CV), after $NBDBF_4$ modification (blue CV) and after electrolysis in 90:10 H_2O/Ethanol for 100 minutes (green CV). All CV's were recorded at 0.1 V s^{-1} at a glassy carbon electrode (0.15 cm^2).

Figure 40. (A.) Multiple overlaid voltammograms (first CV is the given by the thick black line) of 1.0 mM diazonium-4-diethylamine tetrafluoroborate (DDEA) in acetonitrile with 0.1 M $TBABF_4$ as supporting electrolyte. (B.) Voltammograms of 1.0 mM 1,4-QH_2 in acetonitrile with 0.2 M $TBAPF_6$ before DDEA modification (black CV) and after DDEA modification (blue CV). All CV's were recorded at 0.1 V s^{-1} at a glassy carbon electrode (0.15 cm^2).

Figure 41. (A.) Voltammograms of 1.0 mM $Ru(NH_3)_6^{3+}$ in pH ~ 2 0.1 M KCl at a glassy carbon rod electrode (0.13 cm^2) before (black CV), after DDEA modification (blue CV) and after performing several scans in a solution of 1.0 mM $Fe(CN)_6^{3-}$ (green CV). (B.) Voltammograms of

LIST OF SCHEMES

LIST OF ABBREVIATIONS AND SYMBOLS

1,4-Q	1,4-Benzoquinone, para-Benzoquinone or p-Benzoquinone
1,2-QD_2	Deuterated 1,2-Hydroquinone
1,4-QD_2	Deuterated 1,4-Hydroquinone
1,2-QH_2	1,2-Hydroquinone, ortho-Hydroquinone, o-Hydroquinone or Catechol
1,4-QH_2	1,4-Hydroquinone, para-Hydroquinone or p-Hydroquinone
α	Electrochemical Transfer Coefficient
a	Radius of Molecule
A	Ampere, also area of the electrode
ACN	Acetonitrile
Ag/AgCl	Silver/silver chloride
$AgNO_3$	Silver Nitrate
B	Calibration constant used in solution viscosity calculation
B3LYP	Becke Three Parameter Lee, Yang and Parr Theory
C	Concentration or coulombs, depending on context
CBSB7	Gaussian 03 keyword that selects the 6-311G** basis set used by CBS-QB3
CBS-QB3	Complete Basis Set
CECE	Acronym representing a redox process where the order of steps proceeds as Chemical step, Electron transfer, Chemical step, Electron transfer.
CEEC	Acronym representing a redox process where the order of steps proceeds as Chemical step, Electron transfer, Electron transfer, Chemical step.

CPC	Controlled Potential Coulometry
CPCM	Conductor Polarizable Continuum Model
$CPDBF_4$	4-Carboxyphenyl diazonium tetrafluoroborate
CPET	Concerted Proton Electron Transfer
CV	Cyclic Voltammogram
δ	Frequency shift in ^{1}H-NMR, also delay time in PGE-^{1}H-NMR
δ_n	Frequency shift in ^{1}H-NMR for some number *n* ligands
Δ	Long Delay time (PGE-^{1}H-NMR) or change in some parameter (generic)
d*n*	Individual time delay for PGE-^{1}H-NMR sequence, *n* is some number 0-4
D	Diffusion Coefficient
D_C	Corrected Diffusion Coefficient
D_{NMR}	Diffusion Coefficient determined by PGE-^{1}H-NMR
DDEA	Diazonium-4-diethylamine
DIPEA	N,N-diisopropylethylamine
$DIPEAH^+$	N,N-ethyldiisopropylamine perchlorate (H^+ indicates protonation)
DOSY	Diffusion Ordered Spectroscopy
D_2O/H_2O	Deuterated Water/Water
d_3-ACN	Deuterated Acetonitrile
$\partial Ep/\partial \log \nu$	Variation of peak potential, determined from slope of E_p vs. log ν
ε_o	Vacuum Permittivity (8.85419 x 10^{-12} C^2 N^{-1} m^{-2})
ε_{op}	Optical Dielectric Constant (= 1.776 in H_2O)
ε_s	Static Dielectric Constant (78.39 in H_2O and 37.5 in ACN)
e^-	Electron

e_o	Charge of an electron (1.60219×10^{-19} C)
ΔE	Potential Change
E_p	Peak Potential
ΔE_p	Peak Potential Change
$E_{p/2}$	Potential where $i = i_p/2$
E^o	Formal Potential
$E_p - E_{p/2}$	Peak Broadness, determined from y-intercept of $E_p - E_{p/2}$ vs. log ν
ECEC	Acronym representing a redox process where the order of steps proceeds as Electron transfer, Chemical step, Electron transfer, Chemical step
ET	Electron Transfer
F	Faraday's constant (96485 C mol^{-1})
Fc/Fc^+	Ferrocene/Ferrocenium Redox Couple
ΔG	Gibbs Free Energy Change
G	Gauss
GC	Glassy Carbon Electrode
η	Solvent or Medium viscosity
H^+	Proton
HF	Hartree-Fock
$HNMBC^{2+}$	Protonated N-Methyl-4,4'-Bipyridyl Chloride
^{1}H-NMR	Proton Nuclear Magnetic Resonance
$HPPC^{2+}$	Protonated 1-(4-Pyridyl)Pyridinium Chloride
I	Intensity
i_p	Peak Current

$i_{p,a}$	Anodic peak current
$i_{p,c}$	Cathodic peak current
k	Boltzmann's Constant
K	Equilibrium Constant
K_n	Association Equilibrium Constant for *n* molecules
k_b	Backward Rate Constant
k_f	Forward Rate Constant
K_{homo}	Homoconjugation rate constant
KCl	Potassium Chloride
K_{equ}	Equilibrium Constant
KIE	Kinetic Isotope Exchange
λ	Wavelength
λ_i	Inner Reorganization Energy
λ_o	Outer Reorganization Energy
λ_T	Overall Reorganization Energy
m	Mass of Electroactive Species
MHz	Mega Hertz
n	Number of electrons transferred
N	Molecular Weight
ν	Scan rate in cyclic voltammetry
$NBDBF_4$	4-nitrobenzenediazonium tetrafluoroborate
$NMBC^+$	N-Methyl-4,4'-Bipyridyl Chloride
NaCl	Sodium Chloride

NaH_2PO_4	Sodium Phosphate Monobasic
Na_2HPO_4	Sodium Phosphate Dibasic
NaOH	Sodium hydroxide
NOESY	Nuclear Overhauser Effect Spectroscopy
OH^-	Hydroxyl Ion
ρ	Solution density
p1	Pulse width (90^o)
pK_a	Logarithmic acid dissociation constant
PCET	Proton-Coupled Electron Transfer
PGE-^{1}H-NMR	Pulsed Gradient Echo Proton Nuclear Magnetic Resonance
PGSE	Pulsed Gradient Stimulated Echo
PPC^+	1-(4-Pyridyl)Pyridinium Chloride
PT	Proton Transfer
pw	Pulse width (180^o)
Q	Charge
QM	Quantum Mechanical, refers to computational chemistry calculations
γ	Gyromagnetic ratio
r_h	Hydrodynamic Radius
RDS	Rate Determining Step
ROESY	Rotational Frame Nuclear Overhauser Effect Spectroscopy
$Ru(NH_3)^{2+/3+}$	Ruthenium Hexamine Chloride
t	Time
T	Temperature

$TBAClO_4$	Tetrabutylammonium Perchlorate
$TBAPF_6$	Tetrabutylammonium Hexafluorophospate
TEA	Triethylamine
TS	Transition State
UV-Vis	Ultra Violet - Visible
V	Volt

ABSTRACT

Mechanistic Studies on the Electrochemistry of Proton Coupled Electron Transfer and the Influence of Hydrogen Bonding

Timothy M. Alligrant, Ph.D.

A dissertation submitted in partial fulfillment of the requirements for the degree of Doctor of Philosophy at Virginia Commonwealth University.

Virginia Commonwealth University, 2010

Major Director: Julio C. Alvarez, Ph.D., Department of Chemistry

This research has investigated proton-coupled electron transfer (PCET) of quinone/hydroquinone and other simple organic PCET species for the purpose of furthering the knowledge of the thermodynamic and kinetic effects due to reduction and oxidation of such systems. Each of these systems were studied involving the addition of various acid/base chemistries to influence the thermodynamics and kinetics upon electron transfer. It is the expectation that the advancement of the knowledge of acid/base catalysis in electrochemistry gleaned from these studies might be applied in fuel cell research, chemical synthesis, the study of enzymes within biological systems or to simply advance the knowledge of acid/base catalysis in electrochemistry. Furthermore, it was the intention of this work to evaluate a system that involved concerted-proton electron transfer (CPET), because this is the process by which enzymes are believed to catalyze PCET reactions. However, none of the investigated systems were found to transfer an electron and proton by *concerted* means. Another goal of this work was to investigate a system where hydrogen bond formation could be controlled or studied via

electrochemical methods, in order to understand the kinetic and thermodynamic effects complexation has on PCET systems. This goal was met, which allowed for the establishment of *in situ* studies of hydrogen bonding via ^{1}H-NMR methods, a prospect that is virtually unknown in the study of PCET systems in electrochemistry, yet widely used in fields such as supramolecular chemistry. Initial studies involved the addition of Brønsted bases (amines and carboxylates) to hydroquinones (QH_2's). The addition of the conjugate acids to quinone solutions were used to assist in the determination of the oxidation processes involved between the Brønsted bases and QH_2's. Later work involved the study of systems that were initially believed to be less intricate in their oxidation/reduction than the quinone/hydroquinone system.

The addition of amines (pyridine, triethylamine and diisopropylethylamine) to QH_2's in acetonitrile involved a thermodynamic shift of the voltammetric peaks of QH_2 to more negative oxidation potentials. This effect equates to the oxidation of QH_2 being thermodynamically more facile in the presence of amines. Conjugate acids were also added to quinone, which resulted in a shift of the reduction peaks to more positive potentials. To assist in the determination of the oxidation process, the six pK_a's of the quinone nine-membered square scheme were determined. ^{1}H-NMR spectra and diffusion measurements also assisted in determining that none of the added species hydrogen bond with the hydroquinones or quinone. The observed oxidation process of the amines with the QH_2's was determined to be a CEEC process. While the observed reduction process, due to the addition of the conjugate acids to quinone were found to proceed via an ECEC process without the influence of a hydrogen bond interaction between the conjugate acid and quinone.

Addition of carboxylates (trifluoroacetate, benzoate and acetate) to QH_2's in acetonitrile resulted in a similar thermodynamic shift to that found with addition of the amines. However,

depending on the concentration of the added acetate and the QH_2 being oxidized, either two or one oxidation peak(s) was found. Two acetate concentrations were studied, 10.0 mM and 30.0 mM acetate. From ^{1}H-NMR spectra and diffusion measurements, addition of acetates to QH_2 solutions causes the phenolic proton peak to shift from 6.35 ppm to as great as ~11 ppm, while the measured diffusion coefficient decreases by as much as 40 %, relative to the QH_2 alone in deuterated acetonitrile (ACN-d_3). From the phenolic proton peak shift caused by the titration of each of the acetates, either a 1:1 or 1:2 binding equation could be applied and the association constants could be determined. The oxidation process involved in the voltammetry of the QH_2's with the acetates at both 10.0 and 30.0 mM was determined via voltammetric simulations. The oxidation process at 10.0 mM acetate concentrations involves a mixed process involving both oxidation of QH_2 complexes and proton transfer from an intermediate radical species. However, at 30.0 mM acetate concentrations, the oxidation of QH_2-acetate complexes was observed to involve an ECEC process. While on the reverse scan, or reduction, the process was determined to be an CECE process. Furthermore, the observed voltammetry was compared to that of the QH_2's with amines. From this comparison it was determined that the presence of hydrogen bonds imparts a thermodynamic influence on the oxidation of QH_2, where oxidation via a hydrogen bond mechanism is slightly easier.

In order to understand the proton transfer process observed at 10.0 mM concentrations of acetate with 1,4-QH_2 and also the transition from a hydrogen bond dominated oxidation to a proton transfer dominated oxidation, conjugate acids were added directly to QH_2 and acetate solutions. Two different acetate/conjugate acid ratios were focused on for this study, one at 10.0 mM/25.0 mM and another at 30.0 mM/50.0 mM. The results of voltammetric and ^{1}H-NMR studies were that addition of the conjugate acids effects a transition from a hydrogen bond

oxidation to a proton transfer oxidation. The predominant oxidation species and proton acceptor under these conditions is the uncomplexed QH_2 and the homoconjugate of the particular acetate being studied, respectively. Furthermore, voltammetry of QH_2 in these solutions resembles that measured with the QH_2's and added amines, as determined by scan rate analysis.

In an attempt to understand a less intricate redox-active system under aqueous conditions, two viologen-like molecules were studied. These molecules, which involve a six-membered fence scheme reduction, were studied under buffered and unbuffered conditions. One of these molecules, N-methyl-4,4'-bipyridyl chloride ($NMBC^+$), was observed to be reduced reversibly, while the other, 1-(4-pyridyl)pyridinium chloride (PPC^+), involved irreversible reduction. The study of these molecules was accompanied by the study of a hypothetical four-membered square scheme redox system studied via digital simulations. In unbuffered solutions each species, both experimental and hypothetical, were observed to be reduced at either less negative (low pH) or more negative (high pH), depending on the formal potentials, pK_a's of the particular species and solution pH. The presence of buffer components causes the voltammetric peaks to thermodynamically shift from a less negative potential (low pH buffer) to a more negative potential (high pH buffer). Both of these observations have been previously noted in the literature, however, there has been no mention, to our knowledge, of kinetic effects. In unbuffered solutions the reduction peaks were found to separate near the $pK_{a,1}$. While in buffered solutions, there was a noted peak separation throughout the pH region defined by pK_a's 1 and 2 ($pK_{a,1}$ and $pK_{a,2}$) of the species under study. The cause for this kinetic influence was the transition from a CE reduction at low pH to an EC reduction process at high pH in both buffered and unbuffered systems. This effect was further amplified via the study of the hypothetical species by decreasing the rate of proton transfer.

In an effort to further this work, some preliminary work involving the attachment of acid/base species at the electrode surface and electromediated oxidation of phenol-acetate complexes has also been studied. The attachment of acid/base species at the surface is believed to assist in the observation of heterogeneous acid/base catalysis, similar to that observed in homogeneous acid/base additions to quinone/hydroquinone systems. Furthermore, our efforts to visualize a *concerted* mechanism are advanced in our future experiments involving electromediated oxidation of phenol-acetate complexes by inorganic species. It may be possible to interrogate the various intermediates more efficiently via homogeneous electron-proton transfer rather than heterogeneous electron transfer/homogeneous proton transfer.

1.0 Overview

Electron and proton transfer, ET and PT, are two of the most fundamental reactions in all of chemistry. These two reactions are as ubiquitous as they are important. Furthermore, both the electron and proton are two of the fundamental constituents of matter. Usually, these two particles, especially the electron, are invoked in the study of structure and reactivity of various molecules and to describe nearly all chemical reactions. Exceptions to this would be the study of nuclear chemistry. ET and PT constitute two key steps in a number of biological processes such as metabolism, respiration, photosynthesis, signal and energy transduction, etc. Additionally, ET and PT are also critical steps in technological devices such as fuel cells.

The study of electrochemistry, usually, but not exclusively, focuses on ET, primarily heterogeneous ET, and the chemistry associated with this transfer. Heterogeneous meaning that the donor and acceptor of the electron are in different phases. Typically, the electron is transferred to a solid electrode by a solvated molecule in a solution of considerable ionic strength. This research focuses on this mode of ET. The transfer of an electron to or from an electrode surface, by or to an electroactive species often results in a variety of chemical reactions. PT, bond dissociation and association, dimerization, association of molecules via hydrogen bonding or other forms of intermolecular forces and structural change are just a few examples. The study of electrochemistry is appealing to the study of such reactions as it is able to give thermodynamic, kinetic and mechanistic insights that could be difficult to interpret if studied by other methods alone. However, electrochemistry is not the ultimate technique to use to study all of the aforementioned reactions. Often, it is advisable to use other techniques, such as UV-vis, IR or NMR spectroscopy or even computational methods to determine if a

hypothesized interaction is viable. Spectroscopic methods allow for analyses to be conducted *in situ* under certain conditions.

This thesis deals with a special class of reactions, proton-coupled electron transfer (PCET) reactions, in which the heterogeneous transfer of an electron is coupled to the transfer of a proton. Such reactions can be classified as either *concerted* or *stepwise*. Where the electron and proton are either transferred one at a time, *stepwise,* or in a single kinetic step, *concerted,* where the electron is transferred and the proton tunnels across the energy barrier in the transition state complex. A hydrogen bonding interaction is often thought to be a pre-requisite for a *concerted* reaction. This presents a compelling argument in many cases for the evidence presented in studies of the addition of hydroxylic reagents to electroactive species. However, there is often very little *in situ* evidence presented to support the complexation hypothesis. The studies described in this dissertation seek to address these issues and describe the mechanism of several PCET systems upon addition of Brønsted acids and bases. The ultimate goal is to determine the effects on the voltammetry brought about by ET and PT transfer via acid/base catalysis under various conditions such as differences in solvent, intermolecular interaction (no complexation versus complexation) and structural changes. Furthermore, it is the expectation that the advancement of the knowledge of acid/base catalysis in electrochemistry gleaned from these studies might be applied in fuel cell research, efficient chemical synthesis, the study of enzymes within biological systems or to simply advance the knowledge of acid/base catalysis in electrochemistry.

1.1 Quinones and Hydroquinones

Both quinones and hydroquinones have many important chemical, biological and industrial functions. In industrial settings, dihydroanthraquinone is oxidized by oxygen to

produce several billion kilograms of hydrogen peroxide annually.[1] In biological systems, quinones function in energy transfer systems as mobile carriers of protons and electrons in energy transducing membranes. Furthermore, quinones have been widely studied in organic chemical and electrochemical systems for their use as proton and electron carriers.[2-4]

1.1.1 Quinones and Hydroquinones as Energy Transfer Species in Cellular Systems

Most quinones involved in energy transfer systems consist of long chain quinones, or quinones substituted with side chains of considerable length. Some of the common examples are shown in Scheme 1. As mobile carriers of electrons and protons in plant and mammal cells, quinones are found in several cellular locations. Within mammalian and bacterial cells, quinones are found in the membrane bilayer of the mitochondria, while in plants and photosynthetic bacteria quinones are found within the membrane bilayer of the thylakoid membrane.[3, 4]

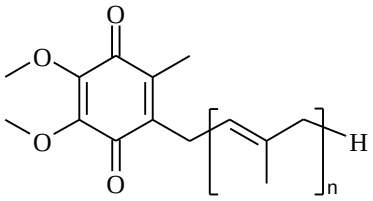

Ubiquinone

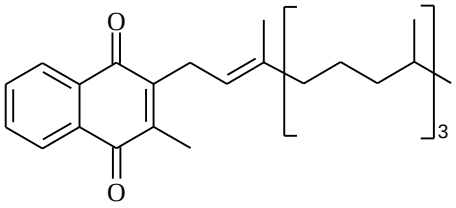

Phylloquinone

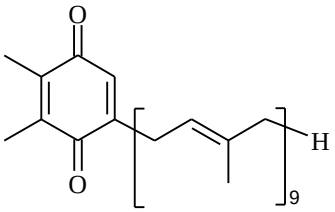

Plastoquinone

Scheme 1. Quinones commonly found in biological systems.

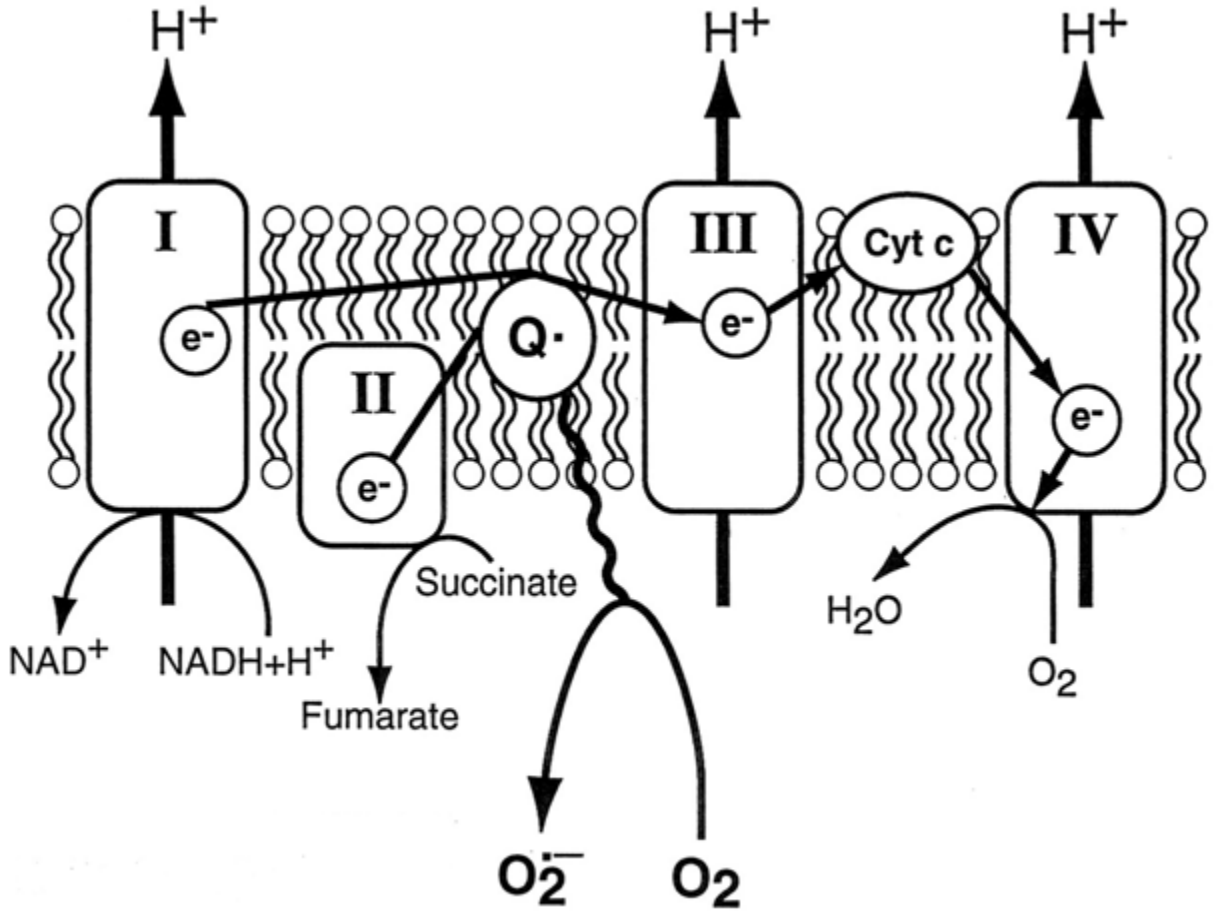

Figure 1. Mitochondrial electron transfer chain, adapted from reference 5.

In mammalian and bacterial cells, quinones are involved in aerobic respiration via complexes I, II and III of the electron transport chain, labeled in Figure 1. Aerobic respiration or oxidative metabolism is one of the primary ways a cell gains useful energy by synthesis of adenosine triphosphate (ATP).[3-5] A full representation of the mitochondrial electron transport chain is shown in Figure 1.[6] Complex IV is also shown, yet will not be discussed. Complex I, otherwise referred to as nicotinamide adenine dinucleotide (NADH) dehydrogenase, removes two electrons from NADH to form NAD^+. Those electrons are then transferred to a lipid soluble quinone, ubiquinone via flavin mononucleotide, FMN, and a Fe-S cluster one electron at a time.[3,

[7] Two protons are also delivered into the intermembrane space to form ubiquinol. Ubiquinol, produced by complex I, is then bound to cytochrome b (cyt b), where it is oxidized back to ubiquinone.[3, 8] In complex II, ubiquinone acts as an electron and proton carrier by first binding within the succinate dehydrogenase enzyme active site. Upon binding, ubiquinone is then reduced by the electrons from succinate oxidation to fumarate.[3] Here again, two protons are transferred from the matrix of the mitochondria into the intermembrane space and ubiquinol is produced. As before with complex I, production of ubiquinol leads to oxidation by complex III,

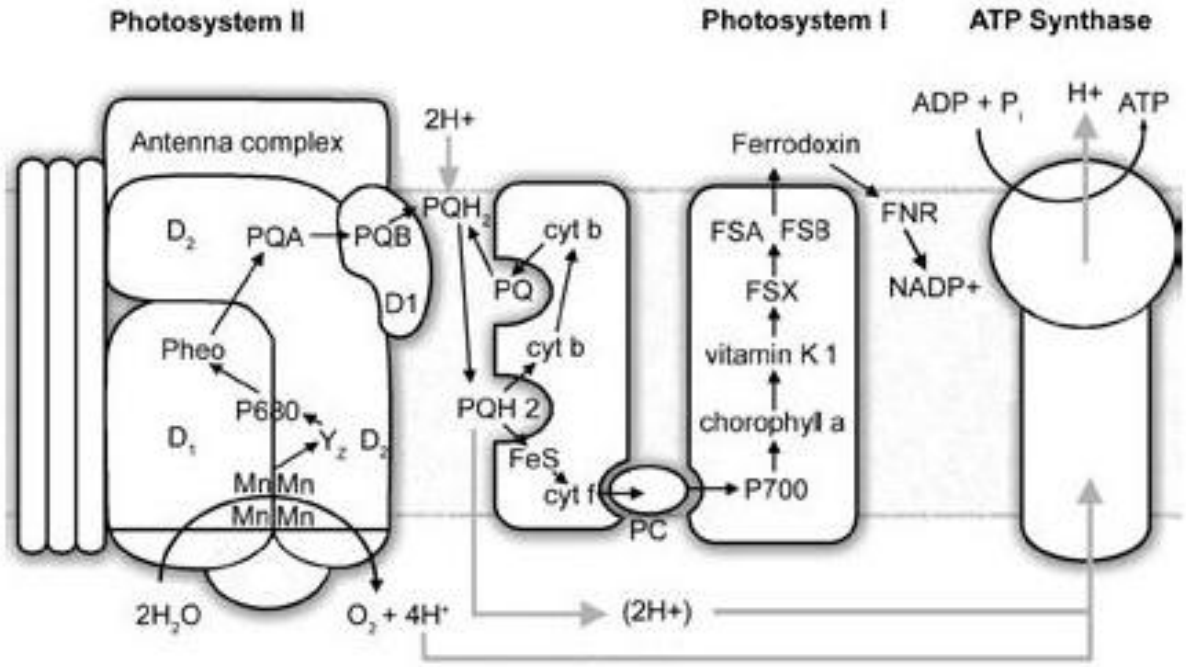

generating ubiquinone.[3, 8]

Figure 2. Photosystems I and II involved in photosynthesis, adapted from reference 9.

Quinones are also involved in photosystems (PS) I and II of photosynthesis in plants, algae and photosynthetic bacteria as depicted in Figure 2. In photosystem I (PS I) phylloquinones, vitamin K_1, act as an intermediate electron transfer center.[9, 10] A photon first excites chlorophyll molecules located in the antenna complex of PS I. From here, the photon

energy is transferred to the P700 reaction center, which causes an electron to be raised to a higher energy level. The electron is then transferred to an acceptor chlorophyll *a* molecule (termed site A_o). The reduced chlorophyll *a* molecule then reduces vitamin K_1 located in site A_1, which subsequently transfer the electron to three different iron-sulfur proteins (FSX, FSA and FSB in Figure 2), the last of which reduces ferredoxin. Ultimately, ferredoxin transports the electron to ferredoxin-$NADP^+$ reductase (FNR), where $NADP^+$ is reduced to NADPH.[3-5, 9, 10] As in PS I the quinone cofactors of photosystem II (PS II), plastoquinones, act as intermediate electron transfer centers.[3, 5, 10] In PS II water is oxidized to dioxygen and four protons at the oxygen evolving complex, a manganese complex, upon absorption of four photons by the P680 reaction center. The electrons from water oxidation are transferred to pheophytin (pheo in Figure 2), a chlorophyll molecule lacking a manganese cation, which then transfers the electrons to plastoquinone.[11] This reduction of plastoquinone produces plastoquinol by also accepting two protons from the stromal matrix of the chloroplast. Oxidation of plastoquinol by the cytochrome b_6f protein complex, or plastoquinol-plastocyanin reductase, leads to the transfer of two protons to the luminal side of the chloroplasts, while the electrons continue on through the electron transport chain.[3, 5, 10, 12] The oxidation of water to dioxygen and four protons along with the proton transfer process, which occurs upon plastoquinol oxidation creates a proton gradient across the membrane. This proton gradient assists in the production of adenosine triphosphate (ATP) via ATP-synthase, as illustrated in Figure 2.[3, 5, 10]

1.1.2 Electrochemical Reactions of Quinones and Hydroquinones

The quinone/hydroquinone redox couple is one of the most fundamental in all of electrochemistry given its wide use in many varied electrochemical studies.[2] In fact, quinoid species can be thought as keystones in the development of modern electroanalytical techniques[13] and despite the multiple electrochemical studies since, novel aspects of quinones continue to be actively investigated. An interesting recent discovery is that the reduction of quinones in aqueous unbuffered solution leads to a different mechanism of reduction than is typically found in buffered aqueous solution. Reduction in unbuffered solutions where the concentration of protons, H^+, is less than the concentration of the quinone leads to a reduced quinone dianion, Q^{2-}, that is hydrogen bound to several water molecules, Figure 3.[14] The mechanism of reduction or oxidation of quinones is defined by a nine-membered square scheme, Scheme 2. Under certain circumstances, aqueous

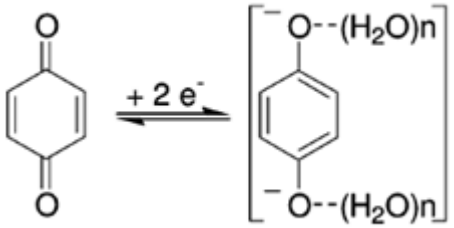

Figure 3. Reduction of 1,4-quinone in ubuffered solution, where $[H^+] < [1,4\text{-Q}]$, adapted from reference 14.

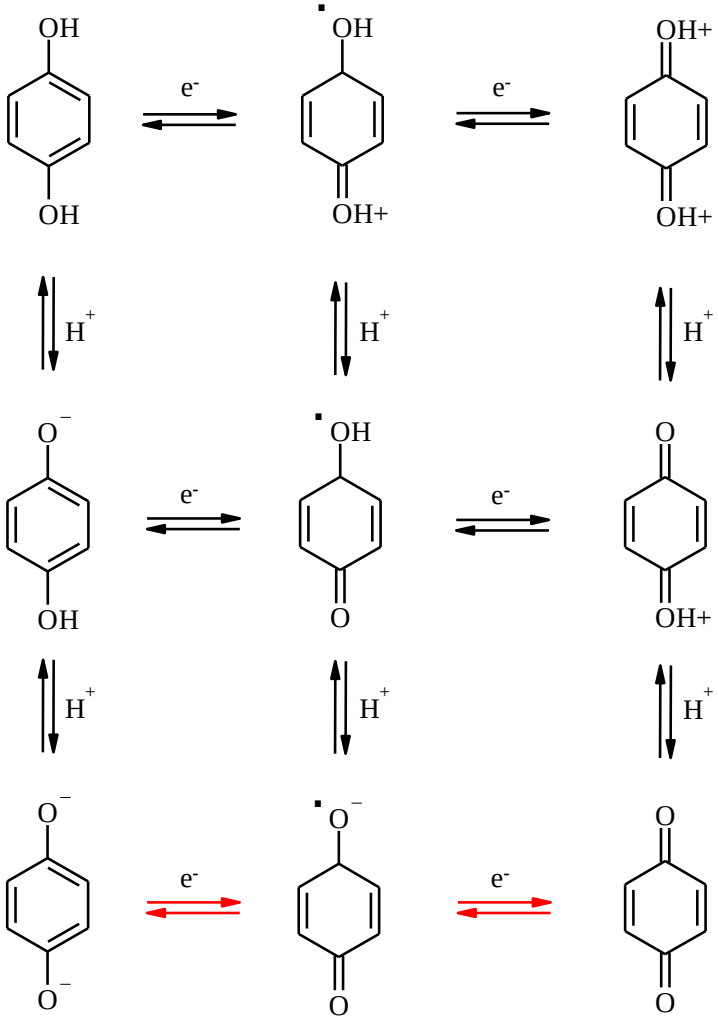

Scheme 2. Nine-membered square scheme of 1,4-benzoquinone/1,4-hydroquinone. Red arrows indicate quinone oxidation in aprotic solution.

versus non-aqueous or buffered versus unbuffered solution, the consideration of a number of the members of this square scheme need to be considered to determine the mechanism of reaction. The reduction or oxidation of quinone or hydroquinone, respectively, in aqueous buffer solution, depending on the pH, will involve multiple members of the square scheme. In aqueous solution, a cyclic voltammogram (CV) typically shows only a single two-electron oxidation and reduction peak for the reduction or oxidation of the quinone redox couple. In non-aqueous media, the CV of hydroquinone (upper left-hand species in Scheme 2, QH_2) will also only display a single two-electron oxidation and reduction peak and multiple members of the square scheme will need to be considered in determining the mechanism of oxidation. However, the reduction of 1,4-benzoquinone (lower right-hand species in Scheme 2, 1,4-Q) in non-aqueous media only involves the three lower members of the nine-membered square scheme, mechanism shown by the red arrows. A CV of 1,4-Q will show two sets of one-electron reduction and oxidation peaks. An example of this voltammetry is shown in Figure 4, where 5.0 mM 1,4-Q is reduced to the radical anion ($1,4\text{-}Q^{\cdot-}$) and then to the dianion ($1,4\text{-}Q^{2-}$) at peaks I and II, respectively. At peak III $1,4\text{-}Q^{2-}$ is oxidized back to the radical anion, which is finally reduced back to 1,4-Q.

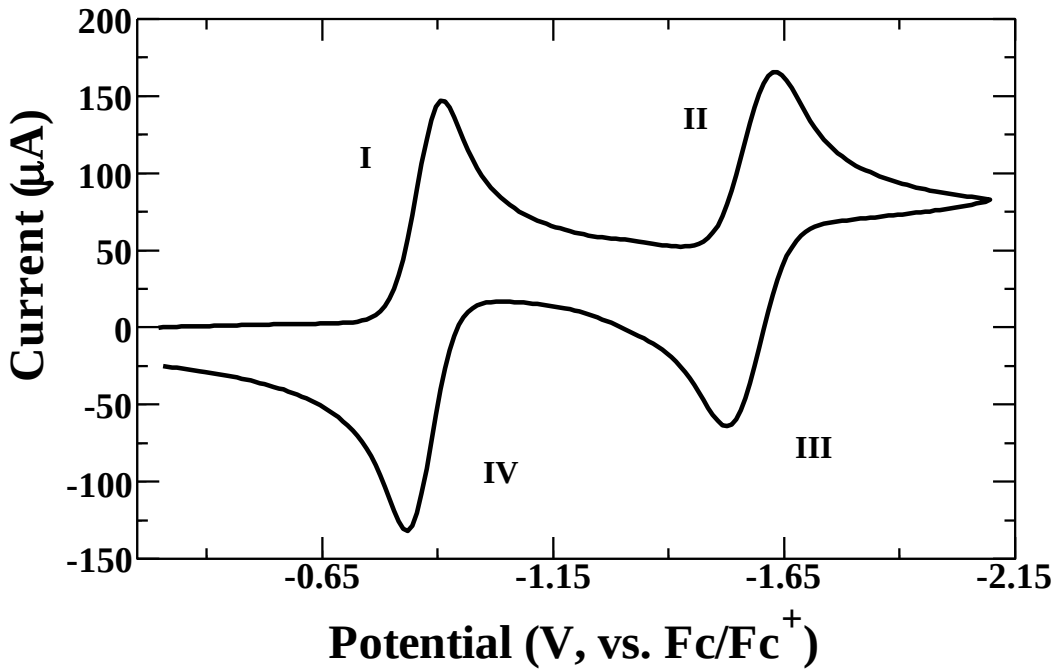

Figure 4. Cyclic voltammogram of 5.0 mM 1,4-benzoquinone with 0.2 M $TBAPF_6$ as supporting electrolyte. Voltammetry performed at 0.1 V s^{-1} at 27 ^{o}C in acetonitrile at a glassy carbon electrode (0.059 cm^2).

1.2 Proton-Coupled Electron Transfer

Electron transfer and proton transfer are two of the most basic and prevalent reactions in all of chemistry. Some chemical reactions involve the transfer of both electrons and protons and such reactions take place in numerous organic, biological and inorganic reactions. Reactions that involve both electron and proton transfer are referred to collectively as proton-coupled electron transfer (PCET), which is of great current interest.[11, 15-19] In such reactions, either the proton or electron transfer can occur first, *stepwise*, or the reaction can occur in a *concerted* manner, otherwise known as concerted-proton electron

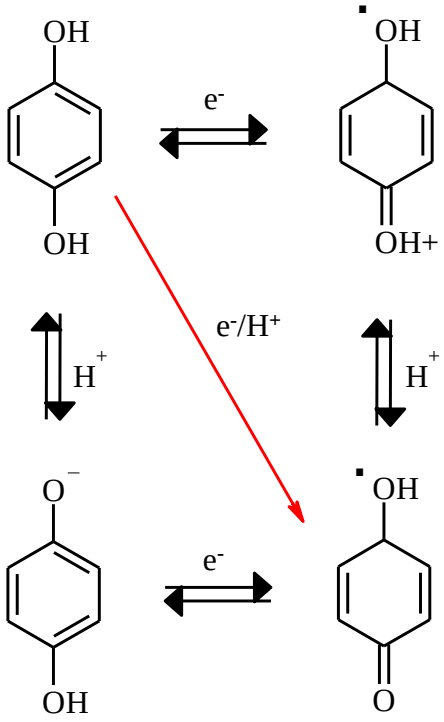

Scheme 3. Abbreviated square scheme of 1,4-Q. The red arrow indicates the CPET mechanism.

transfer (CPET). In a CPET reaction, both the electron and proton are transferred in a single kinetic step.[15-17, 20] An example of this reaction is illustrated by the abbreviated quinone square scheme, Scheme 3. The horizontal and vertical lines in Scheme 3 represent the *stepwise* ET and PT, respectively, while the diagonal red line represents the *concerted* reaction. Intermolecular and intramolecular hydrogen bonds between reactants involved in PCET reactions are thought to increase the likelihood of a *concerted* reaction over a *stepwise* reaction, especially in aprotic solvents.[15, 19] However, there is some research to suggest that CPET reactions are much less favorable in aprotic solvents.[21]

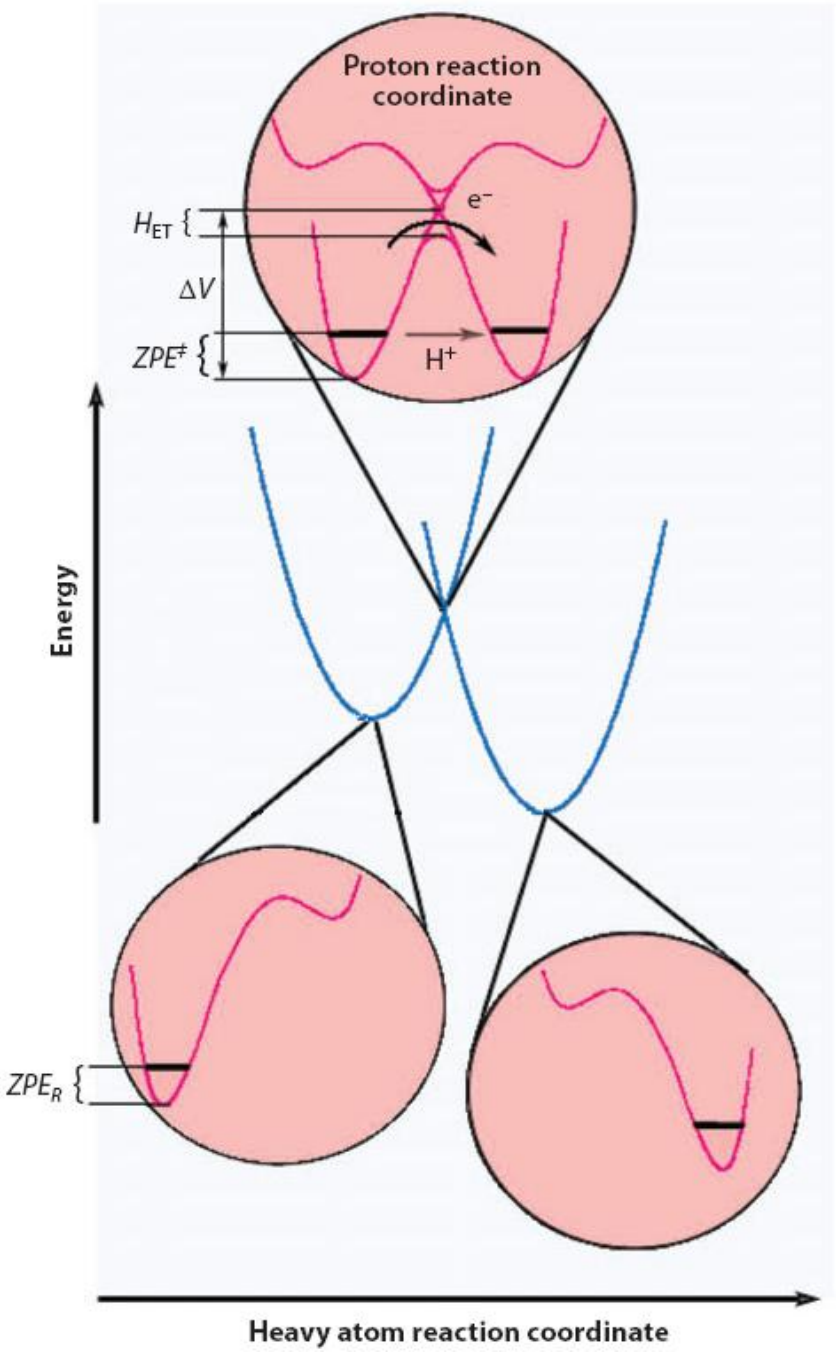

Figure 5. CPET reaction two-dimensional potential energy profiles. The pink circles represent the vibrational energy surface for the transferring hydrogen atom at the lowest energy level at the, from left to right, reactant, transition state and product. Adapted from reference 23.

Yet, it is believed that many enzymatic or catalytic reactions occur via a *concerted* manner, and aprotic solvents are often touted as a dielectric mimic for the interior or reaction sites of enzymes.[15, 22] Furthermore, CPET reactions are thought to be nature's way of avoiding high energy intermediates.[11, 16] Due to the avoidance of these intermediates, energy is conserved and the PCET process in biological reactions is favorable, versus a *stepwise* mechanism where the reaction is often energetically unfavorable.[11, 17] Thus, such reactions are known or thought to occur in important biological reactions such as respiration, nitrogen fixation and photosynthesis.[11, 16, 17] Furthermore, the scope of CPET also encompasses many other terms associated with *concerted* ET/PT reactions.[15, 17]

To understand the kinetics of CPET, one should envision an intermolecular hydrogen bonded complex reacting with an electrode surface. As a complex, the proton activation barrier at the transition state, ΔV (see Figure 5), is much greater than the proton vibrational ground state of the reactant or product molecules. Generally, the electron resonance energy, H_{ET}, is small compared to the proton activation barrier, ΔV. However, the greatest probability of the proton to tunnel across the energy barrier occurs at the reaction transition state where the lowest proton vibrational wavefunction is the same in the reactant and product wells, Figure 5.[19, 20, 23] To distinguish between a CPET and a *stepwise* mechanism deuterated reagents or solvent, in the case of aqueous experiments, are used. Once kinetic rate constants are determined for the protiated and deuterated experiments the kinetic isotope effect (KIE) can be determined using the relation, $KIE = k_H/k_D$. If the result of the KIE relation is found to be greater than 1.6 the mechanism is considered *concerted*.

1.3 Electrochemical Methods

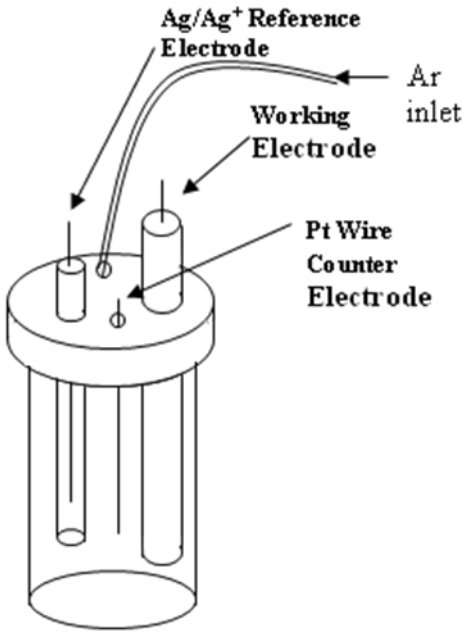

Figure 6. Typical three electrode cell.

Electrochemical methods have been applied in nearly every branch of science to study a broad range of reactions and for many applications.[24] The four electrochemical techniques involved in this research are cyclic voltammetry, chronoamperometry, chronocoulometry and bulk electrolysis.

1.3.1 Cyclic Voltammetry

Cyclic voltammetry involves the use of a three-electrode cell setup and a cyclic potential scan as shown in Figures 6 and 7, respectively. The slope of the potential scan indicates the scan rate of the cyclic voltammetry experiment. The result of this potential scan gives a cyclic voltammogram (CV), as shown in Figure 8. This is a CV for 1.0 mM ruthenium hexaamine chloride ($Ru(NH_3)_6^{3+}$) in unbuffered 0.5 M KCl at a glassy carbon electrode (surface area = 0.059 cm^2). $Ru(NH_3)_6^{3+}$ is a readily used redox couple due to its reversible electron transfer (usually accepted to be a process where $\Delta E_p \sim 60$ mV, and the peak current ratio, i_{pa}/i_{pc}, close to unity) nature as a redox couple. The scanned potential range in Figure 8 is measured versus an Ag/AgCl reference electrode.

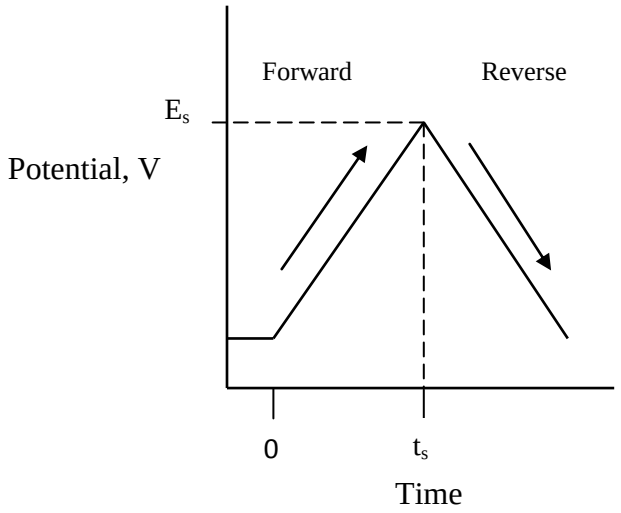

Figure 7. Cyclic potential sweep program for cyclic voltammetry. In this figure, t_s and E_s are the switching potentials and the arrows represent the forward and reverse scans.

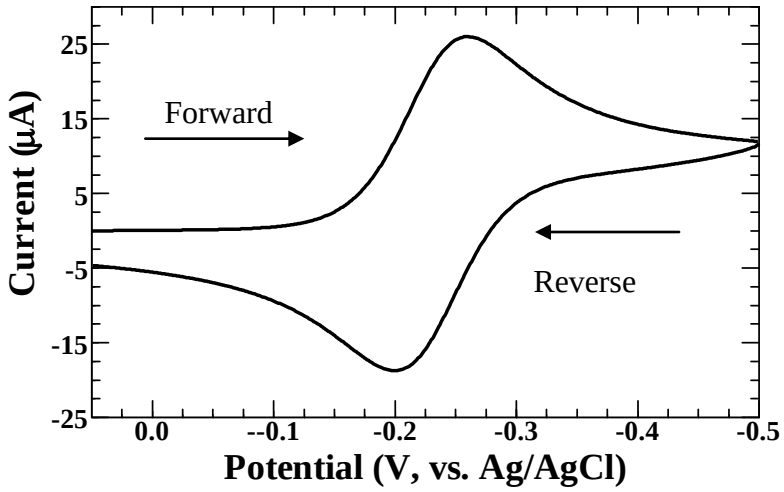

Figure 8. Cyclic voltammogram of 1.0 mM $Ru(NH_3)_6^{3+}$ in 0.5 M KCl at pH 7.05. Voltammetry performed at a glassy carbon electrode at 0.1 V s^{-1}.

Both the general potential diagram and the CV in Figures 7 and 8, respectively, show the direction of the potential scan, in both the forward and reverse direction.[24-26] From the CV, we see that initially there is no faradic current observed from 0.05 V (vs. Ag/AgCl) to approximately -0.1 V (vs. Ag/AgCl), due to the absence of electron transfer. Any measure of current within this region is considered charging or nonfaradic current, where charge is accumulating at the electrode interface with the solution. The peak at -0.259 V, referred to as the cathodic peak, corresponds to the reduction of $Ru(NH_3)_6^{3+}$ at the electrode surface to $Ru(NH_3)_6^{2+}$. During reduction there is a flux of $Ru(NH_3)_6^{3+}$ to the surface and the peak results when the concentration of $Ru(NH_3)_6^{3+}$ at the surface approaches zero and mass transfer to the electrode is at a maximum. The peak potential in the reverse scan, at -0.200 V, referred to as the anodic peak, corresponds to the oxidation of $Ru(NH_3)_6^{2+}$ back to

$Ru(NH_3)_6^{3+}$. Like the reduction process, the oxidation current of $Ru(NH_3)_6^{2+}$ reaches a maximum when the surface concentration of $Ru(NH_3)^{2+}$ approaches zero.

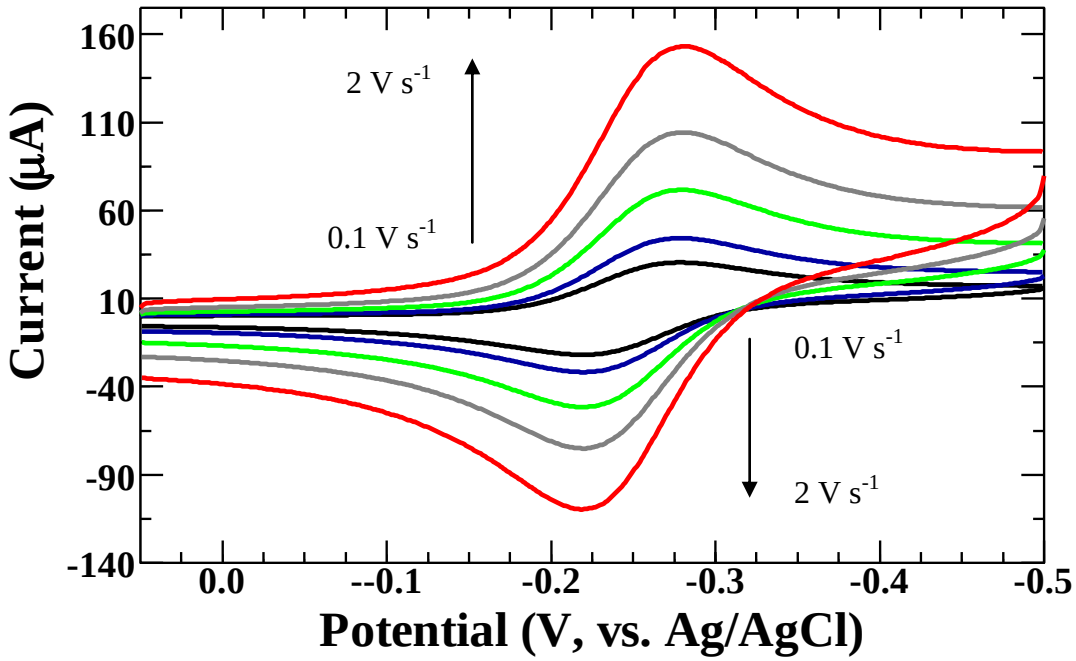

Figure 9 Cyclic voltammetry of 1.0 mM $Ru(NH_3)_6^{3+}$ in 0.5 M KCl at pH 7.05. Voltammetry performed at a glassy carbon electrode. Arrows represent increase in scan rate.

$$i_p = (2.69 \times 10^5) n^{3/2} A D^{1/2} C v^{1/2} \quad (1)$$

For a reversible electrochemical system, like $Ru(NH_3)_6^{3+}$, the peak current is directly related to the concentration of the analytes by the Randles-Sevcik equation, equation 1.[24] Where *n* represents the number of electrons transferred in the redox reaction; A the area of the electrode, in cm^2; D the diffusion coefficient, in $cm^2\ s^{-1}$; C the concentration, in mol cm^{-3}; and *v* the scan rate, in V s^{-1}.[24] Often equation 1 is used to plot the peak current versus the square root of the scan rate to obtain the area of the electrode or the diffusion coefficient of the analyte. Figure 9 shows how the peak current changes as the scan rate is increased from 0.1 to 2 V s^{-1}. Notice the

near complete lack of cathodic or anodic movement of each of the peaks. This is another indication of a reversible or near reversible electrochemical couple. Varying the scan rate can assist one to determining the mechanism of the redox process via various mathematical and conceptual means.[18, 24, 27] Furthermore, kinetic and thermodynamic influences on oxidation processes are easily visualized via cyclic voltammetry. Kinetic influences typically involve a separation of the voltammetric peaks, while thermodynamic effects are found when the measurement of the redox process occurs at more or less positive potentials. However, kinetic and thermodynamic effects are not limited to these observations.

1.3.2 Chronoamperometery/Chronocoulometery

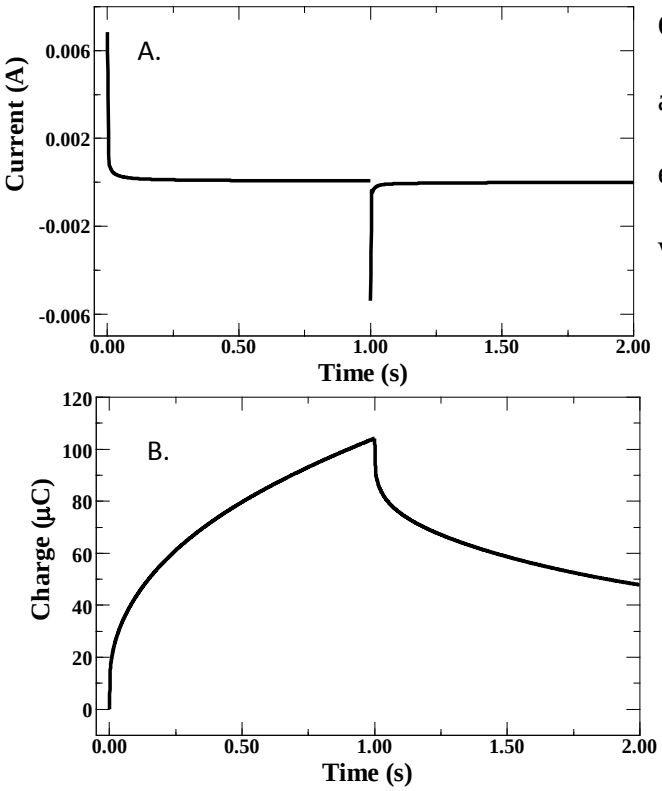

Figure 10. (A.) Typical double-step chronoamperometic response curve. (B.) Typical double-step response curve to a chronocoulometry potential step experiment.

Chronoamperometry and chronocoulometry are two of the most basic of all electrochemical techniques. The potential waveform for a single step chronoamperometry experiment involves a step from one potential to another while the current is measured versus time.[24] Chronocoulometry involves the same step from an initial potential to another, while measuring the charge produced. A typical chronoamperogram is presented in Figure 10A, while 10B shows the result of a chronocoulometry experiment.

Chronoamperometry and chronocoulometry are commonly used to determine diffusion coefficients or the area of the electrode using the Cottrell equation, equation 2, or it's integral, respectively. Where *i*, represents current in amperes; *n*, the number of electrons transferred; F, the Faraday constant (96485.3 C); A, the area of the electrode in cm^2; D, the diffusion coefficient in cm^2 s^{-1}; C, the bulk concentration of the electroactive species in mol cm^{-3}; and *t*, time in seconds.[24]

$$i = \frac{n\mathrm{FAD}^{1/2}\mathrm{C}}{\pi^{1/2} t^{1/2}} \qquad (2)$$

1.3.3 Controlled Potential Coulometry

Previously discussed electrochemical techniques only affected a small quantity of the sample within the electrochemical cell. However, controlled potential coulometry (CPC) is a bulk electrolysis technique, and generally involves the entire sample. This technique can be used for studying the products of a redox reaction, by electrolyzing the solution at some potential beyond the half-wave potential. Typically, the potential used is 0.118/*n* V more negative than the formal potential, E^o, for a reduction at 25 ^oC.[24] Using Faraday's Law, equation 3, one can determine the number of electrons transferred in an electrode reaction. Here, Q represents the charge passed, in coulombs; N the molecular weight, in grams per mole; F, Faraday's constant,

$$n = \frac{\mathrm{QN}}{m\mathrm{F}} \qquad (3)$$

in coulombs per mole; *m* the mass of the electroactive species, in grams; and *n* the number of electrons. To use this method the background charge at the same potential must also be determined and subtracted from the total charge passed with the electroactive species present. For CPC experiments involving the determination of the number of electrons passed, the final charge ratio should be ≤ 0.1 %.[24] This technique requires a large working and counter electrode.

The counter electrode must be in contact with, but separate from the electrolysis solution, thus in a fritted chamber filled with the solvent and supporting electrolyte.[24] The research discussed below involved this technique for the evaluation of the number of electrons transferred and for studying electrolysis products by UV-vis.

1.4 Nuclear Magnetic Resonance

Nuclear magnetic resonance (NMR) is simply a form of absorption spectroscopy, where under the appropriate conditions in a magnetic field a sample can absorb electromagnetic radiation in the radio frequency region of the sample. The absorption is a function of certain nuclei of a molecule in the sample.[28] There are many nuclei with which NMR techniques can be used, however, the focus of the research reported herein involves the use of proton NMR, or ^{1}H-NMR.

1.4.1 Pulsed Gradient Echo Proton Nuclear Magnetic Resonance

The pulsed field gradient technique has been used extensively in many areas of science and medicine to determine the self-diffusion coefficient (D) since the discovery by Stejkal and Tanner in 1965.[29-31] A common pulse sequence diagram for the pulsed gradient echo (PGE) technique is gradient pulses are inserted into each period τ o

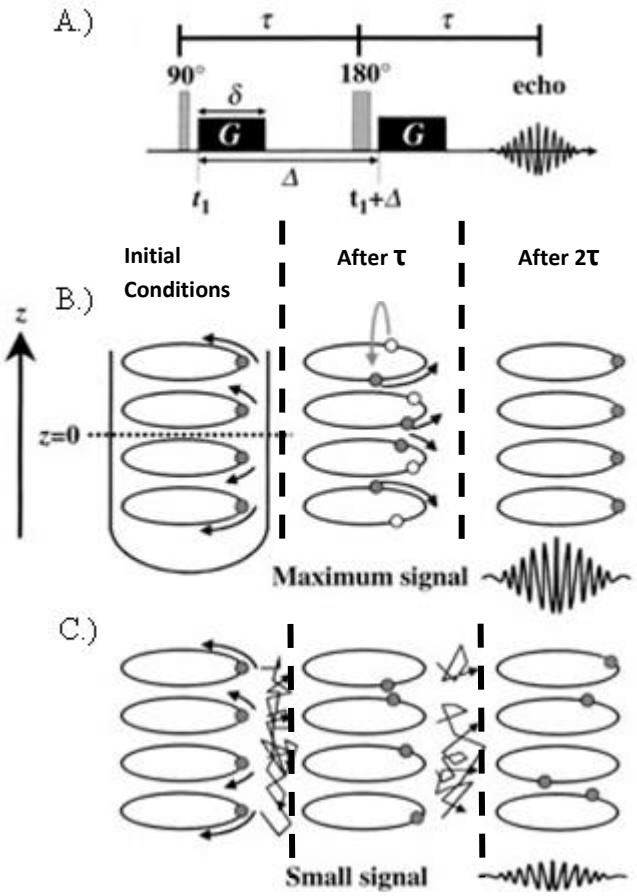

Figure 11. A.) The PGE pulse sequence. Also shown is the effect of the absence (B.), and presence (C.) of diffusion on the phase shift and signal intensity in a PGE experiment. Adapted from Reference 29.

effect that the PGE technique has on the magnetization of an ensemble of spins are shown in Figures 11B and 11C. The ensembles of spins are in thermal equilibrium, and the net magnetization is oriented along the z-axis. First, a 90° radiofrequency (RF) pulse is applied resulting in a shift of the magnetization from the z-axis to the x-y plane. Then, a pulse gradient of some duration δ and magnitude G is then applied at time t_1. As a result, each spin experiences a phase shift at the end of the first period τ, before the application of the 180° RF pulse.[29, 32] The 180° RF pulse causes the reversal of the sign of the processing and the sign of the phase angle, as shown in Figure 11B, where open circles become filled circles. Then, the second gradient, equal in duration and

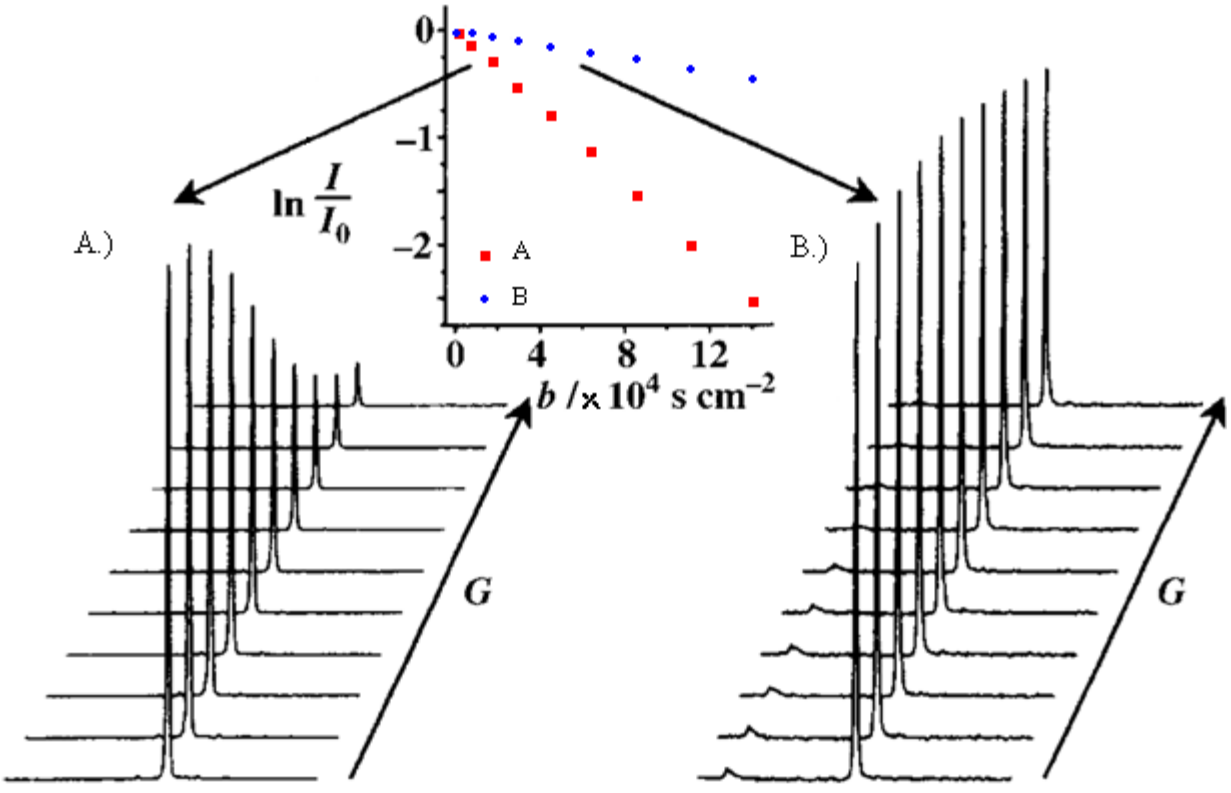

Figure 12. Signal decays of two separate species, A and B. Inset, plot of natural log of peak intensity versus the product of $\gamma^2G^2\delta^2(\Delta-\delta/3)$, or *b*, from equation 4. Adapted from Reference 29.

magnitude to the first, is applied at time $t_1 + \Delta$. Here there are two possible scenarios, represented in Figures 11B and 11C. In the first scenario, Figure 11B, the spins do not undergo translational motion along the z-axis, thus no diffusion during the time interval. In this case, the phase shift of each spin after each time τ is equal. Thus, the maximum echo signal is obtained.[29] However, in the presence of diffusion, Figure 11C, the phase shift of each spin is different after each time period τ. This effect is due to the difference in position of each species under study at the times t_1 and $t_1 + \Delta$, and hence each species is oriented in the magnetic field differently. Therefore, a smaller echo signal is found. By intuition, one can deduce that a smaller echo signal reflects larger diffusion.[29] A clear description of the differences in echo signals by different species is given by Figure 12, where one species has a diffusion coefficient (D) of 1.81×10^{-5} $cm^2\ s^{-1}$ (A.) while the other has a D equal to 0.33×10^{-5} $cm^2\ s^{-1}$ (B.).[29] To determine the values of D, the natural log of the intensity after 2τ, I, divided by the intensity of the echo signal after the 90^o RF pulse, I_0, is plotted versus the product $\gamma^2G^2\delta^2(\Delta-\delta/3)$, otherwise known as *b*.[29] This plot should give a straight line, the slope of which is equal to –D, as given by equation 4.[29, 32] In equation 4, γ is the gyromagnetic ratio (in $T^{-1}\ s^{-1}$), G is pulsed gradient strength (in $G\ cm^{-1}$), Δ is the time separation in seconds between the pulsed gradients (t_1 to $t_1 + \Delta$, Figure 11A) and δ is the duration in seconds of the gradient pulse.[29]

$$\ln(I/I_0) = -\gamma^2G^2\delta^2(\Delta-\delta/3)D = -bD \qquad (4)$$

1.5 Computational Methods

The proliferation of computational methods in many areas of chemistry is ever increasing. From the use of simulation programs for various forms of spectroscopy[33, 34] and voltammetry[35-40] to the use of more quantitative methods[41, 42] for the calculation of pK_a's, formal

potentials and free energies, computational chemistry is becoming a part of nearly every thorough study in chemistry.

1.5.1 Digital Simulations of Cyclic Voltammetry

The simulation of cyclic voltammetry was developed as a method to analyze the complex hetero- and homogeneous processes that make up a cyclic voltammogram (CV).[35] The following will describe how the CV simulator works and then will explain the user input that allows for the fitting of an experimental CV. To do so, the electrolytic solution must be broken up, or

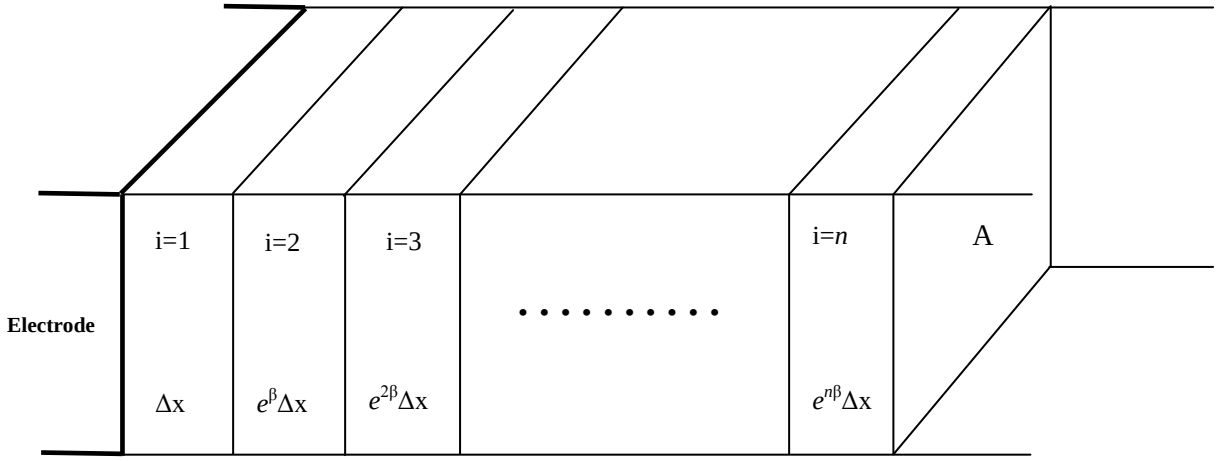

Figure 13. Exponentially expanding space grid model for the digital simulation of electrochemical experiments on an electrode with a projected area A.[35, 37]

discretized, into small volume elements, i. These volume elements start at the working electrode face and are projected into the bulk solution, as shown in Figure 13. The first volume element is in contact with the electrode surface and the *n*th volume element represents bulk solution. An exponentially expanding space grid, expanding by a factor β, causes an increase in the thickness of the volume elements as the distance from the electrode increases. The exponentially expanding space grid allows for an efficient and accurate treatment of the concentration profiles,

which are associated with the volume elements, produced by homogeneous chemical reactions. The program user can manipulate the value of β, from 0 to 0.5. Obviously, a β value of 0 corresponds to a uniform grid space of Δx. Decreasing β to approximately 0 will increase computation time and enhance the accuracy, while increasing β will decrease computation time and have detrimental effects on accuracy.[35-40] Once the user has input an appropriate mechanism and parameters pertaining to this mechanism, the parameters can be refined by the use of a Gauss-Newton algorithm. This iterative method seeks values that minimize the residuals of the fitting. To further minimize the error of the fitting the user should attempt the fittings of CV's at multiple scan rates and attempt to determine as many of the parameters involved in the fitting as possible. As the number of fitted parameters increases the probability of finding a true value decreases.[35, 43]

1.5.2 Quantum Mechanical Calculations

Computational chemistry, more importantly, quantum mechanical (QM) chemistry, simulates chemical structures and reactions based on the fundamentals of physics. The methods discussed in this section are a much generalized view of computational QM chemistry, for use in understanding the methods used herein. Various calculations of reaction parameters can be determined using energies determined from QM calculations. Through QM calculations bond dissociation energies, enthalpies, entropies, Marcus reorganization energies (λ), pK_a's, and more can be determined. There are many ways in which to conduct these calculations. The two primary types of calculations are those determined by electronic structure methods and those determined by density functional methods. Electronic structure methods use the laws of quantum mechanics and therefore involve the solving of the Schrödinger equation for the structures of interest. An example level of theory that uses electronic structure methods is

Hartree-Fock (HF).[44] Density functional methods, however, include the effects of electron correlation, or how electrons in a system react to each other's motion and attempt to avoid collisions. An example level of theory that uses the principles of density functional theory is the B3LYP theory.[44] However, electronic structure methods address electron movements in an average sense, thus each electron sees and reacts to an averaged electron density. Typically, for most systems density functional methods are much more accurate than those of electronic structure methods.[44] However, under some circumstances the use of both electronic structure and density functional methods allow for more accurate and computationally less expensive calculations. Compound models use this methodology to determine very accurate energies. An example of this is the complete basis set (CBS) methods.[44, 45]

Often a thermodynamic cycle must be constructed to determine a parameter of interest. To do so, the structure of the molecule is optimized under each state of a reaction in the gas phase and in simulated solvation conditions to arrive at a final value of interest. Solvation models all reproduce the solvent as a continuum of uniform dielectric constant, ε. Various energetic parameters are calculated on the molecule of interest within the modeled solvation continuum. There are several different models for solvation modeling; the only difference is the way each defines the cavity into which the solute is placed. The most commonly used solvation models are those developed by Tomasi *et al.*, the polarized continuum models (PCM).[46, 47] These models define a cavity around the solute or molecule of interest as a union of a series of interlocking atomic spheres .[44, 46, 47] PCM models the interaction of the solute with the solvent by measuring the electrostatic interaction with the surface of the cavity, which is characterized by the solvent's dielectric constant.[44]

2.0 Hydroquinones and Quinones in the Presence of Amines and Their Conjugate Acids

2.1 Introduction

Electron and proton transfer, ET and PT, in biological systems have been intensively studied through natural quinoid species, whose redox chemistry is greatly influenced by acidic and basic functionalities.[48-53] Likewise, studies in protic and aprotic media have revealed the effects of Brønsted acids and bases in the electrochemistry of quinoid species through proton transfer and hydrogen bonding.[2, 14, 54-61] In this work, we intend to determine whether hydrogen bonding takes place and possibly determine its role in proton-coupled electron transfer (PCET) reactions of some quinoid species in the presence of weakly acidic and basic compounds. Hydrogen bonding was determined by ^{1}H-NMR and support for the proposed mechanisms was collected from digital simulations, cyclic voltammetry and quantum mechanical calculations.

The redox chemistry of quinoid compounds typically involves the reduction of the Q species to produce QH_2 with the uptake of two electrons and two protons: $Q + 2e^- + 2H^+ = QH_2$, or the oxidation of QH_2 by the reverse reaction. As written, these reactions are an over-simplification of a very complex mechanism that depends on the electrode surface,[62, 63] the protic nature of the solvent and the presence of Brønsted acids or bases.[2, 14, 54-61] For instance, in aprotic media, the reduction of Q is better represented by Equation 5, in which no chemical steps involving proton transfer (PT) are possible because of the lack of protons. However, a number of studies have shown that the disproportionation reaction in Equation 6 can occur when the dianion, Q^{2-}, is produced.[2, 57, 64, 65] In contrast, the protic nature of QH_2 implies that its oxidation even in aprotic media does involve PT steps and the possibility of hydrogen bonding of QH_2 with itself or any of the oxidation products.[2, 54, 56, 57, 60] These characteristics make the electrochemical behavior of hydroquinones far more challenging to interpret than the corresponding quinones,

however over the years several accepted mechanisms have been proposed.[2, 54, 56, 61, 66, 67] The present work is aimed at evaluating the redox mechanisms of selected QH_2 and Q species in the light of research collected by ^{1}H-NMR and the *ab initio* pK_a estimation of each quinoid redox species in acetonitrile.

$$Q + e^- \rightleftharpoons Q^{\cdot -} \quad (5a)$$

$$Q^{\cdot -} + e^- \rightleftharpoons Q^{2-} \quad (5b)$$

$$2\,Q^{\cdot -} \rightleftharpoons Q + Q^{2-} \quad (6)$$

In the past, hydrogen bonding for quinoid and similar systems has been inferred indirectly from UV-vis and computational studies as well as from standard mathematical treatments based on the redox shift of the voltammetric peaks caused by the association with hydroxylic reagents.[2, 14, 54-61, 68-72] These studies clearly indicated that hydrogen bonding on its own can significantly alter the electrochemistry of quinoid compounds even though actual PT does not occur. Recently this was confirmed for some quinoid and phenolic systems that display inter- and intra-molecular hydrogen bonding.[54, 57-59, 68-70, 73-76] Unlike the techniques used in such studies, ^{1}H-NMR can provide direct evidence of hydrogen bonding because molecular association in solution decreases the diffusion coefficient (D) of the species involved and the spatial location of hydrogen bonding within the molecules can be traced from the chemical shift in titration experiments.[29] The Pulsed Gradient Echo (PGE-^{1}H-NMR) experiment allows the accurate estimation of D values in solution by monitoring Brownian motion.[24, 30, 77] Electrochemical methods can also be used to determine D values but require independent knowledge of the electrode area and the number of electrons involved, and can be influenced by

electrode surface effects.[54] Therefore, the PGE-^{1}H-NMR experiment provides an alternate and reliable way to determine D values which can be used in electrochemical simulations. In the study below, no hydrogen bonding interactions were found and the mechanism is thought to proceed via a CEEC reaction in the presence of Brønsted bases, where C represents a chemical step or PT and E represents an electrochemical step or ET. To the best of our knowledge, this is the first time this approach is used for investigating hydrogen bonding effects in the electrochemical behavior of quinoid species. For the compounds selected in this work, the availability of decent ^{1}H-NMR spectra for both redox states of the quinoid couple makes this method very appropriate. Besides the only direct experimental evidence of hydrogen bonding for quinones comes from x-ray diffraction measurements.[78] On the other hand, we believe this to be the first instance in which the pK_a's of all redox states in the quinone nine-membered square system has been estimated in acetonitrile and used as a guide for electrochemical simulations.

2.2 Experimental

2.2.1 Reagents and Materials

Anhydrous acetonitrile, (ACN, Aldrich, St. Louis, MO, 99.8% with < 10 ppm H_2O), pyridine (Aldrich, anhydrous, ≥ 99.8 %), and N,N-diisopropylethylamine (DIPEA, Aldrich, redistilled, anhydrous, 99.5 %) were used as received and transferred via microsyringe under argon. Triethylamine (TEA, Fluka, St. Louis, MO, ≥ 99.5 %) was kept cold until used and transferred via microsyringe. Tetrabutylammonium hexafluorophosphate ($TBAPF_6$, Fluka, electrochemical grade, ≥ 99.0 %) was heated to ~100 ^oC in a vacuum oven for at least 24 hours prior to use as supporting electrolyte. Pyrocatechol (1,2-QH_2, Fluka, ≥ 99.0 %), hydroquinone (1,4-QH_2, Riedel-deHaën, St. Louis, MO, 99.5 %), Hexaammineruthenium (III) chloride (Aldrich, $Ru(NH_3)_6Cl_3$ 98 %), D_2O (Aldrich, 99 % atom D), acetonitrile-d_3 (d_3-ACN, Aldrich, 99 % atom

D), ferrocene (Fc, Fluka, ≥ 99 %), p-benzoquinone (1,4-Q, Acros Organics, Geel, Belgium, 99+ %), N-ethyldiisopropylamine perchlorate ($DIPEAH^+$, Aldrich), hydrogen peroxide (Acros Organics, 35 wt. % in H_2O), silver nitrate (Aldrich, ≥ 99.0 %), Potassium chloride (EM Science, Gibbstown, NJ, 99.0-100.5 %), sulfuric acid (EM Science, 95-98 %), nitric acid (Aldrich, ACS Reagent, 70 %), hydroquinone-d_6 (1,4-QD_2, C/D/N Isotopes, Pointe-Claire, Quebec, Canada, 99.2 atom % D), and 1,2-dihydroxylbenzene-d_6 (1,2-QD_2, C/D/N Isotopes, 99.4 atom % D) were all used as received. Pyridinium nitrate was prepared by mixing equimolar volumes of pyridine and 1M nitric acid, then filtering the precipate and washing the filtrate with 1 M nitric acid, then drying at ~40 ^oC under reduced pressure for ~2 hours.

2.2.2 Electrochemical Methods

All electrochemical experiments were performed with a hydroquinone or quinone concentration of 5.0 mM in 10 mL dry acetonitrile with 200 mM tetrabutylammonium hexafluorophosphate ($TBAPF_6$) at a glassy carbon electrode. The electrochemical experiments were performed using a CHI660C potentiostat (CH Instruments, Austin, TX) incorporating a CHI200B Faraday cage and picoampbooster using either a three electrode cell (10 mL) in an inert argon atmosphere or a jacketed, three electrode cell (10 mL). Experiments involving the jacketed cell were conducted at 300 K with the use of a circulating water bath constructed in-house using a Solid State Water Recirculator (RPR Corp.; Fisher Scientific). The jacketed cell experiments were used to determine the ($\partial E_p/\partial \log v$) and ($E_p - E_{p/2}$) values accurately, as they can be affected by variable temperature. Experiments were also repeated under a dry argon atmosphere to ensure the results were not affected by ubiquitous atmospheric water, which gave similar results to those obtained at constant temperature. Several different 0.3 cm diameter

glassy carbon electrodes (CH Instruments, areas were consistent, between 0.059 to 0.060 cm^2) were used during this work and the areas associated with each are given in the respective figures (determined by the Randles-Sevcik equation using a 1.0 mM solution of $Ru(NH_3)^{3+}$ in deionized water with 0.1 M KCl as supporting electrolyte, where D = 6.3 x 10^{-6}).[77] The same electrode was always used for a particular set of data, for instance, data involving the addition of a particular base to protiated 1,4-QH_2 was used again to record similar measurements with deuterated 1,4-hydroquinone (1,4-QD_2). A platinum flag electrode served as the auxiliary electrode, and the reference electrode was an Ag/Ag^+ electrode (a silver wire immersed in the supporting electrolyte, 0.2 M $TBAPF_6$/3 mM silver nitrate/acetonitrile). The reference electrode was separated from the rest of the solution by a glass tube capped with a porous vycor frit (CH Instruments). The potential of the silver reference electrode was periodically measured versus the formal potential (measured as the average of the peak potentials) of the ferrocene/ferrocenium (Fc/Fc^+) couple under the same conditions as the other experiments and thus all potentials are reported versus ferrocene as Fc/Fc^+. Prior to each experiment, the polished glassy carbon electrode was first polished using 0.05 μm alumina paste (Buhler, Lake Bluff, Il) washed with deionized water, carefully wiped, and then sonicated for three minutes in acetonitrile. In each experiment the solution resistance (R_u) was totally compensated via positive feedback.

2.2.3 NMR and UV-vis Spectroscopic Methods

^1H NMR spectra were recorded on a Varian Mercury-300 MHz and a Varian Inova-400 MHz spectrometer. These measurements were always conducted at room temperature, with the exception of the pulsed gradient echo (PGE-) -^1H NMR experiments,[30, 77, 79] which were performed at 27°C on the 400 MHz instrument. All NMR samples were prepared under a dry

argon atmosphere and placed in screw-cap NMR sample tubes (600-MHz, 5 mm, 7" length, Norell, Inc., Landisville, NJ). The applied gradients in the PGE-^{1}H NMR experiments were calibrated by measuring the diffusion coefficient of HDO[29] (2.23×10^{-5} cm^2 s^{-1}, at 25°C, 0.03%) in a D_2O sample and the diffusion coefficient of 1,6-diaminohexane[77] (6.98×10^{-6} cm^2 s^{-1}, at 25°C, 0.04%). The pulse sequences and associated parameters are reported in the appendix.[79] The diffusion coefficients were measured under the same conditions as the electrochemical experiments, with the exceptions of measurements in deuterated acetonitrile and without supporting electrolyte. For a discussion on the correction of diffusion coefficients and control experiments see the appendix.[68-70]

UV-Vis measurements were obtained as reported by Uno[41, 80, 81] on a Hewlett-Packard 8453 spectrophotometer, incorporating a 1-mm path-length quartz flow cell (Agilent Technologies) and a Varian 9002 HPLC Solvent delivery module, using a calibrated flow rate of 10.00 mL/min, and connected with PTFE 20 thin wall tubing, 1/16 inch internal diameter (Cole-Parmer Vernon Hills, IL). The cells used for bulk electrolysis were either a 100 mL bulk electrolysis set from Bioanalytical Systems (BAS, West Lafayette, IN) or a specially made 25 mL bulk electrolysis cell. The specially made cell incorporated two large Pt flag working and counter electrodes and a typical Ag/Ag^{+} electrode was used as a reference electrode. The electrodes used in the bulk electrolysis experiments using the BAS kit included a large pyrolytic carbon-working electrode, a typical Ag/Ag^{+} reference electrode, and the same Pt flag counter electrode used in the other bulk electrolysis cell, separated from the analytical solution by a fritted glass cylinder. When the large Pt flag electrodes were not being used, they were stored in piranha solution (25% of H_2O_2 35 wt. % and 75% of H_2SO_4 98%) to clean them so that any absorbed material would not interfere with future experiments. In the electrolysis experiments,

the counter electrode was isolated from the electrolyzed solution so that the electrolysis material would not be converted back. In UV/electrolysis experiments, a solution of acetonitrile and the supporting electrolyte was used to blank the spectra. When experiments were performed that did not require electroylsis, but required a dry atmosphere, acetonitrile was cycled through the system to clean it and obtain a blank spectra. For UV-vis experiments not involving electrolysis, yet still requiring an oxygen-free environment, a 25 mL cell with influx, efflux, and gas ports was used.

2.2.4 Computational Methods and Digital Simulations

Digital simulations were conducted using DigiSim version 3.03b (Bioanalytical Systems, Inc., West Lafayette, IN). For a particular set of experimental conditions, cyclic voltammograms (CV's) were recorded at six different scan rates in the range 0.1 to 2 V s^{-1}, and fittings were attempted at each of these scan rates involving known and determined values of D, pK_a, and the assumption that α=0.5 (except for CV's where α was determined). Concentrations used in the voltammetric fittings were the same as those used in the experiments. Unknown parameters (E°, heterogeneous rate constants (k_{sp}) and homogeneous rate constants (k_f and k_b)) were allowed to vary iteratively, until a fit to the experimental CV was attained. The fitting of the heterogeneous rate constant for a set of different scan rates was computed as an average and the obtained standard deviation for this and other averaged estimated parameters was used as criterion for the validity of the fitting and ultimately the selected mechanism (in addition to the actual matching of the current and peak potentials on the experimental CV). If fittings could not be obtained using the quantum mechanically determined pK_a values of the quinone redox species, the kinetic constants were varied slightly. Care was taken to not allow the fitted kinetic constants attain unrealistic values. Examples of fitted CVs and determined parameters not found in the text can

be found in the appendix along with the relevant fitted parameters. Relevant mechanisms proposed in the literature were tested in the light of the new pK_a estimations and the hydrogen bonding evidence, and the ones with best fits (lower standard deviation of parameters determined at different scan rates) were selected as best to represent the experimental voltammetry.

Geometries were fully optimized in the gas-phase using Hartree-Fock (HF) and the 6-31+G** basis set, B3LYP density functional theory and the 6-31+G** basis set and using the complete basis set, CBS-QB3, using the *Gaussian 03* suite of programs.[41, 82] Minima were verified to have all real vibrational frequencies. The vibrational frequency calculations also provided the necessary parameters to compute zero-point and thermochemical corrections to energies. Geometry optimization and vibrational frequency analyses were also performed in the presence of implicit acetonitrile ($\varepsilon = 37.5$) as solvent using the conductor polarizable continuum model, CPCM.[83-86] The solvation phase geometries were optimized using Hartree-Fock (HF), B3LYP density functional theory and with the 6-31*, 6-31+G* and 6-31+G** basis sets. Open-shell species were treated using the unrestricted formalism of the aforementioned levels of theory, UHF and UB3LYP, respectively.

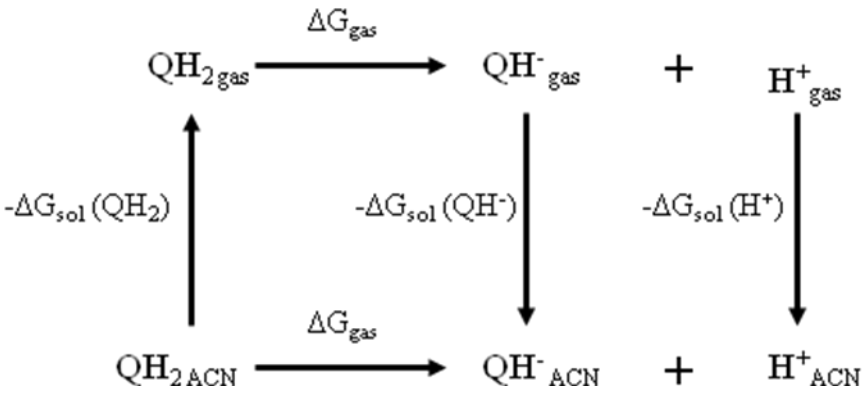

Figure 13. Thermodynamic cycle used for the calculation of the pK_a's for both of the QH_2's.

pK_a's were determined using a thermodynamic cycle as reported previously and shown in Figure 13.[87] From this scheme, the pK_a of QH_2 (or relative acid/conjugate base couple) in acetonitrile is related to the basicity of the first deprotonation state, QH^-, gas phase acidity ΔG_{gas} and solvation Gibbs energies for QH_2, QH^-, and H^+. This is related through equation 7, where ΔG_{gas} is the Gibbs energy for the deprotonation of QH_2 in the gas phase at 1 atm and 25°C, while $\Delta G_{sol}(QH_2)$ and $\Delta G_{sol}(QH^-)$ are the absolute Gibbs energies of solvation for the QH_2 and QH^-. Calculations of gas phase Gibbs energies uses a reference state of 1 atm, while the calculation of the ΔG_{sol} values uses a 1 M reference state. This was converted using equation 8, where the reference state is converted from 1 atm (using 24.46 L at 298.15 K) to 1 M. $\Delta G_{sol}(H^+)$ is the absolute Gibbs energy of solvation for the proton, -260.2 kcal mol^{-1}, in acetonitrile.[88] The value of $\Delta G_{gas}(H^+)$, -6.28 kcal mol^{-1}, comes from the Sackur-Tetrode equation. The most accurate pK_a calculations, discussed below in the results and discussion, involved the use of the gas phase energies determined from B3LYP/CBSB7 (from the first step in the CBS-QB3 calculation) with the solvation phase energies determined from CPCM/B3LYP/6-31+G**. Only the pK_a values determined by this procedure will be used and discussed in the text.

$$pK_a(QH_2) = -\log K_a = \frac{\Delta Gaq}{2.303RT} = [\Delta G_{gas}(QH_2) + \Delta G_{sol}(QH^-) + \Delta G_{sol}(H^+) - \Delta G_{sol}(QH_2)]/2.303RT \quad (7)$$

$$\Delta G_{gas}(1\ M) = \Delta G_{gas}(1\ atm) + RT \ln(24.46) \quad (8)$$

2.3 Results and Discussion

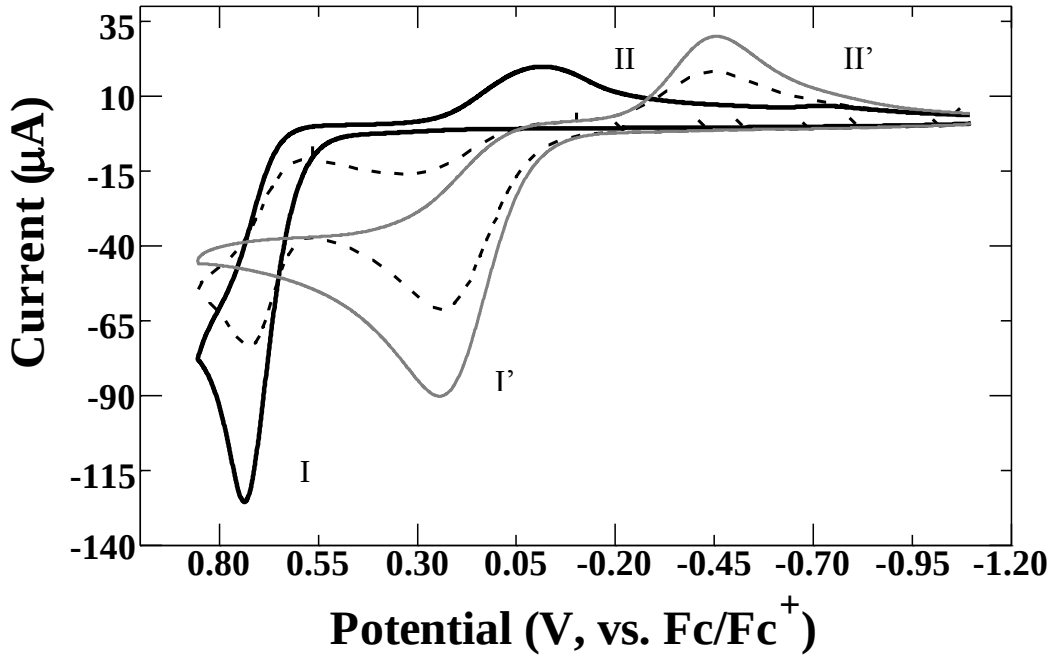

Figure 14. Cyclic voltammograms of 5.0 mM 1,4-QH_2 without pyridine (thick black CV), with 5.0 mM pyridine (dashed black line) and 10.0 mM pyridine (thin gray line). Voltammetry measured with 0.2 M $TBAPF_6$ as supporting electrolyte in acetonitrile at a glassy carbon electrode (0.059 cm^2) with a scan rate of 0.1 V s^{-1}.

The addition of various Brønsted bases significantly influenced the kinetics and thermodynamics of QH_2 oxidation. Figure 14 shows an example of the shift observed after addition of 5.0 and 10.0 mM pyridine to 1,4-QH_2, which results in the development of a new peak system (I' and II') at the cost of the original peaks I and II. In this case, a shift of -0.493 and -0.506 V was observed for peaks I and II, respectively, after addition of 10.0 mM pyridine to 1,4-QH_2. Addition of more than 10.0 mM showed no further significant change in the voltammetry of the QH's with the amines. Table 1 gives the literature pK_a values for pyridine, N,N-diisopropylethylamine (DIPEA), and triethylamine (TEA) along with some CV parameters (peak separation (ΔE_p), anodic and cathodic peak potentials) for both QH_2's upon addition of two

equivalents of different Brønsted bases. Table 1 shows that as the pK_a of the base increases, the oxidation peak potentials for QH_2's become more negative.

Table 1. Peak potential of oxidizable bases, pK_a of bases and resultant peak potentials of 1,4-QH_2 and 1,2-QH_2 upon addition of two or approximately two equivalents of base.

			Bases added to 1,4-QH_2[e]			**Bases added to 1,2-QH_2[e]**		
Base	**E_p (V)[a,b]**	**pK_a[88]**	**$E_{p,a}$ (V)[a]**	**$E_{p,c}$ (V)[a]**	**ΔE_p (V)**	**$E_{p,a}$ (V)[a]**	**$E_{p,c}$ (V)[a]**	**ΔE_p (V)**
TEA	0.443	18.46	-0.045 (-0.091)	-0.651 (-0.732)	0.606 (0.641)	0.153 (-0.078)	-0.342 (-0.487)	0.495 (0.409)
DIPEA	0.305	18.10[d]	-0.060 (-0.168)	-0.748 (-0.681)	0.688 (0.513)	-0.030 (-0.003)	-0.551 (-0.569)	0.521 (0.566)
Pyridine	-[c]	12.33	0.194 (0.239)	-0.437 (-0.438)	0.631 (0.677)	0.508 (0.381)	-0.025 (-0.310)	0.533 (0.691)

[a.] Potential reported vs. Fc/Fc^+ and the reported potential was obtained from a CV of the indicated base at 10 mM at 0.1 V s^{-1}.
[b.] Values determined from a single CV of the indicated base at a concentration of 2.5 mM measured in anhydrous acetonitrile at a glassy carbon electrode (0.059 cm^2) at 27°C with 0.2 M $TBAPF_6$.
[c.] No peak exhibited within the potential window 2 V to -2 V vs. Ag/Ag^+.
[d.] pK_a estimated from pK_a of Tripropylamine.[61, 66]
[e.] Values in parentheses are the peak potential and peak separation values for deuterated QH_2's (1,4-QD_2 and 1,2-QD_2).

The addition of the amines to 1,2-QH_2 produces analogous CV's to those obtained with 1,4-QH_2 (see Appendix). However, the average peak separation (ΔE_p) for 1,2-QH_2 (0.516 V) is less than that of 1,4-QH_2 (0.660 V). Previous reports have suggested that the reaction taking place at peak I' is the oxidation of the hydroquinone anion (QH^-), whereas peak II' represents the reduction of the protonated quinone (QH^+).[22] It has also been suggested that hydrogen bonding between bases and 1,4-QH_2 takes place, however no *in situ* confirmation has been performed. This argument is valid, because the aprotic environment of acetonitrile can be thought as a

dielectric mimic of the interior of proteins, where some Q/QH_2 couples are known to be stabilized through hydrogen bonds.[88]

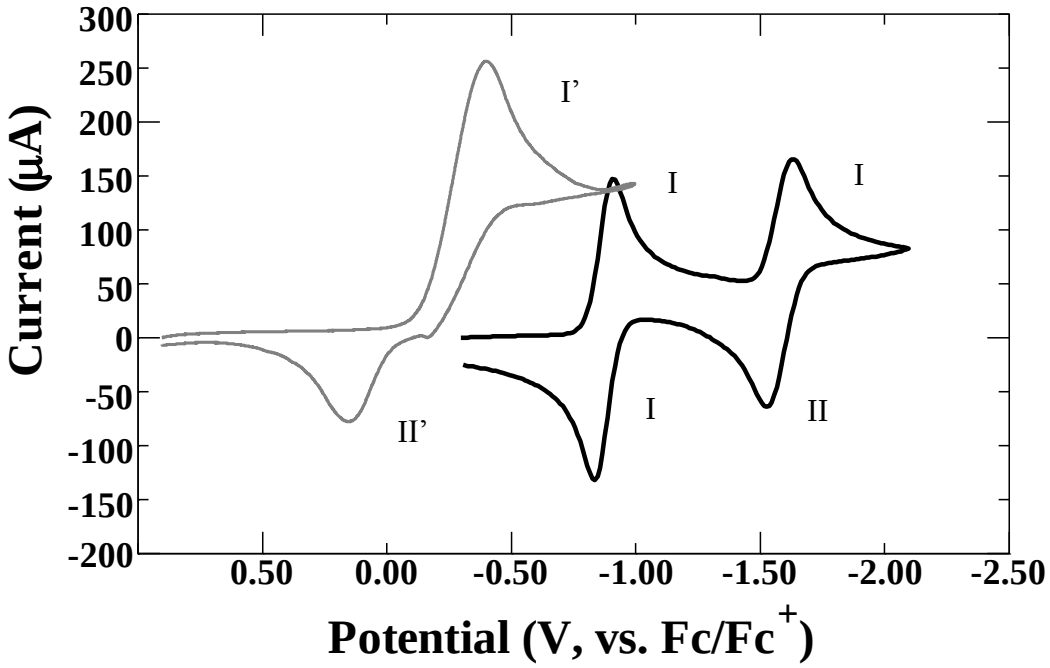

Figure 15. Cyclic voltammograms of 5.0 mM 1,4-Q alone (thick black CV) and 5.0 mM 1,4-Q with 13.0 mM pyridinium nitrate (thin gray CV) added. Voltammetry conducted at 27 ^{o}C in 0.2 M $TBAPF_6$ at 0.1 V s^{-1} in acetonitrile at a glassy carbon electrode (0.059 cm^2).

Table 2. pK_a's of Brønsted acids, peak potentials of 1,4-Q with the acids, peak separation of peak potentials for 1,4-Q with the acids and the separation of peak I' of the 1,4-Q/acid CV at 0.1 V s^{-1} and peak I of the 1,4-Q alone CV at 0.1 V s^{-1}.

Acid	pK_a [a]	$E_{p,a}$ (V)	$E_{p,c}$ (V)	ΔE_p (V)	$\Delta E_{p,\ BQ\ I\ to\ BQ/HA+\ I'}$ (V) [b]
$DIPEAH^+$	18.10[c]	-0.219	-0.689	0.470	0.221
Pyridinium	12.33	0.158	-0.401	0.559	0.509

[a.] From ref.[88]
[b.] Measured from a CV of 1,4-Q alone (first reduction peak, I) and a CV of 1,4-Q with the indicated acid (reduction peak I') at 0.1 V s^{-1} at 300 K at a glassy carbon electrode (0.059 cm^2).
[c.] pK_a estimated from pK_a of Tripropylamine.[89, 90]

Addition of the conjugate acids to 1,4-benzoquinone (1,4-Q) was believed to assist in the elucidation of the processes taking place between the QH_2's and the bases. Figure 15 depicts the

CV of 5.0 mM 1,4-Q before and after the addition of 13.0 mM pyridinium nitrate, which results in the advent of peaks I' and II' at the cost of the original one-electron transfer peaks I-IV and II-III. The addition of 13.0 mM pyridinium causes the appearance of peak I' at 0.509 V positive of peak I. Furthermore, chronoamperometry data of peak I' reveals that the electrochemical reaction taking place is a two-electron transfer. Addition of N-ethyldiisopropylamine perchlorate ($DIPEAH^+$) produces similar effects to those of pyridinium. Table 2 displays the peak potentials of peaks I' and II' for each of the conjugate acid additions to 1,4-Q and the shift of peak I' relative to peak I in 1,4-Q when no conjugate acid is present. From the data given in Table 2, it is uncertain if there is a trend between the pK_a of the acid and the potential shift between peaks I' and I, as data from only two acids are displayed. Attempts were made to either synthesize $TEAH^+$ or add nitric or perchloric acid to the solution prior to adding TEA in a 1:1 ratio. However, $TEAH^+NO_3^-$ (or ClO_4^-) would not crystallize and additions of acid prior to addition of TEA to 1,4-Q solutions seemed to lead to 1,4-Michael addition.[91] When examining the peak potentials for 1,4-Q in the presence of acids or 1,4-QH_2 in the presence of the corresponding conjugate bases, there is a similarity in the values, especially when comparing pyridine/1,4-QH_2 with pyridinium/1,4-Q. This similarity is probably a consequence of the fact that 1,4-Q and 1,4-QH_2 are complementary redox states of the same redox couple. The proton and electron transfer in the presence of an acid for 1,4-Q or a base for 1,4-QH_2 might go through the same intermediate.

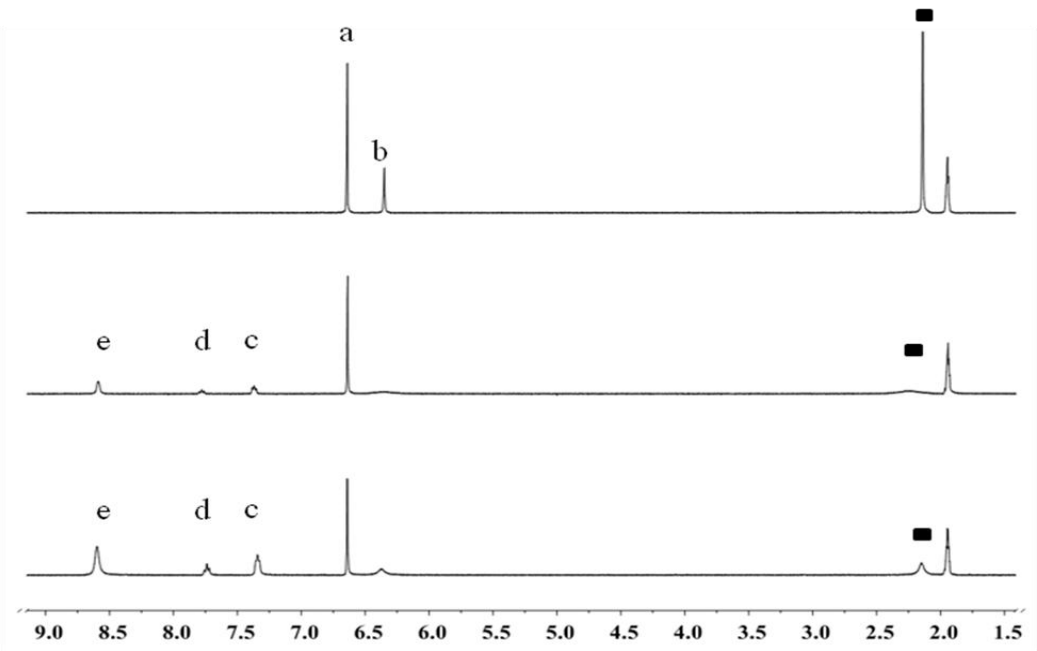

Figure 16. ^{1}H-NMR spectra of 5.0 mM 1,4-QH_2 in the presence of 0, 3.0 and 10.0 mM pyridine.

In order to investigate the extent of hydrogen bonding at the conditions employed herein, UV-vis and ^{1}H-NMR experiments were performed. The spectra and spectroelectrochemistry of the QH_2's and quinone did not show changes in the spectra upon additions of the Brønsted acids and bases, even at extreme concentrations of the base (see Appendix). Therefore, ^{1}H-NMR experiments were relied on to determine the interactions between the QH_2's and quinone with the bases and acids, respectively. As with the voltammetric analysis, the ^{1}H-NMR spectra were recorded by adding bases to the QH_2's and the corresponding conjugate acids to 1,4-Q. Data from ^{1}H-NMR experiments can be used to determine hydrogen bonding in solution if such interaction changes the local chemical environment and causes a shift in the resonance frequency of the protons involved.[92] After addition of 10.0 mM of the amines to the QH_2's, the phenolic proton signal shifted very little from its original position at 6.35 ppm. Figure 16 gives an

example of this, where the phenolic proton peak, *b*, shifts only 0.023 ppm from 0 mM to 10.0 mM pyridine added to 1,4-QH_2. The 1,4-QH_2 aromatic proton peak, *a*, and the pyridine ring proton peaks, *e*, *d* and *c*, are not affected by increasing pyridine additions. The HDO peak, marked by a black square in Figure 16, decreases in intensity with the addition of pyridine to 1,4-QH_2, yet this peak and the phenolic proton peak were relatively unaffected by additions of DIPEA, shifting down-field only 0.003 ppm (see Appendix). However, addition of TEA to the QH_2's causes complete loss of the phenolic proton and HDO peaks, while a new very broad peak centered at approximately 5 ppm is apparent. The decrease and loss of the phenolic proton peak intensity was also noted for the addition of pyridine to 1,2-QH_2. The loss of the HDO peak and possibly the phenolic peak is likely due to variations in chemical exchange caused by the uneven amounts of ubiquitous water present in the nominally dry deuterated acetonitrile (ACN-d_3). However, the NMR spectra of the conjugate acids added to 1,4-Q did not show any shifting or broadness in the peaks. The decrease in peak intensity and loss of the phenolic proton peak of the QH_2's with the addition of the bases, could indicate either deprotonation or hydrogen bonding between the QH_2's and these bases.[61, 93] To investigate the possibility of deprotonation, the NMR spectrum of the conjugate acids for the added bases was recorded independently so the proton frequency of the protonated base could be identified. In acetonitrile the acidic proton peak of the protonated amines was absent, probably due to chemical exchange with ubiquitous water.

To determine changes in diffusion coefficients (D) that would occur if hydrogen bonding was taking place, D values were measured by pulsed gradient echo-^{1}H-NMR (PGE) for the QH_2's, 1,4-Q, the bases, the conjugate acids and the corresponding mixtures. Table 3 displays these data. The D values of the individual species in ACN-d_3 match those reported in the

literature and determined by other means.[29] The utility of this PGE technique relies on the ability to determine complexation between molecules because the complexed species have a smaller D than the individual molecules.[79] Furthermore, the determination of the D does not involve other interfering processes, such as those found by determining D values by electrochemical methods, where absorption can take place and affect the determined value. However, for this study the change of the D values for the QH_2's upon addition of the amine bases was negligible indicating that hydrogen bonding at the concentrations investigated is minimal and that either no interaction is present or PT from the QH_2 to the amine should be responsible for the broadness of the phenolic proton peak. Thus, attempts to fit the voltammetry of the QH_2's in the presence of amine bases (B) employing hydrogen bonding equilibria like equation 9, where *n* is the number of base molecules bound to the QH_2, were abandoned and instead proton transfer reactions were included. For 1,4-Q the D values did not change upon addition of the conjugate acids used for the QH_2's. Overall these results confirm that for the oxidation of QH_2, a chemical step involving PT or hydrogen bonding can precede the ET whereas for the reduction of quinones this chemical step will most likely follow the ET. The implication for PCET is that a concerted PT-ET is more likely to occur if pre-association in a hydrogen bonded complex is attained prior to ET.

$$QH_2 + nB \rightleftharpoons QH_2(B)_n \qquad (9)$$

Table 3. PGE-^{1}H-NMR diffusion coefficient results.

Q/HQ Evaluated[a]	D (x 10^{-5} cm^2 s^{-1})[b]	Acid/Base Evaluated[a]	D (x 10^{-5} cm^2 s^{-1})[b]
1,4-Q	3.50	*10 mM TEA*	3.12
1,4-QH_2	2.79	*10 mM DIPEA*	3.34
1,2-QH_2	3.01	*10 mM $DIPEAH^+$*	2.32
10 mM Pyridinium	2.59	*10 mM Pyridine*	4.39
1,4-QH_2 + 10 mM TEA	2.96	1,4-QH_2 + *10 mM TEA*	3.13
1,4-QH_2 + 10 mM DIPEA	3.09	1,4-QH_2 + *10 mM DIPEA*	3.33
1,4-QH_2 + 10 mM Pyridine	2.71	1,4-QH_2 + *10 mM Pyridine*	4.45
1,4-Q + 10 mM Pyridinium	3.54	1,4-Q + *10 mM Pyridinium*	2.70
1,4-Q + 10 mM $DIPEAH^+$	3.57	1,4-Q + *10 mM $DIPEAH^+$*	2.40
1,2-QH_2 + 10 mM TEA	2.79	1,2-QH_2 + *10 mM TEA*	3.29
1,2-QH_2 + 10 mM DIPEA	2.65	1,2-QH_2 + *10 mM DIPEA*	3.26
1,2-QH_2 + 10 mM Pyridine	2.78	1,2-QH_2 + *10 mM Pyridine*	4.18

[a.] Text underlined and *italicized* indicate the species whose diffusion coefficient in given in the column to the right of the text.
[b.] Values measured in heavy acetonitrile at 27°C, and then corrected for differences in viscosity in 0.2 M $TBAPF_6$ in light acetonitrile.[88]

Knowledge of the pK_a's of the constituents of the nine-membered square scheme of the QH_2's in acetonitrile remains an outstanding issue when simulating QH_2 electrochemistry. Often the pK_a's are assumed based on the knowledge of the pK_a's of the QH_2's in water or the

pK_a of phenol in acetonitrile. Here, we attempt to computationally determine the pK_a's of the constituents of the nine-membered square scheme of the QH_2's in acetonitrile. Table 4 displays the pK_a values for the QH_2's studied here using the gas phase values determined from B3LYP/CBSB7 and the solvation phase energies determined from CPCM/B3LYP/6-31+G**. The pK_a values determined from calculations using this procedure are believed to be more reliable than the assumed values in the literature for a couple of reasons. First, the pK_a of phenol determined using this same method is 25.2, which is only 1.4 pK_a units smaller than the experimentally determined pK_a of phenol in acetonitrile, 26.6.[94] Second, the $pK_{a,1}$ (9.85) for 1,4-QH_2 is slightly lower than the $pK_{a,2}$ (11.4) in water, therefore a similar or larger difference should be expected in acetonitrile especially because of the less efficient charge solvation in this aprotic solvent.[83] Furthermore, because the QH_2's are substituted by two hydroxyl groups, an electron donating group, the first pK_a should be more basic than that of unsubstituted phenol (25.2, using this procedure). This is the case here, the first pK_a of 1,4-QH_2 is more basic than that of phenol, by 1 pK_a unit, 26.2. The procedure for the determination of the pK_a values was selected due to the very accurate values determined in similar manner for phenols and 1,4-QH_2 in water.[35] Overall, the values determined this way served as a guide for the fitting of the voltammetry, using the pK_a's as a starting point for the determination of the equilibrium constants.

Table 4. pK_a values as determined by theory.

1,4-QH_2	
Deprotonation Reaction	**pK_a[a]**
$QH_2 \rightarrow QH^- + H^+$	26.20
$QH^- \rightarrow Q^{2-} + H^+$	40.96
$QH_2^{\cdot+} \rightarrow QH^{\cdot} + H^+$	-3.89
$QH^{\cdot} \rightarrow Q^{\cdot-} + H^+$	16.56
$QH^{2+} \rightarrow QH^+ + H^+$	-36.02
$QH^+ \rightarrow Q + H^+$	-17.01
1,2-QH_2	
Deprotonation Reaction	**pK_a[a]**
$QH_2 \rightarrow QH^- + H^+$	21.67
$QH^- \rightarrow Q^{2-} + H^+$	43.08
$QH_2^{\cdot+} \rightarrow QH^{\cdot} + H^+$	-9.18
$QH^{\cdot} \rightarrow Q^{\cdot-} + H^+$	19.86
$QH^{2+} \rightarrow QH^+ + H^+$	-42.54
$QH^+ \rightarrow Q + H^+$	-16.37

[a.] Determined using the CPCM/theory/basis set//gas phase theory/basis set combination CPCM/B3LYP/6-31+G**// B3LYP/CBSB7.

Scheme 4. Oxidation scheme for 1,4-QH_2 and 1,2-QH_2.

$$QH_2 \rightleftharpoons QH_2^{\cdot+} + e^- \quad (10)$$

$$QH_2^{\cdot+} \rightleftharpoons QH^{\cdot} + H^+ \quad (11)$$

$$QH^{\cdot} \rightleftharpoons QH^+ + e^- \quad (12)$$

$$QH^+ \rightleftharpoons Q + H^+ \quad (13)$$

$$QH^{\cdot} + QH^{\cdot} \rightleftharpoons Q + QH_2 \quad (14)$$

Simulations allow one to determine the mechanism responsible for the voltammetry observed through attempted fittings with several plausible mechanisms.[24] Although numerous studies have discussed the mechanism of oxidation of the QH_2's, not one of those studies has attempted to simulate the voltammetry of QH_2's alone in acetonitrile. The fitting of the QH_2's alone is represented as an ET first, PT second and a second ET third, (equations 10-14, Scheme 4) called an ECE mechanism in electrochemical literature.[18, 95] The order of reactions was determined by the measurement of the peak potential and half peak potential versus the logarithm of scan rate. A transition from a situation where the chemical step is the rate determining step to a situation where the electron transfer is the rate determining step can be derived from the values of $(E_p - E_{p/2})$ and $\partial E_p / \partial \log \nu$. This transition is characterized by an increase of $(E_p - E_{p/2})$ from 47.5 to 95 mV and an increase in $\partial E_p / \partial \log \nu$ from 29.6 to 59.2 mV decade^{-1}, for a two electron process at 25 ^{o}C. Because the values that we determined for $(E_p - E_{p/2})$ and $\partial E_p / \partial \log \nu$ are approximately equal to 95 mV and 59.2 mV decade^{-1}, Table 5, we know that the process is at least an ECE process.[18, 27] However, based on the values for peak II we know that the process is undefined, but is a two-electron reduction of Q, yet with dramatically

slower kinetics.[24] The other reactions in Scheme 4, equations 13 and 14, were used to describe the second deprotonation reaction, equation 13, and the disproportionation reaction, equation 14. Multiple electron transfer mechanisms typically involve disproportionation reactions.[54, 61, 65-67] However, the proposed disproportionation reaction, equation 14, has been a source of controversy and its occurrence has been questioned.[66] The fittings of 1,4-QH_2 to Scheme 4 included equation 14, while those to 1,2-QH_2 did not. The fittings to 1,4-QH_2 actually included the fitting of equation 14 in the form discussed by Eggins and Chambers, where a hemiketal (see hemiketal Structure below) is formed as an intermediate.[88] From this fitting it is found that the oxidation of both QH_2's occurs at significant overpotential, based on the peak potential, at 0.812 V vs. Fc/Fc^+ for 1,4-QH_2 (peak I in Figure 14 and Figure 17), versus the determined formal potential, E^o, 0.357 V vs. Fc/Fc^+. Simulations of both QH_2's alone in acetonitrile at various scan rates and the kinetic constants associated with these fittings can be found in the appendix (together with associated discussion).

Table 5. Data showing the various calculated parameters from cyclic voltammetric experiments, presenting evidence of a two electron ECE reaction.

Hydroquinone*	**E^o (V)[a]**	***n*[b]**	**$\partial Ep/\partial \log v$ (V decade^{-1}, Peak I)**	**$\partial Ep/\partial \log v$ (V decade^{-1}, Peak II)[c]**	**$E_p - E_{p/2}$ (V, peak I)**	**$E_p - E_{p/2}$ (V, peak II)[c]**
1,2-QH_2	0.611	1.99	0.058	-0.082	0.094	-0.134
1,4-QH_2	0.442	1.81	0.059	-0.072	0.090	-0.123

* All measurements displayed determined in acetonitrile with 0.2 M $TBAPF_6$.
a. Determined by taking the average of the anodic and cathodic peak potentials.
b. Determined by chronocoulometry from the first peak (oxidation peak) of the indicated hydroquinone.
c. Convention to represent reduction values as negative, rather than take the absolute value.

Hemiketal Structure

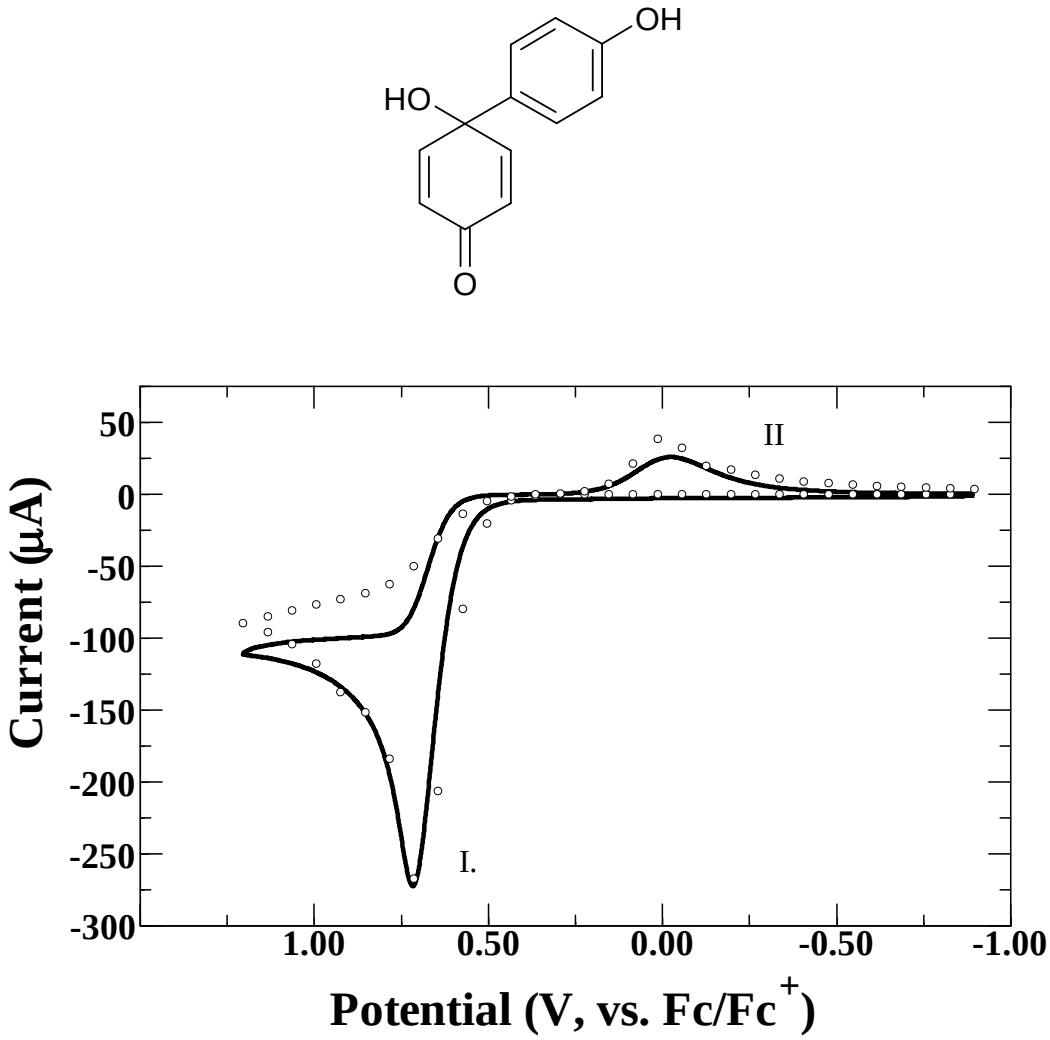

Figure 17. Cyclic voltammogram (solid line) and simulation (circles) of 5.0 mM HQ with 0.2 M $TBAPF_6$ as supporting electrolyte in acetonitrile at a glassy carbon electrode (0.06 cm^2) at a scan rate of 0.1 V s^{-1}.

Scheme 5. Oxidation scheme for both QH_2's with 10.0 mM of the amines.

$$QH_2 + B \rightleftharpoons QH^- + BH^+ \quad (15)$$

$$QH^- \rightleftharpoons QH^{\cdot} + e^- \quad (16)$$

$$QH^{\cdot} \rightleftharpoons QH^+ + e^- \quad (17)$$

$$QH^+ + B \rightleftharpoons Q + BH^+ \quad (18)$$

$$QH^{\cdot} + QH^{\cdot} \rightleftharpoons Q + QH_2 \quad (14)$$

Based on the ^{1}H-NMR evidence, several schemes can be envisioned for fitting the voltammetry for the addition of the amines to the QH_2's. However, only one scheme, Scheme 5, was found to fit the voltammetry of the addition of the amines to the QH_2's at each scan rate. Other mechanisms investigated can be found in the appendix together with a brief discussion of these schemes. Scheme 5 describes the mechanism of QH_2 oxidation as an initial PT followed by two consecutive electron transfers and a disproportionation reaction. The disproportionation reaction, equation 14, was used in Scheme 5, because without it peak II' could not be fit. Figure 18 shows the fitting of 5.0 mM 1,4-QH_2 with 10.0 mM pyridine using Scheme 5. Fittings to both QH_2's with two equivalents of the other amines can be found in the appendix. The average $pK_{a,1}$ of 1,4-QH_2 (19.85) and 1,2-QH_2 (18.58) as determined by the fitted values of the equilibrium constants of equation 15 (using $K_{equ,15} = (K_{a,QH2})((K_{a,\ BH+})^{-1})$ for the amines, knowing the pK_a values of the conjugate acids (BH^+) [96, 97]) were somewhat lower than the pK_a values determined using the *ab initio* methods described above (Table 4). Furthermore, the average pK_a of 1,4-QH^+ (-7.03) and 1,2-QH^+ (-6.99) determined using the fitted equilibrium constants of equation 18 from simulations of TEA, DIPEA and pyridine, produced higher values than those found by

quantum mechanical simulations, -17.0 and -16.37, respectively. This discrepancy in the fitted values versus the calculated values can be explained by several likely scenarios. Ubiquitous water could alter the pK_a of both the amine and the QH_2, though steps to guarantee dry working conditions using a dry glove box under argon were taken. Furthermore, the computational estimation of the pK_a of the various species of the QH_2 square scheme only takes into account the solvation free energies in the pure dielectric medium of the indicated solvent, thus the presence of water is not considered. It is also possible that the homoconjugation (self-association, discussed below) of pyridine, which enhances the acidity of weak acids, has a significant influence on the kinetics that could not be revealed through simulations or other instrumental methods.[55, 57]

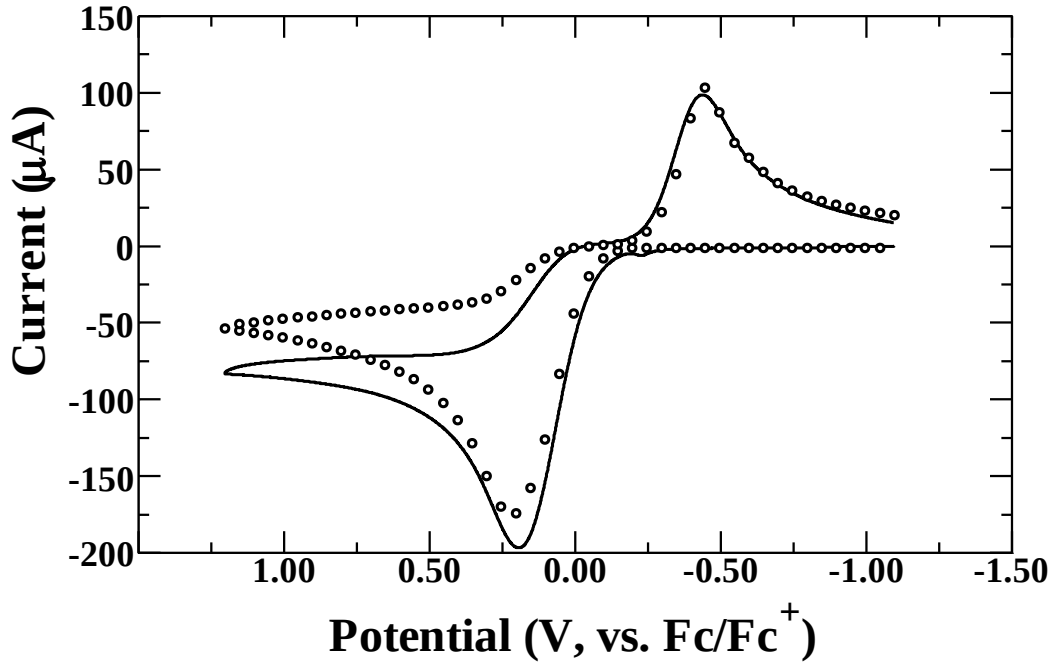

Figure 18. Voltammetry (solid line) and simulation (circles) of 5.0 mM 1,4-QH_2 with 10.0 mM pyridine. Voltammetry was recorded at 0.1 V s^{-1} in anhydrous acetonitrile with 0.2 M $TBAPF_6$ at a glassy carbon electrode (0.060 cm^2), under dry conditions.

Scheme 6. Reduction scheme for 1,4-Q in the presence of the conjugate acids.

$$Q + e^- \rightleftharpoons Q^{\cdot -} \quad (19)$$

$$Q^{\cdot -} + H^+ \rightleftharpoons QH^{\cdot} \quad (20)$$

$$QH^{\cdot} + e^- \rightleftharpoons QH^- \quad (21)$$

$$QH^- + H^+ \rightleftharpoons QH_2 \quad (22)$$

$$Q + QH_2 \rightleftharpoons QH^{\cdot} + QH^{\cdot} \quad (23)$$

Thus far we have described the oxidation of two selected QH_2's in the presence of bases. In this last section we show the mechanistic details for the reduction of 1,4-Q with the conjugate

acids, pyridinium nitrate (pyridinium), acetic acid and N-ethyldiisopropylamine perchlorate ($DIPEAH^+$). Previously, the reduction of quinone in the presence of benzoic acid and trifluoroacetic acid has been described as an ECEC mechanism of the type displayed in Scheme 6 including a comproportionation reaction, equation 23.[88] Mechanisms have also been described where an initial complexation of the quinone and acid are involved, but this was not found under the present conditions. An ECEC mechanism is the only feasible mechanism as PT occurring first, is not plausible because the pK_a of 1,4-Q in acetonitrile (-19.93, Table 4) is much too low. Incorporation of Scheme 6 into the simulations of 1,4-Q with the selected conjugate acids yielded acceptable fittings. Figure 19 displays the experimental and simulated voltammetry of 1,4-Q with13.0 mM pyridinium, while voltammetry of 1,4-Q with $DIPEAH^+$ at selected scan rates can be found in the appendix.

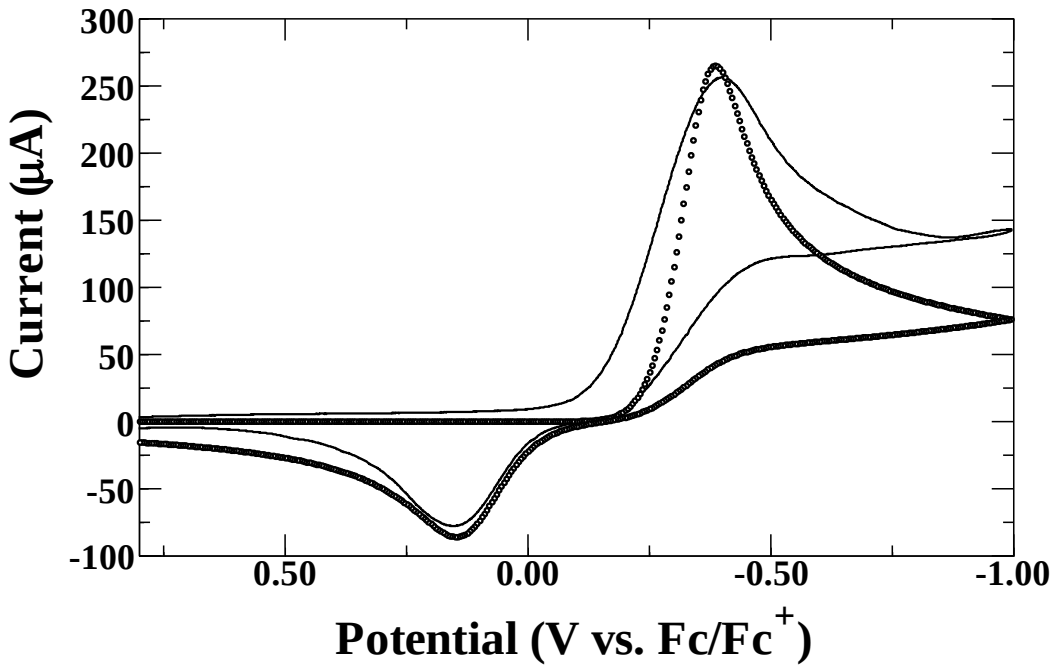

Figure 19. Voltammetry (solid line) and simulation (circles) of 5.00 mM 1,4-Q with 13 mM pyridinium. Voltammetry was recorded at 0.1 V s^{-1} in anhydrous acetonitrile with 0.2 M $TBAPF_6$ at a glassy carbon electrode (0.059 cm^2) under dry conditions.

$$HA + A^- \rightleftharpoons HA_2^- \quad (24)$$

Other processes such as homoconjugation as displayed in equation 24, where HA and A^- represent the acid and its conjugate base, respectively, are also believed to be at work in solution. This reaction enhances the acidity of weak acids through hydrogen bonding with the protonated forms of itself.[15, 58, 59, 73] In this study, pyridine is known to be involved in such reactions. Inclusion of this reaction, equation 24, in the simulations for pyridine did not improve the accuracy of the fittings or influence the fitting upon dramatic changes in the kinetics or the diffusion coefficients pertaining to this reaction. The other kinetic constants involved in the fittings of the QH_2's with the bases (Scheme 5) or the fittings of 1,4-Q with the conjugate acids (Scheme 6) remained constant while attempting the fittings of this homoconjugation reaction.

To this point, consideration of the mechanism of Q reduction and QH_2 oxidation under the influence of acid and base addition as either *stepwise* or *concerted* has not been addressed thoroughly. Kinetic analysis of fitted voltammograms and experiments involving deuterated reagents, are two general methods for classifying a mechanism as *concerted* or *stepwise*.[59] In the literature, *concerted* mechanisms in aprotic media have been characterized by fast proton transfer ($k_f \approx 1 \times 10^8$ M) and slow electron transfer ($k_s \approx 1x10^{-5}$ cm s^{-1}).[19, 73] Discussion of *concerted* mechanisms in this way is a result of simulation software limitations. *Concerted* mechanisms must therefore be fit as two separate reactions, an ET and a PT. The kinetic values of electron and proton transfer determined here (appendix) do not fit this criterion, whether alone or in the presence of acid or base. Furthermore, little peak potential shift was noted when bases were added to QD_2's, values in parentheses in Table 1. To determine the kinetic isotope effect, Scheme 5 was applied to fit the QD_2 voltammetry with base. These simulations confirmed that a concerted mechanism is unlikely with this system, as the KIE values determined were on the

order of 0.64 to 1.29, below the characteristic value of 1.6 needed to classify a reaction as *concerted*.[78] Similar studies involving 1,4-Q and deuterated conjugate acids were deemed unnecessary, as the electron and proton transfers were fast, relative to electron and proton transfers involved in a *concerted* mechanism. Overall, the KIE findings show that the presence of a *concerted* mechanism is unlikely. However, a *concerted* mechanism cannot be ruled out as the *concerted* step may not be rate determining, thus the KIE results are lower than if the *concerted* step were rate determining.

2.4 Conclusion

In summary, herein we have presented a thorough electrochemical study of the oxidation of hydroquinones and reduction of quinones, both alone and in the presence of non-hydrogen bonding Brønsted acids and bases. PGE-^{1}H-NMR results concluded that none of the amines were involved in hydrogen bonded complexes with the QH_2's. This knowledge coupled with determined pK_a values for each of the quinone redox species allowed for fitting of the QH_2 with amine and 1,4-Q with conjugate acid voltammetry. The mechanism of QH_2 oxidation in the presence of amines was determined to undergo a *stepwise* CECE mechanism. 1,4-Q, however, in the presence of the conjugate acids was determined to be involved in an ECEC mechanism. Based on the findings of this work and the similarity of the chemistry involved to previous intramolecular proton/electron studies, it seems that there may be some requirements for observing *concerted* reactions. They seem to be favored in conditions that allow a rather restrained geometry such as hydrogen bonded complex, or the active site of an enzyme. This will be examined further by exploring the mechanism of QH_2 oxidation in the presence of acetate in the following chapter.

3.0 Hydroquinones and Quinones in the Presence of Acetates and Their Conjugate Acids and Comparision to Hydroquinones and Quinones in the Presence of Amines and Their Conjugate Acids

3.1 Introduction

In order to understand the effects that different bases have on the electrochemistry of QH_2's, the addition of several carboxylates, acetate, benzoate and trifluoroacetate, were made to QH_2 solutions in acetonitrile and this voltammetry was compared to that from Chapter 2. Each of the species studied in this Chapter are found in Scheme 7. Since carboxylates are initially charged in acetonitrile, while amines are uncharged, the probability of hydrogen bond formation between the carboxylate and the QH_2's is enhanced. This enhanced ability of carboxylates to form hydrogen bonds with QH_2's is due to the reduced ability of acetonitrile to solvate charged species.[98] The additions of the two types of Brønsted base produce somewhat similar results, the shift of the anodic and cathodic peaks of the QH_2's to more negative potentials, meaning oxidation of QH_2 is more favorable. However, the addition of carboxylates was found to lower the diffusion coefficient of both the carboxylate and the QH_2's by as much as 40 % and the phenolic proton peak in ^{1}H-NMR was found shifted to higher frequencies. Such effects have been previously discussed in voltammetric and ^{1}H-NMR studies of other molecular systems.[29, 55, 76, 99] Furthermore, concentrations of 10.0 mM of the carboxylates with 1,4-QH_2 causes the formation of two anodic peaks versus the single anodic peak found for the addition of the amines to QH_2 solutions. The two peaks are defined as the hydrogen bonding peak and the proton transfer (PT) peak. The confirmation of this assignment is corroborated by voltammetry at various concentrations of each of the acetates, ^{1}H-NMR and digital simulations. Comparison of the voltammetry of the amines and the carboxylates shows that the presence of hydrogen bonds

imparts a thermodynamic advantage to the oxidation of the QH_2's. In previous reports, the presence of hydrogen bonds has been a prerequisite for *concerted* reactions.[15, 19, 58, 59, 73-76, 100, 101] However, the presence of hydrogen bonds between the acetates and QH_2 show no evidence of a *concerted* reaction. Discussion of the absence of a *concerted* reaction is thoroughly discussed below.

Scheme 7. Molecular species investigated in this chapter.

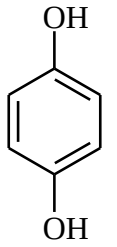

1,4-QH_2

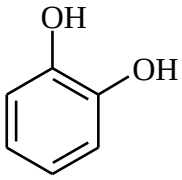

1,2-QH_2

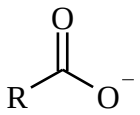

R = CF_3, CH_3 or C_6H_5

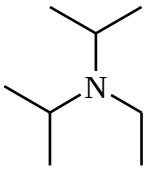

Diisopropylethylamine

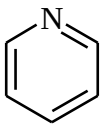

Pyridine

3.2 Experimental

3.2.1 Reagents and Materials

Anhydrous acetonitrile (ACN, Aldrich, St. Louis, MO, 99.8 % with < 10 ppm H_2O), pyridine (Aldrich, anhydrous, ≥ 99.8 %), and N,N-diisopropylethylamine (DIPEA, Aldrich, redistilled, anhydrous, 99.5 %) were used as received and transferred via microsyringe under argon. Tetrabutylammonium hexafluorophosphate ($TBAPF_6$, Fluka, electrochemical grade, ≥ 99.0 %) was heated to ~100 ^oC in a vacuum oven for at least 24 hours prior to use as supporting

electrolyte. Tetrabutylammonium acetate (acetate, Fluka, electrochemical grade, ≥ 99.0 %) was treated similarly to the $TBAPF_6$, because it is extremely hygroscopic, however, it was heated to only ~60 ^oC for at least 24 hours before use. The less hygroscopic acetates, tetrabutylammonium benzoate (benzoate, Fluka, electrochemical grade, ≥ 99.0 %) and tetraethylammonium trifluoroacetate (trifluoroacetate, Fluka, ≥ 99.0 %) were only opened and used under a nominally dry argon atmosphere. Pyrocatechol (1,2-QH_2, Fluka, ≥ 99.0 %), hydroquinone (1,4-QH_2, Riedel-deHaën, St. Louis, MO, 99.5 %), Hexammineruthenium (III) chloride (Aldrich, $Ru(NH_3)_6Cl_3$ 98 %), D_2O (Aldrich, 99 % atom D), acetonitrile-d_3 (d_3-ACN, Aldrich, 99 % atom D), ferrocene (Fc, Fluka, ≥ 99 %), p-benzoquinone (1,4-Q, Acros Organics, Geel, Belgium, 99+ %), N-ethyldiisopropylamine perchlorate ($DIPEAH^+$, Aldrich), acetic acid (Aldrich, glacial, ≥ 99.85 %), benzoic acid (Aldrich, ≥ 99.5 %), trifluoroacetic acid (Aldrich, ≥ 99 %), hydrogen peroxide (Acros Organics, 35 wt.% in H_2O), silver nitrate (Aldrich, ≥99.0%), Potassium chloride (EM Science, Gibbstown, NJ, 99.0-100.5 %), sulfuric acid (EM Science, 95-98%), nitric acid (Aldrich, ACS Reagent, 70 %), hydroquinone-d_6 (1,4-QD_2, C/D/N Isotopes, Pointe-Claire, Quebec, Canada, 99.2 atom % D), and 1,2-dihydroxylbenzene-d_6 (1,2-QD_2, C/D/N Isotopes, 99.4 atom % D) were all used as received. Pyridinium nitrate was prepared by mixing equimolar volumes of pyridine and 1 M nitric acid, then filtering the precipate and washing the filtrate with 1 M nitric acid, then drying at ~40 ^oC under reduced pressure for ~2 hours.

3.2.2 Electrochemical Methods

All electrochemical experiments were performed with a hydroquinone or quinone concentration of 5.0 mM in 10 mL dry acetonitrile with 0.2 M tetrabutylammonium hexafluorophosphate ($TBAPF_6$) at a glassy carbon electrode. The electrochemical experiments were performed using a CHI660C potentiostat (CH Instruments, Austin, TX) incorporating a

CHI200B Faraday cage and picoampbooster using a three electrode cell (10 mL) in an inert argon atmosphere. Several different 0.3 cm diameter glassy carbon electrodes (CH Instruments, areas were consistent, between 0.07 to 0.073 cm^2) were used during this work and the areas associated with each are given in the respective figures (determined by the Randles-Sevcik equation using a 1.0 mM solution of $Ru(NH_3)_6^{3+}$ in deionized water with 0.1 M KCl as supporting electrolyte, where D = 6.3 x 10^{-6} cm^2 s^{-1}).[77] The same electrode was always used for a particular set of data, for instance, data involving the addition of a particular base to protiated 1,4-QH_2 was used again to record similar measurements with deuterated 1,4-hydroquinone (1,4-QD_2). A platinum flag electrode served as the auxiliary electrode, and the reference electrode was an Ag/Ag^+ electrode (a silver wire immersed in the supporting electrolyte, 0.2 M $TBAPF_6$/3 mM silver nitrate/acetonitrile). The reference electrode was separated from the rest of the solution by a glass tube capped with a porous vycor frit (CH Instruments). The potential of the silver reference electrode was periodically measured versus the formal potential (measured as the average of the peak potentials) of the ferrocene/ferrocenium (Fc/Fc^+) couple under the same conditions as the other experiments and thus all potentials are reported versus ferrocene as Fc/Fc^+. Prior to each use, the polished glassy carbon electrode was first polished using 0.05 μm alumina paste (Buhler, Lake Bluff, Il) washed with deionized water, carefully wiped, and then sonicated for three minutes in acetonitrile. In each experiment the solution resistance (R_u) was totally compensated via positive feedback.

3.2.3 NMR Spectroscopic Methods

Variable temperature and ROESY and NOESY 2-D ^{1}H-NMR experiments were performed with a Brucker AVANCE III 600 MHz NMR. Standard ^{1}H-NMR and Pulsed Gradient Echo (PGE-) ^{1}H-NMR were performed on a Varian Inova 400 MHz NMR at 25 ^oC.

The applied gradients in the PGE-^{1}H NMR experiments were calibrated by measuring the diffusion coefficient of HDO (2.23×10^{-5} cm^2 s^{-1}, at 25°C, 0.03%) in a D_2O sample and the diffusion coefficient of 1,6-diaminohexane (6.98×10^{-6} cm^2 s^{-1}, at 25°C, 0.04%). The pulse sequences and associated parameters are reported in the appendix.[79] The diffusion coefficients were measured under the same conditions as the electrochemical experiments, with the exceptions of measurements in deuterated acetonitrile and without supporting electrolyte. For a discussion on the correction of diffusion coefficients see the appendix.[41, 80, 81]

3.2.4 Computational Methods and Digital Simulations

Digital simulations were conducted using DigiSim version 3.03b (Bioanalytical Systems, Inc., West Lafayette, IN). For a particular set of experimental conditions, cyclic voltammograms (CV's) were recorded at six different scan rates in the range 0.1 to 2 V s^{-1}, and fitting attempted involving known and determined values of D, pK_a, and the assumption that α=0.5 (except for CV's where α was determined). Concentrations of all the species entered for fitted simulations were the actual values used in the experiments. Unknown parameters (E°, heterogeneous rate constants (k_{sp}) and homogeneous rate constants (k_f and k_b)) were allowed to vary iteratively, until a fit to the experimental CV was attained. The fitting of the heterogeneous rate constant for a set of different scan rates was computed as an average and the obtained standard deviation for this and other averaged estimated parameters was used as criterion for the validity of the fitting and ultimately the selected mechanism (in addition to the actual matching of the current and peak potentials on the experimental CV). If fittings could not be obtained using the quantum mechanically determined pK_a values of the quinone redox species, the kinetic constants were varied slightly. Care was taken to not allow the fitted kinetic constants attain unrealistic values. Examples of fitted CVs and determined parameters not found in the text can be found in the

appendix along with the relevant fitted parameters. Relevant mechanisms proposed in the literature were tested in the light of the new pK_a estimations and the hydrogen bonding evidence, and the ones with best fits (lower standard deviation of parameters determined at different scan rates) were selected as best to represent the experimental voltammetry.

Geometries of the QH_2-acetate complexes were fully optimized in the gas-phase using B3LYP density functional theory and the 6-31G* and 6-31+G* basis sets using the *Gaussian 03* suite of programs.[41, 82] Minima were verified to have all real vibrational frequencies. The vibrational frequency calculations also provided the necessary parameters to compute zero-point and thermochemical corrections to energies. Geometry optimization and vibrational frequency analyses were also performed in the presence of implicit acetonitrile ($\varepsilon = 37.5$) as solvent using the conductor polarizable continuum model, CPCM.[54, 91] The solvation phase geometries were optimized using B3LYP density functional theory and with the 6-31* and 6-31+G* basis sets. Open-shell species were treated using the unrestricted formalism of the aforementioned level of theory, UB3LYP, respectively.

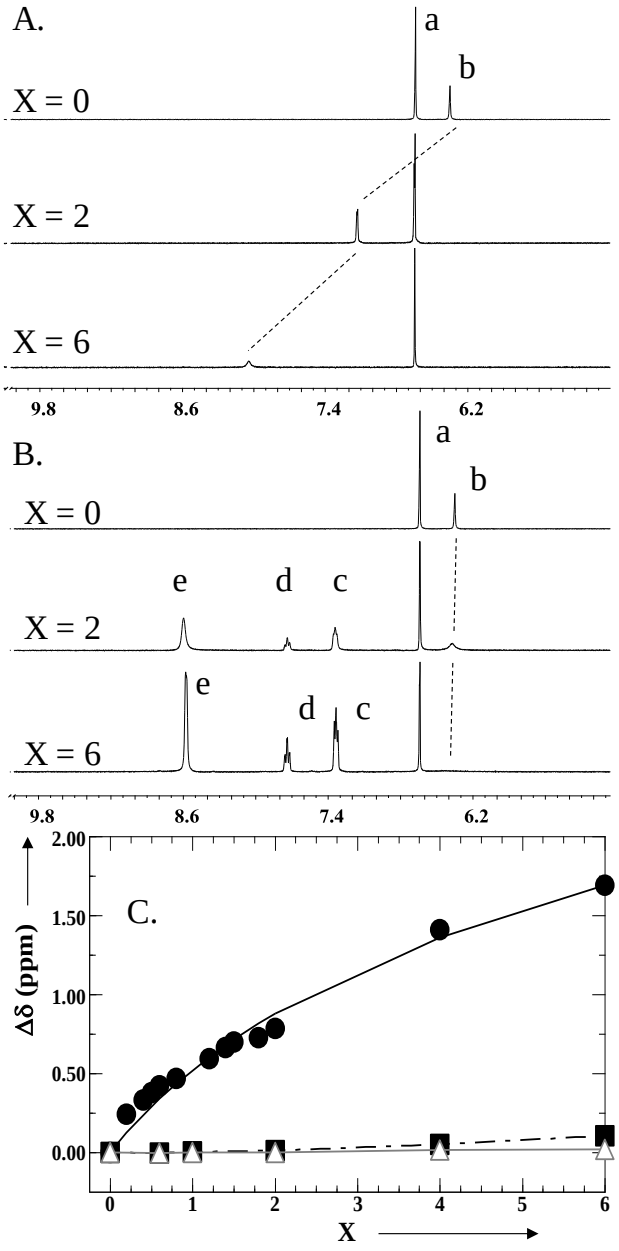

Figure 20. A.) ^{1}H-NMR spectra of 1,4-QH_2 with 0, 10 and 30 mM trifluoroacetate. B.) ^{1}H-NMR spectra of 1,4-QH_2 with 0, 10 and 30 mM pyridine. C.) Molar ratio plot from the ^{1}H-NMR titration of 1,4-QH_2 with trifluoroacetate (circle), pyridine (square) and DIPEA (triangle).

3.3 Results and Discussion

Hydrogen bonds between the QH_2's and acetates were readily detected by ^{1}H-NMR spectroscopy. Figure 20A shows the shift of the phenolic protons, *b*, of 1,4-QH_2 to lower frequencies, from 6.35 ppm without trifluoroacetate to 8.043 ppm upon addition of 30 mM trifluoroacetate (X = 6, six equivalents added). While, the peak assigned to the aromatic protons of 1,4-QH_2, *a* at 6.63 ppm, and the peaks assigned to the counterion, tetraethylammonium (not shown), remain unchanged throughout the titration of trifluoroacetate. In terms of the ^{1}H-NMR experimental timescale, the exchange between the free and complexed state for the QH_2's with trifluoroacetate is in the fast exchange limit. However, the exchange limit for the QH_2's with the other acetates, benzoate and acetate, is defined as intermediate at 25 ^{o}C, and a peak for this

complex is often broad or not observed at 25 ^{o}C.[91] However, upon lowering the temperature a single peak is noted at lower frequencies. The shifts noted with acetate and benzoate with 5.0 mM 1,4-QH_2, 11.769 and 11.1373 upon addition of 30.0 mM at 5 ^{o}C, are significantly greater than that of trifluoroacetate. Thus, acetate and benzoate are associated much more strongly with 1,4-QH_2 than is trifluoroacetate. A similar shift in the phenolic protons was noted upon addition of the acetates to 5.0 mM 1,2-QH_2. In contrast to this, the addition of pyridine to 1,4-QH_2 shows no significant shift of any of the peaks of 1,4-QH_2, *a* and *b*, or pyridine, peaks *c*, *d* and *e*, Figure 20B. However, the height of the phenolic proton peak for 1,4-QH_2 and the HDO peak, at ~2.0 ppm (not shown) decrease. The decrease in peak height only correlates to a net shift of 0.023 ppm from 0 to 10.0 mM added pyridine. Furthermore, the addition of DIPEA to 1,4-QH_2 does not influence the shift of the phenol proton peaks significantly, as only a shift of 0.020 ppm difference was found from 0 to 30 mM added DIPEA. Similar effects were found upon addition of pyridine and DIPEA to 1,2-QH_2. Overall, it is unlikely that the amines are associated with the QH_2's since such a small shift in the phenol proton peak was observed. The observed broadening of the phenolic and HDO peaks is likely due to the increase of ubiquitous water found in the solvent and the added amine.

To determine the stoichiometry of the complexes formed between the acetates and the QH_2's, molar ratio analyses were performed. The molar ratio analysis revealed that a 1:2 complex was formed between the QH_2's and the acetates. The only exception to this was the addition of benzoate to 1,2-QH_2 where a 1:1 complex is apparent (see appendix).[91] Therefore, by monitoring the shift of the phenolic protons, *b*, of the QH_2's during titration of trifluoroacetate (Figure 20C) from 0 (6.35, 1,4-QH_2) to 30.0 mM added trifluoroacetate (8.043) we can determine the association constants (K_1 and K_2) of this interaction. By fitting the data of the

phenolic proton shift to a 1:2 binding isotherm, equation 25, the K_1 and K_2 for 1,4-QH_2 with trifluoroacetate are determined, 55 ± 14 and 5 ± 8, respectively.[91] However, to determine the association constants for the QH_2's with acetate and benzoate at 25.0 ^oC ^{1}H-NMR spectra were measured between 5.0 ^oC and 15.0 ^oC where the exchange peak for the QH_2 and acetate complex is observed. A van't Hoff plot, ln K versus T^{-1}, for this data allowed for extrapolation of the K values at 25.0 ^oC (see appendix).[29] The association constants for the QH_2's with each of the acetates are presented in Table 6.

$$\Delta\delta = (\delta_1 K_1[\text{acetate}] + \delta_2 K_1 K_2[\text{acetate}]^2)/(1 + K_1[\text{acetate}] + K_1 K_2[\text{acetate}]^2) \quad (25)$$

Table 6. Association constants determined by ^{1}H-NMR titration data.

1,4-QH_2			**1,2-QH_2**	
Base	**K_1 (M^{-1})**	**K_2 (M^{-1})**	**K_1 (M^{-1})**	**K_2 (M^{-1})**
Acetate	202 ± 10	155 ± 10	1250 ± 70	404 ± 20
Benzoate	473 ± 30	209 ± 20	(9.91 ± 0.3) x 10^4	-[a]
Trifluoroacetate	55 ± 10	5 ± 10	270 ± 30	82 ± 20

[a.] This data was fit using a 1:1 binding isotherm, due to the molar ratio analysis.[91]

The use of pulsed gradient echo (PGE-) ^{1}H-NMR also supports the claims of hydrogen bonding, by determination of the diffusion coefficient (D) of the individual molecules believed to be involved in molecular association.[79] The diffusion coefficients of molecules involved in a complex will decrease relative to the diffusion coefficients of the molecules alone. Table 7 gives the diffusion coefficients of the individual molecules from Scheme 7 alone as well as 1,4-Q and the conjugate acids. The diffusion coefficients of 5.0 mM of each of the QH_2's with base concentrations of 10.0 mM and 30.0 mM and the diffusion coefficients of the base at 10.0 and 30.0 mM concentrations in the presence of the QH_2's are also presented in Table 7. The

diffusion coefficients of 5.0 mM 1,4-Q with various concentrations of the conjugate acids (concentration dictated by voltammetry results, discussed below) are also found in Table 7. The diffusion coefficients of the QH_2's decrease by 30 to 46 % when in the presence of 10.0 to 30.0 mM acetate or benzoate. The addition of 10.0 mM trifluoroacetate does not significantly affect the diffusion coefficient of the QH_2's, yet concentrations greater than 10.0 mM show considerable changes. Upon addition of 10.0 mM trifluoroacetate there is only an approximate 9 % decrease in the diffusion coefficient of the QH_2's. While, addition of 30.0 mM trifluoroacetate causes a 21 - 26 % decrease in the diffusion coefficient of the QH_2's. However, the change in the diffusion coefficients of the QH_2's in the presence of DIPEA and pyridine is negligible, within error, even at concentrations of 30.0 mM added base.

Table 7. PGE-^{1}H-NMR diffusion coefficient results.

Q/HQ or Acid/Base Evaluated[a]	**D (x 10^{-5} cm^2 s^{-1})[b]**	**Acid/Base Evaluated[a]**	**D (x 10^{-5} cm^2 s^{-1})[b]**
1,4-Q	3.37 ± 0.03	*10 mM Acetate*	2.67 ± 0.07 (2.69 ± 0.05)
1,4-QH_2	2.79 ± 0.04	*100 mM Acetic Acid*	3.95 ± 0.02
1,2-QH_2	3.01 ± 0.003	*10 mM Benzoate*	2.71 ± 0.003 (2.72 ± 0.09)
10 mM DIPEA	3.34 ± 0.001 (3.38 ± 0.004)	*18 mM Benzoic Acid*	3.58 ± 0.06
12 mM $DIPEAH^+$	2.32 ± 0.04	*10 mM Trifluoroacetate* [c]	3.06
10 mM Pyridine	4.39 ± 0.09 (4.36 ± 0.0008)	*30 mM Trifluoroacetic Acid*	-
13 mM Pyridinium	2.59 ± 0.04		
1,4-Q + 100 mM Acetic Acid	3.42 ± 0.05	1,4-Q + *100 mM Acetic Acid*	3.63 ± 0.08 (-6.7 %)
1,4-Q + 18 mM Benzoic Acid	3.29 ± 0.03 (-2.4 %)	1,4-Q + *18 mM Benzoic Acid*	3.05 ± 0.02 (-15 %)
1,4-Q + 12 mM $DIPEAH^+$	3.57 ± 0.05 (+5.6 %)	1,4-Q + *12 mM $DIPEAH^+$*	2.40 ± 0.06 (+3.3 %)
1,4-Q + 30 mM Trifluoroacetic Acid	3.54 ± 0.07 (+4.8 %)	1,4-Q + *30 mM Trifluoroacetic Acid*	-
1,4-Q + 13 mM Pyridinium	3.54 ± 0.04 (+4.8 %)	1,4-Q + *13 mM Pyridinium*	2.70 ± 0.08 (+4.1 %)
1,4-QH_2 + 10 mM Acetate	1.65 ± 0.04 (1.67 ± 0.02)	1,4-QH_2 + *10 mM Acetate*	2.11 ± 0.04 (2.24 ± 0.009)
1,4-QH_2 + 10 mM Benzoate	1.97 ± 0.05 (1.50 ± 0.009)	1,4-QH_2 + *10 mM Benzoate*	2.09 ± 0.08 (2.03 ± 0.01)
1,4-QH_2 + 10 mM DIPEA	3.09 ± 0.02 (2.95 ± 0.04)	1,4-QH_2 + *10 mM DIPEA*	3.33 ± 0.003 (3.36 ± 0.08)
1,4-QH_2 + 10 mM Trifluoroacetate	2.56 ± 0.02 (2.07 ± 0.02)	1,4-QH_2 + *10 mM Trifluoroacetate*	-
1,4-QH_2 + 10 mM Pyridine	2.71 ± 0.02 (2.76 ± 0.04)	1,4-QH_2 + *10 mM Pyridine*	4.45 ± 0.01 (4.15 ± 0.03)
1,2-QH_2 + 10 mM Acetate	1.87 ± 0.05 (1.67 ± 0.04)	1,2-QH_2 + *10 mM Acetate*	2.52 ± 0.04 (2.60 ± 0.05)
1,2-QH_2 + 10 mM Benzoate	1.92 ± 0.03 (2.02 ± 0.09)	1,2-QH_2 + *10 mM Benzoate*	2.09 ± 0.02 (2.24 ± 0.08)
1,2-QH_2 + 10 mM DIPEA	2.65 ± 0.02 (2.87 ± 0.07)	1,2-QH_2 + *10 mM DIPEA*	3.26 ± 0.04 (3.30 ± 0.06)
1,2-QH_2 + 10 mM	2.76 ± 0.02 (2.39 ± 0.009)	1,2-QH_2 + *10 mM*	-

Trifluoroacetate		*Trifluoroacetate*	
1,2-QH_2 + 10 mM Pyridine	2.78 ± 0.003 (3.07 ± 0.5)	1,2-QH_2 + *10 mM Pyridine*	4.18 ± 0.04 (4.22 ± 0.03)

[a.] Text underlined and *italizied* indicate the species who's diffusion coefficient in given in the column to the right of the text.
[b.] Values measured in heavy acetonitrile at 27°C, and then corrected for differences in viscosity in 0.2 M $TBAPF_6$ in light acetonitrile.[88]
[c.] D value of trifluoroacetate alone measured by chronoamperometry of a solution containing 10 mM trifluoroacetate in dry acetonitrile with 0.2 M $TBAPF_6$.

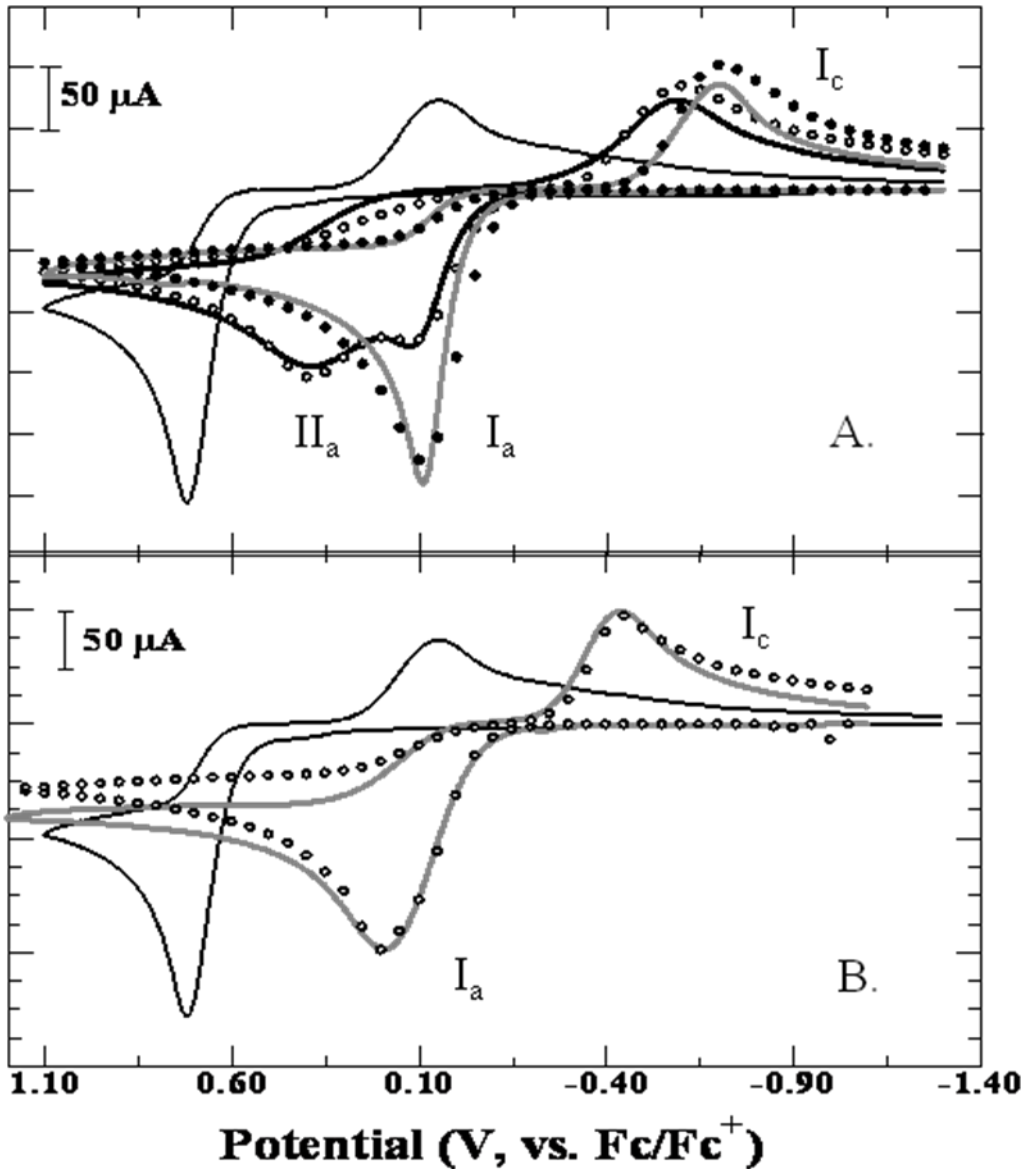

Figure 21. A.) Cyclic voltammetry of 5.0 mM 1,4-QH_2 alone (thin black line), with 10.0 mM trifluoroacetateTEATfa (thick black line), with 30.0 mM trifluoroacetate (thick gray line) and simulations of 5.0 mM 1,4-QH_2 with 10.0 mM trifluoroacetate and with 30.0 mM trifluoroacetate (open and closed black circles, respectively). B.) Cyclic voltammetry of 5.0 mM 1,4-QH_2 alone (thin black line), with 10.0 mM pyridine (gray line) and the simulation (open circles). Voltammetry measured at a glassy carbon electrode in 0.2 M $TBAPF_6$ at 0.1 V s^{-1}.

Table 8. Voltammetric data from 1,4-QH_2 alone and with the amines and acetates.

	pK_a [a]	E_{pIa} (V) [c, d]	E_{pIIa} (V) [c]	E_{pIc} (V) [c, d]	ΔE_{pI} (V) [d]	$\Delta E_{pIIa-Ia}$ (V)	ΔE_{pa} (V)	$\Delta E_{p\ QH2-Ia}$ (V) [d]	ΔG (kJ mol^{-1}) [d, f]
1,4-QH_2	26.20	0.722	-	0.050	0.672	-	-	-	-
1,2-QH_2	21.67	0.834	-	0.196	0.638	-	-	-	-
Acetate	22.3	-0.406 (-0.428)	-0.337	-0.824 (-0.901)	0.418 (0.473)	0.069	-0.032	-1.128 (-1.150)	-217.6 (-221.9)
Benzoate	20.7	-0.329 (-0.365)	-0.238	-0.805 (-0.857)	0.476 (0.492)	0.091	-0.036	-1.051 (-1.087)	-202.8 (-209.8)
DIPEA [e]	18 [b]	-0.061	-	-0.749	0.688	-	-	-0.783	-151.1
Trifluoroacetate	12.65	0.128 (0.093)	0.392	-0.586 (-0.700)	0.714 (0.793)	0.264	-0.035	-0.594 (-0.629)	-114.6 (-121.4)
Pyridine	12.33	0.194 (0.204)	-	-0.437 (-0.440)	0.631 (0.644)	-	-	-0.528 (-0.518)	-101.9 (-100.0)
Acetate (with 1,2-QH_2)	22.3	-0.044 (-0.016)	-	-0.677 (-0.759)	0.633 (0.743)	-	+0.028	-0.878 (-0.850)	-169.4 (-164.0)
Benzoate (with 1,2-QH_2)	20.7	-0.003 (-0.012)	-	-0.698 (-0.715)	0.695 (0.703)	-	-0.009	-0.837 (-0.846)	-161.5 (-163.3)
DIPEA [e] (with 1,2-QH_2)	18 [b]	-0.030	-	-0.551	-0.521	-	-	-0.864	166.7
Trifluoroacetate (with 1,2-QH_2)	12.65	0.296 (0.249)	0.392	-0.472 (-0.535)	0.768 (0.784)	0.096	-0.047	-0.538 (-0.585)	-103.8 (-112.9)
Pyridine (with 1,2-QH_2)	12.33	0.369 (0.360)	-	-0.299 (-0.303)	0.668 (0.677)	-	-	-0.465 (-0.474)	-89.7 (-91.5)

[a.] The pK_a's of the QH_2's are the same as reported in Chapter 2, by QM calculations, others determined from the literature.[88]
[b.] Estimated from the pK_a's of tripropylamine and triisopentylamine.[88]
[c.] All reported values are determined from voltammograms at 0.1 V s^{-1} at room temperature vs. Fc/Fc^+.
[d.] Values in parentheses are from voltammograms recorded with 30 mM of the indicated base.
[e.] Voltammetry of 1,4-QH_2 was not recorded with 30 mM DIPEA, due to passivation of the electrode by oxidation of DIPEA at concentrations greater than 10 mM.
[f.] Determined by $-\Delta G = nFE_{QH2-Ia}$, assuming the number of electrons transferred, n, is equal to 2 at this point.

Cyclic voltammetry shows that addition of 10.0 mM of the Brønsted base, amines or acetates, to the QH_2's causes a new redox peak system (Figure 21, I_a, II_a and I_c) to form at negative potentials relative to the redox peaks for 1,4-QH_2 alone in acetonitrile. Cyclic voltammetry of 1,4-QH_2 with the acetates shows two overlapped oxidation peaks (Figure 21, I_a and II_a) at acetate concentrations of 10.0 mM. At higher concentrations, 20.0 to 30.0 mM of the acetates, the first oxidation peak is resolved at the expense of the second oxidation peak, gray CV, Figure 21. However, voltammetry of both QH_2's with amines and voltammetry of 1,2-QH_2 with acetate and benzoate shows only a single oxidation peak regardless of the concentration,

Table 8 (see appendix). Chronocoulometry, chronoamperometry and controlled potential coulometry (CPC) results indicate that the new oxidation peak after addition of the amines involve the transfer of two electrons. However, for acetate additions to the QH_2's less than two electrons are transferred ($n \approx 1.6$-1.7) using the D values found for the QH_2's alone. The use of the D values for the QH_2's with each acetate (Table 7) shows that two electrons are transferred, as further evidence that the hydrogen bound QH_2 is being oxidized.

Figure 21 gives two examples of the voltammetry for 5.0 mM 1,4-QH_2 with 10.0 and 30.0 mM trifluoroacetate (Figure 21A) and 5.0 mM 1,4-QH_2 with 10.0 mM pyridine (Figure 21B). The first oxidation peak, I_a, from the addition of 10.0 mM trifluoroacetate to 1,4-QH_2 is 0.264 V ($\Delta E_{pIIa\text{-}Ia}$) relative to the second oxidation peak, II_a. Upon addition of 20.0 mM more trifluoroacetate to the same solution the first oxidation peak shifts to more negative potentials by 0.035 V (ΔE_{pa}) and the second oxidation peak is absent. This addition highlights the significant difference in potential between the oxidation, I_a, and reduction peaks, I_c (0.793 V, ΔE_{pI}). Similar voltammetric changes are observed for the addition of 10.0 mM and 30.0 mM acetate and benzoate to 1,4-QH_2 and additions of 10.0 mM and 30.0 mM trifluoroacetate to 1,2-QH_2. However, the difference in the oxidation peak potentials ($\Delta E_{pIIa\text{-}Ia}$, Table 8) is smaller for these additions. It is possible that the larger K values, Table 6, coupled with the larger pK_a's for acetate (22.3) and benzoate (20.7) likely influence the smaller values for $\Delta E_{pIIa\text{-}Ia}$.[88] While, the smaller K values, Table 6, for 1,2-QH_2 with trifluoroacetate, relative to the K values for 1,2-QH_2 with acetate and benzoate, influence the observation of two peaks. Interestingly, the shift of peak II_a to I_a, ΔE_{pa}, for each of the acetates with 1,4-QH_2, going from 10.0 mM to 30.0 mM, is similar, within error, Table 8. The similarity in ΔE_{pa} with each of the acetates with 1,4-QH_2 is likely due to the same process taking place as the concentration of acetate increases.

From Table 8, there is an obvious dependence of the shift in the oxidation peak, I_a, with the pK_a of the added base.[18, 27] As the pK_a of the base increases the oxidation peak shifts towards more negative potentials, overall making the oxidation of 1,4-QH_2 easier. Interestingly, the pK_a's of pyridine (12.33) and trifluoroacetate (12.65) are similar, yet the oxidation of 1,4-QH_2 is 0.111 V easier in the presence of 30.0 mM trifluoroacetate versus 30.0 mM pyridine. Overall, this equates to about 21.4 kJ of stabilization of 1,4-QH_2 by trifluoroacetate. Another interesting find is that the K's of the QH_2's with benzoate are considerably higher than those of the QH_2's with trifluoroacetate or acetate. A possible explanation for this is the added influence of other intermolecular interactions such as π-stacking of benzoate and the QH_2's. NOESY and ROESY 2D ^{1}H-NMR experiments were undertaken to determine the orientational effects of each of the acetates with the QH_2's, however no correlational cross-peaks were noted. A possible reason for this is that the hydrogen atoms of the base and the QH_2 are greater than 5 Å apart, limiting the effectiveness of these 2D NMR techniques.[28, 102] Simple QM calculations of the QH_2-acetate complexes were performed and measurements between the hydrogen atoms that were in closest proximity confirmed this assumption. Measurements showed the closest distance to be between benzoate aromatic hydrogen atoms and the aromatic hydrogen atoms of the QH_2's was ~6 Å.[28, 102]

Table 9. Voltammetric measurements recorded from multiple voltammograms at various scan rates to determine the mechanism of oxidation.

1,4-QH_2					
Base	**$\partial Ep/\partial \log v$ (V/decade, Peak I_a)[a]**	**$\partial Ep/\partial \log v$ (V/decade, Peak II_a)**	**$\partial Ep/\partial \log v$ (V/decade, Peak I_c)[a]**	**$E_p - E_{p/2}$ (V, peak I_a)[a]**	**$E_p - E_{p/2}$ (V, peak I_c)[a]**
Acetate	0.074 ± 0.03 (0.063 ± 0.003)	0.057 ± 0.03	-0.031 ± 0.03 (-0.015 ± 0.01)	0.127 ± 0.01 (0.106 ± 0.01)	-0.089 ± 0.004 (-0.052 ± 0.002)
Benzoate	0.043 ± 0.007 (0.069 ± 0.01)	0.051 ± 0.009	-0.024 ± 0.003 (-0.027± 0.01)	0.111 ± 0.006 (0.116 ± 0.02)	-0.092 ± 0.02 (-0.059 ± 0.002)
DIPEA[b]	0.108 ± 0.01	-	-0.059 ± 0.01	0.194 ± 0.009	-0.094 ± 0.01
Trifluoroacetate	0.042 ± 0.01 (0.053 ± 0.002)	0.047 ± 0.01	-0.080 ± 0.009 (-0.069 ± 0.01)	0.105 ± 0.01 (0.073 ± 0.01)	-0.204 ± 0.03 (-0.151 ± 0.01)
Pyridine	0.153 ± 0.02 (0.109 ± 0.002)	-	-0.105 ± 0.02 (-0.135 ± 0.005)	0.187 ± 0.009 (0.152 ± 0.004)	-0.145 ± 0.02 (-0.175 ± 0.009)
1,2-QH_2					
Base	**$\partial Ep/\partial \log v$ (V/decade, Peak I_a)[a]**	**$\partial Ep/\partial \log v$ (V/decade, Peak II_a)**	**$\partial Ep/\partial \log v$ (V/decade, Peak I_c)[a]**	**$E_p - E_{p/2}$ (V, peak I_a)[a]**	**$E_p - E_{p/2}$ (V, peak I_c)[a]**
Acetate	0.041 ± 0.01 (0.060 ± 0.01)	-	-0.033 ± 0.02 (-0.025 ± 0.004)	0.101 ± 0.009 (0.092 ± 0.005)	-0.112 ± 0.008 (-0.061 ± 0.0008)
Benzoate	0.023 ± 0.008 (0.049)	-	-0.053 ± 0.02 (-0.0262)	0.101 ± 0.01 (0.087)	-0.115 ± 0.03 (-0.063)
DIPEA[b]	0.146 ± 0.02	-	-0.109 ± 0.005	0.183 ± 0.02	-0.114 ± 0.008
Trifluoroacetate	0.048 ± 0.005 (0.060 ± 0.001)	0.036 ± 0.006	-0.069 ± 0.0001 (-0.065 ± 0.004)	0.103 ± 0.002 (0.089 ± 0.002)	-0.170 ± 0.007 (-0.123 ± 0.002)
Pyridine	0.084 ± 0.02 (0.081 ± 0.002)	-	-0.101 ± 0.01 (-0.117 ± 0.01)	0.133 ± 0.01(0.123 ± 0.01)	-0.114 ± 0.01 (-0.144 ± 0.02)

[a.] Values in parentheses are from voltammograms recorded with 30.0 mM of the indicated base.
[b.] There was only a single voltammogram recorded at 30.0 mM DIPEA due to oxidation of DIPEA at the electrode at concentrations greater than 10.0 mM.

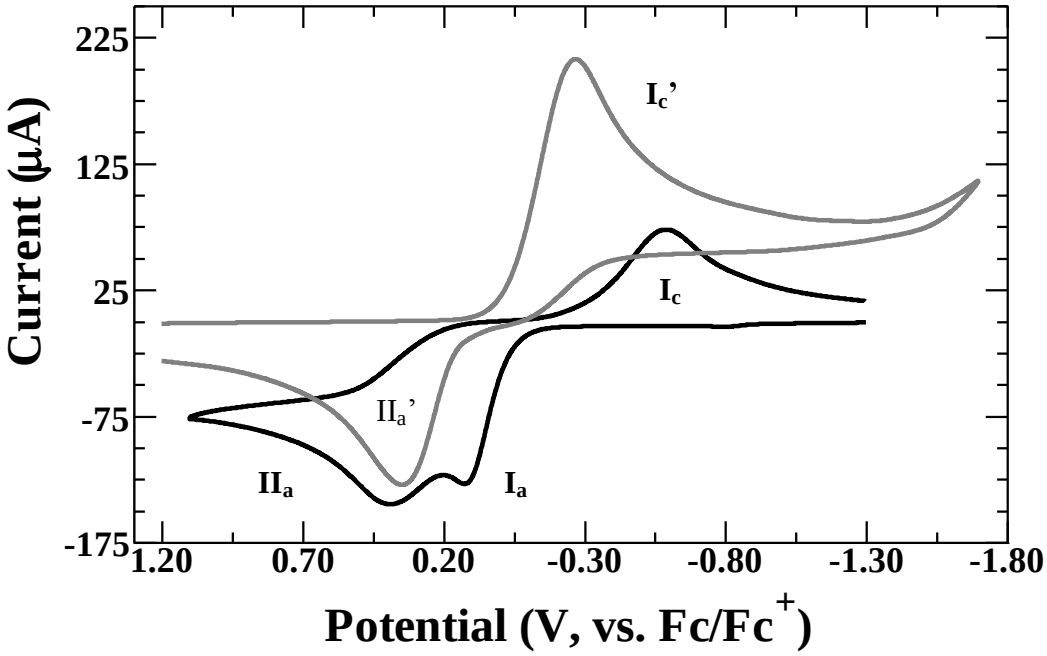

Figure 22. Cyclic voltammetry of 5.0 mM 1,4-QH_2 with 10.0 mM trifluoroacetate (black CV) and 5.0 mM 1,4-Q with 30.0 mM trifluoroacetic acid (gray CV). All voltammetry recorded at 0.1 V s^{-1} at a glassy carbon electrode at 25 ^{o}C under dry conditions in anhydrous acetonitrile with 0.2 M tetrabutylammonium hexafluorophosphate.

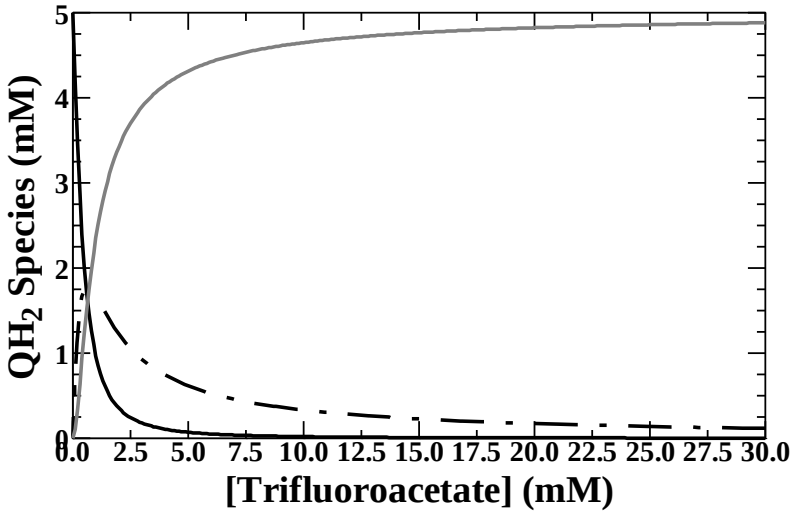

Figure 23. Equilibrium concentrations of 1,4-QH_2 species as a function of the total trifluoroacetate concentration, where K_1 = 55 M^{-1} and K_2 = 5 M^{-1}: 1,4-QH_2 (solid black line), 1,4-QH_2(B) (dashed black line) and 1,4-$QH_2(B)_2$ (solid gray line).

The simulations displayed in Figure 21 for 1,4-QH_2 upon addition of each base were envisioned based on the ^{1}H-NMR and the electrochemical data. By monitoring the voltammetry at various scan rates the mechanism of oxidation, whether a chemical or electron transfer step occurs first, can be derived from the values of ($E_p - E_{p/2}$) and $\partial E_p / \partial \log \nu$. This transition is characterized by an increase of ($E_p - E_{p/2}$) from 47.5 to 95 mV and an increase in $\partial E_p / \partial \log \nu$ from 29.6 to 59.2 mV/decade, for a two electron process at 25 ^oC.[15, 61, 66] Values between these characteristic values are said to be of an intermediate or mixed kinetic nature, meaning the reaction is not fixed on one kinetic scheme (ET first versus PT first). The values determined for ($E_p - E_{p/2}$) and $\partial E_p / \partial \log \nu$ for the oxidation of the QH_2's in the presence of 30.0 mM of the acetates, represented by peak I_a, Figure 21A, are approximately equal to 95 mV and 59.2 mV decade^{-1}, Table 9, for both of the QH_2's each of the acetates at 30.0 mM. Therefore, it is known that the process is an ECE process. Interestingly enough, the values determined for the reduction, peak I_c, roughly correspond to an CECE process. However, the values determined for the amines at all concentrations and the acetates at 10.0 mM do not correlate well to this theory (Table 9). Therefore, to determine the processes taking place at peaks I_a and II_a, voltammetry of 1,4-benzoquinone (1,4-Q), the completely oxidized form of 1,4-QH_2, with the conjugate acids was measured. Figure 22 shows the voltammetry of 5.0 mM 1,4-QH_2 with 10.0 mM trifluoroacetate and 5.0 mM 1,4-Q with 30.0 mM trifluoroacetic acid. The oxidation taking place at peak II_a, Figures 21 and 22, has a similar peak potential to the oxidation peak potential of 1,4-Q with trifluoroacetic acid, peak II_a' (0.391 and 0.350 V, respectively). Similar voltammetry is found when comparing the voltammetry of acetate and benzoate additions to 1,4-QH_2 with acetic acid and benzoic acid additions to 1,4-Q. Therefore, it is reasonable to assume that because 1,4-

Q and 1,4-QH_2 are complementary redox states of the same couple, a reaction occurring at a similar redox potential may involve the same intermediate. Since the diffusion measurements of 1,4-Q with the conjugate acid indicated that no complexation was taking place, the process at peak II_a is an electron-proton transfer. However, peak I_a represents the oxidation of the complexed 1,4-QH_2, both $QH_2(B)$ and $QH_2(B)_2$, where the B in parentheses represents the hydrogen bound acetate. The determined association constants, K_1 and K_2 (Table 6), were used to determine the equilibrium concentrations of QH_2 alone, the singularly bound QH_2 ($QH_2(B^-)$) and the doubly bound QH_2 ($QH_2(B^-)_2$) prior to oxidation. Figure 23 displays the equilibrium concentration plot for 1,4-QH_2 with trifluoroacetate up to 30.0 mM trifluoroacetate. From this plot it is obvious that the doubly bound QH_2 ($QH_2(B^-)_2$) is the predominant species in solution at 10.0 (93.0 %) and 30.0 (97.6 %) mM trifluoroacetate. Knowledge of the predominant species in solution defines the initial conditions and a starting point for the simulations. Oxidation of the QH_2 complexes at 10.0 mM acetate concentrations was envisioned to involve the oxidation of both the singly and doubly bound QH_2 due to the significant concentration (4.8 to 6.6 % for each of the acetates at 10.0 mM) of this species in solution under these conditions, equations 28 and 29, Scheme 8A. Upon oxidation of the QH_2-acetate complexes the concentration of acetate and acetate bound to QH_2 dramatically decreases due to the production of acetic acid and the homoconjugate of the respective acetic acids. Homoconjugate species are complexes of a base and its conjugate acid, in this study, each of the acetates forms a homoconjugate where the strength of the interaction for each is greater than 10^4 M^{-1}.[88] The production of the conjugate acids and the homoconjugate at the surface is the cause for the measurement of two oxidation peaks at acetate concentrations of 10.0 mM. At 30.0 mM acetate, only a single peak is found because the concentration of acetate at the surface of the electrode is far greater than that of the

acid or homoconjugate. Thus, from the scan rate analysis, the reduction of 1,4-Q in the presence of the conjugate acids and the equilibrium plot data the mechanisms of Scheme 8 were conceived. Schemes 8A and B represent the mechanism fitted to 1,4-QH_2 in the presence of 10.0 and 30.0 mM of the acetates, respectively. Support for the difference in oxidation of QH_2 at two different acetate concentrations can be found for numerous hydrogen bonding systems in the literature.[58, 59, 71] Scheme 8A also fit the voltammetry of 1,2-QH_2 in the presence of trifluoroacetate, while Scheme 8B fit the voltammetry of 1,2-QH_2 at every investigated concentration of acetate. However, the voltammetry of 1,2-QH_2 in the presence of any concentration of benzoate (10.0 to 30.0 mM) could only be fit by Scheme 8C because the interaction between 1,2-QH_2 and benzoate is 1:1. The binding constants, K_1 and K_2, for each of the hydrogen bonding events, Table 6, and the determined diffusion coefficients (Table 7) were incorporated into the simulations. Scheme 8D (equivalent to Scheme 5, Chapter 2.3) is the mechanism fitted to 1,4-QH_2 in the presence of 10.0 and 30.0 mM of the amines, the principle of which, deprotonation of 1,4-QH_2, equation 15, is supported by the literature.[58, 59]

Scheme 8. Oxidation schemes for the QH_2's in the presence of various concentrations of the acetates and amines.

Scheme 8A

$$QH_2 + B \rightleftharpoons QH_2(B) \quad (26)$$

$$QH_2(B) + B^- \rightleftharpoons QH_2(B)_2 \quad (27)$$

$$QH_2(B) \rightleftharpoons QH_2^{+\cdot}(B) + e^- \quad (28)$$

$$QH_2(B)_2 \rightleftharpoons QH_2^{+\cdot}(B)_2 + e^- \quad (29)$$

$$QH_2^{+\cdot}(B) \rightleftharpoons QH^{\cdot} + HB \quad (30)$$

$$QH_2^{+\cdot}(B)_2 \rightleftharpoons QH^{\cdot} + HB_2 \quad (31)$$

$QH^{\cdot} \rightleftharpoons QH^{+} + e^{-}$ (32)

$QH^{+} + \mathbf{H}B_2^{-} \rightleftharpoons Q + H_2B_2$ (33)

$QH^{\cdot} + QH^{\cdot} \rightleftharpoons Q + QH_2$ (14)

$HB \rightleftharpoons B^{-} + H^{+}$ (34)

$HB + B \rightleftharpoons HB_2$ (35)

Scheme 8B

$QH_2 + B \rightleftharpoons QH_2(B)$ (26)

$QH_2(B) + B \rightleftharpoons QH_2(B)_2$ (27)

$QH_2(B)_2 \rightleftharpoons QH_2^{+\cdot}(B)_2 + e^{-}$ (31)

$QH_2^{+\cdot}(B)_2 \rightleftharpoons QH^{\cdot}(B) + HB$ (36)

$QH^{\cdot}(B) \rightleftharpoons QH^{+}(B) + e^{-}$ (37)

$QH^{+}(B) \rightleftharpoons Q + HB$ (38)

$QH^{\cdot}(B) + QH^{\cdot}(B) \rightleftharpoons Q + QH_2(B)_2$ (39)

Scheme 8C

$QH_2 + B \rightleftharpoons QH_2(B)$ (26)

$QH_2(B) \rightleftharpoons QH_2^{+\cdot}(B) + e^{-}$ (28)

$QH_2^{+\cdot}(B) \rightleftharpoons QH^{\cdot} + HB$ (30)

$QH^{\cdot} + B \rightleftharpoons QH^{\cdot}(B)$ (40)

$QH^{\cdot}(B) \rightleftharpoons QH^{+}(B) + e^{-}$ (37)

$QH^{+}(B) \rightleftharpoons Q + HB$ (38)

$QH^{\cdot} + QH^{\cdot}(B) \rightleftharpoons Q + QH_2(B)$ (41)

Scheme 8D

$QH_2 + B \rightleftharpoons QH^{-} + HB$ (15)

$QH^{-} \rightleftharpoons QH^{\cdot} + e^{-}$ (16)

$QH^{\cdot} \rightleftharpoons QH^{+} + e^{-}$ (17)

$QH^{+} + B \rightleftharpoons Q + HB$ (18)

$QH^{\cdot} + QH^{\cdot} \rightleftharpoons Q + QH_2$ (14)

To this point, the oxidation of the QH_2's as a hydrogen bonded complex or after proton transfer as a *stepwise* or *concerted* mechanism has not been addressed. Defining an electrochemical oxidation or reduction mechanism as *stepwise* or *concerted* often involves the use of deuterated reagents and determination of the kinetic isotope effect (KIE). The KIE is determined from the simulated rate constants ($KIE = k_H/k_D$) found from simulated voltammetry of deuterated reagents, in this case, deuterated QH_2's (QD_2) in the presence of the acetates and amines. The KIE's determined for the QH_2's in the presence of the amines and acetate ranged from 0.64 to 1.3 at low concentrations of the amines and acetates. While at higher concentrations the KIE values were unity. This range of KIE values is less than the characteristic value of 1.6 needed to classify a reaction as *concerted*.[78] However, this does not overturn the possibility of a *concerted* reaction taking place under these conditions; it only denotes that the *concerted* reaction, if it does take place, is not the rate determining step.[103] Another possibility is that the QH_2's are not involved in a hydrogen bonded complex in the transition state, which limits the possibility of perceiving a *concerted* reaction.[18, 19, 104, 105] Furthermore, there is some evidence that *concerted* reactions are less likely in aprotic solvents such as acetonitrile.[21]

3.4 Conclusion

In conclusion, though the pK_a's of the amines and acetates are similar, their mode of action on the oxidation of the QH_2's are significantly different. The acetates are involved in at least one hydrogen bond with the QH_2's as determined by ^{1}H-NMR spectra and diffusion

coefficients determined by PGE-^{1}H-NMR. The PGE-^{1}H-NMR method is a very valuable technique under conditions such as these as it allows for the determination of the diffusion coefficients of both species suspected of interacting. Significant shifts of the phenolic proton peak upon addition of the acetates allowed the determination of the association constants. The amines, however, do not hydrogen bond with the QH_2's and very small changes were found in the ^{1}H-NMR and diffusion coefficients determined by PGE-^{1}H-NMR. The voltammetry of the two QH_2's differ due to the positioning of the phenolic groups on the benzene ring, *ortho* versus *para*. As a result, two peaks are noted with the oxidation of 1,4-QH_2 with each of the acetates at 10.0 mM concentrations, while oxidation of 1,2-QH_2 in the presence of 10.0 mM acetate and benzoate show a single oxidation peak. Scan rate analyses and voltammetry of 1,4-Q in the presence of the conjugate acids allows for the discrimination of the two peaks found upon oxidation of 1,4-QH_2 in the presence of 10.0 mM of the acetates. The first peak was determined to be the oxidation of the hydrogen bonded complex, while the second peak belongs to the oxidation of the one proton-one electron transfer from the protonated quinone radical, QH^o. At 30.0 mM added acetate, only a single oxidation peak was found for all added bases. The simulations of the voltammetry show that the stoichiometry of the complexes found increases upon addition of greater concentrations of the acetates as the concentration of the acetate becomes much greater than that of the protons released by oxidation of the QH_2's. The presence of hydrogen bonds between the QH_2's and the acetates actually stabilizes the oxidation of 1,4-QH_2 relative to oxidation following proton transfer.

4.0 Hydroquinones in an Aprotic Buffered Solution: The Transition from a Hydrogen Bonded Proton Transfer Mechanism to a Purely Proton Transfer Mechanism

4.1 Introduction

Since the inception of electrochemical studies, mechanistic transitions in proton-coupled electron transfer (PCET) have been of particular interest. Early descriptions of mechanistic transitions involved the study of proton-coupled electron transfers of simple systems, both actual and hypothetical systems in aqueous solution.[106-114] These model systems involved four-, six- and nine-membered square schemes and even probed the study of such systems bound to electrode surfaces.[107, 108, 110-113, 115-119] Mathematical models were even introduced to determine what mode of electron-proton transfer was taking place; electron transfer before or after proton transfer.[18, 27] Furthermore, there have also been accounts discussing the transition of coupled-proton electron transfer reactions to a stepwise dissociative reaction upon changing the substituents on a class of molecules, the temperature or driving force.[120-122] The model molecular system for several of these studies and more not mentioned here has been the quinone/hydroquinone couple.[14, 113, 114] Herein, we report on the transition from an acetate hydrogen-bound 1,4-hydroquinone (1,4-QH_2) mechanism to a proton-transfer based 1,4-QH_2 mechanism upon addition of acetic acid to 1,4-QH_2-acetate solutions. To our knowledge, no previous studies have discussed such a transition. Furthermore from these studies it appears that the oxidation process is a further example of a CEEC oxidation reaction.

This work seeks to advance the growing body of similar studies by understanding the kinetic effects imparted from the transition from an ECEC reaction (a process found to occur with QH_2 alone in ACN and in the presence of acetates, Chapters 2 and 3), to a CEEC mechanism (a process observed upon titration of the amines with QH_2, Chapter 2). The addition

of conjugate acids to QH_2-acetate complex solutions causes the increase in the measured diffusion coefficient (D) back to or approximately to the measured D of QH_2 alone in acetonitrile (ACN). Voltammetry measured at two different acetate/conjugate acid ratios helped to determine that the predominant species present in solution is the uncomplexed QH_2 and that virtually the only proton acceptor is the homoconjugate of the acetate being studied. Furthermore, current studies indicate that the oxidation occurs via *stepwise* proton-coupled electron transfer (PCET) as opposed to *concerted* PCET.

4.2 Experimental

4.2.1 Reagents and Materials

Anhydrous acetonitrile (ACN, Aldrich, St. Louis, MO, 99.8 % with < 10 ppm H_2O) was used as received and transferred via syringe under argon. Tetrabutylammonium hexafluorophosphate ($TBAPF_6$, Fluka, electrochemical grade, ≥ 99.0 %), tetrabutylammonium acetate (acetate, Fluka, electrochemical grade, ≥ 99.0 %) tetrabutylammonium benzoate (benzoate, Fluka, electrochemical grade, ≥ 99.0 %) and tetraethylammonium trifluoroacetate (trifluoroacetate, Fluka, ≥ 99.0 %) were only opened and used under a nominally dry argon atmosphere. Hydroquinone (1,4-QH_2, Riedel-deHaën, St. Louis, MO, 99.5 %), hexaammineruthenium (III) chloride (Aldrich, $Ru(NH_3)_6Cl_3$ 98 %), D_2O (Aldrich, 99 % atom D), acetonitrile-d_3 (d_3-ACN, Aldrich, 99 % atom D), ferrocene (Fc, Fluka, ≥ 99 %), acetic acid (Aldrich, glacial, ≥ 99.85 %), trifluoroacetic acid (Aldrich, ≥ 99 %), silver nitrate (Aldrich, ≥ 99.0 %), Potassium chloride (EM Science, Gibbstown, NJ, 99.0-100.5 %), nitric acid (Aldrich, ACS Reagent, 70 %), hydroquinone-d_6 (1,4-QD_2, C/D/N Isotopes, Pointe-Claire, Quebec, Canada, 99.2 atom % D), trifluoroacetic acid-*d* (Aldrich, 99.5 atom % D), benzoic acid-*d* (Aldrich, 98 atom % D) and acetic acid-*d* (Aldrich, 99 atom % D) were all used as received.

4.2.2 Electrochemical Methods

All electrochemical experiments were performed with a hydroquinone or quinone concentration of 5.0 mM in 10 mL dry acetonitrile with 0.2 M tetrabutylammonium hexafluorophosphate ($TBAPF_6$) at a glassy carbon electrode. The electrochemical experiments were performed using a CHI660C potentiostat (CH Instruments, Austin, TX) incorporating a CHI200B Faraday cage and picoampbooster using a three electrode cell (10 mL) in an inert argon atmosphere. Several different 0.3 cm diameter glassy carbon electrodes (CH Instruments, areas were consistent, between 0.07 to 0.073 cm^2) were used during this work and the areas associated with each are given in the respective figures (determined by the Randles-Sevcik equation using a 1.0 mM solution of $Ru(NH_3)^{3+}$ in deionized water with 0.1 M KCl as supporting electrolyte, where $D = 6.3 \times 10^{-6}$).[77] The same electrode was always used for a particular set of data, for instance, data involving the addition of a particular base to protiated 1,4-QH_2 was used again to record similar measurements with deuterated 1,4-hydroquinone (1,4-QD_2). A platinum flag electrode served as the auxiliary electrode, and the reference electrode was an Ag/Ag^+ electrode (a silver wire immersed in the supporting electrolyte, 0.2 M $TBAPF_6$/3 mM silver nitrate/acetonitrile). The reference electrode was separated from the rest of the solution by a glass tube capped with a porous vycor frit (CH Instruments). The potential of the silver reference electrode was periodically measured versus the formal potential (measured as the average of the peak potentials) of the ferrocene/ferrocenium (Fc/Fc^+) couple under the same conditions as the other experiments and thus all potentials are reported versus ferrocene as Fc/Fc^+. Prior to each use the polished glassy carbon electrode was first polished using 0.05 μm alumina paste (Buhler, Lake Bluff, Il) washed with deionized water, carefully wiped, and then

sonicated for three minutes in acetonitrile. In each experiment the solution resistance (R_u) was totally compensated via positive feedback.

4.2.3 NMR Spectroscopic Methods

Standard ^{1}H-NMR and Pulsed Gradient Echo (PGE-) ^{1}H-NMR were performed on a Varian Inova 400 MHz NMR at 25 ^{o}C. The applied gradients in the PGE-^{1}H NMR experiments were calibrated by measuring the diffusion coefficient of HDO (2.23×10^{-5} cm^2 s^{-1}, at 25°C, 0.03%) in a D_2O sample and the diffusion coefficient of 1,6-diaminohexane (6.98×10^{-6} cm^2 s^{-1}, at 25°C, 0.04%). The pulse sequences and associated parameters are reported in the appendix.[79] The diffusion coefficients were measured under the same conditions as the electrochemical experiments, with the exceptions of measurements in deuterated acetonitrile and without supporting electrolyte. For a discussion on the correction of diffusion coefficients see the appendix.[88]

4.3 Results and Discussion

The addition of the conjugate acid to the solution containing 1,4-QH_2 and acetate causes the loss of the hydrogen bond exchange peak in the ^{1}H-NMR spectra. Figure 24A presents an example of this, where the ^{1}H-NMR spectra of 5.0 mM 1,4-QH_2 alone, 5.0 mM 1,4-QH_2 with 10.0 mM trifluoroacetate and 5.0 mM 1,4-QH_2 with 10.0 mM trifluoroacetate and 5.0 mM trifluoroacetic acid are shown. Upon addition of 10.0 mM trifluoroacetate to 5.0 mM 1,4-QH_2 the phenolic proton peak (*b*) shifts from 6.350 to 7.134 ppm. However, upon addition of 5.0 mM trifluoroacetic acid peak *b* is lost. Although, the addition of only 5.0 mM trifluoroacetic acid is given in Figure 24A, the addition of any of the conjugate acids to a solution of 1,4-QH_2 with an acetate shows no new peaks or the return of the phenolic peak to its initial position (at 6.350 ppm) regardless of temperature from 25 to 5 ^{o}C. The aromatic proton peak remains essentially

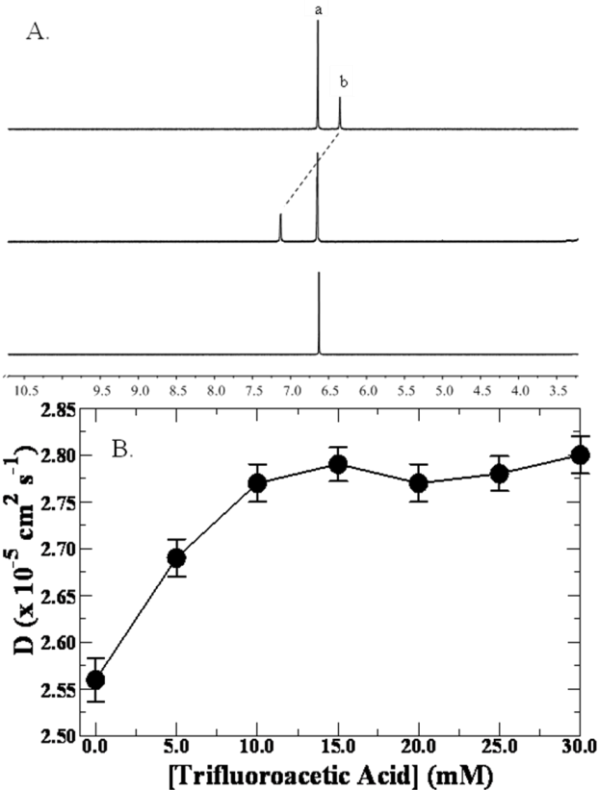

Figure 24. (A.) ^{1}H-NMR spectra of 5.0 mM 1,4-QH_2 alone (top spectra), 5.0 mM 1,4-QH_2 with 10.0 mM trifluoroacetate (middle spectra) and 5.0 mM 1,4-QH_2 with 10.0 mM trifluoroacetate and 5.0 mM trifluoroacetic acid in ACN-d_3. (B.) Change in the diffusion coefficient of 5.0 mM 1,4-QH_2 in the presence of 10.0 mM trifluoroacetate as trifluoroacetic acid is titrated.

constant throughout the additions of both trifluoroacetate and trifluoroacetic acid at 6.63 ppm. Although the phenolic proton peak is lost during the titration of the conjugate acids of each of the acetates the process taking place can be investigated by determining the diffusion coefficients of 1,4-QH_2 and the acetate using the PGE-^{1}H-NMR technique. The titration of each of the conjugate acids causes the steady shift of the diffusion coefficient (D) as illustrated in Figure 24B for the addition of 5.0 mM aliquots to trifluoroacetic acid to a solution of 5.0 mM 1,4-QH_2 with 10.0 mM trifluoroacetate. In Figure 24B, the D value for 5.0 mM 1,4-QH_2 with 10.0 mM trifluoroacetate shifts from 2.56 x 10^{-5} cm^2 s^{-1} without trifluoroacetic acid to 2.80 x 10^{-5} cm^2 s^{-1} after addition of 25.0 mM trifluoroacetic acid. The D measured upon addition of 25.0 mM trifluoroacetic acid, 2.80 x 10^{-5} cm^2 s^{-1}, is the same as that measured for 1,4-QH_2 alone in ACN-d_3. A similar shift in D to 2.80 x 10^{-5} cm^2 s^{-1} is found with the titration of trifluoroacetic acid in 5.0 mM aliquots up to 50.0 mM to a 5.0 mM 1,4-QH_2 with 30.0 mM trifluoroacetate solution (appendix). The titration of acetic acid and benzoic acid to solutions of 5.0 mM 1,4-QH_2 with 10.0 and 30.0 mM acetate and benzoate, respectively, also causes an increase in the measured D

as the concentration of the conjugate acid increases. However, the measured D of 1,4-QH_2 with 10.0 mM acetate and benzoate only approaches the expected value of 2.8 x 10^{-5} cm^2 s^{-1} after addition of 150 to 200 mM of acid. However, the measured D of 1,4-QH_2 with 30.0 mM acetate and benzoate never attains the expected value of 2.80 x 10^{-5} cm^2 s^{-1} with the titration of benzoic and acetic acid, even after addition of up to 700.0 mM titrated acid (appendix). Titrations of larger concentrations of the acids were not made because control experiments involving the addition of acetic and benzoic acid to 1,4-QH_2 alone revealed a decrease in the measured D with the increase in the acid concentration. The decrease in D in these control experiments is likely due to changes in viscosity brought about by the large concentration of acid in solution. Overall, the largest D's measured for 1,4-QH_2 with 30.0 mM acetate or benzoate was around 2.40 x 10^{-5} cm^2 s^{-1}. The titration of acetic and benzoic acid to solutions of 10.0 and 30.0 mM solutions of acetate and benzoate solutions alone, respectively, causes the measured D of the acid/base to decrease or remain somewhat constant throughout the titration. The noted decrease in D for the titration of acetic and benzoic acid to solutions of their conjugate bases alone indicates the expected formation of the homoconjugate species, as depicted in equation 42 (similar to equation 35, Chapter 3, but with modified notation to reflect acetate chemistry).

$$HA + A^- \rightleftharpoons HA_2^- \qquad (42)$$

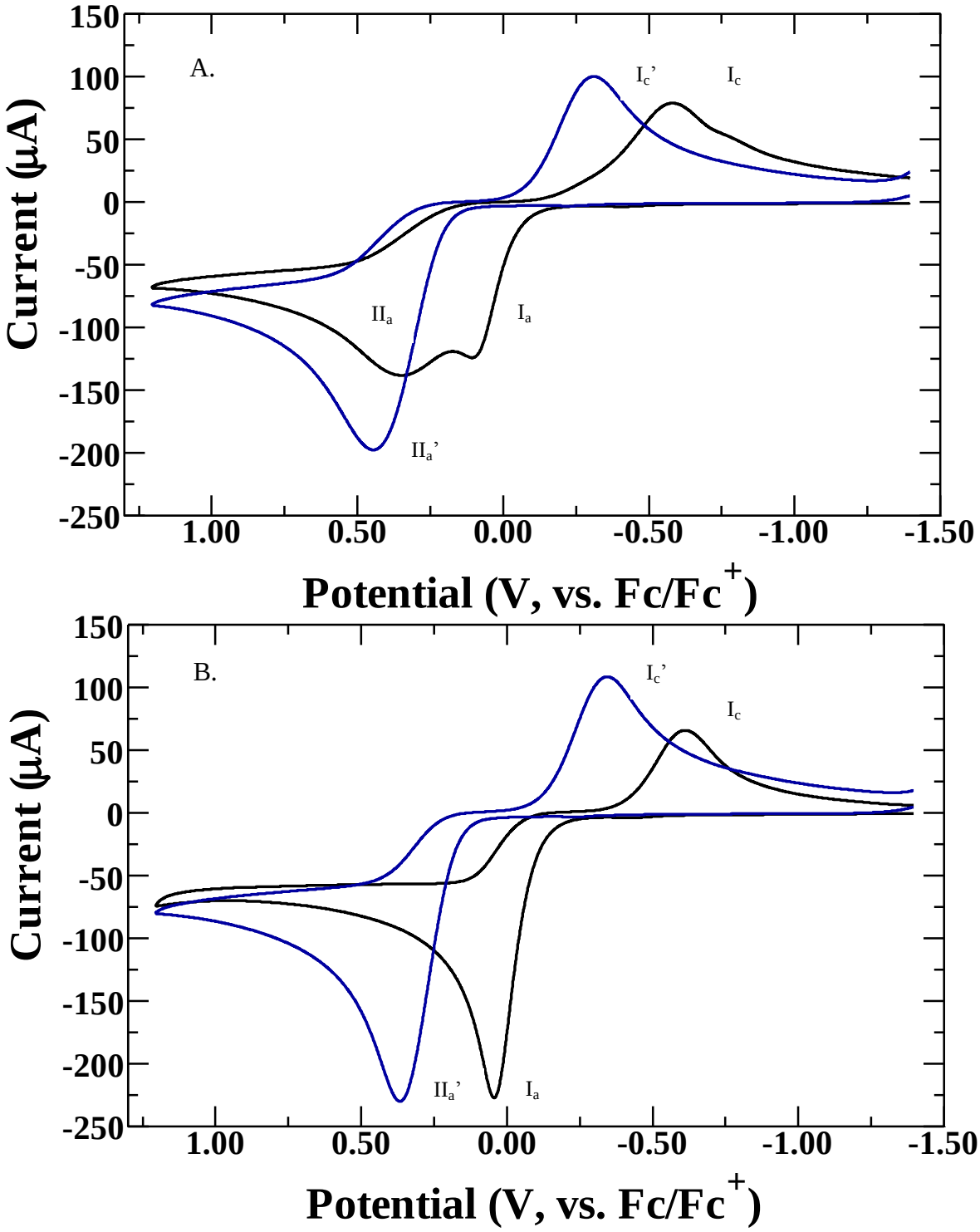

Figure 25. Cyclic voltammetry of (A.) 5.0 mM 1,4-QH_2 with 10.0 mM trifluoroacetate alone (black CV) and 5.0 mM 1,4-QH_2 with 10.0 mM trifluoroacetate and 25.0 mM trifluoroacetic acid (blue CV). Cyclic voltammetry of (B.) 5.0 mM 1,4-QH_2 with 30.0 mM trifluoroacetate alone (black CV) and 5.0 mM 1,4-QH_2 with 30.0 mM trifluoroacetate and 50.0 mM trifluoroacetic acid. All voltammetry recorded at 0.1 V s^{-1} at a glassy carbon electrode at 25 ^oC under dry conditions in anhydrous acetonitrile with 0.2 M tetrabutylammonium hexafluorophosphate.

The redox peaks of 5.0 mM 1,4-QH_2 with 10.0 and 30.0 mM of various acetates shift to more positive potentials upon addition of their conjugate acids. Figure 25 illustrates two examples of this. Figure 25A presents the CV of 5.0 mM 1,4-QH_2 with 10.0 mM trifluoroacetate alone, which shows two anodic peaks, peaks I_a and II_a, at 0.106 and 0.349 V. Upon addition of trifluoroacetic acid to the same solution in aliquots of 2.5 mM trifluoroacetic acid, a steady positive shift of peak II_a and an increase in the anodic peak current (i_{pa}) with each addition up to 25.0 mM is found. The growth and shift of peak II_a to peak II_a' is accompanied by the steady loss of peak I_a. After addition of 25.0 mM trifluoroacetic acid only a single anodic peak is found, peak II_a', at 0.445 V. Peak II_a' is given this notation due to the similarities in peak potentials of peaks II_a and II_a'. Since the potentials of these reductions are somewhat similar it is thought that the oxidation may go through the same process or at least involve the same intermediate. The addition of trifluoroacetic acid in 5.0 mM aliquots to a solution of 5.0 mM 1,4-QH_2 with 30.0 mM trifluoroacetate produced similar results to those discussed above. The addition of trifluoroacetic acid causes a positive shift of peak I_a to peak II_a' up to 50.0 mM trifluoroacetic acid, after which the peak potential (E_{pIIa}) and current (i_{pIIa}) remain approximately constant. However, the i_{pa} of peak II_a' (i_{pIIa}, -225.9 μA) is not much less than that of peak I_a (-223.6 μA), as displayed in Figure 25B. Yet, during the transition from peak I_a to peak II_a' during the titration of trifluoroacetic acid to 1,4-QH_2 with 30.0 mM trifluoroacetate the i_{pa} steadily decreases up to the addition of 25.0 mM trifluoroacetic acid. After addition of 25.0 mM trifuloroacetic acid, the trend in i_{pa} reverses and the i_{pa} increases up to the addition of 50.0 mM trifluoroacetic acid. Figure 25B presents the voltammetry found upon addition of 30.0 mM trifluoroacetate to 1,4-QH_2 and addition of 50.0 mM trifuloroacetic acid to the same solution. In Figure 25B peak I_a is found at 0.044 V, while peak II_a' is found at 0.367 V. Again, the notation

in Figure 25B is the same as that of Figure 25A since the peak potentials of peak II_a' in both figures is comparable. The voltammetry of 1,4-QH_2 with acetate and benzoate also proved to illustrate similar findings. Table 10 below, gives several electrochemical values of interest for the addition of 25.0 mM and 50.0 mM of the conjugate acids to 1,4-QH_2 with 10.0 and 30.0 mM of each acetate. Similar to the potentials of peak I_a, the peak potential of peak II_a' ($E_{p,IIa}$) in Table 10 correlate well with the pK_a of the acids; the higher the pK_a the more negative the peak potential of peak II_a'.

Table 10. Voltammetric data from 1,4-QH_2 with 10.0 and 30.0 mM of the acetates alone and voltammetric data from after the addition of 25.0 and 50.0 mM of the conjugate acids.

10.0 mM Base/25.0 mM Acid	**pK_a**[a]	**$E_{p,Ia}$ (V)**[b]	**$E_{p,IIa}$ (V)**[b, c]	**$E_{p,Ic}$ (V)**[b, c]	**$\Delta E_{pIIa-Ic}$ (V)**[c, d]	**$i_{pa,IIa}$ (μA)**[b,c,d]	**$i_{pa,Ic}$ (μA)**[b, c]
Acetate/Acetic Acid	22.3	-0.487	-0.389 (-0.182)	-0.837 (-0.685)	0.448 (0.503)	-132.4 (-180.6)	110.3 (126.0)
Benzoate/Benzoic Acid	20.7	-0.398	-0.293 (-0.144)	-0.807 (-0.596)	0.409 (0.452)	-119.6 (-169.0)	60.56 (84.35)
Trifluoroacetate/Trifluoroacetic Acid	12.65	0.106	0.349 (0.445)	-0.582 (-0.311)	0.931 (0.756)	-120.9 (-192.8)	74.26 (95.63)
30.0 mM Base/50.0 mM Acid							
Acetate/Acetic Acid	22.3	-0.474	- (-0.270)	-0.850 (-0.685)	- (0.415)	- (213.4)	136.9 (222.2)
Benzoate/Benzoic Acid	20.7	-0.385	- (-0.184)	-0.840 (-0.635)	- (0.451)	- (201.7)	101.9 (149.9)
Trifluoroacetate/Trifluoroacetic Acid	12.65	0.044	- (0.367)	-0.611 (-0.344)	- (0.711)	- (-225.9)	61.48 (102.4)

[a] Literature values.[123]
[b] Determined from voltammetry at 0.1 V s^{-1}.
[c] Values in parentheses are those from voltammetry measured after the indicated aliquot of acid, either 25.0 mM (top set of values) or 50.0 mM (bottom set of values). Values not in parentheses come from voltammetry of 1,4-QH_2 with indicated base.
[d] Determined from the peak current of either peak II_a (no parentheses) or peak II_a'(value in parentheses).

The voltammetry of 1,4-QH_2 with acetate and the conjugate acids were measured at multiple scan rates in an attempt to classify the mechanism as an ECE or a CECE process, where E represents an electron transfer and C a proton transfer. Classifying a process as an ECE or a CECE mechanism via scan rate analysis involves the interpretation of the values of ($E_p - E_{p/2}$) and $\partial E_p / \partial \log \nu$, where E_p and $E_{p/2}$ are the peak potential and potential where the current is half of the measured peak current. An ECE process is found via scan rate analysis as having $\partial E_p / \partial \log \nu$

and ($E_p - E_{p/2}$) values of 0.0592 V decade^{-1} and 0.095 V at 25 ^{o}C, respectively. However, a CECE process is determined if the values of $\partial E_p / \partial \log \nu$ and ($E_p - E_{p/2}$) are found to be 0.0296 V decade^{-1} and 0.0475 V. $\partial E_p / \partial \log \nu$ and ($E_p - E_{p/2}$) values found from evaluation of the voltammetry of 5.0 mM 1,4-QH_2 with 10.0 and 30.0 mM acetate with 25.0 and 50.0 mM conjugate acid, respectively, are given in Table 11. The values of $\partial E_p / \partial \log \nu$ and ($E_p - E_{p/2}$) do not correlate well with theory. However, they are similar to those measured from the titration of amines with the QH_2's (Chapter 2), which was found to be a CEEC process from voltammetric fittings.

Table 11. Voltammetric measurements recorded from multiple voltammograms at various scan rates to determine the mechanism of oxidation.

10.0 mM Base/25.0 mM Acid	**$\partial E_{pIIa'} / \partial \log \nu$ (V)**	**$\partial E_{pIc'} / \partial \log \nu$ (V)**	**($E_{pIIa'} - E_{pIIa'/2}$) (V)**	**($E_{pIc'} - E_{pIc'/2}$) (V)**
Acetate/Acetic Acid	0.0719 ± 0.004	-0.0466 ± 0.0001	0.1669 ± 0.0002	-0.0991 ± 0.0004
Benzoate/Benzoic Acid	0.0843 ± 0.008	-0.0614 ± 0.002	0.1621 ± 0.001	-0.1283 ± 0.001
Trifluoroacetate/Trifluoroacetic Acid	0.0834 ± 0.0004	-0.0962 ± 0.002	0.1659 ± 0.004	-0.1591 ± 0.002
30.0 mM Base/50.0 mM Acid				
Acetate/Acetic Acid	0.0682 ± 0.008	-0.0450 ± 0.002	0.1144 ± 0.0002	-0.0833 ± 0.0007
Benzoate/Benzoic Acid	0.0897 ± 0.003	-0.0673 ± 0.003	0.1353 ± 0.002	-0.1666 ± 0.004
Trifluoroacetate/Trifluoroacetic Acid	0.0621 ± 0.003	-0.0757 ± 0.0007	0.1205 ± 0.003	-0.1405 ± 0.005

The discussion above focused on the addition of 25.0 and 50.0 mM of the acids to the 10.0 and 30.0 mM acetate solutions, respectively. The above discussion facilitated the description of the bulk effects of the transition from a hydrogen bond dominated mechanism to a proton transfer mechanism. Larger concentrations of the acids and a study involving the addition of both the acetate and acid in a 1:1 ratio were also studied. Additions of conjugate acids up to 700 mM to the acetate solutions only illustrated the fact that the voltammetry shown in Figure 25 essentially represents the final outcome of the addition of the conjugate acids to the acetate

solutions. Conjugate acid additions beyond 700 mM limited the information that could be obtained due to the lower solubility of benzoic acid in ACN at concentrations greater than this and voltammetry measured at these concentrations indicated a change in solution viscosity was affecting the measured voltammetry due to a decrease in measured current. However, the major influence that the larger additions of the conjugate acids have on the measured voltammetry is that the $\Delta E_{pIIa'\text{-}Ic'}$ value decreases for each of the acetate/acid solutions to an average value of 0.433 V. Furthermore, the addition of the acetates and acids to 1,4-QH_2 in a 1:1 ratio beginning with the addition of 10.0 mM acetate and 10.0 mM acid results in voltammetry with constant anodic ($i_{pIIa'}$) and cathodic peak currents ($i_{pIc'}$), regardless of the acid/acetate concentration. In order to understand this transition an equilibrium plot was constructed using the determined association constants of the acetates with 1,4-QH_2 (Table 6, Chapter 3.3), the initial concentrations of each species and the homoconjugation constants (K_{homo}) for each acetate ($K_{homo,}$ = 7.6 x10^4 M^{-1} (trifluoroacetate), 4.0 x 10^4 M^{-1} (benzoate), 6.0 x 10^4 M^{-1} (acetate)).[88] Figure 26 presents two example equilibrium plots, the addition of trifluoroacetic acid to 1,4-QH_2 with 10.0 mM trifluoroacetate (Figure 26A) and to 1,4-QH_2 with 30.0 mM trifluoracetate (Figure 26B), that were constructed to describe the voltammetric measurements. From these plots, we can determine that the predominant species in the 10.0 and 30.0 mM acetate solutions after addition of 25.0 and 50.0 mM conjugate acid is 1,4-QH_2 (63.2 to 83.2 %). However, the singly bound hydroquinone-acetate species (1,4-QH_2(B)) is still present in significant proportion (14.8 to 28%) at added conjugate acid concentrations of 25.0 and 50.0 mM. Therefore, the oxidation mechanism is a mixed process, yet primarily classified as a proton transfer mechanism at the studied concentrations. Also, the predominant proton acceptor in solution is the homoconjugate of the particular acetate/conjugate acid being studied, as represented in Figure 26 by the thick red

line. Knowledge that the homoconjugate is the predominant proton acceptor in solution also assists in the determination of the rate determining step (RDS). From Table 10, we notice that the average peak current of peaks $i_{p,IIa'}$ and $i_{pIc'}$ increases substantially as the concentration of the homoconjugate increases ([homoconjugate] = 9.90 mM at 10.0 mM/25.0 mM acetate/conjugate acid to [homoconjugate] = 29.84 mM 30.0 mM/50.0 mM acetate/conjugate acid). Therefore, since the i_p scales with the proton acceptor concentration the rate determining step is proton transfer, confirming the discussion elaborated by the voltammetric scan rate analysis study (Table 11). Furthermore, inspection of the equilibrium plots made to describe these studies at 1:1 acetate to conjugate acid ratios shows that the solution composition of the 1,4-QH_2 species is constant for each of the acetates studied. Therefore, voltammetry of 1:1 acetate/conjugate acid solutions should depict peak currents of similar values regardless of the overall acetate/conjugate acid concentration. This result explains the voltammetric measurements at 1:1 acetate/conjugate acid ratios.

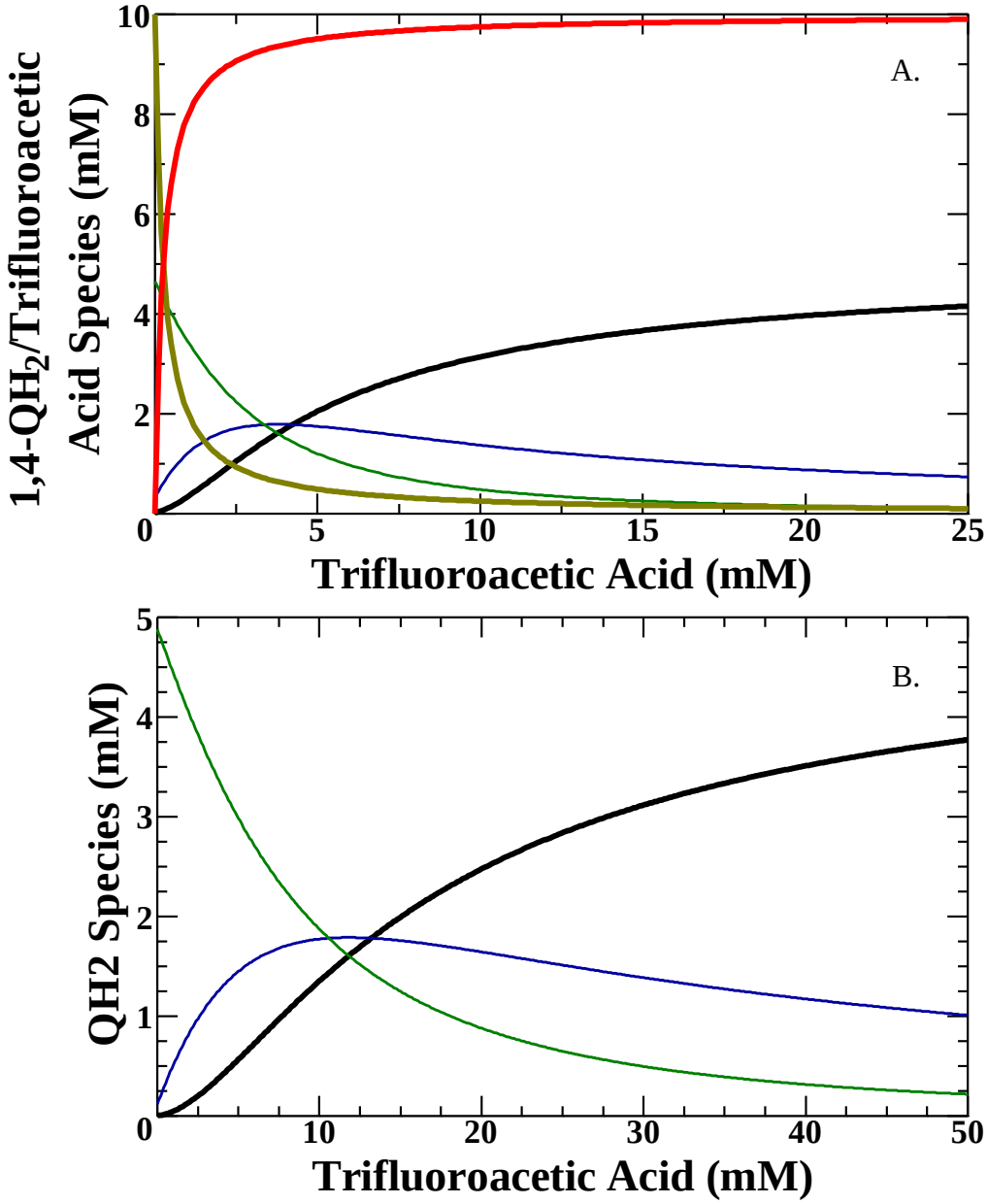

Figure 26. Equilibrium concentrations of 1,4-QH_2 (both A. and B.) and trifluoroacetic acid homoconjugate species (A. only) as a function of the total trifluoroacetic acid concentration for the addition of trifluoroacetic acid to 1,4-QH_2 solutions of (A.) 10.0 and (B.) 30.0 mM trifluoroacetate. In both A. and B. 1,4-QH_2 is represented by the thick black line, 1,4-QH_2(B) the thin blue line and 1,4-QH_2 the thin green line. In A. trifluoroacetate is represented by the thick gold line and its homoconjugate the thick red line.

The addition of deuterated conjugate acids to deuterated 1,4-QH_2 (1,4-QD_2) for the purpose of evaluating the redox mechanism as *concerted* or *stepwise* illustrated similar

voltammetry to that found for the addition of protiated conjugate acids to 1,4-QH_2. Voltammetry of the addition of deuterated conjugate acids to 1,4-QD_2 showed similar peak potential shifts and measured peak currents to those found with the addition of protiated conjugate acids to 1,4-QH_2 as shown in Figure 27. Figure 27A shows the peak potentials (E_p) found for the addition of a total of 50.0 mM trifluoroacetic acid, both deuterated and protiated, to 5.0 mM solutions of 1,4-QD_2 and 1,4-QH_2, respectively, containing 30.0 mM trifluoroacetate. The measured peak currents (i_p) for the addition of a total of 50.0 mM trifluoroacetic acid, both deuterated and protiated, to 5.0 mM solutions of 1,4-QD_2 and 1,4-QH_2, respectively, containing 30.0 mM trifluoroacetate is found in Figure 27B. These shifts are fairly small compared to those obtained from the addition of deuterated and protiated reagents to quinones and dissolved oxygen in acetonitrile.[58, 101] However, without a plausible mechanism and associated kinetic constants the observed voltammetry cannot be classified as *concerted* or *stepwise*.

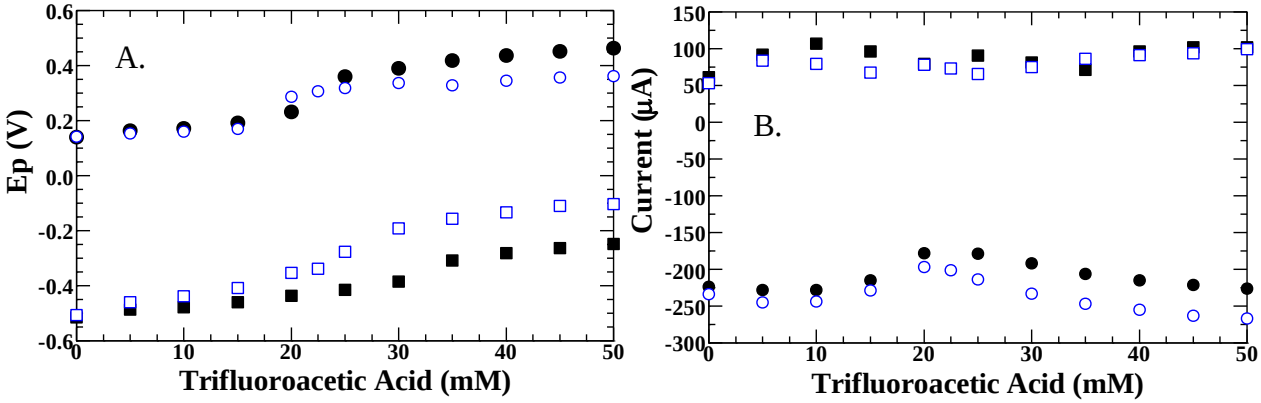

Figure 27. A.) Anodic (circles) and cathodic (squares) peak potential (E_p) as a function of the total concentration of added protiated (closed shapes) and deuterated (open shapes) trifluoroacetic acid to a solution of 1,4-QH_2 or 1,4-QD_2, respectively. B.) Anodic (circles) and cathodic (squares) peak current (i_p) as a function of the total concentration of added protiated (closed shapes) and deuterated (open shapes) trifluoroacetic acid to a solution of 1,4-QH_2 or 1,4-QD_2, respectively.

4.4 Conclusion

Overall, the description of the titration of conjugate acids to solutions containing hydrogen bound species of acetate with hydroquinone shows a sequential dissolution of the hydrogen bound species in acetonitrile. Via ^{1}H-NMR methods the peaks corresponding to the hydrogen bound acetate-hydroquinone species vanished and the diffusion coefficient increased to values determined for the 1,4-QH_2 alone in acetonitrile upon addition of conjugate acids. Furthermore, the voltammetry was found to evolve from a hydrogen bond mechanism to a proton transfer mechanism as determined by the evaluation of the voltammetry at various scan rates. The values found from scan rate analysis were similar to those measured when amines where added to QH_2 solutions, which from voltammetric fitting was found to operate through proton transfer from the QH_2 to the amine (Chapter 2). Furthermore, the peak potentials of the voltammetry measured after addition of the conjugate acids to 1,4-QH_2 and acetate solutions roughly coincided with the second overlapped peak of CV's of 1,4-QH_2 with 10.0 mM acetate. From simulations this process was found to involve proton transfer from the deprotonated hydroquinone radical ($QH^{\cdot}$) to the homoconjugate (Scheme 8A, Chapter 3.3). Construction of equilibrium plots found that the predominant species in solutions of 5.0 mM 1,4-QH_2 with 10.0 and 30.0 mM acetate, where 25.0 mM and 50.0 mM conjugate acid had been titrated was the uncomplexed 1,4-QH_2. Also, the predominant species involved in proton transfer was the homoconjugate of the particular acid under study. Though the process cannot be completely defined at the moment, it appears that the overall electron-proton transfer process is *stepwise*.

5.0 Voltammetric Simulations of One Electron – One Proton Transfer and Similar Studies Involving Viologen-Like Molecules: Understanding the Effects of Aqueous Buffer Solutions on Voltammetry

5.1 Introduction

Since the first reported electrochemical study of viologens[124] and their discovery as an herbicide,[125] the electrochemistry of various viologens or various forms of 1,1-disubstituted 4,4'-bipyridyl has been thoroughly studied.[126] However, a thorough discussion of the electron-proton transfer of the monoalkylated viologen, or N-methyl-4,4'-bipyridyl chloride ($NMBC^+$, structure 1, below), and 1-(4-Pyridyl)Pyridinium Chloride (PPC^+, structure 2, below), is nearly absent.[110, 123] In fact, to our knowledge, the cyclic voltammetry of both $NMBC^+$ and PPC^+ has never been displayed or discussed systematically in the literature. These compounds can be studied as organic "one-electron, one-proton" transfer reagents. To our knowledge most organic electron, proton transfer reagents typically display pK_a's that are close and involve the transfer of two electrons, which complicates interpretation of the voltammetry. This chapter reports on the use of these compounds as models for the description of the effects of conducting voltammetry in buffer versus non-buffered aqueous solutions.

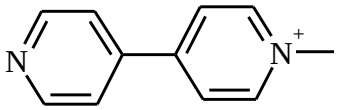

N-methyl-4,4'-bipyridyl Chloride ($NMBC^+$), **1**

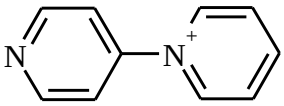

1-(4-Pyriyl)pyridinium Chloride (PPC^+), **2**

Scheme 9. Six-membered Fence Scheme for the Reduction of $NMBC^+$

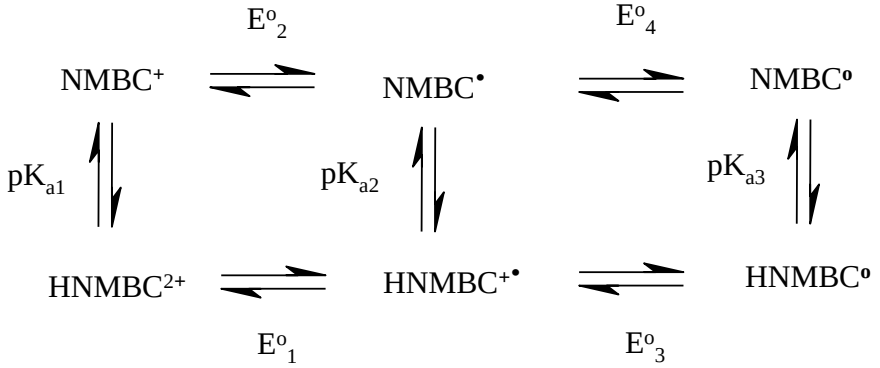

Scheme 10. Six-membered Fence Scheme for the Reduction of PPC^+

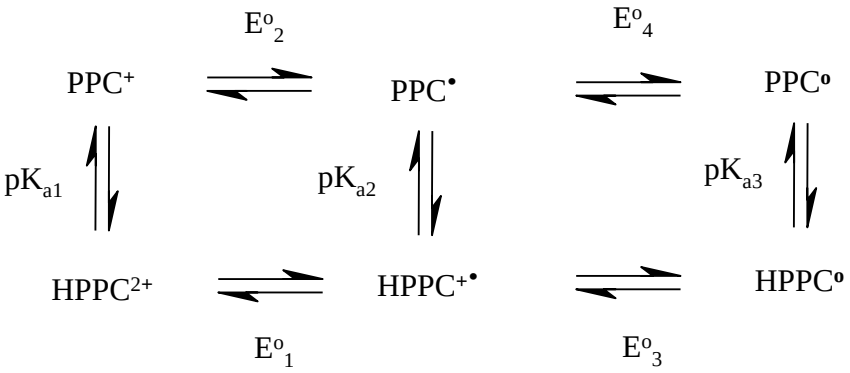

Knowledge of electrochemistry in buffered versus unbuffered systems has recently been discussed to a brief extent with another popular electrochemical staple, the quinone.[14] However, quinone chemistry, which involves 2 electron, 2 proton transfer and a nine-membered square scheme, is difficult to use to describe the intricacies of buffered versus unbuffered systems. Furthermore, as Quan et al. described, hydrogen bonding influences the voltammetric results obtained.[14] This report will focus on the reduction of $NMBC^+$ and PPC^+ and a hypothetical compound B, which are involved in a six-membered (Schemes 9 and 10) and a four-membered (Scheme 11) reduction scheme, respectively. Since the reduction of $NMBC^+$ and PPC^+ involves reversible and irreversible electron transfer, respectively, the electron transfer of B will change depending on which viologen-like compound is being discussed.

Scheme 11. Four-membered Square Scheme for the Reduction of the model compound B.

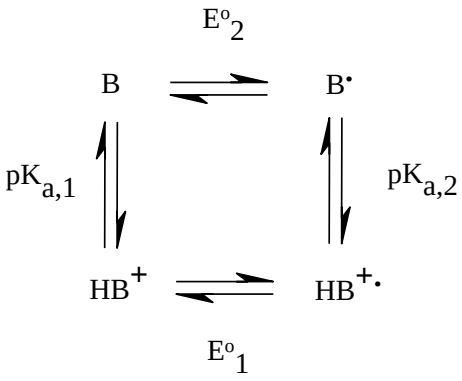

Some evidence presented below suggests that the reduction of PPC^+ involves inverted potentials, while the reduction of NMBC involves normal ordering of potentials. As an example, when a neutral organic molecule is reduced, the electron transfer (ET) produces the radical anion first and then the dianion second at a more negative potential than the first ET. The reason that the two potentials are not the same is traced to electrostatic effects, where it is more difficult to insert an electron into the negatively charged anion radical than into the neutral radical. Such an arrangement of potentials is referred to as "normal ordering."[127] Normal ordering of potentials corresponds to E^o_1 being situated at less negative potentials than E^o_2, or $E^o_1 - E^o_2 > 0$.[127] However, under certain circumstances, one finds that introduction of the second electron occurs with greater ease than the first. Under such conditions, the second reduction potential lies to the positive side of the first, or $E^o_1 - E^o_2 < 0$.[127] This ordering of potentials has been referred to as "potential inversion." In nearly every known case the cause of potential inversion is significant structural changes that accompany the electron transfer.[127-131]

This chapter is an extension of previous studies involving the study of weak acid and base effects on quinones/hydroquinones in acetonitrile (Chapters 2-4), using electrogenerated protons to enhance electrochemical currents and remove electroactive interferences with

overlapping redox potentials.[132, 133] As with previous related work, this chapter will discuss how the presence of protons, whether from a strong acid/base or weak acid/base, can influence the kinetics and thermodynamics of the reaction and the voltammetry. Furthermore, the influence of structural changes on the kinetics of the reactions and a discussion of inverted potentials also follows the goals of this dissertation.

5.2 Experimental

5.2.1 Reagents and Materials

4,4'-bipyridyl (Fluka, anhydrous, 99.9 %), idomethane (Fluka, ≥ 99.5 %), benzene (Sigma-Aldrich, 99+ %), toluene (Sigma-Aldrich, 99.8 %) Dowex 1 X 8 (Fluka, Cl^- form, 20-50 mesh), 1-(4-Pyridyl)pyridinium chloride hydrochloride hydrate (TCI America, > 98.0 %), citric acid (Fluka, anhydrous, ≥ 99.5 %), succinic acid (Fluka, ≥ 99.5 %), acetonitrile (Sigma-Aldrich, anhydrous, 99.8 %), ammonium hexafluorophosphate (Sigma, 99.99 %), tetrabutylammonium hexafluorophosphate ($TBAPF_6$, Fluka, electrochemical grade, ≥ 99.0 %), trifluoromethanesulfonic acid (Sigma, ≥ 99 %), silver nitrate (Sigma, ≥ 99 %), potassium chloride (Fluka, ≥ 99.5 %), sodium dihydrogen phosphate monohydrate (Fluka, ≥ 99.5 %), potassium hydroxide (Fisher, ≥ 85 %), deuterium hydroxide (D_2O, Sigma-Aldrich, 99.9 atom % D), sodium deuteroxide (Sigma-Aldrich, 40 wt. % solution in D_2O, 99+ % D), deuterium chloride (Sigma-Aldrich, 35 wt. % solution in D_2O, 99 atom % D), hydrochloric acid (Fisher, 37.3 % solution) and phosphoric acid (Acros Organics, 85+ % solution) were all used as received. All deionized water (18 MΩ cm) was provided by a Milli-Q Academic water filtration system (Millipore; Billerica, MA).

The synthesis of N-methyl-4,4'-bipyridyl chloride was carried out similar to that described in a previous work.[123] Equimolar quantities of 4,4'-bipyridyl and idomethane were

added to 50.0 mL of benzene. This mixture became yellow and turbid after stirring at room temperature for approximately ten minutes. Stirring of the reaction mixture continued for four days. The precipitate was filtered of and dried by vacuum. The dried precipitate was then placed into a soxhlet extractor. Extraction with 100 mL of toluene for ~4 hours removed any unreacted 4,4'-bipyridyl from the precipitate. The remaining product was then dried under vacuum at ~50-60 ^{o}C for about an hour. Then the dried material underwent a second extraction with 100 mL of acetonitrile for six hours. Using this extraction procedure any dialkylated 4,4'-bipyridyl (viologen) remains in the extraction filter. The acetonitrile was then evaporated and the resulting product was dissolved in 50 mL of deionized water and then passed through a Dowex 1 X 8 anion exchange resin, which was further eluted with deionized water. The water was then removed under reduced pressure until ~10 mL remained. The rest of the water was removed by azeotropic distillation with benzene in a Dean-Stark trap to obtain off-white crystals (0.30648 g). ^{1}H-NMR in D_2O of the product revealed a singlet at 4.282 ppm and doublets centered at 7.76, 8.23, 8.63, and 8.73 ppm. The ratio of the integration of the singlet to each of the doublets revealed a value of 1.5, indicating production of the monoalkylated 4,4'-bipyridyl.

Synthesis of 1-(4-pyridyl)pyridinium hexafluorophosphate involved a methathesis reaction of 1.00048 g of 1-(4-Pyridyl)pyridinium chloride hydrochloride hydrate (4.36681 mmol) with 2.14626 g of ammonium hexafluorophosphate (13.1672 mmol) in 50 mL of deionized water. The metathesis reaction produced a white precipate that was washed with three 50 mL aliquots of deionized water and dried by vacuum filtration.

5.2.2 Electrochemical Methods

All electrochemical experiments were performed using a CHI660C potentiostat (CH Instruments, Austin, TX) incorporating a CHI200B Faraday cage and picoampbooster.

Electrochemical measurements were conducted under nitrogen in a jacketed, three electrode cell (10 mL) incorporating a GCA Precision water recirculator (model R10a) set to 300 K. A single 0.3 cm diameter glassy carbon electrode (CH Instruments, with area 0.072 cm^2) was used during this work. A large platinum flag electrode served as the auxiliary electrode, and the reference electrode was an Ag/AgCl electrode (CH Instruments). Prior to each experiment the highly polished glassy carbon electrode was polished using 0.05 μm alumina paste (Buhler, Lake Bluff, Il) and then washed with deionized water, then the body of the electrode was carefully wiped. In each experiment the solution resistance (R_u) was totally compensated via positive feedback. For each set of experimental conditions described CV's were recorded at seven different scan rates.

For work in acetonitrile, a platinum flag electrode was used, while the reference electrode was an Ag/Ag^+ electrode (a silver wire immersed in the supporting electrolyte, 0.2 M $TBAPF_6$/3.0 mM silver nitrate/acetonitrile). The potential of the Ag/Ag^+ reference electrode in acetonitrile was periodically measured versus the formal potential (measured as the average of the peak potentials) of the ferrocene/ferrocenium (Fc/Fc^+) couple under the same conditions as the other experiments and thus all potentials in acetonitrile are reported versus ferrocene as Fc/Fc^+. Prior to each experiment in acetonitrile the polished glassy carbon electrode was first polished using 0.05 μm alumina paste (Buhler, Lake Bluff, Il) washed with deionized water, carefully wiped, washed with acetonitrile and then sonicated for three minutes in acetonitrile.

5.2.3 NMR Spectroscopic Methods

^{1}H-NMR spectra and pulsed gradient echo (PGE-) ^{1}H-NMR diffusion coefficients were obtained on a Varian Inova-400 MHz spectrometer. The same procedure involving PGE-^{1}H-NMR as used in the QH_2/Q chapters (Chapters 2-4) was used here to determine the diffusion coefficients of $NMBC^+$ and PPC^+ at various pH's.[126] The applied gradients in the PGE-^{1}H NMR

experiments were calibrated by measuring the diffusion coefficient of HDO (2.23×10^{-5} cm^2 s^{-1}, at 25°C, 0.03%) in a D_2O sample and the diffusion coefficient of 1,6-diaminohexane (6.98×10^{-6} cm^2 s^{-1}, at 25°C, 0.04%). The pulse sequences and associated parameters are reported in the appendix.[79] The diffusion coefficients were measured under the same conditions as the electrochemical experiments, with the exceptions of measurements in D_2O and without supporting electrolyte or buffer. For a discussion on the correction of diffusion coefficients at various pH's and in various buffers see the appendix.[88]

5.2.4 Computational and Digital Simulations

Digital simulations were conducted using DigiSim version 3.03 (Bioanalytical Systems, Inc., West Layfayette, IN). For each of the described simulations, the known or estimated values of the E^o's, α's, pK_a's and D's were input into the simulation, while the other parameters were allowed to fit iteratively at each scan rate until a consistent set of parameters was obtained. The E^o values were determined or estimated from the CV's in unbuffered solution, α remained 0.5, pK_a's were determined by base titration and via reduction in 0.1 M phosphate from pH 1 to 12. D values were determined from the PGE-^{1}H-NMR results of both $NMBC^+$ and PPC^+ (typically 0.73 to 1.6 x 10^{-5} cm^2 s^{-1}). The fitted heterogeneous rate constants for $NMBC^+$ (k_s) were reversible and on the order of 0.12 to 0.01 cm s^{-1}. The fitted heterogeneous constants for PPC^+ in pH 4 succinate buffer were 2 x 10^{-6} ($k_{s,1}$) 5.8 x 10^{-9} ($k_{s,2}$) 2 x 10^{-9} ($k_{s,3}$) and 1.7 x 10^{-4} cm s^{-1} ($k_{s,4}$). The disproportionation constant for PPC^+ was K_{dis} = 0.256 and the associated forward rate constant was determined to be 5 x 10^4 M^{-1} s. However, the variation in peak height noted in the CV's is likely due to weak absorption.

For the simulations involving reduction of the hypothetical compound, B, in simulated unbuffered conditions, the following set of equations were incorporated,

$$B + H^+ \rightleftharpoons BH^+ \quad (43)$$

$$B + e^- \rightleftharpoons B^\cdot \quad (44)$$

$$B^\cdot + H^+ \rightleftharpoons BH^{+\cdot} \quad (45)$$

$$BH^+ + e^- \rightleftharpoons BH^{+\cdot} \quad (46)$$

For the simulation of B under buffered conditions the following equations were employed,

$$B + AH_n \rightleftharpoons BH^+ + AH_{n-1}^{-n} \quad (47)$$

$$B + e^- \rightleftharpoons B^\cdot \quad (48)$$

$$B^\cdot + AH_n \rightleftharpoons BH^{+\cdot} + AH_{n-1}^{-n} \quad (49)$$

$$BH^+ + e^- \rightleftharpoons BH^{+\cdot} \quad (50)$$

where *n* represents the number of protons that the acid species (AH) of the buffer has to transfer. For each proton that AH has to transfer the number of equations to model this system increases by two. Using the same notation as given in Scheme 11, above, the reversible model is simulated using E^o_1 = 0 V, $pK_{a,1}$ = 2, $pK_{a,2}$ = 10, α_1 and α_2 = 0.5, and the D values for all species was 1 x 10^{-5} cm^2 s^{-1}. Reversible values of $k_{s,1}$ and $k_{s,2}$ were incorporated (0.1 cm s^{-1}). E^o_2 was determined using equation 51. The irreversible model is simulated using the parameters, E^o_1 = 0.238 V, $pK_{a,1}$ = 2, $pK_{a,2}$ = 6, α_1 and α_2 = 0.5, and the D values for all species was 1 x 10^{-5} cm^2 s^{-1}. Irreversible values of $k_{s,1}$ and $k_{s,2}$ were incorporated (1 x 10^{-5} cm s^{-1}). The simulated concentrations of B in both the reversible and irreversible case were 2.0 mM, the same as for the studies of $NMBC^+$ and PPC^+. The values for the homogeneous rate constants were fast and were not allowed to fit to values greater than 1 x 10^9 for the simulations of $NMBC^+$, PPC^+ and B, except where noted.

$$E^o_1 = E^o_2 + (2.3RT/F)(pK_{a,2} - pK_{a,1}) \quad (51)$$

Geometries were fully optimized in the gas-phase using B3LYP density functional theory and the 6-31G* basis set using the *Gaussian 03* suite of programs.[41] Minima were verified to have all real vibrational frequencies. The vibrational frequency calculations also provided the necessary parameters to compute zero-point and thermochemical corrections to energies. Geometry optimization and vibrational frequency analyses were also performed in the presence of implicit water ($\varepsilon = 78.39$) as solvent using the polarizable continuum model, PCM.[54, 91, 134] The solvation phase geometries were optimized using B3LYP density functional theory and with the 6-31* basis set. Open-shell species were treated using the unrestricted formalism of the aforementioned level of theory, UB3LYP, respectively. The radius of the geometry optimized structures of the reactant species for use in determining the total reorganization energies (λ_T) was determined through a volume *ab initio* calculation. The volume calculation involves the use of the *volume* keyword in Gaussian 03. The *volume* calculation requests that the molecular volume be computed, which is defined as the volume inside a contour of 0.001 electrons/bohr^3 density.

5.3 Results and Discussion

5.3.1 Results of a Reversible Hypothetical One Electron – One Proton Transfer Molecule and Correltation with N-Methyl-4,4'-Bipyridyl Chloride

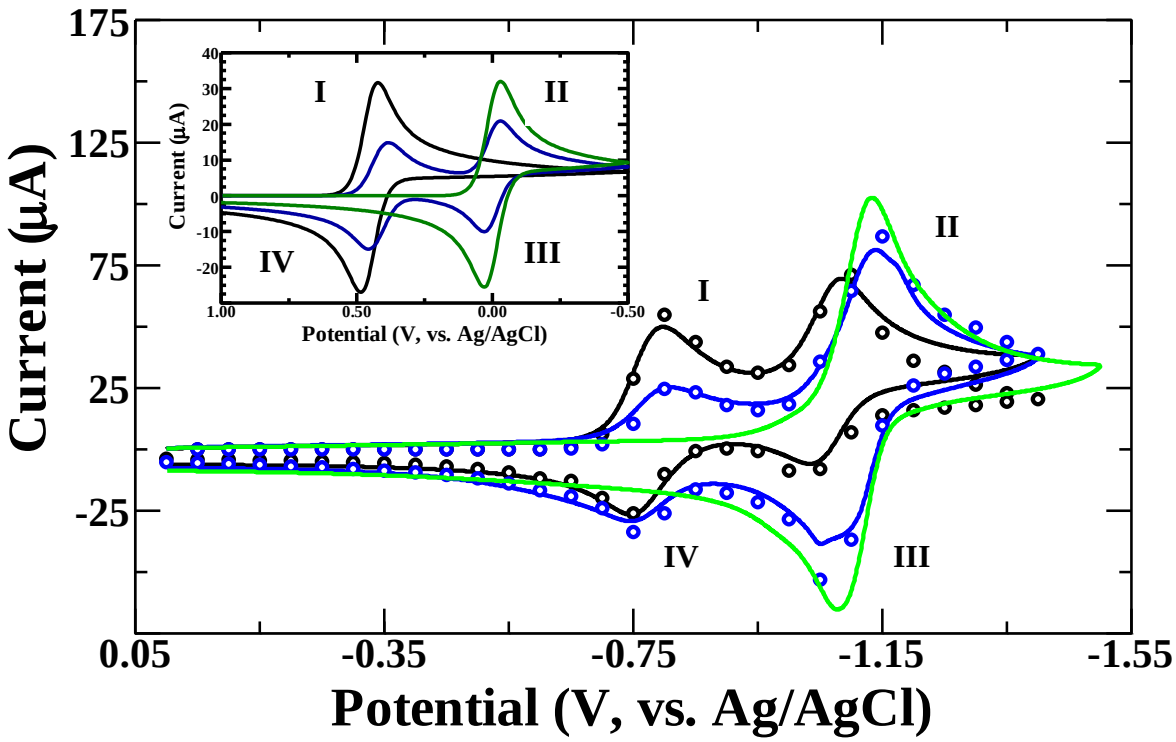

Figure 28. Experimental (solid lines) and simulated (circles) CV's of N-Methyl-4,4'-Bipyridyl Chloride ($NMBC^+$) in unbuffered solution with KCl (I = 0.5) at pH 3.35 (black), 4.01 (blue) and 7.00 (green). Experiments performed at a glassy carbon electrode (0.073 cm^2) at 0.2 V s^{-1} at 300 K. Inset: Simulations of the reduction of 2.0 mM of the theoretical compound, B, at pH 2 (black), 3 (blue) and 7 (green).

Figure 28 shows three cyclic voltammograms (CV's) of 2.0 mM N-methyl-4,4'-bipyridyl chloride ($NMBC^+$) in three solutions of constant ionic strength (I = 0.5) at pH 3.35, 4.01 and 7.00. The CV's at pH 3.35 and 4.01 show two redox peak systems. The peak at -0.75 V (vs. Ag/AgCl, E^o_1), peak I, is the reversible ($k_{s,1}$ = 0.05 cm s^{-1}, from simulation) one-electron reduction, as determined by chronocoulometry, of protonated $NMBC^+$ ($HNMBC^{2+}$). Peak II

centered at -1.06 V (vs. Ag/AgCl, E^o_2) is the reduction of the protonated $NMBC^+$ radical cation ($HNMBC^{+\cdot}$). The number of electrons transferred at peak II at this pH is assumed to be one, judging from the similarity of the peak current of peaks I and II. However, the peak II peak current at lower pH (< 3) indicates that weak absorption of $HNMBC^{+\cdot}$ takes place.[24] At pH < 3, peak II is sharp and exhibits a large peak current, while peak III is nonexistent, and peak IV displays a smaller than expected peak current. Furthermore, numerous scans at any particular scan rate show the same amount of peak current for each of the peaks. This further indicates that the adsorption event is weak, versus a strong adsorption which significantly influences future scans due to electrode modification.[24, 135] Peaks I and IV can be studied alone at lower pH's (pH < 5) by narrowing the potential window (starting potential = -0.4 V, switching potential = -0.9 V) studied to encompass only the reduction of $HNMBC^{2+}$. Narrowing of this potential window at pH < 3.5 results in a nearly perfect CV, with a peak current ratio near unity ($i_{p,IV}/i_{p,I}$) and peak separation ($\Delta E_p = E_{p,I} - E_{p,IV}$) of -0.052 V. As the pH increases beyond 3.5, ΔE_p increases as the peak system related to the reduction and oxidation of $HNMBC^{2+}$ and $HNMBC^{+\cdot}$, respectively, becomes broader until it vanishes at pH ~4.5.

Peaks II and III, in the CV at pH 4.01, are broader, by 0.014 V, than at pH 3.35 or 7.00. This displays the overlap of the reduction of $HNMBC^{+\cdot}$ and the unprotonated $NMBC^+$ radical ($NMBC^{\cdot}$**)**. The reduction potential of $HNMBC^{+\cdot}$ **(**E^o_3, -1.06 V vs. Ag/AgCl) is more positive than that of $NMBC^{\cdot}$ (E^o_4, -1.12 V vs. Ag/AgCl), as determined by simulation and CV inspection. Figure 28 also displays the CV of $NMBC^+$ at pH 7.00, where only the two-electron reduction, as determined by chronocoulometry, of $NMBC^+$ is centered at approximately -1.13 V (vs. Ag/AgCl). Voltammetry collected at higher scan rate at pH ≥ 5 indicates the weak adsorption of $NMBC^o$. As the scan rate increases at pH > 5 the $i_{p,III}/i_{p,II}$ increases to greater than unity.[35, 136]

Since it is not possible to simulate a CV exhibiting electrode adsorption, whether weak or strong, using DigiSim, CV's with simulations are only shown for CV's where 3.35 < pH < 5, where the observed influence of electrode absorption is small.[137] The Scheme used for simulating the reduction of $NMBC^+$ in unbuffered H_2O is given in Scheme 12. Equation 59, below, was the only ion-pairing/disproportionation reaction that was found to fit the voltammetric data.[24, 135]

Scheme 12. Reduction process used for the simulation of $NMBC^+$ in unbuffered aqueous solution.

$$NMBC^+ + H^+ \rightleftharpoons HNMBC^{2+} \quad (52)$$

$$NMBC^+ + e^- \rightleftharpoons NMBC^{\cdot} \quad (53)$$

$$NMBC^{\cdot} + H^+ \rightleftharpoons HNMBC^{+\cdot} \quad (54)$$

$$HNMBC^{2+} + e^- \rightleftharpoons HNMBC^{+\cdot} \quad (55)$$

$$HNMBC^{+\cdot} + e^- \rightleftharpoons HNMBC^{o} \quad (56)$$

$$NMBC^{\cdot} + e^- \rightleftharpoons NMBC^{o} \quad (57)$$

$$NMBC^{o} + H^+ \rightleftharpoons HNMBC^{o} \quad (58)$$

$$HNMBC^{2+} + HNMBC^{o} \rightleftharpoons (HNMBC)_2^{2+} \quad (59)$$

From Figure 28 we note that as the pH increases from 3.35 to 7.00 the peak current of peaks II and III increase at the expense of peaks I and IV. The inset of Figure 28 demonstrates a similar case to that of $NMBC^+$, with reduction of the hypothetical model, B. As with the reduction of $NMBC^+$, reduction of B causes peaks II and III to increase at the expense of peaks I and IV as the pH increases from 2 to 7. Here, B undergoes electron and proton transfer with pK_a ($pK_{a,1}$ = 2 and $pK_{a,2}$ = 10) values similar to $NMBC^+$. Displacement of the first peak system (peaks I and IV) to the second peak system (peaks II and III) can be determined by equation 51, and is set by the pK_a's of the compound of interest. Therefore, the reduction of $NMBC^+$ under

unbuffered conditions is governed primarily by the single thermochemical parameter, pK_a. The only influence on kinetics is noted within the range of pH = $pK_{a,1}$ ± 1 for both the reduction of $NMBC^+$ and B, as determined by the change in the peak-to-peak separation (ΔE_p). The average ΔE_p of $NMBC^+$ (measured from peak I and IV, pH ≤ $pK_{a,1}$) was consistent and averaged 0.052 V, except within the pH range of ~3.5 to ~7 for peak systems I-IV and II-III, where the peak separation was ~0.08 V and ~0.07, respectively throughout this range. This was also noted for the reduction of B, where the peak separation averaged 0.06 V, until pH ~ 2.5, when it increased to 0.075 V. At higher pH values the peak separation decreased to the expected values of 0.059 V for B and ~0.030 V for $NMBC^+$ (higher pH only the two electron peaks II and III are noted, where 0.029 V is an ideal ΔE_p for a two ET process).[24] This kinetic change is due to the decreased proton concentration at the electrode due to the increase in pH_{bulk} and the influence of the reduced $NMBC^+$ species, $HNMBC^o$ ($pK_{a,2}$ = 8.5, from simulations) and $NMBC^o$ ($pK_{a,3}$ = 9.5, from simulations). Between pH 3 and 4 the pH at the electrode can be estimated to be ~6.10, based on the $pK_{a,2}$ and $pK_{a,3}$ of $NMBC^+$.[24] Therefore, within the range of pH = $pK_{a,1}$ ± 1 the kinetic change could be described as moving from an CE (C, chemical step or proton transfer (PT) first; E, electron transfer (ET) second) path at pH < $pK_{a,1}$ to an EC path at pH < $pK_{a,2}$.

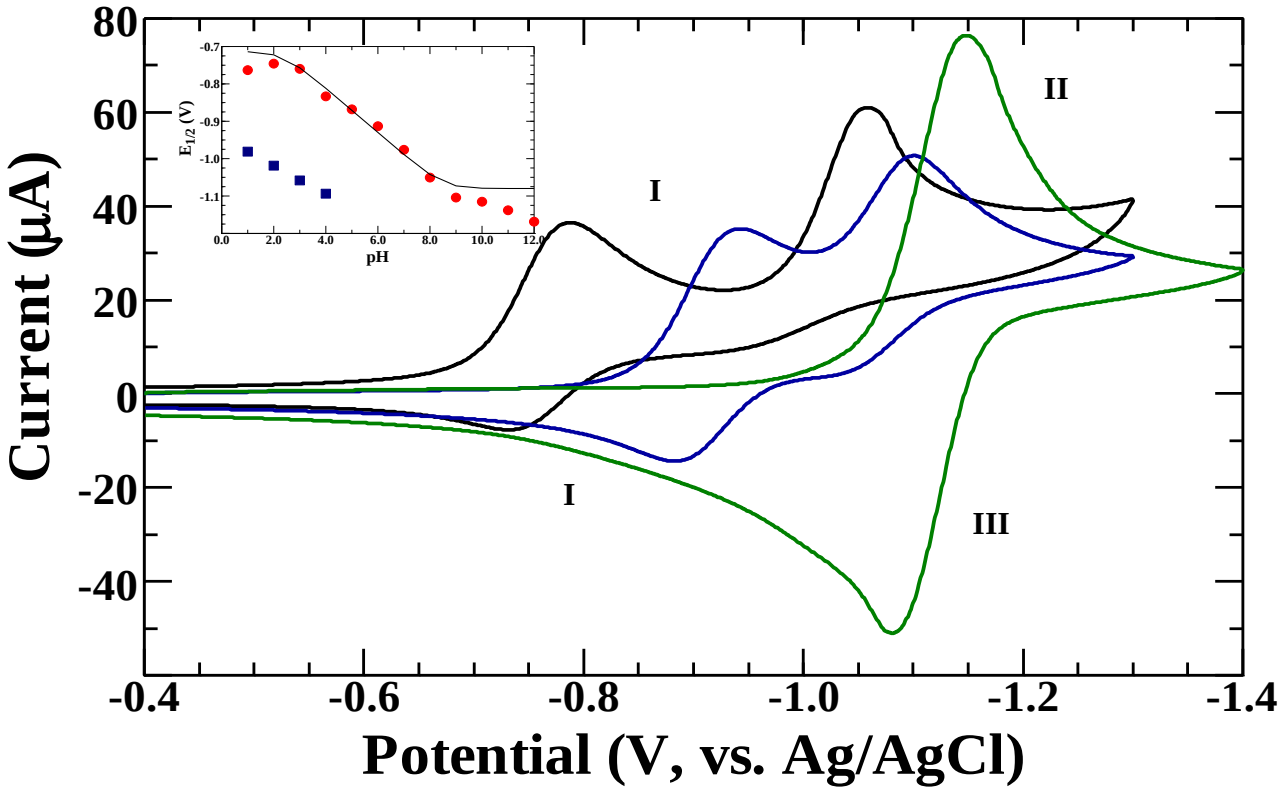

Figure 29. CV's of 2.0 mM N-Methyl-4,4'-Bipyridyl Chloride (NMBC) in 0.1 M phosphate buffer with KCl (I = 0.5) at pH 3 (black), 6 (blue) and 10 (green). Experiments performed at a glassy carbon electrode (0.073 cm^2) at 0.1 V s^{-1} at 300 K. Inset: Plot of $E_{1/2}$ versus pH for peaks I and IV (red circles) and peaks II and III (blue squares). Fitted black line represents the fitting of equation 60 to the $E_{1/2}$ versus pH data for peaks I and IV.

Reduction of $NMBC^+$ in the presence of 0.1 M phosphate buffer, ionic strength 0.5, causes an incremental thermodynamic shift as the pH increases from pH 3 to 9 as depicted in Figure 29. Figure 29 shows the reduction of $HNMBC^{2+}$, peak I, shift from -0.78 V at pH 3 to -0.943 V at pH 6. At pH 10 this thermodynamic shift is complete and a single two electron peak is found at -1.148 V. Again, due to weak surface adsorption of both $HNMBC^{+\cdot}$ and $NMBC^o$ throughout the buffered studies, accurate simulations could not be attempted. Weak adsorption caused very little current from peak IV to be noted and peak III was nonexistent until pH 8. At pH > 8 the peak current of peak III was found to increase with increase in scan rate. Likewise, the $i_{p,III}/i_{p,II}$ increased to greater than unity with increase in scan rate. Similar effects with 0.1 M

citrate buffer solutions were also found. This demonstrates that there is no chemical dependence on the buffer itself.

Elementary knowledge of the Nernst equation shows that for any *m* H^+, *n* e^- electrochemical reaction the observed redox potential will change by –(*m*/*n*)0.059 V/pH unit.[138, 139] From the discussion of Figures 28 and 29, above, we know that peak I represents a 1 H^+, 1 e^- transfer. Therefore, varying the pH between $pK_{a,1}$ and $pK_{a,2}$ of $NMBC^+$ one should note a change in the observed half potential ($E_{1/2}$) of approximately -0.060 V pH^{-1} unit. $pK_{a,1}$ and $pK_{a,2}$ can be found at the inflexion points of the plot of $E_{1/2}$ versus pH, inset of Figure 29. The slope of the line in the inset of Figure 29 was found to be -0.053 V pH^{-1} unit (R^2 = 0.99). Fitting the data of the Figure 29 inset to equation 60 using nonlinear least squares regression gives the solid black line.[117] The fitting of this line corresponds to E^o_2 = -1.08 V (vs. Ag/AgCl), $pK_{a,1}$ = 2.35 and $pK_{a,2}$ = 8.52. Also displayed in the inset is the plot of the shift of peak II between pH 1 and 4, which was found to have a slope of -0.038 V pH^{-1} unit (R^2 = 0.99). At pH > 4, the $E_{1/2}$ versus pH plot goes through a plateau until peaks I and II merge. Since the plot of the $E_{1/2}$ versus pH for peak II through most of this pH range (1 to 4) represents a one-electron, one-proton transfer, the slope should be -0.060 V pH^{-1} unit. However, this reduction is likely influenced by the weak adsorption of $HNMBC^{+\cdot}$ and $NMBC^o$.

$$E_{1/2} = E^o_2 + (2.3RT/F)\log((1+[H^+]/K_{a,2})/(1+[H^+]/K_{a,1})) \quad (60)$$

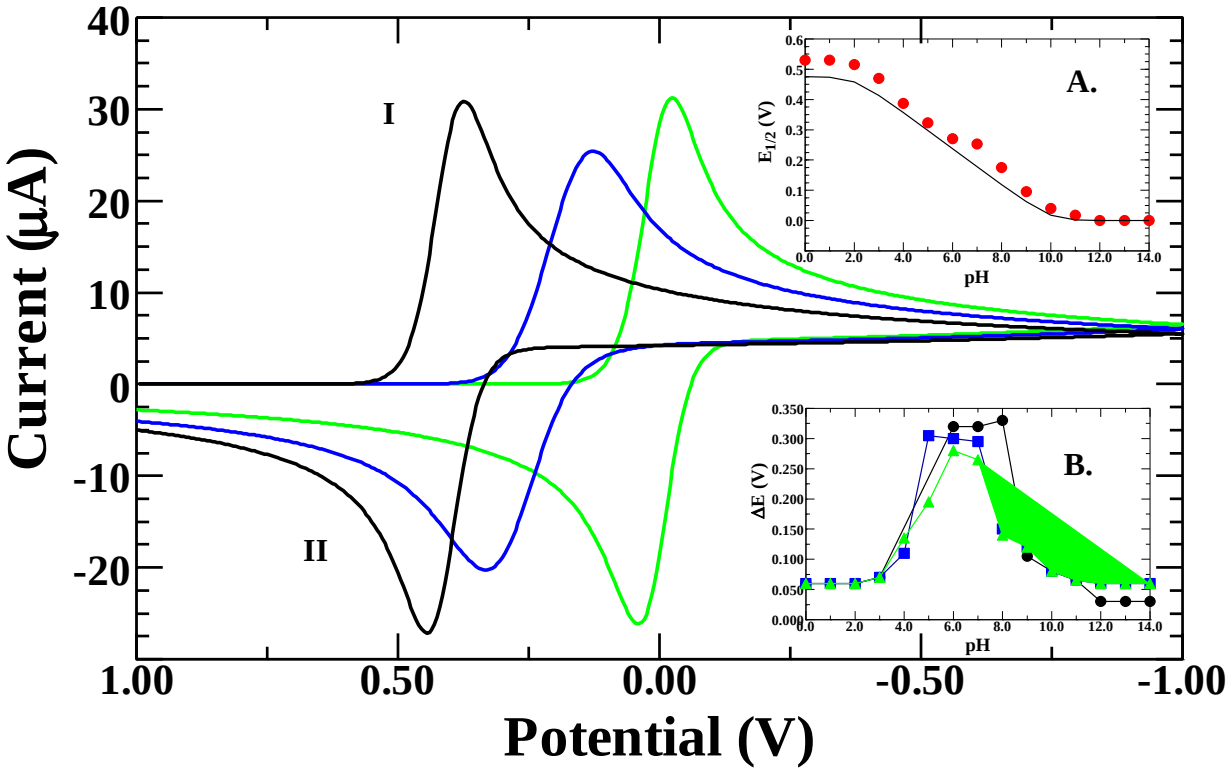

Figure 30. Simulated CV's of 2.0 mM B in a simulated 0.1 M phosphate buffer at pH 3 (black), 6 (blue) and 10 (green). Inset: (A.) Plot of $E_{1/2}$ versus pH for peaks I and II (red circles), fitted black line represents the fitting of equation 60 to the $E_{1/2}$ versus pH data for peaks I and II. (B.) Plot of ΔE_p versus pH for proton transfer rate constant values of 1 x 10^7 (black dots and line), 1 x 10^8 (blue squares and line) and 1 x 10^9 M^{-1} s^{-1} (green triangles and line).

The reduction of the hypothetical compound, B, in a simulated 0.1 M phosphate buffer (buffer component concentrations determined from an α plot) solution, Figure 30, shows a similar thermodynamic shift between $pK_{a,1}$ and $pK_{a,2}$.[140] As the pH of the simulated phosphate buffer solution increases from 3 to 10, peak I shifts -0.059 V/pH unit (inset Figure 30, R^2 = 0.99). The plotted black line in inset A of Figure 30 uses equation 60 and the parameters assigned to the model (Scheme 11 and Experimental section). This model reduction further demonstrates the similarity of the reduction of $NMBC^+$ and B.

The thermodynamic effects of increasing the pH are further complicated between the two pK_a's of $NMBC^+$ and B by kinetic effects. The peak separation of the cathodic and anodic peaks again increase between $pK_{a,1}$ and $pK_{a,2}$. The peak separation of peak I for $NMBC^+$ in 0.1 M phosphate increases from 0.059 V at pH 1 to 0.091 V at pH 8. However, the peak separation of B increases from 0.059 V to as high as 0.280 V at pH 8 using the maximum studied proton transfer rate constant of 1 x 10^9 M^{-1} s^{-1}. At higher pH, pH ~ 12, the peak separation of the cathodic and anodic peaks of $NMBC^+$ becomes 0.05 V while that of B, becomes 0.059 V. Obviously, peak separation is not consistently large for both studies, but the separation is expected to decrease to approximately 0.0295 V for $NMBC^+$ at pH 12, as this is a two electron reduction. The cause of this kinetic influence is due to the switching of the reaction path from a CE to an EC mechanism. This conclusion is affirmed and amplified by changing the maximum rate constant for each of the proton transfers of B in simulated phosphate at varied pH, inset B of Figure 30. At approximately the midpoint (between pH 6 and 8) between $pK_{a,1}$ and $pK_{a,2}$, the peak separation increases as the maximum rate constant for proton transfer decreases from 1 x 10^9 to 1 x 10^7 M^{-1} s^{-1} (ΔE_p = 0.28 to 0.33 V, respectively). Recently, another work has performed similar findings, yet monitored the logarithm of the apparent standard rate constant versus pH in the study of surface bound species involved in concerted-proton electron transfer (CPET).[103, 141]

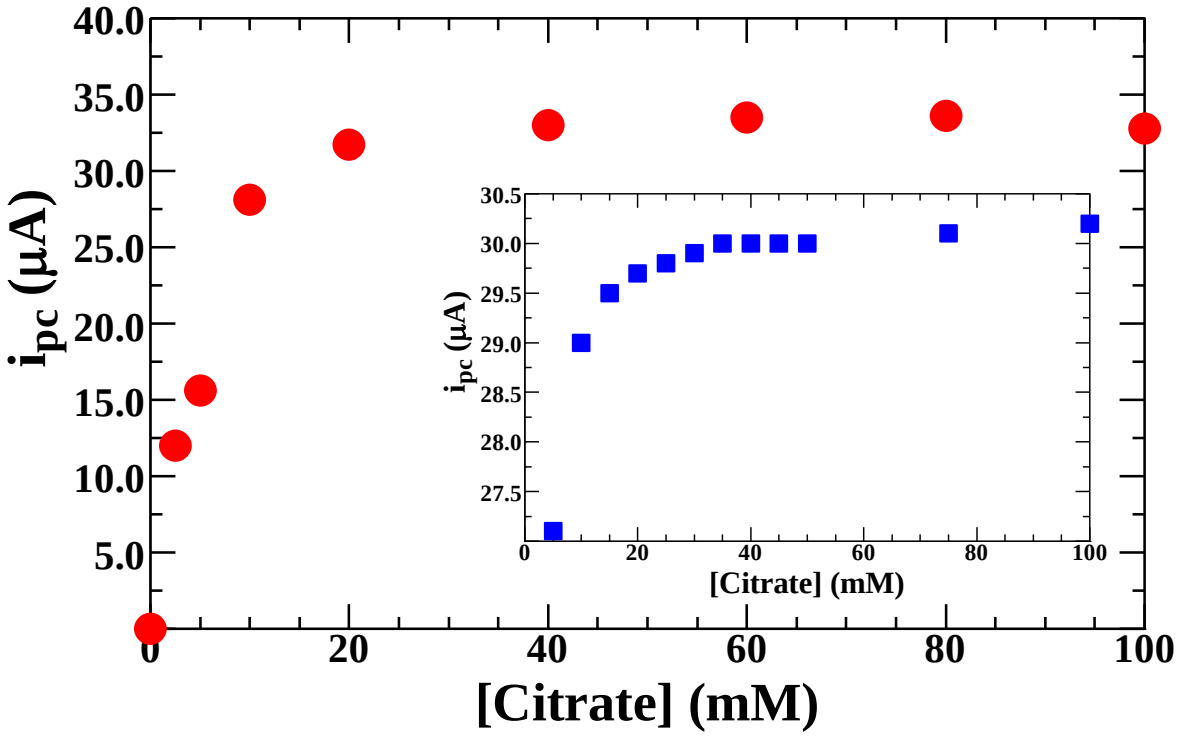

Figure 31 – Plot of i_{pc} (peak I) versus citrate buffer concentration for 2.0 mM of $NMBC^+$. Inset: Plot of i_{pc} versus simulated citrate buffer concentration for the hypothetical model compound, B.

Furthermore, one can amplify the CE to EC transition experimentally or through simulations by studying the effect of buffer concentration at pH 6 (pH between $pK_{a,1}$ and $pK_{a,2}$) for both $NMBC^+$ and B. As the buffer concentration decreases the peak current for peak I decreases. A plot of the peak current of peak I (i_{pc}) as a function of buffer concentration reveals an inflection point in these plots for both $NMBC^+$ (at 20 mM citrate) and B (~40 mM citrate). The inflection point divides the reduction into two kinetic regimes for $NMBC^+$ and B, Figure 31 and inset, respectively. Such behavior has been observed in studies involving general acid/base catalysis, and has been considered an indication of a change in the rate-determining step of the reaction.[103, 141] At lower concentrations of buffer, proton transfer is rate limiting. Reduction of $NMBC^+$ or B at the electrode causes the pH to increase, which limits the peak current measured at peak I. However, at higher concentrations of buffer the electron transfer is rate limiting,

because the proton concentration is fixed. Furthermore, the ΔE_p of both $NMBC^+$ and B increase as the concentration of citrate decreases. The ΔE_p increases from an average of 0.052 V between 100 mM citrate to 20 mM citrate to as high as 0.124 V at 2.5 mM citrate. Likewise, the ΔE_p of B increases from an average of 0.059 V between 100 to 25 mM citrate to as high as 0.085 V at 2.5 mM citrate.

5.3.2 Results of an Irreversible Hypothetical One Electron – One Proton Transfer Molecule and Correltation with 1-(4-Pyridyl)Pyridinium Chloride

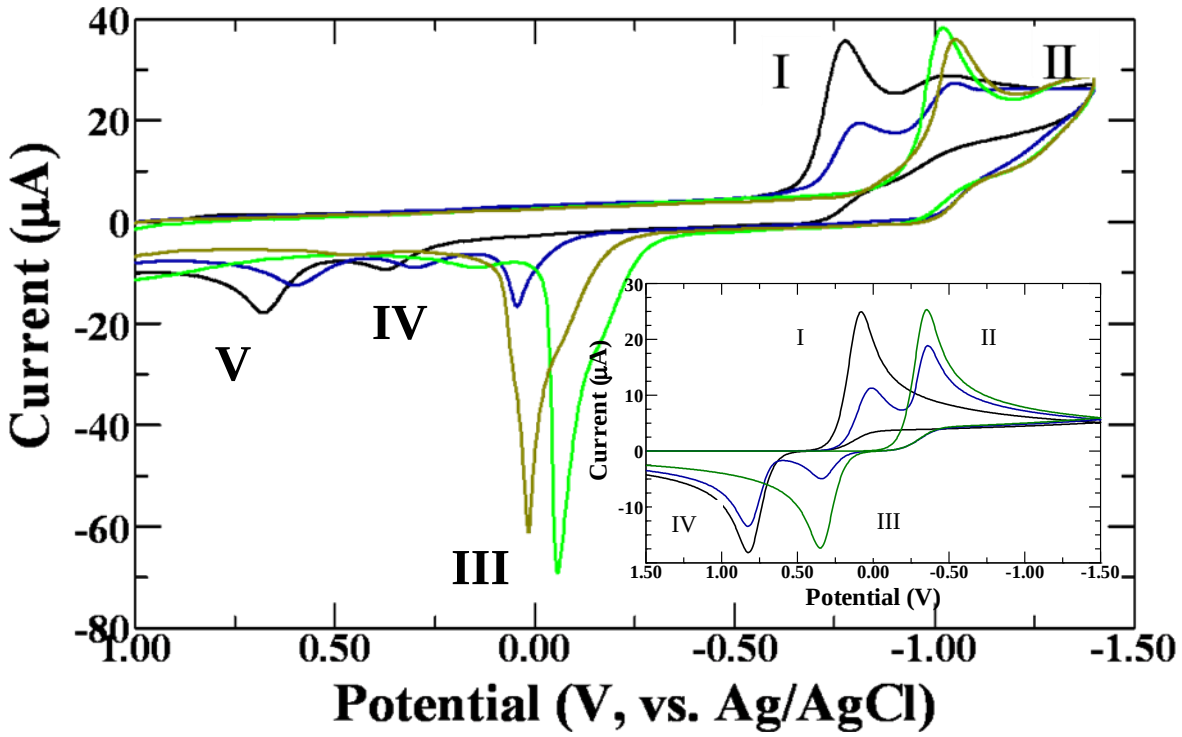

Figure 32. Experimental CV's of 1-(4-Pyridyl)pyridinium Chloride (PPC) in unbuffered solution with KCl (I = 0.5) at pH 2.87 (black), 3.65 (blue), 7.80 (gold) and 10.82 (green). Experiments performed at a glassy carbon electrode (0.073 cm^2) at 0.1 V s^{-1} at 300 K. Inset: Simulations of the reduction of 2.0 mM of the theoretical compound, B, at pH 2 (black), 3 (blue) and 7 (green).

Figure 32 shows four irreversible cyclic voltammograms (CV's) of 2.0 mM 1-(4-pyridyl)pyridinium chloride (PPC^+) in three solutions of constant ionic strength (I = 0.5) at pH

2.87, 3.65, 7.80 and 10.82. The CV at pH 2.87 shows two reduction peaks labeled I and II. Peak I at -0.776 V (vs. Ag/AgCl) is the irreversible one electron reduction, as determined by chronocoulometry, of protonated PPC^{+} ($HPPC^{2+}$). Peak II centered at -1.038 V (vs. Ag/AgCl) is the reduction of the protonated PPC^{+} radical cation ($HPPC^{+\cdot}$) to completely reduced $HPPC^{2+}$, or $HPPC^{o}$. The number of electrons transferred at peak II at pH < 3 is found to be one, based on the subtraction of the total number of electrons transferred between -0.5 and -1.4 from those transferred between -0.5 to -0.9 V measured via chronoamperometric scans. As the pH increases, the current of peak II increases at the expense of peak I. At higher pH, specifically pH = 10.82, the cathodic peak is found at -1.021 V vs. Ag/AgCl. The number of electrons transferred at peak II at higher pH is one based on chronoamperometric data. Another cathodic peak (unlabeled) is found at higher pH just beyond the potential window -1.33 V that exhibits much slower kinetics than that found at either -0.776 or -1.021 V. However, upon widening the potential window by 0.2 V, no further reduction peaks are found.

The description of the oxidation peaks is more complex. The oxidation peaks of PPC^{+} as displayed in Figure 32 are labeled III through V. At lower pH, pH 1 to 3, only two oxidation peaks are found, IV and V, around 0.4 and 0.65 V. These two peaks shift to more negative potentials as the pH increases until pH > 3, where a new sharp anodic peak, III, found ~0.05 V, develops at the cost of peak V, as peak IV remains, yet continues to shift to more negative potentials. Peak III shifts as well, as the pH increases to -0.057 V at pH 10.82. The sharp anodic peak at greater pH's is likely due to the oxidation of adsorbed PPC^{+} dimers, $(PPC)_2$. The $(PPC)_2$ is likely less soluble in water due to its molecular size and high concentration at the electrode face. The oxidation process at peak III involves the one electron splitting of the $(PPC)_2$, then the one electron one electron oxidation of the completely reduced PPC^{+}, referred to as PPC^{o}.

Finally, the reduction of the PPC^+ radical cation, $PPC^{+\cdot}$, takes place at peak IV. Overall, the oxidation process at high pH involves the transfer of three electrons, as confirmed by double-step chronoamperometry and coulometry.

With the intention of understanding the voltammetry of PPC^+ over the pH range of 1 to 12, a hypothetical redox species B was studied via digital simulations. The inset of Figure 32 displays the CV's of B, an irreversible reduction (where $k_s = 1 \times 10^{-5}$ cm s^{-1}) at pH 2, 3 and 7. At pH 2 a single one-electron redox peak system is found, peaks I and IV, these peaks are centered at -0.097 and 0.646 V. As the pH increases, by increasing the proton concentration in the simulator, a new peak system, peaks II and III, develops at the cost of peaks I and IV. The potential difference of this peak displacement is governed by $pK_{a,1}$ (2) and $pK_{a,2}$ (7), defined in the simulation parameters. These new peaks, II and III, are found at -0.353 and 0.349 V at pH 7, and do not shift to other potentials as the pH increases. Interestingly, the peaks I through IV do not shift significantly upon their formation as the pH increases or decreases. However, those of PPC^+ do shift as the pH changes.

Kinetic effects on the reduction of PPC^+ and B are significantly different. The kinetic effects of increasing the pH of the solution involve the broadening of the peak separation, ΔE_p. This effect is more easily visualized in the reduction of B rather than PPC^+. At pH 0 and the pH range between 4 and 12 the ΔE_p is 0.704 V. However, within the pH range of 1 to 3 the ΔE_p increases dramatically to as great as 1.266 V. Such an effect is not as easily visualized with the reduction of PPC^+ over the same pH range 1 to 12. At pH 1 the ΔE_p is 1.109 V and this increases to 1.137 V at pH 3. However, under moderate to high pH conditions, 7.8 to 12, the ΔE_p averages at 0.987 V.

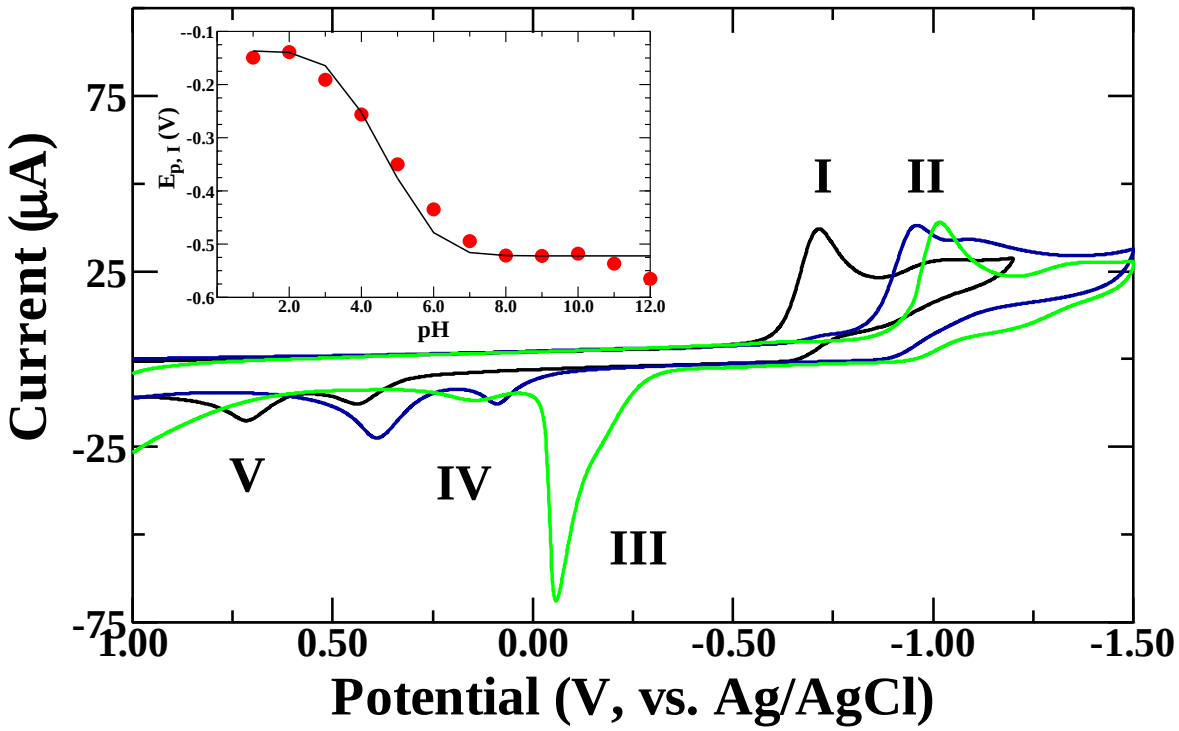

Figure 33. CV's of 2.0 mM (4-Pyridyl)pyridinium Chloride (PPC) in 0.1 M phosphate buffer with KCl (I = 0.5) at pH 2 (black), 6 (blue) and 11 (green). Experiments performed at a glassy carbon electrode (0.073 cm^2) at 0.1 V s^{-1} at 300 K. Inset: Plot of $E_{1/2}$ versus pH for peak I (red circles). Fitted black line represents the fitting of equation 61 to the $E_{p, I}$ versus pH data for peaks I and IV.

The reduction of PPC^+ in the presence of 0.1 M phosphate buffer, ionic strength 0.5, causes an incremental thermodynamic shift of each of the peaks as the pH increases from pH 3 to 9 as shown in Figure 33. Figure 33 shows the reduction of $HPPC^{2+}$, peak I, shift from -0.702 V at pH 2 to the reduction of PPC^+, peak II, at -1.033 V at pH 11. At pH ~7 this thermodynamic shift is complete and only peak II and the kinetically slow single electron transfer peak (unlabeled) are found at -1.03 and -1.331 V, respectively. The oxidation peaks of PPC^+, as displayed in Figure 33, are more difficult to interpret than those discussed previously under unbuffered conditions, Figure 32, due to the shifting peak potentials. Peak V, shown in the CV at pH 2, disappears as the pH is increased and is no longer noted in the CV at pH 6. The CV at

pH 6 displays two oxidation peaks, III and IV, at 0.031 and 0.333 V. At pH 11 the oxidation peaks, III and IV, are found at -0.001 and 0.204 V. Though each of the peaks shifts in the study of PPC^+ reduction the thermodynamic shift of peak I to peak II was of primary interest. The extent of this thermodynamic shift is found in the inset from pH 1 to 12. The slope of the line from pH 3 to about pH 7 was -0.068 V pH^{-1}, which represents a -0.009 V difference in the expected value of -0.059 V pH^{-1} for a one electron-one proton transfer. With the aid of equation 61, shown below modified from its original form (equation 60), to interpret the thermodynamic shift of the peak potential of peak I to peak II, $E_{p,\,I}$, the formal potential for the reduction of PPC^+ to $PPC^{\cdot}$, $pK_{a,\,1}$ and $pK_{a,\,2}$ could be determined. The E^o_2, $pK_{a,\,1}$ and $pK_{a,\,2}$ were determined to be -0.522, 2.21 and 6.03, respectively. The observed decrease in the peak I potential found in the inset of Figure 33, was likely due to the effect that minute amounts of dissolved oxygen had on the oxidation of PPC^+ at high pH. Spectroelectrochemical results and the study of PPC^+ at high pH (~12) confirmed the production of the PPC^+ radical cation ($PPC^{+\cdot}$) even under a nitrogen atmosphere.

$$E_{p,\,I} = E^o_2 + (2.3RT/F)\log((1+[H^+]/K_{a,2})/(1+[H^+]/K_{a,1})) \quad (61)$$

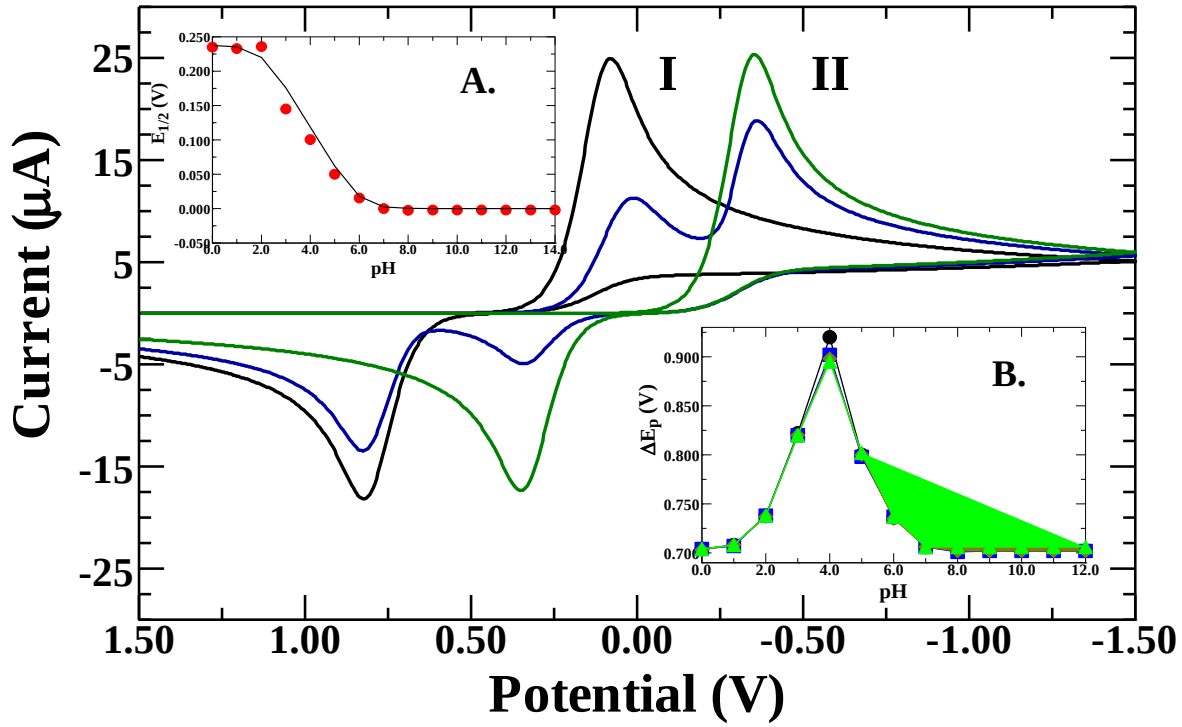

Figure 34. Simulated CV's of 2.0 mM B in a simulated 0.1 M phosphate buffer at pH 2 (black), 4 (blue) and 11 (green). Inset: (A.) Plot of $E_{1/2}$ versus pH for peaks I and II (red circles), fitted black line represents the fitting of equation 60 to the $E_{1/2}$ versus pH data for peaks I and II. (B.) Plot of ΔE versus pH for proton transfer rate constant values of 1 x 10^6 (black dots and line), 1 x 10^7 (blue squares and line), 1 x 10^8 (gold diamonds and line) and 1 x 10^9 M^{-1} s^{-1} (green triangles and line).

The reduction of the hypothetical compound, B, in a simulated 0.1 M phosphate buffer (buffer component concentrations determined from an α plot) solution, Figure 34, shows a thermodynamic shift between $pK_{a,1}$ and $pK_{a,2}$ similar to that of PPC^+.[140] As the pH of the simulated phosphate buffer solution increases from 3 to 7, peak I shifts -0.059 V pH^{-1} unit (inset A Figure 34, R^2 = 0.99) to peak II. The plotted black line in inset A of Figure 34 involves the fitting of equation 60 and the parameters assigned to the model (Scheme 11 and Experimental section).[139] This model reduction further demonstrates the similarity of the first electron transfer reduction of PPC^+ and B.

The thermodynamic effects of increasing the solution pH are further complicated between the two pK_a's of PPC^+ and B by kinetic effects. The ΔE_p of the cathodic and anodic peaks again increases between $pK_{a,1}$ and $pK_{a,2}$. The ΔE_p of PPC^+ between $pK_{a,1}$ and $pK_{a,2}$ decreases from an average ΔE_p of 1.129 V from pH 1 to 6 to 1.008 V between pH 7 to 12. A similar trend is found when studying the ΔE_p of B, where ΔE_p increases from 0.704 V to at pH 0 to 0.895 V at pH 4, after which it decreases back to 0.704 V. The trend in increasing ΔE_p with changing pH is found in inset B of Figure 34. The effect of changing the maximum kinetic rate constant from 1 x 10^9 M s^{-1} to 1 x 10^6 M s^{-1} can be found in inset B of Figure 34 as well. The purpose of studying the effect of altering the maximum rate constant on ΔE_p as the pH changes was to demonstrate the effect of slowing PT in the transition from a CE to an EC reaction. By slowing PT throughout the studied pH range the effect of the transition from a CE to an EC reaction is amplified. However, the order of this amplification is not as great as that found for a reversible system (section 5.3.1). There is only a 0.025 V difference noted between the maximum ΔE_p between changing the maximum rate constants from 1 x 10^6 (0.920 V) to 1 x 10^9 M s^{-1} (0.895 V).

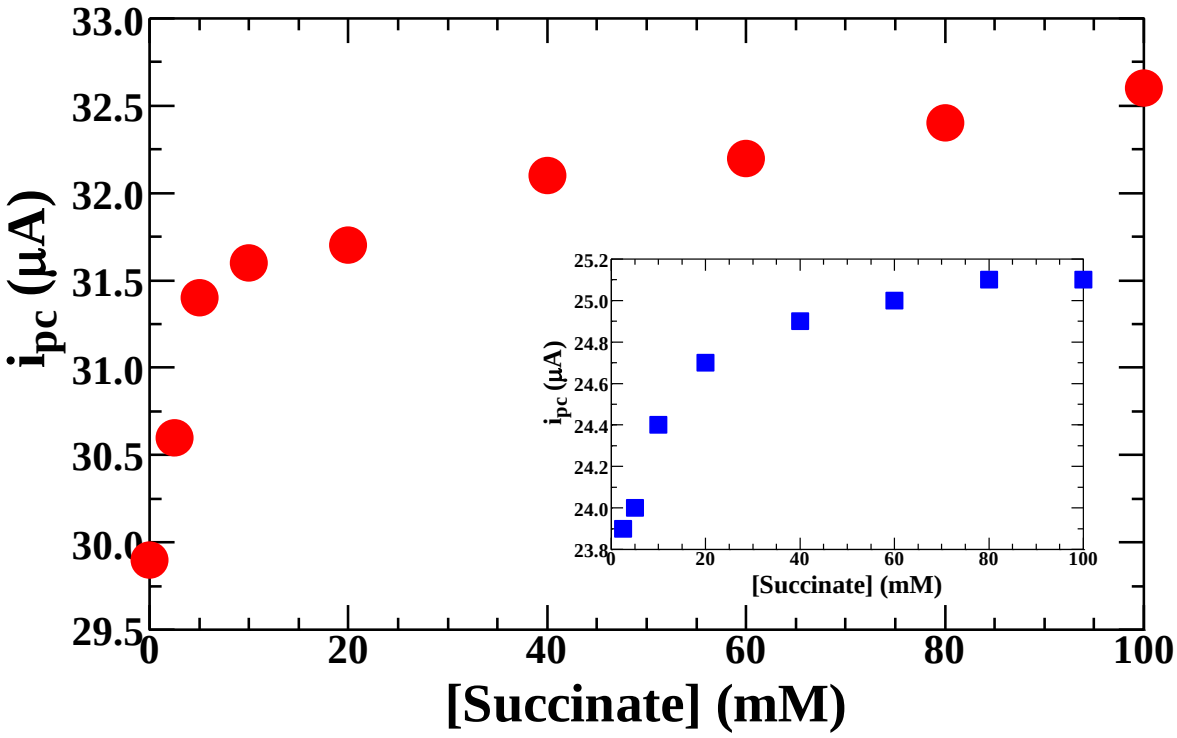

Figure 35. Plot of i_{pc} (peak I) versus succinate buffer concentration for 2.0 mM of PPC^+. Inset: Plot of i_{pc} versus simulated succinate buffer concentration for the hypothetical model compound, B.

Varying the buffer concentration at the mid-point between the two pK_a's of the species of interest allows for the study of the CE to EC transition for heterogeneous electron-proton transfers via experimentation or simulation. As the buffer concentration decreases the peak current for peak I in CV's of both PPC^+ and B decreases. A plot of the peak current of peak I (i_{pc}) as a function of buffer concentration reveals an inflection point in these plots for both PPC^+ (at 10 mM succinate) and B (~40 mM succinate). The inflection point divides the reduction into two kinetic regimes for $NMBC^+$ and B, Figure 35 and inset, respectively. Similar behavior has been observed in studies involving general acid/base catalysis, and has been considered an indication of a change in the rate-determining step of the reaction.[18, 142, 143] At lower buffer concentrations, proton transfer is rate limiting. Reduction of PPC^+ or B at the electrode causes the pH to increase at the electrode beyond the capacity of the buffer, which limits the peak

current measured at peak I. However, at higher concentrations of buffer the electron transfer is rate limiting, because the proton concentration is fixed. Furthermore, the ΔE_p of B increases as the concentration of succinate decreases. The ΔE_p of B increases from an average of 0.870 V at 100 to 40 mM citrate to as high as 0.885 V at 2.5 mM citrate. However, the ΔE_p of PPC^+ does not change significantly, and averages at 1.140 V throughout the observed succinate concentration range. Obviously, the changes in ΔE_p are not consistent and under this study and there are likely other processes taking place that may affect these observations.

One possible process taking place at low pH is the inversion of the potentials E^o_1 and E^o_3 (from Scheme 10). To determine if a given molecule undergoes potential inversion upon oxidation or reduction voltammetric studies under various experimental conditions (concentration, solvent, voltammetric parameters, etc.) coupled with voltammetric simulations are typically undertaken. In this study, voltammograms with shorter potential windows were initially measured to obtain knowledge of what was taking place at each of the redox peaks. However, the voltammograms of shorter potential windows, such as that in Figure 36, illustrated the possibility of potential inversion. When the potential window is shortened so that only the first cathodic peak, peak I, is measured on the cathodic sweep, one finds that the more negative anodic peak, peak IV, is found on the anodic sweep. Typically, the first cathodic peak would be coupled to the more positive anodic peak that at 0.717 V or peak V. Voltammograms of PPC^+ were also measured in anhydrous acetonitrile (ACN) alone and with triflic acid, by exchanging the chloride ion for hexafluorophosphate. The voltammetry of PPC^+ in ACN with one to four equivalents of triflic acid illustrated similar features to those in aqueous solution of low pH. With one equivalent of triflic acid the CV at 0.1 V s^{-1} showed two reduction peaks at -0.728 and -1.334 V and two small oxidation peaks at 0.391 and 0.798 V in a similar inverted order to that

in aqueous solution (data not shown). The voltammetry of PPC^+ without triflic acid was similar to the voltammetry measured in aqueous solution of high pH, yet without the presence of a sharp anodic peak at ~ 0 V (peak III). In these CV's peak III was broad and did not indicate adsorption (data not shown).

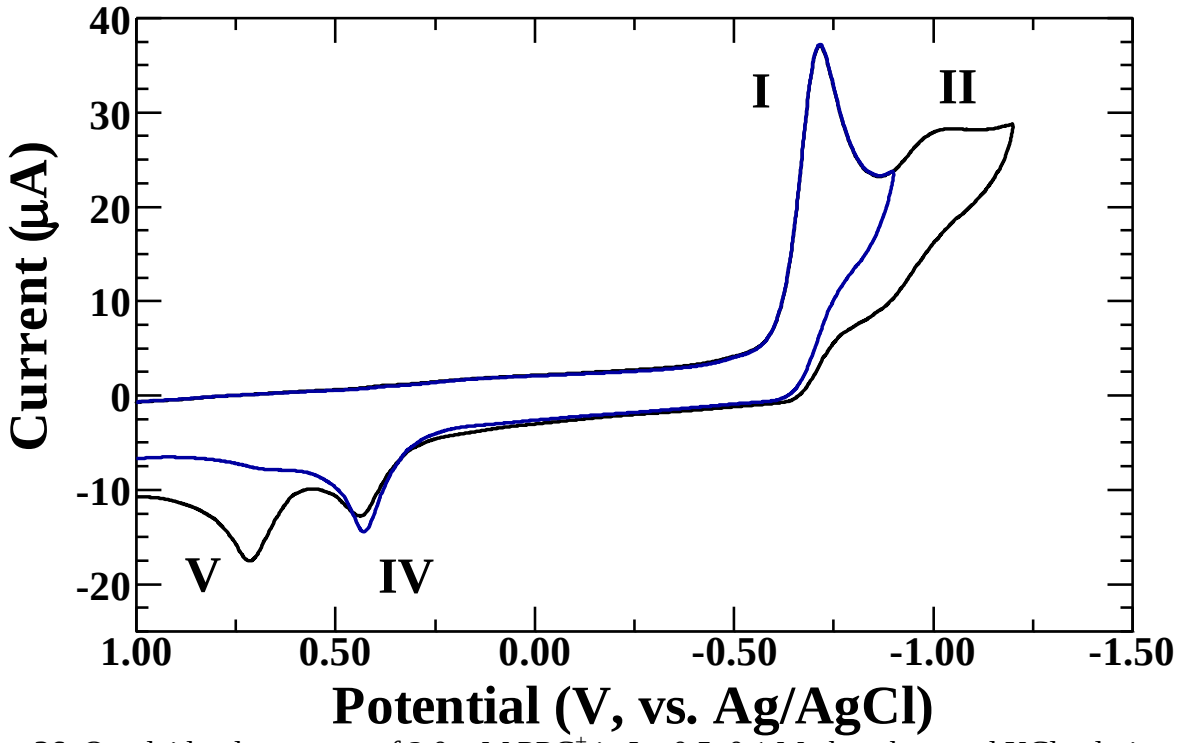

Figure 36. Overlaid voltammetry of 2.0 mM PPC^+ in I = 0.5, 0.1 M phosphate and KCl solution at pH = 2, at 300 K, at a glassy carbon electrode (0.060 cm^2) at two different potential window widths.

To confirm whether potential inversion was possible, quantum mechanical calculations were performed on each of the structures of both PPC^+ and $NMBC^+$ in fence schemes 9 and 10. The structures of $NMBC^+$ were included in this study because both PPC^+ and $NMBC^+$ are structural analogs. Furthermore, based on the discussion of the voltammetry of $NMBC^+$ (above, section 5.3.1) there was no indication that $NMBC^+$ undergoes potential inversion. Therefore, the study of the structures of $NMBC^+$ serves as a control for the study of PPC^+. Figures 37 and 38 show the optimized structures of the PPC^+ and $NMBC^+$ redox species, PPC^o and $NMBC^o$ are omitted

due to the inability to optimize this structure via computational methods. Upon reduction there is an observed dihedral angle twist between the two PPC^+ pyridine rings, while there is only an observed dihedral angle in the optimized structures of $NMBC^+$ and $HNMBC^{2+}$. Table 12 gives the N-C or C-C bond length (depending on whether PPC^+ or $NMBC^+$ species are under study, respectively), dihedral angle and the determined total reorganization energy (λ_T) of the indicated reactions. The outer reorganization energies (λ_o) of PPC^+ reduction were determined using equation 62, where e_o is the charge of an electron, ε_o is the vacuum permittivity, ε_{op} is the optical dielectric constant (=1.776 in H_2O), ε_s static dielectric constant (=78.39 in H_2O) and a represents the radius of the reactant molecule.[18, 19, 134] The inner reorganization energies (λ_i) were determined via Nelsen's four point method and the total reorganization energy was determined by equation 63.[142, 143] Since there is a rearrangement of the PPC^+ species at each reduction and lack of rearrangement of $NMBC^+$ upon reduction, except for the initial rearrangement it is likely that inverted potentials are a part of the PPC^+ reduction chemistry and not of $NMBC^+$.

$$\lambda_o = (e_o^2/4\pi\varepsilon_o)(1/\varepsilon_{op} - 1/\varepsilon_s)(1/2a_{HPPC/PPC}) \quad (62)$$

$$\lambda_T = \lambda_o + \lambda_i \quad (63)$$

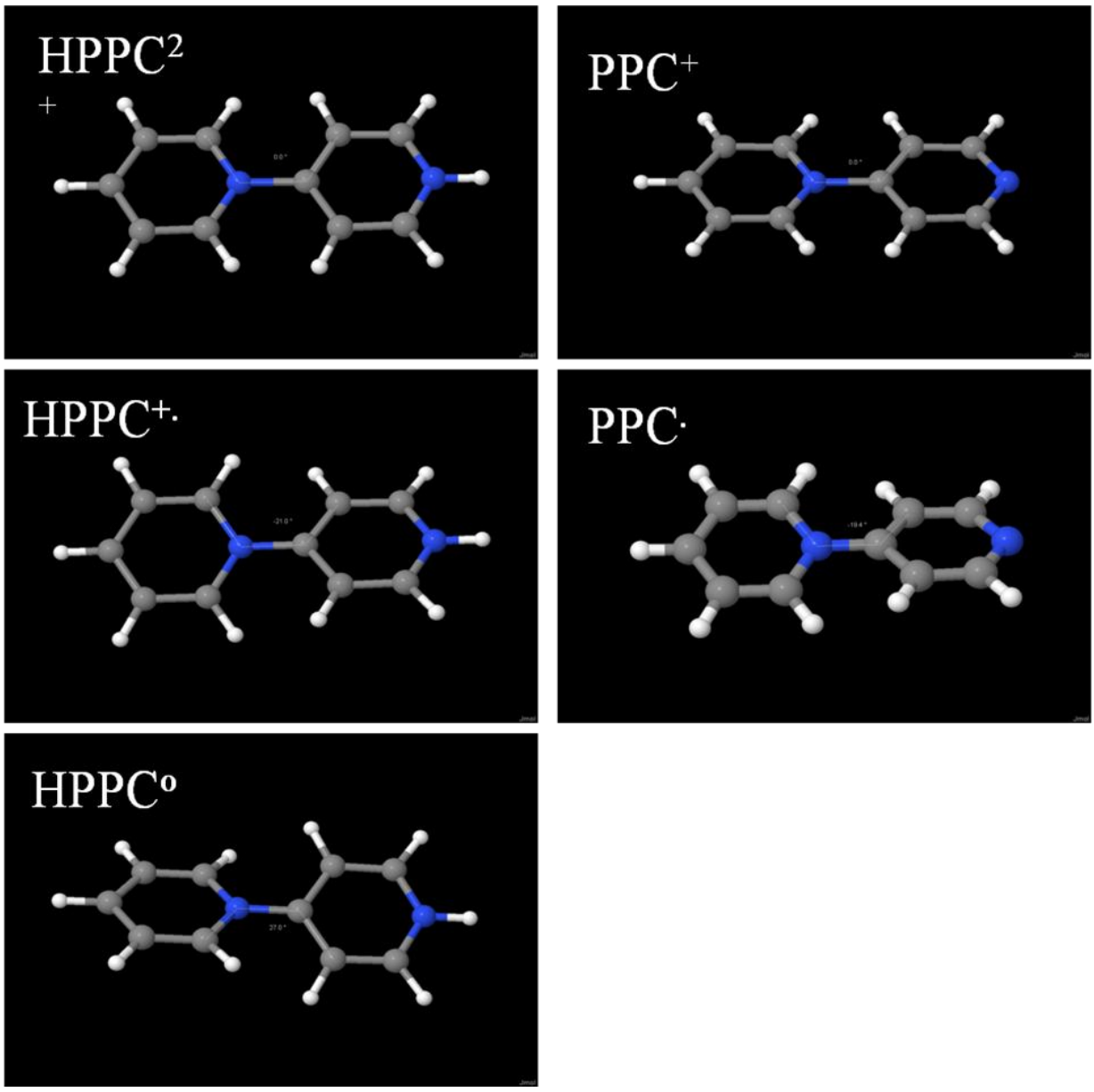

Figure 37. PPC^{+} fence scheme structures determined using PCM/B3LYP/6-31G*.

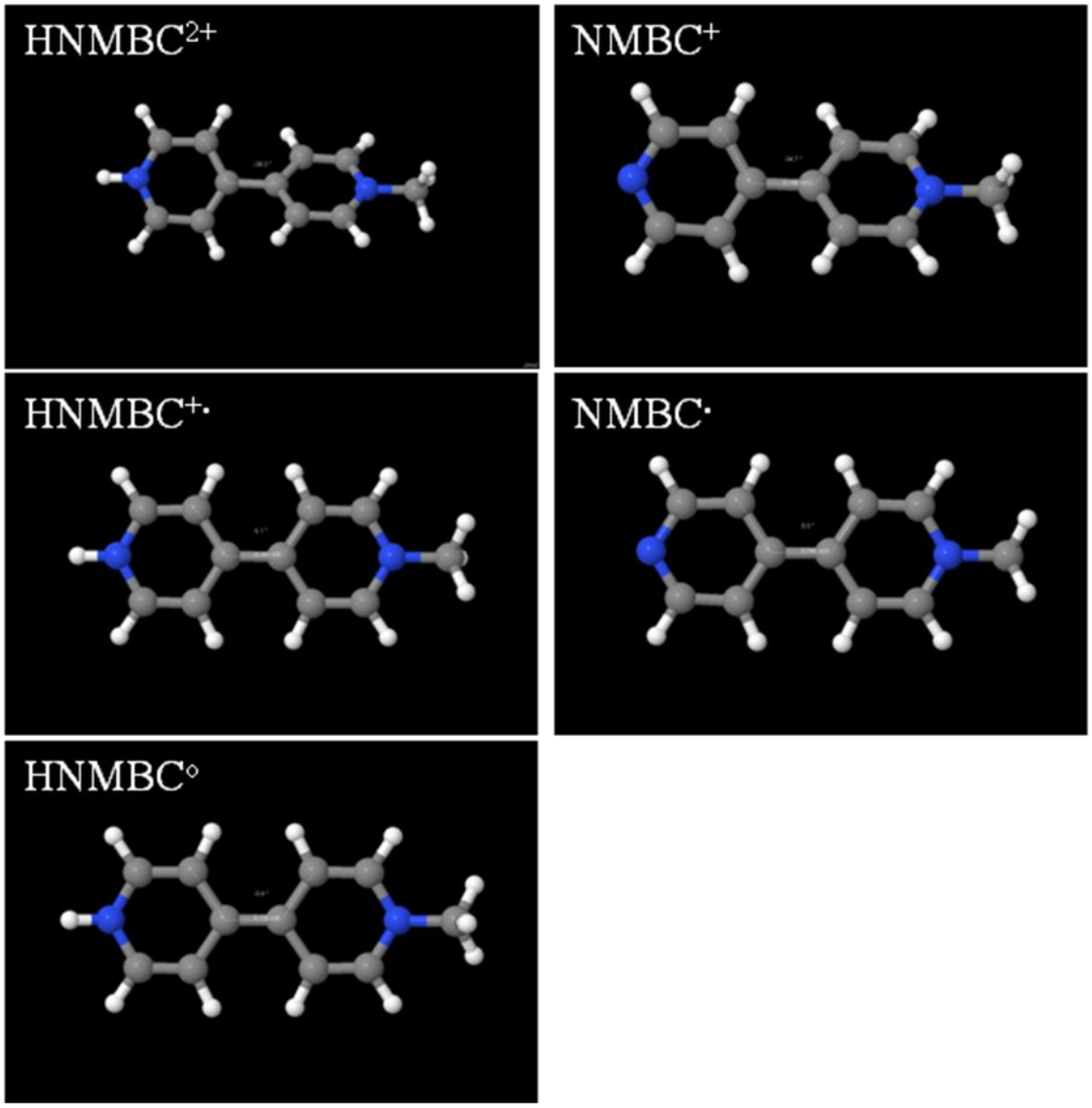

Figure 38. $NMBC^+$ fence scheme structures determined using PCM/B3LYP/6-31G*.

Though not previously discussed, simulations were attempted for PPC^+ under both unbuffered and buffered conditions. These simulations were attempted at all pH's and with each of the studied buffers. However, only somewhat satisfactory fittings were obtained with the fittings of PPC^+ in succinate buffer at pH 4. These fittings employed the formal potential and pK_a values determined by equation 61, and examples of this fitted voltammetry can be found in

the appendix along with the mechanism and fitted parameters (also found in section 5.2.4). The λ_T values along with Marcus kinetics were not included in these simulations, because all attempts using Marcus kinetics provided unsatisfactory fittings. The formal potentials for E^o_1 and E^o_3 (Scheme 10) used in these fittings were -0.22 and -0.185 V, showing that the reduction of PPC^+ can be fit as a potential inversion process.

Table 12. Bond length, dihedral angle and determination of λ_T for the reduction species of PPC^+ and $NMBC^+$.

Species	**N-C or C-C Bond Length (Å)[a]**	**Dihedral Angle[a]**
$HPPC^{2+}$	1.44	0.0^o
$HPPC^{+\cdot}$	1.40	20.8^o
$HPPC^o$	1.38	27.0^o
PPC^+	1.48	0.0^o
$PPC^\cdot$	1.40	19.4^o
$HNMBC^{2+}$	1.48	39.3^o
$HNMBC^{+\cdot}$	1.43	0.0^o
$HNMBC^o$	1.43	0.0^o
$NMBC^+$	1.48	34.7^o
$NMBC^\cdot$	1.44	0.0^o
λ_T Determination[a]		
Reaction	**λ_T (eV)**	
$HPPC^{2+} + e^- \Leftrightarrow HPPC^{+\cdot}$	0.87	
$HPPC^{+\cdot} + e^- \Leftrightarrow HPPC^o$	-[b]	
$PPC^+ + e^- \Leftrightarrow PPC^\cdot$	1.11	
$HNMBC^{2+} + e^- \Leftrightarrow HNMBC^{+\cdot}$	-[b]	
$HNMBC^{+\cdot} + e^- \Leftrightarrow HNMBC^o$	-[b]	
$NMBC^+ + e^- \Leftrightarrow NMBC^{+\cdot}$	-[b]	

[a.] All values from calculations at PCM/(U)B3LYP/6-31G*.
[b.] Values were yet to be determined upon the completion of this thesis.

5.4 Conclusion

In summary, herein a thorough electrochemical study of N-methyl-4,4'-bipyridyl chloride ($NMBC^+$) and 1-(4-Pyridyl)Pyridinium Chloride (PPC^+) in unbuffered and buffered aqueous solution has been presented. The voltammetric study of each species in unbuffered solution results in the complete shift of the reduction peaks to more negative reduction potentials

governed by the pK_a's of the molecule in each reduction state and described by equation 50. Broadening of the redox peaks were the only kinetic effects noted upon increasing or decreasing the pH of the unbuffered solution. The voltammetry within the range pH = $pK_a \pm 1$, were found to exhibit these kinetic effects. The voltammetry of both species in buffered solution demonstrated an expected incremental thermodynamic effect as the pH of the solution increased between $pK_{a,1}$ and $pK_{a,2}$. Fitting of equation 60, to a plot of $E_{1/2}$ (or E_p) versus pH allowed for the determination of E^o_2 and $pK_{a,1}$ and $pK_{a,2}$. Interestingly, the redox peaks of both $NMBC^+$ and PPC^+ both exhibited an increase in the peak width between $pK_{a,1}$ and $pK_{a,2}$. The broadening of the peaks in the specified ranges for both species in buffered and unbuffered solution has been determined to be an indication of the change from a CE reduction process to a EC reduction process as the solution pH increases. This determination was made through the study of a hypothetical model species via Digital simulations. Through such simulations one is able to manipulate constants, such as PT rate constants (k_f and k_b) that should remain constant in situ. However, the manipulation of such constants illustrates that as such constants become smaller the peak width increases within the same range as noted in buffered experiments. This increase in peak width in simulations is similar to the in situ transition from a CE to EC reduction process. A way to study this transition experimentally is to study the effect of decreasing the buffer concentration on the measured current. As the buffer concentration decreases the peak current decreases and shows two kinetic regions, one where PT is the rate determining step (RDS, at lower concentrations) and one where ET is the RDS (higher buffer concentrations). To confirm this transition a similar study was performed with a model compound, however the transition regions between the experimental and simulations were different. In the future, matching the experimental and simulated plots would be beneficial as this could further interpret

the kinetics of the experimental results. Accurate simulations of the experimental results could not be attained because for both $NMBC^+$ and PPC^+ there were obvious issues with dimerization and absorption on the electrode. To suppress the issues of electrode absorption further voltammetric studies of $NMBC^+$ and PPC^+ in acetonitrile should be performed. Interestingly, the voltammetry and computational studies of PPC^+ indicated potential inversion was responsible for some of the complicated irreversible voltammetry.

6.0 Future and Ongoing Research

6.1 Acid/Base Modification of Glassy Carbon Electrodes

6.1.1 Introduction

In the last three decades there have been many examples of chemically modified electrodes. Such electrodes have a broad range of use in analytical and materials science applications.[144, 145] Recently, the reduction of diazonium salts and subsequent covalent modification of electrodes has been of interest.[146-148] The modification by diazonium salts provides a solid and noncorrosive means to attach species of interest to carbon surfaces.[146-150] The originally proposed means by which surfaces are modified by diazonium salts is illustrated in Scheme 13.[149, 150] Here, the diazonium salt is first reduced forming both an aryl radical and nitrogen gas, then the aryl radical forms a covalent bond with the electrode surface forming a supposed monolayer.[146-151] However, more recent studies have shown that the further reduction of diazonium salts at the electrode surface forms multiple layers of the aryl species.[152-157]

Scheme 13. Reduction mechanism of diazonium molecules.

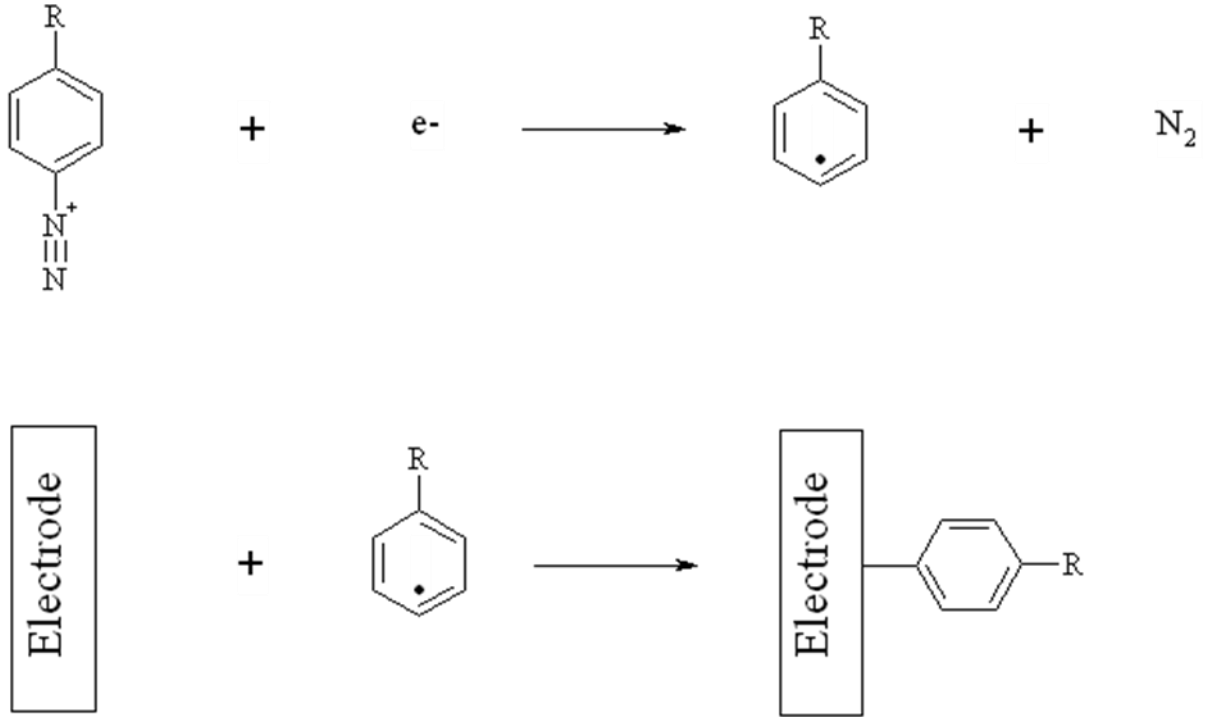

The goal of this work is to investigate amine and carboxylate species on the surface of glassy carbon (GC) electrodes. By modifying the electrodes with amines and carboxylates and reducing or oxidizing quinones or hydroquinones, respectively, at the modified surface a similar thermodynamic shift as found in Chapters 2 through 4 might be found. Furthermore, the effects of proton transfer versus hydrogen bond interactions at the surface can be investigated. The first objective of this work is to investigate the conditions (concentration of the diazonium salt, electrochemical technique, electrochemical parameters, etc.) used to modify glassy carbon electrode surfaces with previously investigated amine and carboxylate diazonium salts in an attempt to form monolayers. Previous reports have discussed the modification of the surface by 4-nitrobenzenediazonium tetrafluoroborate ($NBDBF_4$, **1**), diazonium-4-diethylamine tetrafluoroborate (DDEA, **2**) and 4-carboxyphenyl diazonium tetrafluoroborate ($CPDBF_4$, **3**).[153-156] Scheme 14 provides the structures of these diazonium salts. The reduction of diazonium-4-

diethylamine tetrafluoroborate (DDEA) at the surface is known to produce multiple layers at glassy carbon surfaces, while under similar conditions $NBDBF_4$ and $CPDBF_4$ likely also involve the production of multiple layers.[155, 156] The formation of monolayers is thought to assist in investigating the expected effects without passivating the electrode surface.

Scheme 14. Structures of 4-nitrobenzenediazonium tetrafluoroborate (**1**), diazonium-4-diethylamine tetrafluoroborate (**2**) and 4-carboxyphenyl diazonium tetrafluoroborate (**3**).

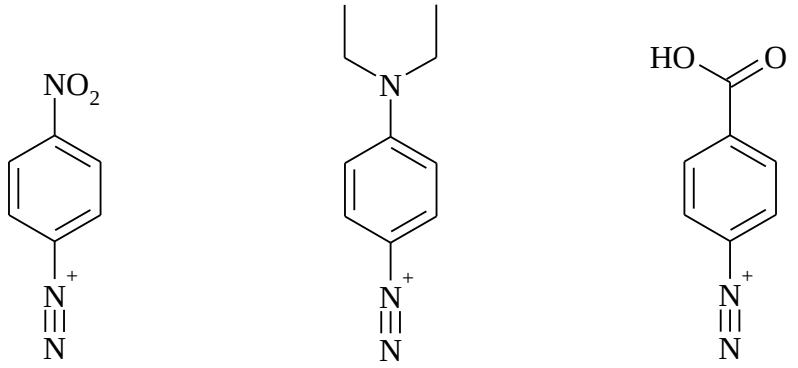

1 **2** **3**

This chapter will discuss the findings to this point based on attempts to address the formation of monolayers on the surface of glassy carbon electrodes. So far, only preliminary work has been completed. The preliminary work to this point has studied the effects of modifying electrodes at reported diazonium concentrations (1.0 to 5.0 mM). The effects the diazonium modification has on redox processes was determined via common electrochemical probes, such as hexaammineruthenium (III) chloride ($Ru(NH_3)_6^{3+}$), potassium ferricyanide ($Fe(CN)_6^{3-}$), hydroquinone (1,4-QH_2) and catechol (1,2-QH_2). Electrodes modified at high concentrations of the diazonium salts seem to indicate that the electrode has become passivated, as the voltammetry of each of the electrochemical probes displays significant kinetic effects with each modification. The effects of lowering the concentration of DDEA in the modification

solution and increasing the scan rate have also been studied. Using these simple changes to the modification procedure led to non-passivation effects of the electrode surface as studied by $Ru(NH_3)_6^{3+}$ and $Fe(CN)_6^{3-}$ in aqueous solution at various pH values. These electrochemical probes were the focus here because of the charge that these molecules possess. At certain pH regions in water, protonation or deprotonation of the aryl amines or carboxylates on the surface of the electrode will impose kinetic effects (ΔE_p broadening) via electrostatic repulsion on the reduction of the electrochemical probes upon reduction. Yet, these effects will only be found provided that the electrode is not passivated. The chemistry at the unpassivated surface is described below, where $Ru(NH_3)_6^{3+}$ displays kinetic effects only at low pH. However, $Fe(CN)_6^{3-}$ displays kinetic effects at higher pH conditions. At this point in this study the reasons behind the ΔE_p broadening for $Fe(CN)_6^{3-}$ are unknown and further studies are required to investigate this process, however it appears that multiple layers are not produced using the new modification procedure. The modification of GC surfaces with 4-carboxyphenyl diazonium tetrafluoroborate involving lower concentrations and higher scan rates will also have to be investigated in a similar manner, using $Ru(NH_3)_6^{3+}$ and $Fe(CN)_6^{3-}$. Overall, spectroscopic methods will have to be used to evaluate whether or not the new modification procedure leads to the production of multiple layers.

If the apparent formation of multiple layers cannot be abated then the next objective is to explore the modification of electrode surfaces with new diazonium salts, which are thought to be synthesized through known routes.[157-159] Molecule **4** of the newly synthesized diazonium salts shown in Scheme 15 is thought to be less likely to form multiple layers due to substitution by two carboxylic acid groups. The other diazonium molecule, **5**, was envisioned based on the work by Cabaniss *et al.* and Thorp, who found that the cycling of a GC electrode in 0.1 M

sulfuric acid lead to more reversible electrochemistry of 1,2-QH_2 due an increase in the surface concentration of primarily phenolic, quinone and ketone groups.[160, 161] Furthermore, studies involving the modification of electrodes with the species in Scheme 15 have not been reported to our knowledge.

Scheme 15. Diazonium molecules to be synthesized.

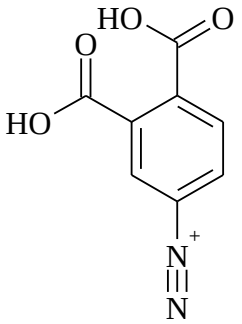

4

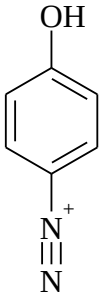

5

6.1.2 Experimental

6.1.2.1 Reagents and Materials

Hexaammineruthenium (III) chloride (Sigma, 98%, $Ru(NH_3)_6^{3+}$), 4-nitrobenzene diazonium tetrafluoroborate(Sigma, 97%, $NBDBF_4$), 4-diazo-N,N-diethylaniline fluoroborate (Sigma, 97%, DDEA), ferrocenium hexafluorophosphate (Sigma, 99%, Fc^+), tetrabutylammonium tetrafluoroborate (Sigma, puriss. ≥99.0%, $TBABF_4$), tetrabutylammonium hexafluorophosphate (Sigma, electrochemical grade, ≥99.0 %, $TBAPF_6$), pyrocatechol (Sigma, ≥99.0%, 1,2-QH_2), hydroquinone (Sigma, 99.5%, 1,4-QH_2), sodium hydroxide (EM Science, Gibbstown, NJ, 97.0%), potassium chloride (Sigma, 99.0-100.5%, NaOH), potassium ferricyanide (Mallinckrodt, Hazelwood, MO, 99 %, $Fe(CN)_6^{3-}$), potassium hexachloroiridate (III)

(Sigma, 99 %, $Ir(Cl)_6^{3-}$), potassium hexacyanoferrate (II) trihydrate (Sigma, ≥99.99 %, $Fe(CN)_6^{4-}$), ethanol (Sigma, 99.50 %, 200 proof), and hydrochloric acid (Fisher, 37.3 % solution) were all used as received. All 18MΩ·cm deionized water was provided by a Milli-Q Academic filtration system (Millipore; Billerica, MA).

6.1.2.2 Glassy Carbon Electrode Construction

For this body of research two different types of glassy carbon electrodes were used and constructed, glassy carbon plate and rod electrodes. Glassy carbon plate electrodes were constructed using glassy carbon plates purchased from Structure Probe Inc. (West Chester, PA) of the SPI-Glas 22 Grade quality and were purchased as 25 x 25 x 2 mm plates. The plates were reduced in size by cutting them into small squares and attaching a copper wire (Fisher Scientific, Pittsburg, PA) to them using silver epoxy (EPO-TEK, Epoxy Technology, Billerica, MA) and then all sides of the plate with the exception of one face was covered using EPON 828 with 14% metaphenylenediamine as the hardener (epoxy and hardener provided by Dr. Collinson). The glassy carbon rod electrodes were prepared using glassy carbon rods purchased from Structure Probe Inc. (West Chester, PA) of the SPI-Glas 25 grade quality and were purchased as 10 mm length rods of 3 mm diameter. The rods were cut in half and the two cut ends were used to make two separate electrodes. Copper wire leads were attached to each of the cut rods via silver epoxy. After the curing of the silver epoxy the rods were sealed within glass tubing (5 mm outer diameter x 0.8 mm wall thickness, 304.8 mm length, Small Parts, Inc., Seattle WA) cut to 40 mm lengths by dipping in a glass container of EPON 828 with 14 % metaphenylenediamine as the harding agent. Upon curing of the sealing epoxy the electrode was sanded using 220 grit sandpaper then 800 grit sandpaper to remove the excess epoxy. After removal of the excess the electrode was successively polished using diamond paste of 6, 3, 1 and then 0.25 μm size

(Buehler, Lake Bluff, IL). Finally, the electrodes were polished on a wet polishing pad with 0.05 μm alumina (Buehler, Lake Bluff, IL).

6.1.2.3 Electrochemical Methods

All electrochemical experiments were performed using a CHI660C potentiostat (CH Instruments, Austin, TX) incorporating a CHI200B Faraday cage and picoampbooster. In each experiment the solution resistance (R_u) was totally compensated via positive feedback. Electrochemical measurements were conducted under nitrogen in a cell containing 10 mL of either acetonitrile or deionized water with 0.2 M $TBABF_4$ (for modification experiments, and 0.2 M $TBAPF_6$ for evaluation experiments) and 0.1 M KCl, respectively. A series of glassy carbon electrodes, either plate or rods (construction described above), were used for this work. Unmodified electrode areas were determined using the Randles-Sevcik equation using a 1.0 mM solution of $Ru(NH_3)_6^{3+}$ in deionized water with 0.1 M KCl as supporting electrolyte, where D = 6.3 x 10^{-6} cm^2 s^{-1}.[77] A large platinum flag electrode served as the auxiliary electrode, and the reference electrode was an Ag/AgCl electrode in aqueous experiments (CH Instruments). For work in acetonitrile, the same platinum flag electrode was used, while the reference electrode was an Ag/Ag^+ electrode (a silver wire immersed in the supporting electrolyte, 0.2 M $TBAPF_6$/3 mM silver nitrate/acetonitrile). The potential of the Ag/Ag^+ reference electrode in acetonitrile was periodically measured versus the formal potential (measured as the average of the peak potentials) of the ferrocene/ferrocenium (Fc/Fc^+) couple under the same conditions as the other experiments and thus all potentials in acetonitrile are reported versus ferrocene as Fc/Fc^+. In both solvents the reference electrode was separated from the rest of the solution by a glass tube capped with a porous vycor frit. Prior to each modification experiment the polished glassy carbon electrode was first polished using 0.05 μm alumina paste (Buhler, Lake Bluff, Il) washed

with deionized water, carefully wiped, and then sonicated for three minutes in acetonitrile. Unless noted otherwise, the modified electrode was never polished after modification, but was instead washed thoroughly with acetonitrile, sonicated in acetonitrile, then ethanol and finally DI H_2O for three minutes each, prior to transfer into an aqueous solution of the various electrochemical probes.

6.1.3 Preliminary Results

6.1.3.1 Reduction of Commercially Available Diazonium Molecules at Glassy Carbon Electrodes and their Effect on Hydroquinone Oxidation

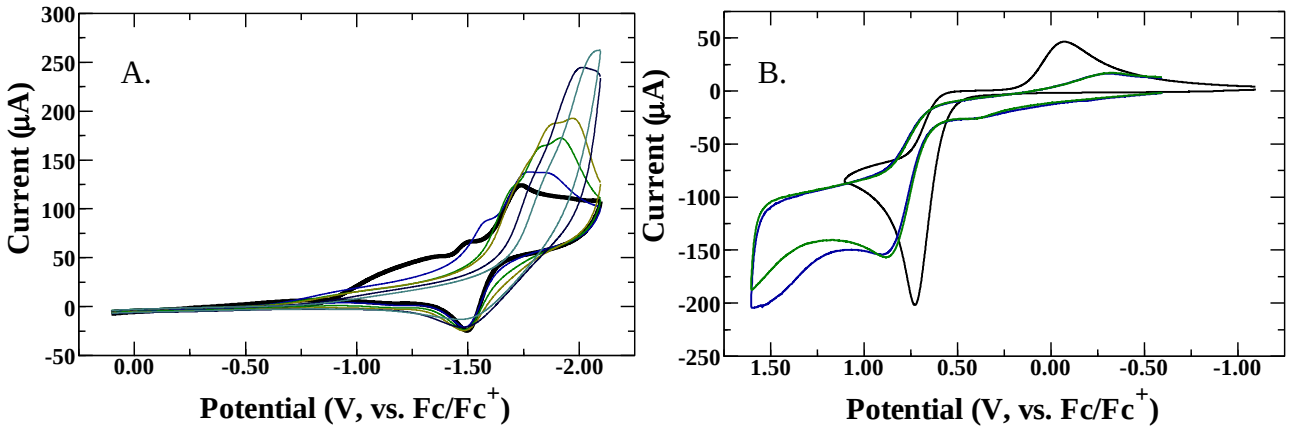

Figure 39. (A.) Multiple overlaid voltammograms (first CV is the given by the thick black line) of 1.0 mM 4-nitrobenzenediazonium tetrafluoroborate ($NBDBF_4$) in acetonitrile with 0.1 M $TBABF_4$ as supporting electrolyte. (B.) Voltammograms of 1.0 mM 1,4-QH_2 in acetonitrile with 0.2 M $TBAPF_6$ before $NBDBF_4$ modification (black CV), after $NBDBF_4$ modification (blue CV) and after electrolysis in 90:10 H_2O/Ethanol for 100 minutes (green CV). All CV's were recorded at 0.1 V s^{-1} at a glassy carbon electrode (0.15 cm^2).

Figure 39 demonstrates the effects that the reduction of 4-nitrobenzenediazonium tetrafluoroborate ($NBDBF_4$) has on the voltammetry of 1,4-QH_2. Figure 39A shows the reduction of $NBDBF_4$ on a GC plate electrode. From the first CV, the peak at approximately -1.25 V is the reduction of the diazo-group, while the peak at -1.75 V is the reduction of the nitro-

group, as determined from CV's of nitrobenzene (reduction peak at -1.72 V) alone in acetonitrile. As the number of scans increases the diazo reduction peak is lost at the cost of the growth in the reduction peak current of the nitro group. For every reduction scan, the number of nitroaryl groups on the surface increases, increasing the surface concentration of the nitro group, thus increasing the peak current related to this reduction. Confirmation of surface modification by the nitroaryl group is found by cycling the modified electrode in a background solution (a solution of 0.1 M $TBABF_4$ in acetonitrile). The voltammetry of the modified electrode in the background solution shows only the peak corresponding to nitro reduction at -1.75 V. Figure 39B demonstrates the effect that modification of the electrode surface with the nitroaryl group has on 1,4-QH_2. Prior to modification, the CV of 1.0 mM 1,4-QH_2 shows similar features to that found at 5.0 mM exhibited in Chapter 2, with a single oxidation peak at 0.728 V and a broad reduction peak at -0.072 V. However, after modification the voltammetry displays significant kinetic effects with the oxidation peak found at 0.903 V and the near absence of the reduction peak. Also found in Figure 39B is the CV of 1,4-QH_2 after electrolysis for 100 minutes in a solution of 90:10 deionized H_2O/ethanol, which reduces the nitro group to an amine group.[146] From this voltammetry the presence of arylamines on the surface seems to have a slightly smaller kinetic effect on the voltammetry of 1,4-QH_2 as the oxidation peak is found at 0.884 V. Furthermore, a smaller oxidation peak is found at negative potentials (0.436 V) relative to the primary oxidation peak at 0.884 V. It is possible that this new oxidation peak is due to heterogeneous proton transfer, from 1,4-QH_2 to the electrode surface, yet further studies have yet to replicate these results. Reduction of $Ru(NH_3)_6^{3+}$ and $Fe(CN)_6^{3-}$ at pH 7.01 at the $NBDBF_4$ electrodes results in the complete absence of redox peaks, which confirms the blocking effect produced by multiple layers.[153, 155, 156]

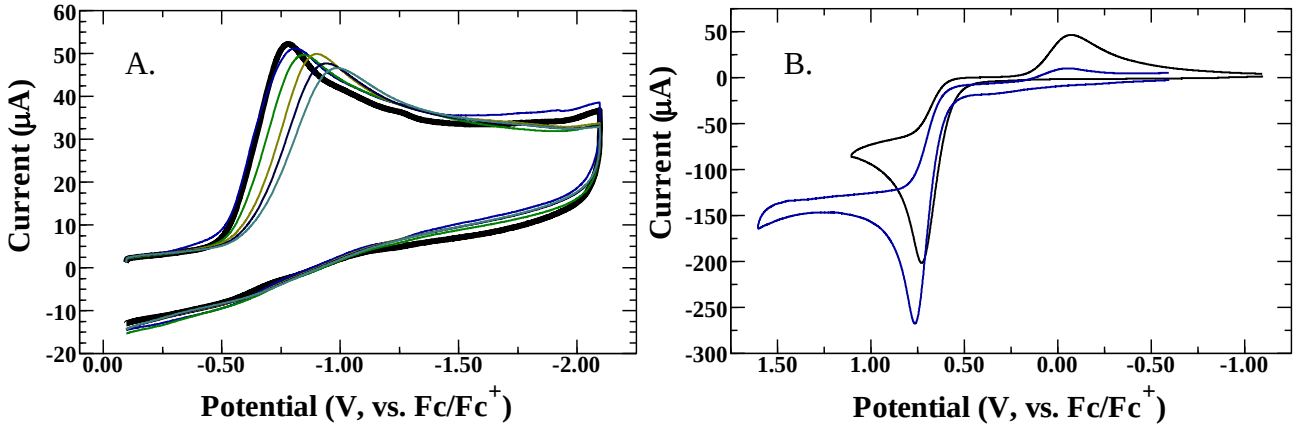

Figure 40. (A.) Multiple overlaid voltammograms (first CV is the given by the thick black line) of 1.0 mM diazonium-4-diethylamine tetrafluoroborate (DDEA) in acetonitrile with 0.1 M $TBABF_4$ as supporting electrolyte. (B.) Voltammograms of 1.0 mM 1,4-QH_2 in acetonitrile with 0.2 M $TBAPF_6$ before DDEA modification (black CV) and after DDEA modification (blue CV). All CV's were recorded at 0.1 V s^{-1} at a glassy carbon electrode (0.15 cm^2).

The reduction of diazonium-4-diethylamine tetrafluoroborate (DDEA) on a glassy carbon plate electrode and its effect on the oxidation of 1,4-QH_2 is found in Figure 40. Figure 40A exhibits the reduction peak of 1.0 mM DDEA at -0.806 V. This irreversible reduction peak at -0.781 V represents the reduction of the diazo group and subsequent modification of the glassy carbon surface with the diethyamine (DEA) aryl groups. Further scans resulted in the reduction peak shifting to more negative potentials as shown in Figure 40A. After DEA modification via multiple scans in a solution of 1.0 mM DDEA and electrolysis for 30 seconds the voltammetry of 1,4-QH_2 was measured and is illustrated in Figure 40B. As with the 1,4-QH_2 voltammetry measured after modification with $NBDBF_4$, surface modification by DEA-aryl groups leads to significant kinetic effects. The CV of 1,4-QH_2 after modification shows an oxidation peak at 0.763 V, only 0.035 V more positive than the CV measured prior to modification. The reduction peak of 1,4-QH_2 in Figure 40B is again nearly absent, decreasing from 195.1 to 112.6 μA. However, unlike after electrolysis of the $NBDBF_4$ solution in a protic solution, no new oxidation

peak was found at more negative potentials relative to the primary oxidation peak at 0.763 V. Similar to the $NBDBF_4$ modified electrodes, reduction of $Ru(NH_3)_6^{3+}$ and $Fe(CN)_6^{3-}$ at the DDEA modified electrodes shows no redox peaks over the expected potential ranges, confirming the blocking effect produced by multiple layers on the surface.[153, 155, 156]

6.1.3.2 Attempts at Producing Monolayers on the Surface of Glassy Carbon Electrodes via Reduction of Diazonium Molecules

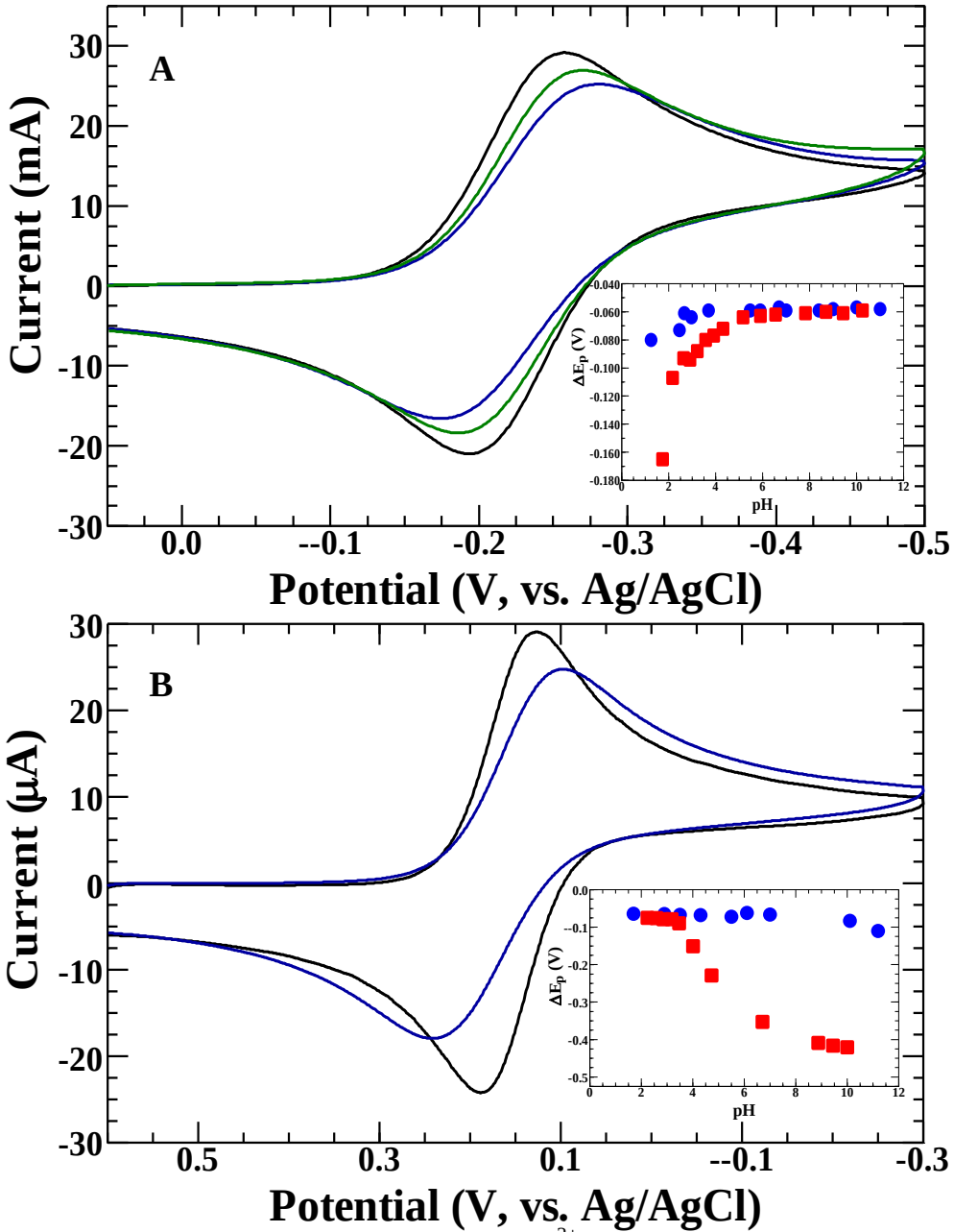

Figure 41. (A.) Voltammograms of 1.0 mM $Ru(NH_3)_6^{3+}$ in pH ~ 2 0.1 M KCl at a glassy carbon rod electrode (0.13 cm^2) before (black CV), after DDEA modification (blue CV) and after performing several scans in a solution of 1.0 mM $Fe(CN)_6^{3-}$ (green CV). (B.) Voltammograms of 1.0 mM $Fe(CN)_6^{3-}$ in pH ~ 5 0.1 M KCl at a glassy carbon rod electrode (0.13 cm^2) before (black CV) and after DDEA modification (blue CV). Inset in both is peak potential difference (ΔE_p) versus solution pH for an unmodified electrode (blue circles) and a DDEA modified electrode.

In an attempt to modify the surface of the electrode with an aryl diethylamine monolayer a single CV of 0.5 mM DDEA was measured at a GC rod electrode (0.13 cm^2) with at a scan rate of 1 V s^{-1} in acetonitrile. This produced a CV similar to that found in Figure 41A, above. Lower diazonium concentrations at 1 V s^{-1} were found to give the best results when evaluated by $Ru(NH_3)_6^{3+}$ $Fe(CN)_6^{3-}$. Other scan rates were attempted, 100, 50 and 20 V s^{-1}, yet little if any difference was found when performing scans with the electrochemical probes, $Ru(NH_3)_6^{3+}$ and $Fe(CN)_6^{3-}$. An expected pH-dependence of the DDEA modified electrode was found when studying the voltammetry of $Ru(NH_3)_6^{3+}$ and $Fe(CN)_6^{3-}$. Voltammetry of $Ru(NH_3)_6^{3+}$ and $Fe(CN)_6^{3-}$ is found in Figure 41A and 41B, respectively. In Figure 41A the voltammetry of $Ru(NH_3)_6^{3+}$ at pH ~ 2 is displayed before modification with DDEA, after modification and after CV's at five scan rates in $Fe(CN)_6^{3-}$ were performed. The ΔE_p of the reduction of $Ru(NH_3)_6^{3+}$ changes from 0.065 V before modification, to 0.107 V after DDEA modification. The voltammetry of $Ru(NH_3)_6^{3+}$ was expected to change on the modified electrode at low pH. This change is due to protonation of the aryl diethylamine groups on the surface of the electrode, which imparts a positive charge on the face of the electrode and causes electrostatic repulsion of positively charged species. The inset of Figure 41A illustrates the pH-dependency of $Ru(NH_3)_6^{3+}$ reduction at DDEA modified electrodes. After several scans at various scan rates were performed in a solution of 1.0 mM $Fe(CN)_6^{3-}$ the ΔE_p of $Ru(NH_3)_6^{3+}$ at pH ~ 2 decreases to 0.084 V. Voltammetric scans in a solution of 1.0 mM $Fe(CN)_6^{3-}$ at the modified electrode at various pH values were intended to act as a control for the CV's of $Ru(NH_3)_6^{3+}$. Since $Fe(CN)_6^{3-}$ is negatively charged, there was believed to be little to no change in the measured voltammetry at the modified electrode regardless of the pH. Figure 41B gives two CV's of $Fe(CN)_6^{3-}$ at pH ~ 5. Under basic conditions the voltammetry of $Fe(CN)_6^{3-}$ was found to have increasingly larger

ΔE_p values, as displayed in the inset of Figure 41B. The completely reduced form of ferricyanide, ferrocyanide ($Fe(CN)_6^{4-}$), and hexachloroiridate (III) ($Ir(Cl)_6^{3-}$) were also used to determine if the voltammetric effects found by $Fe(CN)_6^{3-}$ reduction are solely characteristic of the $Fe(CN)_6^{2-/3-}$ redox couple, or if other negatively charged species exhibit similar results. Oxidation of $Fe(CN)_6^{4-}$ exhibited similar results to those found by $Fe(CN)_6^{3-}$ reduction (results not shown). However, voltammetry of $Ir(Cl)_6^{3-}$ over the pH range of 1.94 to 10.46 revealed little influence due to surface modification, with a change of ΔE_p of 0.058 to 0.060 V, respectively (results not shown). The noted influences on the voltammetry surrounding the $Fe(CN)_6^{3-/4-}$ redox couple was originally envisioned to involve heterogeneous oxidation of the aryl diethylamine groups to aryl ethylamine-*N*-oxide via *N*-demethylation.[162-164] However, similar pH-dependence was discovered with reduction of $Ru(NH_3)_6^{3+}$ and $Fe(CN)_6^{3-}$ upon modification of GC rod electrodes with 0.5 mM 4-nitrobenzenediazonium tetrafluoroborate ($NBDBF_4$) at a scan rate of 0.1 V s^{-1}. The CV of $Ru(NH_3)_6^{3+}$ at pH 2.98 at 0.1 V s^{-1} presented a ΔE_p of 0.110 V, while a CV at pH 11.18 showed a ΔE_p of 0.064 V. Likewise, a CV of $Fe(CN)_6^{3-}$ at pH 10.66 was found to have a ΔE_p of 0.308 V, while at pH 2.72 the ΔE_p was 0.070 V. The values of these ΔE_p displacements are of similar magnitude to those measured at the DDEA modified rod electrodes. Since nitro-aryl groups are neither Brønsted acids nor bases and cannot be protonated, the pH-dependency is expected to be a result of some to be determined interference within electrical double-layer.[24, 165]

Interestingly, modification of GC electrodes at lower diazonium concentrations and scan rates of 1 V s^{-1} is not as robust as modification at higher diazonium concentrations. Polishing with 0.050 μm alumina seems to remove the aryl groups from the surface. Voltammograms of $Ru(NH_3)_6^{3+}$ were measured after DDEA modification and after polishing with alumina. The ΔE_p

was found to decrease from ~0.100 V at pH ~ 2 after modification to 0.060 V after polishing. Similar results were found after modification of $NBDBF_4$.

6.1.4 Conclusion

In summary, the description of the modification of two GC electrode types by two diazonium molecules has been described. The modification of the planar GC electrodes involved the use of commercially available diazonium species, 4-nitrobenzenediazonium tetrafluoroborate ($NBDBF_4$) and diazonium-4-diethylamine tetrafluoroborate (DDEA), by previously discussed modification parameters (diazonium concentration, solvent, scan rate, electrolysis). Modification via these methods forms multilayers of the aryl species, either nitrophenyl or N,N'-diethylaminophenyl groups, on the surface of GC electrodes.[153, 155, 156] Evaluation of GC electrodes modified by $NBDBF_4$ and DDEA shows a significantly detrimental impact on the kinetics of three common electrochemical probes, 1,4-QH_2, $Ru(NH_3)_6^{3+}$ and $Fe(CN)_6^{3-}$. By lowering the diazonium concentration and performing a single modification scan at a fast scan rate the DDEA GC electrodes illustrated the expected effects when used to reduce $Ru(NH_3)_6^{3+}$ at low pH, while reversible CV's were obtained at higher pH. Such effects have never been discussed previously and the reduction of diazonium species has typically been associated with the passivation of electrodes. Interestingly, the reduction of $Fe(CN)_6^{3-}$ at the DDEA modified electrode presented the opposite trend that was found with $Ru(NH_3)_6^{3+}$. Reduction of $Fe(CN)_6^{3-}$ at DDEA modified electrodes showed irreversible kinetics at high pH and reversible kinetics at low pH. Control experiments involving the modification of GC rod electrodes by $NBDBF_4$ demonstrated a similar kinetic influence to DDEA modified electrodes when evaluated by voltammetry of $Ru(NH_3)_6^{3+}$ and $Fe(CN)_6^{3-}$. Currently the cause of this kinetic influence is unknown, but will be studied by impedance measurements in an attempt to interpret these results.

Since studies of GC modification by $NBDBF_4$ and DDEA have never discussed these findings and have typically only evaluated the modification of GC electrodes at one pH, it may be possible to discuss these findings in a future publication. Furthermore, the ultimate aim of this work is to find a diazonium species that demonstrates results similar to those found in Chapters 2 and 3, facilitating PT through surface groups rather than homogeneously. For this to happen, new diazonium molecules will need to be synthesized (Scheme 15), preferably through the newly described *in situ* generation.[157, 159]

6.2 Mediated Oxidation of Phenol Proton-Coupled Electron Transfer

6.2.1 Introduction

There are many examples of mediated electron transfer in the literature, one example involves the oxidation of glutathione by tris(2,2'-bipyridyl)dichlororuthenium (II).[166] In mediated redox systems an electroactive species, the mediator, is oxidized or reduced at the electrode surface and then diffuses away from the electrode where it is involved in a homogeneous electron transfer with some species of interest, the substrate. Through the evaluation of the voltammetry of mediated electron transfer other homogeneous processes, such as proton transfer and the kinetics involved can also be determined. Another means by which to study mediated electron-proton transfer involves the mixing of the completely oxidized mediator with the substrate of interest. Mixing the two species causes the oxidation of the substrate and reduction of the mediator. Studying electron-proton transfer by this method employs various forms of spectroscopy to evaluate the kinetics of the system.[17, 75, 76] Typically, mediators are reversible species that are reduced or oxidized at more positive or negative potentials, respectively, relative to the species of interest. Normally, electromediaton is required for species

that are likely to adsorb on electrodes and/or have unusually slow kinetics which makes the study of other processes, such as proton transfer, difficult to interpret.

The goal is to evaluate whether the means of studying electron-proton transfer, heterogeneous versus homogeneous, affects the outcome of whether a process is *concerted* or *stepwise*. Under heterogeneous means the electron-proton transfer processes of hydroquinone hydrogen bound to various acetates is a *stepwise* mechanism (Chapter 3). However, one may find a difference in the designation of the proton-coupled electron transfer (PCET) if studied using homogeneous electron transfer via electromediation. Through electromediation it may be possible to better evaluate the intermediate of the electron-proton reaction, which may or may not be involved in a hydrogen bonded complex. Although, hydroquinone chemistry has been used in previous studies, oxidation of a phenol may be better suited to evaluating whether the reaction is *concerted* or *stepwise*. Oxidation of phenol involves a six-membered fence scheme, as displayed in Scheme 16, where the OH in the upper left corner represents a generic phenol species. Utilization of phenol oxidation over QH_2 oxidation simplifies the oxidation process by eliminating three possible protonation processes and two possible redox reactions. In this work, 2,4,6-tri-*tert*-butylphenol (TTBP, **1**) was used due to its substitution by large bulky *tert*-butyl groups, which should prevent it from polymerization upon oxidation.[167-169] Three different inorganic complexes have been investigated, yet only two, tris(2,2'-bipyridine)iron (II) hexafluorophosphate ($Fe(bpy)_3(PF_6)_2$, **2**) and tris(1,10-phenanthroline)iron (II) hexafluorophosphate ($Fe(phen)_3(PF_6)_2$, **3**), will oxidize TTBP in preliminary studies. However, it is believed that the third proposed mediator, ferrocene (**4**), will oxidize TTBP upon addition of acetates. The substrate and each of the investigated mediators are given below in Scheme 17. The addition of the acetates, acetate, benzoate and trifluoroacetate, seem to have a similar effect

on the oxidation of TTBP as they had on the oxidation of the QH_2's, however, diffusion ^{1}H-NMR studies have yet to prove this.

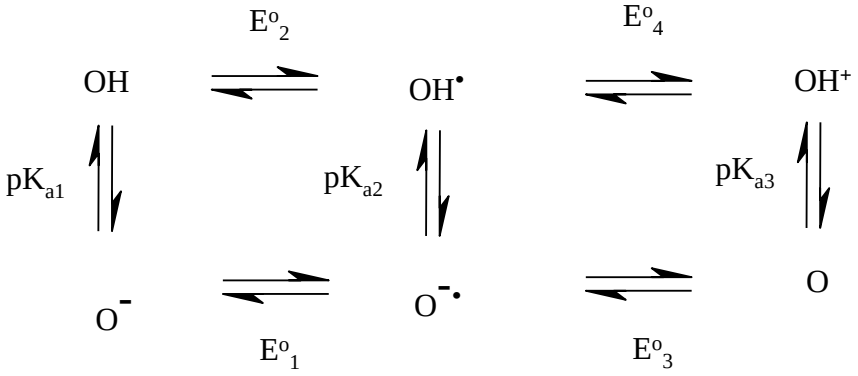

Scheme 16. Six-membered fence scheme for the reduction of phenols.

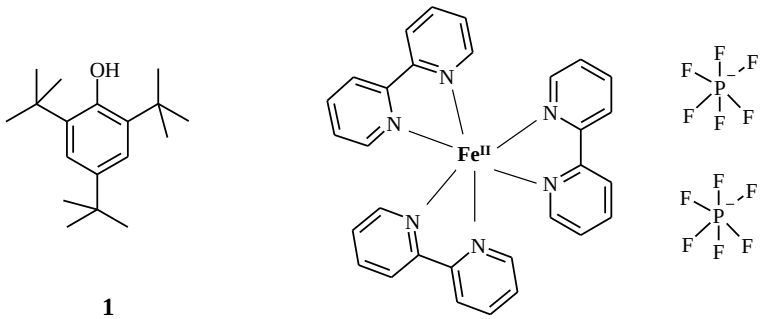

1 **2**

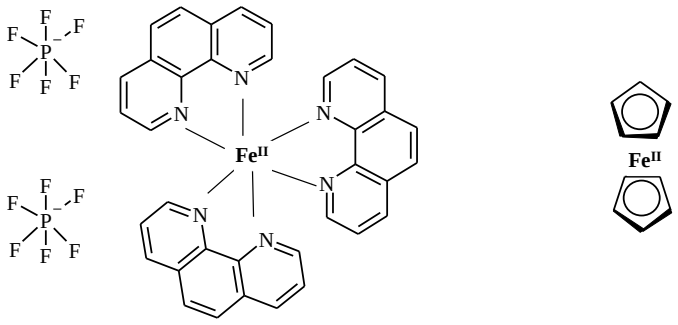

3 **4**

Scheme 17. Structures of 2,4,6-tri-*tert*-butylphenol (**1**), tris(2,2'-bipyridine)iron (II) hexafluorophosphate (**2**), tris(1,10-phenanthroline)iron (II) hexafluorophosphate (**3**) and ferrocene (**4**).

6.2.2 Experimental

6.2.2.1 Reagents and Materials

Tetrabutylammonium hexafluorophosphate ($TBAPF_6$, Fluka, electrochemical grade, ≥ 99.0%) was heated to ~100 ^oC in a vacuum oven for at least 24 hours prior to use as supporting electrolyte. Tetrabutylammonium acetate (acetate, Fluka, electrochemical grade, ≥ 99.0 %) was treated similarly to the $TBAPF_6$, because it is extremely hygroscopic, however, it was heated to only ~60 ^oC for at least 24 hours before use. The less hygroscopic acetates, tetrabutylammonium benzoate (benzoate, Fluka, electrochemical grade, ≥ 99.0 %) and tetraethylammonium trifluoroacetate (trifluoroacetate, Fluka, ≥ 99.0 %) were only opened and used under a nominally dry argon atmosphere. 2,4,6-Tri-*tert*-butylphenol (Sigma, 98 %, TTBP), iron (II) sulfate heptahydrate (Sigma, ≥ 99.0 %), 2,2'-bipyridyl (Sigma, ≥ 99.0 %, bpy), 1,10-phenanthroline (Sigma, ≥ 99 %, phen), potassium hexafluorophosphate (Fluka, ≥ 98.0 %, KPF_6), anhydrous acetonitrile (Sigma, 99.8 % with < 10 ppm H_2O, ACN), ferrocene (Fluka, ≥ 98.0 %, Fc), ferrocenium hexafluorophosphate (Sigma, 98 %, Fc^+), sulfuric acid (EM Science, 95-98 %), ethanol (Sigma, 99.50 %, 200 proof) and diethyl ether (Sigma, ≥ 99.9 %, inhibitor free) were all used as received.

Synthesis of tris(2,2'-bipyridine)iron (II) hexafluorophosphate ($Fe(bpy)_3(PF_6)_2$) and tris(1,10-phenanthroline)iron (II) hexafluorophosphate ($Fe(phen)_3(PF_6)_2$) involved literature procedures by mixing 0.920 g of iron (II) sulfate heptahydrate was mixed with 1.562 g and 2.000 g of 2,2'-bipyridyl and 1,10-phenanthroline, respectively in 25 mL DI H_2O.[170] The preparation of both complexes involved the same procedure. These solutions were then gently warmed to dissolve all remaining solids. Then, these solutions were filtered into two separate flasks and

immersed in an ice bath and 2-3 mL of 1 M H_2SO_4 was added to each. These solutions were then filtered into two separate cold saturated solutions of 0.5 M KPF_6, both of which instantly formed a red precipitate. Then each of these solutions were filtered into a flask and the precipitates were washed with approximately 130 mL cold DI H_2O. Then they were washed with two separate 100 mL aliquots of 200 proof ethanol, and finally each was washed with approximately 60 mL of diethyl ether. The remaining solids were then vacuum filtered for approximately 10 minutes to attempt to remove any remaining solvent. The solids were then dissolved in anhydrous acetonitrile and dried under vacuum at 60 ^oC.

6.2.2.2 Electrochemical Methods

All electrochemical experiments were performed with a hydroquinone or quinone concentration of 5.0 mM in 10 mL dry acetonitrile with 200 mM tetrabutylammonium hexafluorophosphate ($TBAPF_6$) at a glassy carbon electrode. The electrochemical experiments were performed using a CHI660C potentiostat (CH Instruments, Austin, TX) incorporating a CHI200B Faraday cage and picoampbooster using a three electrode cell (10 mL) in an inert argon atmosphere. Several different 0.3 cm diameter glassy carbon electrodes (CH Instruments, areas were consistent, between 0.07 to 0.073 cm^2) were used during this work and the areas associated with each are given in the respective figures (areas determined by the Randles-Sevcik equation using a 1.0 mM solution of $Ru(NH_3)^{3+}$ in deionized water with 0.1 M KCl as supporting electrolyte, where $D = 6.3 \times 10^{-6}$).[77] The same electrode was always used for a particular set of data, for instance, data involving the addition of a particular base to protiated 1,4-QH_2 was used again to record similar measurements with deuterated 1,4-hydroquinone (1,4-QD_2). A platinum flag electrode served as the auxiliary electrode, and the reference electrode was an Ag/Ag^+ electrode (a silver wire immersed in the supporting electrolyte, 0.2 M $TBAPF_6$/3 mM silver

nitrate/acetonitrile). The reference electrode was separated from the rest of the solution by a glass tube capped with a porous vycor frit (CH Instruments). The potential of the silver reference electrode was periodically measured versus the formal potential (measured as the average of the peak potentials) of the ferrocene/ferrocenium (Fc/Fc^+) couple under the same conditions as the other experiments and thus all potentials are reported versus ferrocene as Fc/Fc^+. Prior to each use the polished glassy carbon electrode was first polished using 0.05 μm alumina paste (Buhler, Lake Bluff, Il) washed with deionized water, carefully wiped, and then sonicated for three minutes in acetonitrile. In each experiment the solution resistance (R_u) was totally compensated via positive feedback.

6.2.3 Preliminary Results

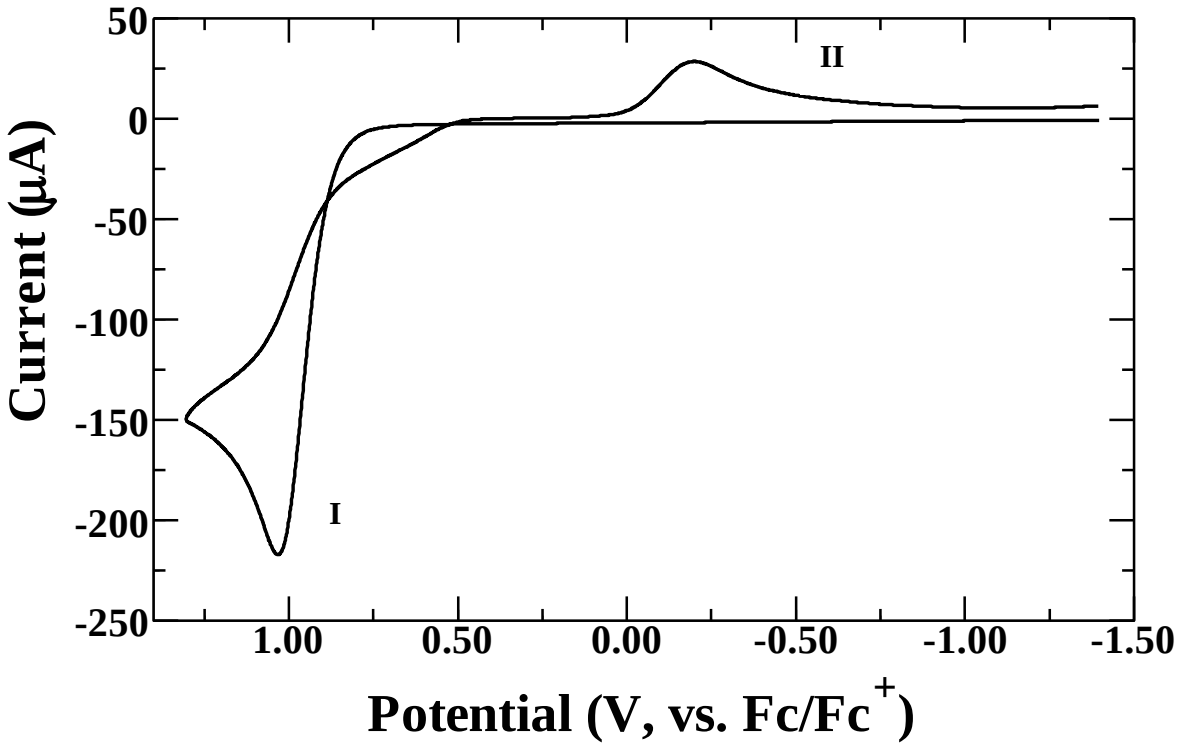

Figure 42. Voltammogram of 5.0 mM 2,4,6-tri-*tert*-butylphenol at a glassy carbon electrode (0.072 cm^2) in dry acetonitrile with 0.2 M $TBAPF_6$ as supporting electrolyte at 0.1 V s^{-1}.

The voltammogram of 2,4,6-tri-*tert*-butylphenol (TTBP) alone is given in Figure 42. Similar to the oxidation of QH_2 only one oxidation peak (I, 1.032 V) and one reduction peak (II, -0.200 V) are found in the voltammogram at 0.1 V s^{-1}. However, unlike the oxidation of QH_2 in acetonitrile, the cathodic peak current (i_{pc}) decreases with increasing scan rate. Initially, the i_{pc} is 37.1 μA, while at scan rates as high as 5 V s^{-1} no reduction peak is found. The oxidation of TTBP was thought to not involve the production of a polymer due to the substitution by the bulky *tert*-butyl groups. However, either polymerization or a slow disproportionation reaction occurs at the surface of the electrode and causes the loss of the reduction peak at higher scan rates, simulations will have to confirm which process takes place. By performing experiments at six different scan rates one can determine the redox mechanism taking place by the measurement of the peak potential and half peak potential versus the logarithm of scan rate. A shift from a situation where the chemical step is the rate determining step (RDS) to a situation where the electron transfer is the RDS can be derived from the values of $(E_p - E_{p/2})$ and $\partial E_p / \partial \log \nu$. This transition is characterized by an increase of $(E_p - E_{p/2})$ from 47.5 to 95 mV and an increase in $\partial E_p / \partial \log \nu$ from 29.6 to 59.2 mV/decade, for a two electron process at 25 ^oC. Since the values determined for $(E_p - E_{p/2})$ and $\partial E_p / \partial \log \nu$ are 0.095 ± 0.01 V and 0.048 ± 0.004 V $decade^{-1}$,the initial electron and proton transfers approximately follow an ECE process, yet are under mixed kinetic control.[18, 27]

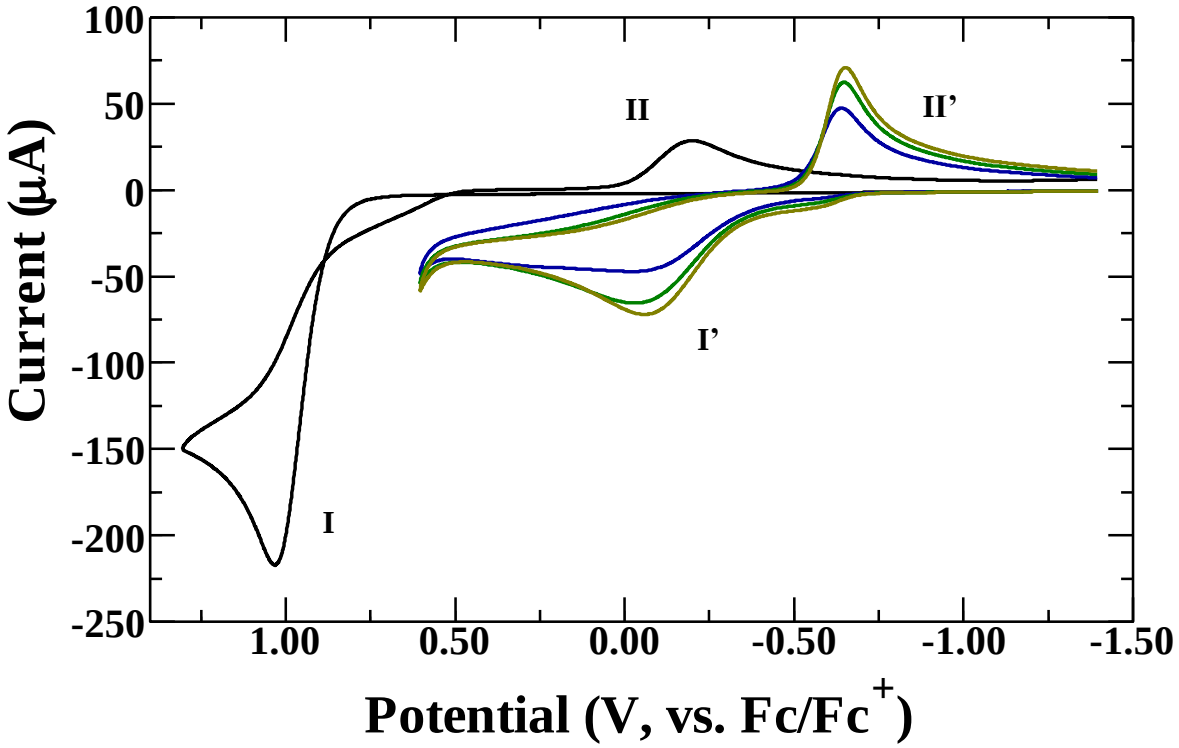

Figure 43. Voltammograms of 5.0 mM TTBP alone (black CV), with 5.0 mM acetate (blue CV), 10.0 mM acetate (green CV) and 20.0 mM acetate (dark yellow CV).

Addition of the acetates discussed in Chapters 3 and 4, acetate, benzoate and trifluoroacetate, causes a similar negative shift as noted with the addition of these same acetates to QH_2. Figure 43 illustrates the growth of a new set of redox peaks (I' and II') at the cost of the original TTBP peaks (I and II) with the addition of 5.0, 10.0 and 20.0 mM acetate. Peaks I' and II' are found at -0.059 and -0.651 V, respectively after addition of 20.0 mM acetate and likely represent the one-electron-one-proton oxidation of the acetate-TTBP complex. Diffusion ^{1}H-NMR studies are required to determine if this assessment of peaks I' and II' is correct. The peak current of peaks I' and II' increases as the concentration of acetate increases due to the increase of acetate and thus complexed TTBP in solution versus its conjugate acid, which is produced by the oxidation of TTBP. The potential window is shortened in the acetate addition CV's because of the oxidation of acetate at 0.820 V, which is responsible for the trailing anodic current at 0.6

V in Figure 43. Oxidation of acetates at the surface of GC electrodes has been known to modify/passivate the electrode.[171] In voltammograms of TTBP with 20.0 mM acetate with larger potential windows, the second one-electron oxidation peak of TTBP can be found at 1.045 V, yet there is no apparent reduction peak coupled to this oxidation. It is likely that reduction of all phenolic species proceeds through the reduction process at peak II', however, further studies are needed to confirm this. The addition of benzoate demonstrates a similar growth of a new redox peak system at negative potentials with respect to the original TTBP redox peaks (I and II). Table 13 presents data taken from voltammograms of 5.0 mM TTBP with acetate, benzoate and trifluoroacetate. From the data in Table 13 there is an apparent correlation between the shift in the oxidation peak, I', and the pK_a of the acetate. Initial experiments with the addition of trifluoroacetate to 5.0 mM TTBP resulted in the growth of a new oxidation peak without an accompanying reduction peak, thus only data corresponding to the addition of 10.0 mM trifluoroacetate is given in Table 13. Further experiments with trifluoroacetate are required to understand this chemistry and determine if this is a reproducible effect. The values of $\partial Ep/\partial \log \nu$ and $E_p - E_{p/2}$ for peak I' are much larger than those found for the addition of the amines or acetates to the QH_2's (Chapters 2 and 3). However, the values of $\partial Ep/\partial \log \nu$ and $E_p - E_{p/2}$ for peak II', -0.036 and -0.064 V, respectively, appear to indicate mixed kinetic control of the electron-proton transfer, assuming a two-electron, one proton transfer.[18, 27]

Table 13. Voltammetric values from the addition of acetate, benzoate and trifluoroacetate to 5.0 mM TTBP.

	pK_a[88]	$E_{p,I'}$ (V)[a]	$E_{p,II'}$ (V)[a]	ΔE_p (V)[a]	$\partial Ep/\partial \log \nu$ (V decade^{-1}, Peak I')	$\partial Ep/\partial \log \nu$ (V decade^{-1}, Peak II')	$E_p - E_{p/2}$ (V, peak I')	$E_p - E_{p/2}$ (V, peak II')
Acetate	22.3	-0.059	-0.651	0.592	0.105	-0.036	0.172	-0.064
Benzoate	20.7	0.177	-0.650	0.827	0.201	-0.044	0.102	-0.069
Trifluoroacetate	12.65	0.846	-	-	-	-	-	-

[a.] All voltammetric data taken from CV's at 0.1 V s^{-1} with 0.2 M $TBAPF_6$ as supporting electrolyte and 20.0 mM of the indicated acetate, except for data from trifluoroacetate CV's, which were from the addition of 10.0 mM trifluoroacetate.

Currently, the only mediators that have been investigated are (2,2'-bipyridine)iron (II) hexafluorophosphate ($Fe(bpy)_3(PF_6)_2$), tris(1,10-phenanthroline)iron (II) hexafluorophosphate ($Fe(phen)_3(PF_6)_2$) and ferrocene. The formal potentials of each of these potential mediators are given in Table 14. Typically, iron (II) complexes are used to oxidize phenols and hydroquinones.[75, 76, 169] Both $Fe(bpy)_3(PF_6)_2$ and $Fe(phen)_3(PF_6)_2$ will oxidize TTBP alone and a CV of 5.0 mM of each mediator with 5.0 mM TTBP shows an enhanced catalytic oxidation current for the oxidation of the mediators (data not shown). Ferrocene will not mediate the oxidation of TTBP alone, however upon addition of the various acetates this oxidation cycle may be possible, since the formal potential of ferrocene is at 0.000 V, similar to the oxidation potentials of TTBP with acetate and benzoate. If ferrocene is found to be an inadequate mediator, then other metal complexes will be investigated, which have more negative formal potentials. Possible chromium (II) mediators and their determined formal potentials are presented in Table 15.[172-174]

Table 14. Formal potentials of investigated possible mediators.

Complex	**E^o (V)[a]**
$Fe(bpy)_3(PF_6)_2$	0.779
$Fe(phen)_3(PF_6)_2$	0.791
Ferrocene	0.000

[a.] Estimated from measurement of $E_{1/2}$ values, where $E_{1/2} = (E_{pa} + E_{pc})/2$.

Table 15. Complexes and their formal potentials to be used as possible mediators in the oxidation of TTBP.

Complex	**E^o (V)[a]**
$Cr(bpy)_3^{2+}$	-0.26
$Cr(phen)_3^{2+}$	-0.28
$Cr(Tpy)_2^{2+}$ [b]	-0.17

[a.] The formal potentials were determined from the chloride salts of the respective complexes in H_2O.[173]
[b.] Tpy = 2,2':6',2"-Terpyridine

6.2.4 Conclusion

In summary, the addition of acetates, acetate, benzoate and trifluoroaceate, to TTBP results in similar voltammetry to that obtained in the oxidation of QH_2-acetate complexes. Diffusion ^{1}H-NMR studies are needed to determine whether TTBP-acetate complexes are formed. Upon determining whether hydrogen bound TTBP-acetate complexes are formed, inorganic complexes will be used in an attempt to mediate this oxidation through homogeneous electron transfer. Of the three complexes investigated to this point, tris(2,2'-bipyridine)iron (II) hexafluorophosphate ($Fe(bpy)_3(PF_6)_2$), tris(1,10-phenanthroline)iron (II) hexafluorophosphate ($Fe(phen)_3(PF_6)_2$) and ferrocene, only ferrocene seems to be a likely candidate based on its low determined formal potential (0.000 V) compared to the oxidation potentials of the supposed TTBP-acetate complexes (-0.059 to 0.846 V). Nevertheless, if the given mediators are found

unsuitable, various polypyridine complexes of chromium will be investigated as possible mediators of the TTBP-acetate complexes.

7.0 Conclusion

The results described in this dissertation show that the type (strong or weak) and state (charged or uncharged) of an added acid/base species can dramatically affect the kinetics and thermodynamics of the quinone/hydroquinone couple and less intricate proton-coupled electron transfer processes (PCET). The goal of this work was to study the electrochemical kinetics and thermodynamics of PCET systems that exhibited proton transfer to or from weak acids and bases and also through complexation. The knowledge established from this body of work could in the future be applied to electrode surfaces in order to make a reusable heterogeneous catalyst to be used in fuel cells or in chemical syntheses. Furthermore, this body of work is also directly applicable to biological enzymes, where within a low dielectric environment, similar to aprotic solvents, electron and proton transfers are catalyzed.

The addition of amines and carboxylates were both shown to make the oxidation of QH_2 easier in acetonitrile, via voltammetry. The observed potential shift from anodic potentials (~1 V) to less positive and even sometimes cathodic potentials was directly proportional to the pK_a of the added species. Complexation via hydrogen bonds was found for the oxidation of QH_2's in the presence of acetates in acetonitrile, while oxidation of QH_2's in the presence of amines was found to undergo proton transfer from the QH_2 to the amine. Complexation of QH_2 by acetate was established via ^{1}H-NMR. Here, a downfield shift of the phenolic proton peak or decrease in the diffusion coefficient (D) indicated complexation between QH_2 and the added species, because a complex will exhibit a smaller D than that of the QH_2 alone. Performing such

measurements is a novel concept in the study of PCET reactions, since this method involves *in situ* measurements of the diffusion coefficient.

The oxidation process of QH_2 both alone and in the presence of added species in acetonitrile is relatively unknown and in the past many assumptions have been made discussing this process. The many parameters that are often unknown and a cause for much of the oxidation process debate are the six pK_a's of the nine-membered square scheme. Here, the six pK_a values were determined and used in the simulations of QH_2's with the added amines and acetates. The simulations also included the determined D's determined by ^{1}H-NMR, reducing the number of fit parameters in simulations, thus enhancing the accuracy of the simulations. Furthermore, the evaluation of the voltammetry of QH_2 with titrated amines and carboxylates also assisted in the determination of the oxidation process, which further enhances the accuracy of the voltammetric fittings. The oxidation of the QH_2's both alone and with 30.0 mM of the acetates in acetonitrile was found to involve an ECEC process, while that of the QH_2's with titrated amines involved a CEEC process. The determination of the oxidation process of 1,4-hydroquinone (1,4-QH_2) in the presence of 10.0 mM acetate was more difficult, as this process exhibited two oxidation peaks. From the determined kinetic association constants of the QH_2's with the acetates the process was determined to involve a mixed complexation reaction and a proton transfer reaction. The proton transfer reaction was also studied via enhancement of this process through addition of conjugate acids to the QH_2-acetate solutions. Through studies of the voltammetry, knowledge of the kinetic constants of the QH_2/acetate species, kinetics of the homoconjugation reaction and the initial concentrations of each species the proton transfer reaction involved a CEEC oxidation.

The study of two viologen-like molecules assisted in the determination of kinetic effects under unbuffered and buffered conditions. In this study, both N-methyl-4,4'-bipyridyl chloride

($NMBC^+$), a reversible electroactive species, and 1-(4-Pyridyl)Pyridinium Chloride (PPC^+**),** an irreversible electroactive species were evaluated. The reduction of these two molecules was initially believed to be more easily understood than the quinone/hydroquinone couple since the reduction of these species only involves electron and proton transfer to six species rather than nine. In order to understand the experimental results a hypothetical model involving a simulated species, B, was undertaken. The experimental and simulated species both exhibited the known thermodynamic effects brought about by performing experiments in buffer or without buffer. However, by measuring the peak-to-peak separation (ΔE_p) during the known voltammetry thermodynamic effects exhibited a broadening of the peaks due to the transition from a CE to EC reaction, when studying only one electron-proton transfer. This effect was further amplified through simulations by lowering the kinetic rate constants for proton transfer, which limits proton transfer during the transition, causing maximum broadening of the voltammetric peaks at the midpoint pH between $pK_{a,1}$ and $pK_{a,2}$. In order to visualize this effect experimentally, the buffer concentration was lowered considerably, which limits proton transfer causing the peaks to separate. Interestingly, another influence on the experimental voltammetry was the apparent potential inversion of the PPC^+ species under aqueous and non-aqueous conditions. This result was further studied by computational methods including simulations, however, the simulations of both PPC^+ and $NMBC^+$ were somewhat inconclusive due to the the influence of inverted potentials and surface absorption.

Some preliminary work has been discussed on potential future directions for this work including the modification glassy carbon electrodes by diazonium species and the study of hydrogen bound species by electromediation. It is the expectation that the knowledge of proton transfer processes and hydrogen bond complexations between QH_2's and amines and

carboxylates, respectively, can be applied to an electrode surface for the purpose of visualizing heterogeneous catalysis. Additionally, in the future the goal is to study hydrogen bound complexes of QH_2 and acetate or phenols with acetate via electromediated oxidation. It is possible that a *concerted* proton-electron transfer may be happening, but it is difficult to visualize via heterogeneous electron transfer at the electrode and homogeneous proton transfer in solution. Therefore, the goal is to study both the electron and proton transfer process homogeneously.

8.0 References

1. Goor, G.; Glenneberg, J.; Jacobi, S., Hydrogen Peroxide. In *Ullmann's Encyclopedia of Industrial Chemistry*, Wiley-VCH: Weinheim, 2007; pp 1-36.
2. Chambers, J. Q., Electrochemistry of Quinones. In *The Chemistry of Quinoid Compounds*, Patai, S.; Rappoport, Z., Eds. John Wiley and Sons: New York, 1988; Vol. 2, pp 719 - 758.
3. Cramer, W. A.; Knaff, D. B., *Energy Transduction in Biological Membranes: A Textbook of Bioenergetics*. Springer-Verlag: New York, 1990.
4. Trumpower, B. L., *Function of Quinones in Energy Conserving Systems*. Academic Press: New York, 1982.
5. Garret, R. H.; Grisham, C. M., *Biochemistry*. 2 ed.; Brooks/Cole: Pacific Grove, 1999.
6. Brownlee, M., The Pathobiology of Diabetic Complications: A Unifying Mechanism. *Diabetes* **2005,** 54, 1615-1625.
7. Hirst, J., Energy Transduction by Respiratory Complex I - an Evaluation of Current Knowledge. *Biochem. Soc. Trans.* **2005,** 33, 525-529.
8. Nicholls, D. G.; Ferguson, S. J., *Bioenergetics*. 3 ed.; Academic Press: San Diego, CA, 2002.
9. Chitnis, P. R., Photosystem I: Function and Physiology. *Annu. Rev. Plant Physiol. Plant Mol. Biol.* **2001,** 52, 593-626.
10. Nelson, N.; Yocum, C. F., Structure and Function of Photosystems I and II. *Annu. Rev. Plant Biol.* **2006,** 57, 521-565.
11. Meyer, T. J.; Huynh, V. H.; Thorp, H. H., The Possible Role of Proton-Coupled Electron (PCET)in Water Oxidation by Photosystem II. *Angew. Chem. Int. Ed.* **2007,** 46, 5284-5304.
12. Hankamer, B.; Barber, J.; Boekema, E. J., Structure and Membrane Organization of Photosystem II in Green Plants. *Annu. Rev. Plant Physiol. Plant Mol. Biol.* **1997,** 48, 641-671.
13. Muller, O. H.; Baumberger, J. P., Oxidation-reduction potentials measured with the dropping mercury electrode. II. Polarographic Investigation. An introduction to a new method. *Trans. Electrochem. Soc.* **1937,** 71, 181-194.
14. Quan, M.; Sanchez, D.; Wasylkiw, M. F.; Smith, D. K., Voltammetry of Quinones in Unbuffered Aqueous Solution: Reassessing the Roles of Proton Transfer and Hydrogen Bonding in the Aqueous Electrochemistry of Quinones. *J. Am. Chem. Soc.* **2007,** 129, 12847-12856.
15. Costentin, C., *Chem. Rev.* **2008,** 108, 2145-2179.
16. Huynh, M. H. V.; Meyer, T. J., Proton-Coupled Electron Transfer. *Chem. Rev.* **2007,** 107, 5004-5064.
17. Mayer, J. M., Proton-Coupled Electron Transfer. *Annu. Rev. Phys. Chem.* **2004,** 55, 363-390.
18. Saveant, J.-M., *Elements of Molecular and Biomolecular Electrochemistry: An Electrochemical Approach to Electron Transfer Chemistry*. Wiley: New York, 2006.
19. Costentin, C.; Robert, M.; Saveant, J.-M., Electrochemical Concerted Proton and Electron Transfers. Potential-Dependent Rate Constant, Reorganization Factors, Proton Tunneling and Isotope Effects. *J. Electroanal. Chem.* **2006,** 588, 197-206.
20. Hammes-Schiffer, S.; Soudackov, A. V., Proton-Coupled Electron Transfer in Solution, Proteins and Electrochemistry. *J. Phys. Chem. B* **2008,** 112, 14108-14123.

21. Weatherly, S. C.; Yang, I. V.; Armistead, P. A.; Thorp, H. H., Proton-Coupled Electron Transfer in Guanine Oxidation: Effects of Isotope, Solvent and Chemical Modification. *J. Phys. Chem. B* **2003,** 107, 372-378.
22. Nakamura, H.; Sakamoto, T.; Wada, A., *Protein Eng.* **1988,** 2, 177-183.
23. Reece, S. Y.; Nocera, D. G., Proton-Coupled Electron Transfer in Biology: Results from Synergistic Studies in Natural and Model Systems. *Annu. Rev. Biochem.* **2009,** 78, 673-699.
24. Bard, A. J.; Faulkner, L. R., *Electrochemical Methods: Fundamentals and Applications*. 2 ed.; Wiley: New York, 2001.
25. Kissinger, P. T.; Hineman, W. R., Cyclic Voltammetry. *J. Chem. Ed.* **1983,** 60, 702-706.
26. Mabbot, G. A., An Introduction to Cyclic Voltammetry. *J. Chem. Ed.* **1983,** 60, 697-702.
27. Nadjo, L.; Saveant, J.-M., Linear Sweep Voltammetry: Kinetic Control by Charge Transfer and/or Secondary Chemical Reactions. *J. Electroanal. Chem.* **1973,** 48, 113-145.
28. Silverstein, R. M.; Webster, F. X.; Kiemle, D. J., *Spectometric Identification of Organic Compounds*. 7 ed.; John Wiley and Sons, Inc.: Hoboken, NJ, 2005.
29. Cohen, Y.; Avram, L.; Frish, L., Diffusion NMR Spectroscopy in Supramolecular and Combinatorial Chemistry: An Old Parameter-New Insights. *Angew. Chem. Int. Ed.* **2005,** 44, 520-554.
30. Stejskal, E. O., Tanner, J.E., Spin Diffusion Measurements: Spin Echoes in the Presence of a Time-Dependent Field Gradient. *J. Chem. Phys.* **1965,** 42, 288-292.
31. Fielding, L., Determination of Association Constants (K_a) from Solution NMR Data. *Tetrahedron* **2000,** 56, 6151-6170.
32. Price, W. S., Pulsed-Field Gradient Nuclear Magnetic Resonance as a Tool for Studying Translational Diffusion: Part 1. Basic Theory. *Concepts Magn. Reson.* **1997,** 9, 299-336.
33. Stoll, S.; Schweiger, A., EasySpin, a Comprehensive Software Package for Spectral Simulation and Analysis in EPR. *J. Magn. Reson.* **2006,** 178, 42-55.
34. Cloverdale, R. T.; Jennings, H. M.; Garboczi, E. J., An Improved Model for Simulating Impedance Spectroscopy. *Comp. Mat. Sci.* **1995,** 3, 465-474.
35. Rudolph, M.; Reddy, D. P.; Feldberg, S. W., A Simulator for Cyclic Voltammetric Responses. *Anal. Chem.* **1994,** 66, 589A-600A.
36. Feldberg, S. W., Simulation of Electroanalytical Systems ~ 1962-2002. In *Historical Perspectives on the Evolution of Electrochemical Tools*, Leddy, J.; Birss, V.; Vanysek, P., Eds. The Electrochemical Society: Pennington, NJ, 2004; pp 189-214.
37. Kaifer, A. E.; Gomez-Kaifer, M., *Supramolecular Electrochemistry*. Wiley-VCH: Weinheim, 2001.
38. Rudolph, M., Digital Simulations with the Fast Implicit Finite Difference Algorithm: The Development of a General Simulator for Electrochemical Processes. In *Physical Electrochemistry: Principles, Methods and Applications*, Rubinstein, I., Ed. Marcel Dekker: New York, 1995; pp 81-130.
39. Rudolph, M., A Fast Implicit Finite Difference Algorithm for the Digital Simulation of Electrochemical Processes. *J. Electroanal. Chem.* **1991,** 314, 13-22.
40. Rudolph, M., Digital Simulations with the Fast Implicit Finite Difference (FIFD) Algorithm: Part II. An Improved Treatment of Electrochemical Mechanisms with Second-Order Reactions. *J. Electroanal. Chem.* **1992,** 338, 85-98.
41. Frisch, M. J.; Trucks, G. W.; Schlegel, H. B.; Scuseria, G. E.; Robb, M. A.; Cheeseman, J. R.; Jr., J. A. M.; Vreven, T.; Kudin, K. N.; Burant, J. C.; Millam, J. M.; Iyengar, S. S.; Tomasi,

J.; Barone, V.; Mennucci, B.; Cossi, M.; Scalmani, G.; Rega, N.; Petersson, G. A.; Nakatsuji, H.; Hada, M.; Ehara, M.; Toyota, K.; Fukuda, R.; Hasegawa, J.; Ishida, M.; Nakajima, T.; Honda, Y.; Kitao, O.; Nakai, H.; Klene, M.; Li, X.; Knox, J. E.; Hratchian, H. P.; Cross, J. B.; Bakken, V.; Adamo, C.; Jaramillo, J.; Gomperts, R.; Stratmann, R. E.; Yazyev, O.; Austin, A. J.; Cammi, R.; Pomelli, C.; Ochterski, J. W.; Ayala, P. Y.; Morokuma, K.; Voth, G. A.; Salvador, P.; Dannenberg, J. J.; Zakrzewski, V. G.; Dapprich, S.; Daniels, A. D.; Strain, M. C.; Farkas, O.; Malick, D. K.; Rabuck, A. D.; Raghavacharti, K.; Foresman, J. B.; Ortiz, J. V.; Cui, Q.; Baboul, A. G.; Clifford, S.; Cioslowski, J.; Stefanov, B. B.; Liu, G.; Liashenko, A.; Piskorz, P.; Komaromi, I.; Martin, R. L.; Fox, D. J.; Keith, T.; Al-Laham, M. A.; Peng, C. Y.; Nanayakkara, A.; Challacombe, M.; Gill, P. M. W.; Johnson, B.; Chen, W.; Wong, W. M.; Gonzalez, C.; Pople, J. A. Gaussian 03, Revision D.02; Gaussian Inc.: Pittsburg, PA, 2003.

42. Hehre, W. J., *A Guide to Molecular Mechanics and Quantum Chemical Calulations*. 2 ed.; Wavefunction, Inc.: Irvine, CA, 2006.

43. Bott, A.; Feldberg, S.; Rudolph, M., Fitting Experimental Cyclic Voltammetry Data with Theoretical Simulations Using DigiSim 2.1. *Curr. Sep.* **1996,** 15, 67-71.

44. Foresman, J. B.; Frisch, A., *Exploring Chemistry with Electronic Structure Methods*. 2 ed.; Gaussian, Inc.: Pittsburgh, PA, 1996.

45. Cramer, C. J., *Essentials of Computational Chemistry: Theories and Models*. John Wiley and Sons, Inc.: New York, 2002.

46. Miertus, S.; Tomasi, J., Approximate Evaluations of the Electrostatic Free Energy and Internal Energy Changes in Solution Processes. *Chem. Phys.* **1982,** 65, 239-245.

47. Miertus, S.; Scrocco, E.; Tomasi, J., Electrostatic Interaction of a Solute with a Continuum. A Direct Utilization of ab initio Molecular Potentials for the Prevision of Solvent Effects. *Chem. Phys.* **1981,** 55, 117-129.

48. Maroti, P.; Hanson, D. K.; Schiffer, M.; Sebban, P., Long Range Electrostatic Interaction in the Bacterial Photosynthetic Reaction Center. *Nature Struct. Biol.* **1995,** 2, 1057-1059.

49. Miksovska, J.; Maroti, P.; Tandori, J.; Schiffer, M.; Hanson, D. K.; Sebban, P., Distant Electrostatic Interactions Modulate the Free Energy Level of QA- in the Photosynthetic Reaction Center. *Biochemistry* **1996,** 35, 15411-15417.

50. Ishikita, H.; Morra, G.; Knapp, E.-W., Redox Potential of Quinones in Photosynthetic Reaction Centers from *Rhodobacter sphaeroides*: Dependence on Protonation of Glu-L212 and Asp-L213. *Biochemistry* **2003,** 42, 3882-3892.

51. Paddock, M. L.; Feher, G.; Okamura, M. Y., Proton and Electron Transfer to the Secondary Quinone (Q_B) in Bacterial Reaction Centers: The Effect of Changing the Electrostatics in the Vicinity of Q_B by Interchanging Asp and Glu at the L212 and L213 Sites. *Biochemistry* **1997,** 36, 14238-14249.

52. Paddock, M. L.; Rongey, S. H.; Feher, G.; Okamura, M. Y., Pathway of proton transfer in bacterial reaction centers: Replacement of glutamic acid 212 in the L subunit by glutamine inhibits quinone (secondary acceptor) turnover. *Proc. Natl. Acad. Sci. USA* **1989,** 86, 6602-6606.

53. Takaashi, E.; Wraight, C. A., Small Weak Acids Reactivate Proton Transfer in Reaction Centers from *Rhodobacter sphaeroides* Mutated at Asp^{L210} and Asp^{M17}. *J. Biol. Chem.* **2006,** 281, 4413-4422.

54. Astudillo, P. D.; Tiburcio, J.; Gozalez, F. J., The role of acids and bases on the electrochemical oxidation of hydroquinone: Hydrogen bonding interactions in acetonitrile. *J. Electroanal. Chem.* **2007,** 604, 57-64.

55. Garza, J.; Vargas, R.; Gomez, M.; Gonzalez, I.; Gonzalez, F. J., Theoretical and Electrochemical Study of Quinone-Benzoic Acid Adduct Linked by Hydrogen Bonds. *J. Phys. Chem. A* **2003,** 107, 11161-11168.
56. Costentin, C., Electrochemical Approach to The Mechanistic Study of Proton-Coupled Electron Transfer. *Chem. Rev.* **2008,** 108, 2145-2179.
57. Gupta, N.; Linschitz, H., Hydrogen-Bonding and Protonation Effects in Electrochemistry of Quinones in Aprotic Solvents. *J. Am. Chem. Soc.* **1997,** 119, 6384-6391.
58. Lehmann, M. W.; Evans, D. H., Mechanism of The Electrochemical Reduction of 3,5-Di-tert-butyl-1,2-benzoquinone. Evidence for a Concerted Electron and Proton Transfer Reaction Involving a Hydrogen Bonded Complex as a Reactant. *J. Phys. Chem. B* **2001,** 105, 8877-8884.
59. Macias-Ruvalcaba, N. A.; Okumura, N.; Evans, D. H., Change in the Reaction Pathway in the Reduction of 3,5-Di-tert-butyl-1,2-benzoquinone with Increasing Concentrations of 2,2,2-Trifluoroethanol. *J. Phys. Chem. B* **2006,** 110, 22043-22047.
60. Aguilar-Martinez, M.; Macias-Ruvalcaba, N. A.; Bautista-Martinez, J. A.; Gomez, M.; Gonzalez, F. J.; Gonzalez, I., Review: Hydrogen Bond and Protonation as Modifying Factors of the Quinone Reactivity. *Curr. Org. Chem* **2004,** 8, 1721-1738.
61. Parker, V. D., The Anodic Oxidation of Hydroquinone in Acetonitrile on the Question of a Possible One Electron Intermediate. *Electrochim. Acta* **1973,** 18, 519-524.
62. Duvall, H. S.; McCreery, R. L., Control of Catechol and Hydroquinone Electron-Transfer Kinetics on Native and Modified Glassy Carbon Electrodes. *Anal. Chem.* **1999,** 71, 4594-4602.
63. Duvall, H. S.; McCreery, R. L., Self-Catalysis by Catechols and Quinones During Heterogenous Electron Transfer at Carbon Electrodes. *J. Am. Chem. Soc.* **2000,** 122, 6759-6764.
64. Lehmann, M. W.; Evans, D. H., Effect of Comproportionation on Voltammograms for Two-Electron Reactions with an Irreversible Second Electron Transfer. *Anal. Chem.* **1999,** 71, (10), 1947-1950.
65. Wipf, D. O.; Wehmeyer, K. R.; Wightman, R. M., Disproportionation of Quinone Radical Anions in Protic Solvents at High pH. *J. Org. Chem.* **1986,** 51, 4760-4764.
66. Eggins, B. R.; Chambers, J. Q., Proton Effects in the Electrochemistry of the Quinone Hydroquinone System in Aprotic Solvents. *J. Electrochem. Soc.* **1970,** 117, 186-192.
67. Stallings, M. D.; Morrison, M. M.; Sawyer, D. T., Redox Chemistry of Metal-Catechol Complexes in Aprotic Media. 1. Electrochemistry of Substituted Catechols and Their Oxidation Products. *Inorg. Chem.* **1981,** 20, 2655-2660.
68. Uno, B.; Okumura, N.; Goto, M.; Kano, K., n-sigma Charge Transfer Interaction and Molecular and Electronic Structural Properties in Hydrogen Bonding Systems Consisting of p-Quinone Dianions and Methyl-Alcohol. *J. Org. Chem.* **2000,** 65, 1448-1455.
69. Uno, B.; Okumura, N.; Seto, K., Bistable Charge-Transfer Complex Formation of Redox-Active Organic Molecules Based on Intermolecular HOMO-LUMO Interaction Controlled by the Redox Reactions. *J. Phys. Chem. A* **2000,** 104, 3064-3072.
70. Okumura, N.; Uno, B., Electronic Spectra of the Electrogenerated 1,4-Benzoquinone pi-dianion and the Strongly Hydrogen Bonded Charge Transfer Complex with Methanol. *Bull. Chem. Soc. Jpn.* **1999,** 72, 1213-1217.
71. Chan-Leonor, C.; Martin, S. L.; Smith, D. K., Electrochemically Controlled Hydrogen Bonding. Redox-Dependent Formation of a 2:1 Diarylurea/Dinitrobenzene^{2-} Complex. *J. Org. Chem.* **2005,** 70, 10817-10822.

72. Bu, J.; Lilienthal, N. D.; Woods, J. E.; Nohrden, C. E.; Hoang, K. T.; Truong, D.; Smith, D. K., Electrochemically Controlled Hydrogen Bonding. Nitrobenzenes as Simple Redox-Dependent Receptors for Arylureas. *J. Am. Chem. Soc.* **2005,** 127, 6423-6429.
73. Costentin, C.; Robert, M.; Saveant, J.-M., Carboxylates as Proton Accepting Groups in Concerted Proton Electron Transfers. Electrochemistry of the 2,5-Dicarboxylate-1,4-Hydroxybenzoquinone/2,5-Dicarboxy-1,4-Benzoquinone Couple. *J. Am. Chem. Soc.* **2006,** 128, 8726-8727.
74. Costentin, C.; Robert, M.; Saveant, J.-M., Electrochemical and Homogeneous Proton-Coupled Electron Transfers: Concerted Pathways in the One Electron Oxidation of a Phenol Coupled with an Intramolecular Amine-Driven Proton Transfer. *J. Am. Chem. Soc.* **2006,** 128, 4552-4553.
75. Rhile, I. J.; Markle, T. F.; Nagao, H.; DiPasquale, A. G.; Lam, O. P.; Lockwood, M. A.; Rotter, K.; Mayer, J. M., Concerted Proton-Electron Transfer in the Oxidation of Hydrogen-Bonded Phenols. *J. Am. Chem. Soc.* **2006,** 128, 6075-6088.
76. Markle, T. F.; Mayer, J. M., Concerted Proton-Electron Transfer in Pyridylphenols: The Importance of the Hydrogen Bond. *Angew. Chem. Int. Ed.* **2008,** 47, 738-740.
77. Berger, S.; Braun, S., 200 and More NMR Experiments A Practical Course. In Wiley-VCH: Weinheim, 2004; pp 467-469.
78. Guillorn, M. A.; McKnight, T. E.; Melecho, A.; Merkulov, V. I.; Britt, P. F.; Austin, D. W.; Lowndes, D. H.; Simpson, M. L., Individually Addressable Vertically Aligned Carbon Nanofiber-based Electrochemical Probes. *J. App. Phys.* **2002,** 91, 3824-3828.
79. Sun, H.; Chen, W.; Kaifer, A. E., A Simple Method Based on NMR Spectroscopy and Ultramicroelectrode Volatmmetry for the Determination of the Number of Electrons in Faradic Processes. *Organometallics* **2006,** 25, 1828-1830.
80. Becke, A. D., *J. Chem. Phys.* **1993,** 98, 5648-5652.
81. Lee, C.; Yang, W.; Parr, R. G., *Phys. Rev. B* **1988,** 37, 785-789.
82. Klampt, A.; Schuurman, G., *J. Chem. Soc. Perkin Trans. 2* **1993**, 799-805.
83. Liptak, M. D.; Gross, K. C.; Seybold, P. G.; Feldgus, S.; Shields, G. C., Absolute pKa Determinations for Substituted Phenols. *J. Am. Chem. Soc.* **2002,** 124, 6421-6427.
84. Liptak, M. D.; Shields, G. C., Accurate pK_a Calculations for Carboxylic Acids Using Complete Basis Set and Gaussian-n Models Combined with CPCM Continuum Solvation Methods. *J. Am. Chem. Soc.* **2001,** 123, 7314-7319.
85. Gao, D.; Svoronos, P.; Wong, P. K.; Maddalena, D.; Hwang, J.; Walker, H., pKa of Acetate in Water: A Computational Study. *J. Phys. Chem. A* **2005,** 109, 10776-10785.
86. Holland, J. P.; Green, J. C.; Dilworth, J. R., Probing the Mechanism of Hypoxia Selectivity of Copper bis(thiosemicarbazonato) complexes: DFT calculation of Redox Potentials and Absolute Acidities in Solution. *Dalton Trans.* **2006**, 783-794.
87. Kelly, C. P.; Cramer, C. J.; Truhlar, D. G., Single-Ion Solvation Free Energies and the Normal Hydrogen Electrode Potential in Methanol, Acetonitrile, and Dimethyl Sulfoxide. *J. Phys. Chem. B* **2007,** 111, 408-422.
88. Izutsu, K., *Acid-Base Dissociation Constants in Dipolar Aprotic Solvents*. Blackwell Scientific Publications: London, 1990.
89. Sasaki, M.; Osugi, J.; Inagaki, Y., High-Pressure Kinetics of the Reactions of p-Benzoquinone with Aliphatic Amines in Aprotic Solvents. *J. Chem. Soc. Perkin Trans. 2* **1985**, 115-119.

90. Yamaoka, T.; Nagakura, S., Reactions of Aliphatic Amines with p-Benzoquinone and it Chloro Derivatives. *Bull. Chem. Soc. Jpn.* **1971,** 44, 2971-2975.
91. Connors, K. A., *Binding Constants, The Measurement of Molecular Complex Stability*. John Wiley and Sons: New York, 1987.
92. Becker, E. D., *High Resolution NMR: Theory and Chemical Applications*. Academic Press: London, 2000.
93. Saiki, H.; Takami, K.; Tominaga, T., Diffusion of Porphyrins and Quinones in Organic Solvents. *Phys. Chem. Chem. Phys.* **1999,** 1, 303-306.
94. Lide, D. R., *CRC Handbook of Chemistry and Physics, 87th ed.* CRC Press: 2007.
95. Nadjo, L.; Saveant, J.-M., Linear Sweep Voltammetry: Kinetic Control by Charge Transfer and/or Secondary Chemical Reactions. *J. Electroanal. Chem.* **1973,** 117, 113-145.
96. Mohammed, O. F.; Pines, D.; Dreyer, J.; Pines, E.; Nibbering, E. T. J., Sequential Proton Transfer Through Water Bridges in Acid-Base Reactions. *Science* **2005,** 310, 83-85.
97. Hibbert, F.; Long, F. A., Proton Transfer from Cyanocarbon Acids. IV. Kinetic Ionization Behavior of p-Nitrobenzyl Cyanide and Bromomalonitrile. *J. Am. Chem. Soc.* **1972,** 94, 2647-2651.
98. Yamdagni, R.; Kebarle, P., Solvation of Negative Ions by Protic and Aprotic Solvents. Gas-Phase Solvation of Halide Ions by Acetonitrile and Water Molecules. *J. Am. Chem. Soc.* **1972,** 94, 2940-2943.
99. Shan, S.-o.; Loh, S.; Herschlag, D., The Energetics of Hydrogen Bonds in Model Systems: Implications for Enzymatic Catalysis. *Science* **1996,** 272, 97-101.
100. Saveant, J.-M., Eletrochemical Concerted Proton and Electron Transfers. Further Insights in the Reduction Mechanism of Superoxide Ion in the Presence of Water and Other Weak Acids. *J. Phys. Chem. C* **2007,** 111, 2819-2822.
101. Singh, P. S.; Evans, D. H., Study of the Electrochemical Reduction of Dioxygen in Acetonitrile in the Presence of Weak Acids. *J. Phys. Chem. B* **2006,** 110, 637-644.
102. Derome, A. E., *Modern NMR Techniques for Chemistry Research*. Pergamon Press: Oxford, 1991; Vol. 6.
103. Fife, T. H.; Natarajan, R., General Acid Catalyzed Acetal Hydrolysis. The Hydrolysis of Acetals and Ketals of Cis- and Trans-1,2-Cyclohexanediol. Changes in Rate-Determining Step and Mechanism as a Function of pH. *J. Am. Chem. Soc.* **1986,** 108, 8050-8056.
104. Kirby, A. J., General Acid-Base Catalysis in Model Systems. In *Hydrogen-Transfer Reactions*, Hynes, J. T.; Klinman, J. P.; Limbach, H.-H.; Schowen, R. L., Eds. Wiley-VCH: Weinheim, 2007; pp 975-1012.
105. Kirby, A. J., Acid-Base Catalysis in Enzymes. In *Handbook of Proteins: Structure, Function and Methods*, 2007; Vol. 1, pp 429-435.
106. Laviron, E., Electrochemical Reactions with Protonations at Equilibrium. Part IV. General Considerations on the Reaction Sequence. *J. Electroanal. Chem.* **1981,** 130, 23-29.
107. Laviron, E., Electrochemical Reactions with Protonations at Equilibrium. Part III. The 1*e*, $2H^+$ Reaction (Six-Member Ladder Scheme) for a Surface or for a Heterogeneous Reaction. *J. Electroanal. Chem.* **1981,** 124, 9-17.
108. Laviron, E., Electrochemical Reactions with Protonations at Equilibrium. Part II. The 1*e* $1H^+$ Reaction (Four-Member Square Scheme) for a Heterogeneous Reaction. *J. Electroanal. Chem.* **1981,** 124, 1-7.

109. Laviron, E., Electrochemical Reactions with Protonations at Equilibrium. Part VI. The Homogeneous Electron Exchange Reaction Between a Monoelectric and a 1*e*, 1 H^+ System. *J. Electroanal. Chem.* **1982,** 137, 1-15.
110. Roullier, L.; Laviron, E., Etude Electochimique de Radicaux Libres - III Etude des Radicaux aux Derives des Naphthyridines -1.5, -1.6, -1.7, -1.8, -2.6 et -2.7 et du Bipyridyl-4,4'. *Electrochim. Acta* **1978,** 23, 773-779.
111. Laviron, E., Electrochemical Reactions with Protonations at Equilibrium. Part VIII. The 2*e*, $2H^+$ Reaction (Nine-Member Square Scheme) for a Surface or for a Heterogeneous Reaction in the Absence of Disproportionation and Dimerization Reactions. *J. Electroanal. Chem.* **1983,** 146, 15-36.
112. O'Connell, K. M.; Waldner, E.; Roullier, L.; Laviron, E., Experimental Study of Redox Modified Electrodes with Simulatneous Electron and Proton Exchange. *J. Electroanal. Chem.* **1984,** 162, 77-85.
113. Laviron, E., Electrochemical Reactions with Protonations ar Equlibrium. Part XIII. Experimental Study of the Homogeneous Electron Exchange in Quinone/Dihydroquinone Systems. *J. Electroanal. Chem.* **1986,** 208, 357-372.
114. Laviron, E., Electrochemical Reactions with Protonations at Equilibrium. Part X. The Kinetics of the *p*-Benzoquinone/Hydroquinone Couple on a Platinum Electrode. *J. Electroanal. Chem.* **1984,** 164, 213-227.
115. Laviron, E., Theoretical Study of a 1*e*, $1H^+$ Surface Electrochemical Reaction (Four-Membered Square Scheme) when the Protonation Reactions are at Equilibrium. *J. Electroanal. Chem.* **1980,** 109, 57-67.
116. Laviron, E., Theoretical Study of a Simple Redox System with Adsorption of the Reactants on a Rotating Disk Electrode. Part I. The Reaction Path in the Case of a Langmuirian Adsorption Equilibrium. *J. Electroanal. Chem.* **1981,** 124, 19-33.
117. Finklea, H. O., Theory of Coupled Electron-Proton Transfer with Potential-Dependent Transfer Coefficients for Redox Couples Attached to Electrodes. *J. Phys. Chem. B* **2001,** 105, 8685-8693.
118. Finklea, H. O., Consequences of a Potential-dependent Transfer Coefficient in AC Voltammetry and in Coupled Electron-Proton Transfer for Attached Redox Couples. *J. Electroanal. Chem.* **2001,** 495, 79-86.
119. Laviron, E.; Roullier, L., Electrochemical Reactions with Protonations at Equilibrium. Part IX. Comparison Between the Surface and Heterogeneous Electrochemical Rate Constants in the System Phenazine/Dihydrophenazine. *J. Electroanal. Chem.* **1983,** 157, 7-18.
120. Maran, F.; Workentin, M. S., Dissociative Electron Transfer. *Interface* **2002**, (Winter), 44-49.
121. Andrieux, C. P.; Saveant, J.-M.; Tallec, A.; Tardivel, R.; Tardy, C., Concerted and Stepwise Dissociative Electron Transfers. Oxidizability of the Leaving Group and Strength of the Breaking Bond as Mechanism and Reactivity Governing Factors Illustrated by the Electrochemical Reduction of a-Substituted Acetophenones. *J. Am. Chem. Soc.* **1997,** 119, 2420-2429.
122. Andrieux, C. P.; Saveant, J.-M.; Tardy, C., Transition between Concerted and Stepwise Dissociative Electron Transfers. An Example of How a Change of Temperature May Trigger a Change in Mechanism in Electrochemical Experiments. *J. Am. Chem. Soc.* **1997,** 119, 11546-11547.

123. Hammarstrom, L.; Almgren, M.; Norrby, T., Transmembrane Electron Transfer Mediated by a Viologen: A Mechanism Involving Diffusion of Doubly Reduced Viologen Formed by Disproportionation of Viologen Radical. *J. Phys. Chem.* **1992,** 96, 5017-5024.
124. Popisil, L.; Kuta, J.; Volke, J., Adsorption Coupled Electrode Kinetics of Bipyridylium-Based Herbicides: Admittance Measurement at the DME in Aqueous 1 M Potassium Fluoride. *J. Electroanal. Chem.* **1975,** 58, (1), 217-227.
125. Michaelis, L.; Hill, E. S., The Viologen Indicators. *J. Gen. Physiol.* **1933,** 16, 859-873.
126. Bird, C. L.; Kuhn, A. T., Electrochemistry of Viologens. *Chem. Soc. Rev.* **1981,** 10, 49-82.
127. Evans, D. H.; Hu, K., Inverted Potentials in Two-Electron Processes in Organic Electrochemistry. *J. Chem. Soc. Faraday Trans.* **1996,** 92, 3983-3990.
128. Macias-Ruvalcaba, N. A.; Evans, D. H., Studies of Potential Inversion in the Electrochemical Reduction of 11,11,12,12-Tetracyano-9,10-anthraquinodimethane and 2,3,5,6-Tetramethyl-7,7,8,8-tetracyano-1,4-benzoquinodimethane. *J. Phys. Chem. B* **2006,** 110, 5155-5160.
129. Gruhn, N. E.; Macias-Ruvalcaba, N. A.; Evans, D. H., Studies of the Inner Reorganization Energies of the Cation Radicals of 1,4-Bis(dimethylamino)benzene, 9,10-Bis(dimethylamino)anthracene and 3,6-Bis(dimethylamino)durene by Photoelectron Spectroscopy and Reinterpretation of the Mechanism of the Electrochemical Oxidation of the Parent Diamines. *J. Phys. Chem. A* **2006,** 110, 5650-5655.
130. Macias-Ruvalcaba, N. A.; Evans, D. H., Electron-Transfer Reactions with Significant Changes in Structure. Unsymmetrical Crowded Ethylenes. *J. Phys. Chem. B* **2006,** 110, 24786-24795.
131. Lehmann, M. W.; Singh, P.; Evans, D. H., Potential Inversion in the Reduction of *trans*-2,3-dinitro-2-butene. *J. Electroanal. Chem.* **2003,** 549, 137-143.
132. Khalid, I. M.; Pu, Q.; Alvarez, J. C., Thermodynamic and Kinetic Enhancement of Electrochemical Sensitivity by Chemical Coupling in Microfluidic Systems. *Angew. Chem. Int. Ed.* **2006,** 45, 5961-5964.
133. Khalid, I. M.; Alvarez, J. C., Removal of Electroanalytical Interferences Using Thermodynamic and Kinetic Effects Induced by in situ Electrogeneration of Protons. *J. Electroanal. Chem.* **2009,** 631, 76-79.
134. Cammi, R.; Cappelli, C.; Corni, S.; Tomasi, J., On the Calculation of Infrared Intensities in Solution within the Polarizable Continuum Model. *J. Phys. Chem. A* **2000,** 104, 9874-9879.
135. Wopschall, R. H.; Shain, I., Effects of Adsorption of Electroactive species in Stationary Electrode Polarography. *Anal. Chem.* **1967,** 39, 1514-1527.
136. *BASi DigiSim FAQ*. BAS: West Lafayette, IN, 2009.
137. Freiser, H., *Concepts and Calculations in Analytical Chemistry: A Spreadsheet Approach*. CRC Press: Ann Arbor, MI, 1992.
138. Laviron, E., Theoretical Study of a 1e-, 1H+ Surface Electrochemical Reaction (four-member square scheme) when the Protonation Reactions are at Equilibrium. *J. Electroanal. Chem.* **1980,** 109, 57-67.
139. The nonlinear least squares regression fit was accomplished using the Levenberg-Marquardt method as implemented in PsiPlot V 7.8.
140. Crouch, S. R.; Holler, F. J., *Applications of Microsoft Excel in Analytical Chemistry*. Brooks/Cole - Thomson Learning: Belmont, CA, 2004.

141. Jencks, W. P.; Salvesen, K., Reaction of Thiols with Acetylimidazole. Evidence for Independent Reaction Pathways. *J. Am. Chem. Soc.* **1971,** 93, 1419-1427.
142. Nelsen, S. F.; Blackstock, S. C.; Kim, Y., Estimation of Inner Shell Marcus Terms for Amino Nitrogen Compounds by Molecular Orbital Calculations. *J. Am. Chem. Soc.* **1987,** 109, 677-682.
143. Nelsen, S. F.; Weaver, M. N.; Luo, Y.; Pladziewicz, J.; Ausman, L. K.; Jentzsch, T. L.; O'Konck, J. J., Estimation of Electronic Coupling for Intermolecular Electron Transfer from Cross-Reaction Data. *J. Phys. Chem. A* **2006,** 110, 11665-11676.
144. Zen, J.-M.; Kumar, A. S.; Tsai, D.-M., Recent Updates of Chemically Modified Electrodes in Analytical Chemistry. *Electroanalysis* **2003,** 15, 1073-1087.
145. Murray, R. W.; Ewing, A. G.; Durst, R. A., Chemically Modified Electrodes. Molecular Design for Electroanalysis. *Anal. Chem.* **1987,** 59, 379A-390A.
146. Saveant, J.-M.; Allongue, P.; Delmar, M.; Desbat, M.; Fagebaume, O.; Hitmi, R.; Pinson, J., Covalent Modification of Carbon Surface by Aryl Radicals Generated from the Electrochemical Reduction of Diazonium Salts. *J. Am. Chem. Soc.* **1997,** 119, 201-207.
147. McCreery, R. L.; Chen, P.; Fryling, M. A., Electron Transfer Kinetics at Modified Carbon Electrode Surfaces: The Role of Specific Surface Sites. *Anal. Chem.* **1995,** 67, 3115-3122.
148. McCreery, R. L.; Chen, P., Control of Electron Transfer Kinetics at Glassy Carbon Electrodes by Specific Surface Modification. *Anal. Chem.* **1996,** 68, 3958-3965.
149. Pinson, J., Electrochemical Modification of Carbon Surfaces. In *Surface Modification Technologies XI*, Sudarshan, T. S.; Jeandin, M.; Khor, K. A., Eds. The Institute of Materials: London, 1998; pp 766-774.
150. Saveant, J.-M.; Pinson, J.; Hitmi, R.; Delmar, M., Covalent Modification of Carbon Surfaces by Grafting of Functionalized Aryl Radicals Produces from Electrochemical Reduction of Diazonium Salts. *J. Am. Chem. Soc.* **1992,** 114, 5883-5884.
151. Liu, Y. C.; McCreery, R. L., Reactions of Organic Monolayers on Carbon Surfaces Observed with Unenhanced Raman Spectroscopy. *J. Am. Chem. Soc.* **1995,** 117, 11254-11259.
152. Louault, C.; D'Amours, M.; Belanger, D., The Electrochemical Grafting of a Mixture of Substituted Phenyl Groups at a Glassy Carbon Electrode Surface. *Chem. Phys. Chem.* **2008,** 9, 1164-1170.
153. Saby, C.; Ortiz, B.; Champagne, G. Y.; Belanger, D., Electrochemical Modification of Glassy Caarbon Electrode Using Aromatic Diazonium Salts. 1. Blocking Effect of 4-Nitrophenyl and 4-Carboxyphenyl Groups. *Langmuir* **1997,** 13, 6805-6813.
154. D'Amours, M. D.; Belanger, D., Stability of Substituted Phenyl Groups Electrochemically Grafted at Carbon Electrode Surfaces. *J. Phys. Chem. B* **2003,** 107, 4811-4817.
155. Kariuki, J. K.; McDermott, M. T., Nucleation and Growth of Functionalized Aryl Films on Graphite Electrodes. *Langmuir* **1999,** 15, 6534-6540.
156. Kariuki, J. K.; McDermott, M. T., Formation of Multilayers on Glassy Carbon Electrodes via the Reduction of Diazonium Salts. *Langmuir* **2001,** 17, 5947-5951.
157. Baranton, S.; Belanger, D., Electrochemical Derivatization of Carbon Surface by Reduction of in Situ Generated Diazonium Cations. *J. Phys. Chem. B* **2005,** 109, 24401-24410.
158. Furniss, B. S.; Hannaford, A. J.; Smith, P. W. G.; Tatachell, A. R., In *Vogel's Textbook of Practical Organic Chemistry*, 5 th ed.; Longman: London, 1989; pp 920-1227.

159. Cougnon, C.; Gohler, F.; Belanger, D.; Mauzeroll, J., In Situ Formation of Diazonium Salts from Nitro Precursors for Scanning Electrochemical Microscopy Patterning of Surfaces. *Angew. Chem. Int. Ed.* **2009,** 48, 4006-4008.
160. Cabaniss, G. E.; Diamantis, A. A.; W. Rorer Murphy, J.; Linton, R.; Meyer, T. J., Electrocatalysis of Proton-Coupled Electron-Transfer Reactions at Glassy Carbon Electrodes. *J. Am. Chem. Soc.* **1985,** 107, 1845-1853.
161. Thorp, H. H., Electrochemistry of Proton-Coupled Redox Reactions: Role of the Electrode. *J. Chem. Ed.* **1992,** 69, 250-252.
162. Agosin, M.; Ankley, G. T., Conversion of N,N-Dimethylaniline to N,N-Dimethylaniline-N-oxide by a Cytosolic Flavin-Containing Enzyme from Trypanosoma cruzi. *Drug Metab. Dispos.* **1987,** 15, 200-203.
163. Thyagarajan, B. S., Oxidations by Ferricyanide. *Chem. Rev.* **1958,** 58, 439-460.
164. Burrows, E. P.; Rosenblatt, D. H., Mechanism of Oxidation of Trialkylamines by Ferricyanide in Aqueous Solution. *J. Org. Chem.* **1983,** 48, 992-995.
165. Delahay, P., *Double Layer and Electrode Kinetics*. Interscience: New York, 1965.
166. Oyesanya, O. O. Mechanistic Studies on the Electrochemistry of Glutathione and Homocysteine. Virginia Commonwealth University, Richmond, VA, 2008.
167. Horswill, E. C.; Ingold, K. U., The Oxidation of Phenols II. The Oxidation of 2,4-Di-*t*-butylphenol with Peroxy Radicals. *Can. J. Chem.* **1966,** 44, 269-277.
168. Ferreira, M.; Varela, H.; Torresi, R. M.; Tremiliosi-Filho, G., Electrode Passivation Caused by Polymerization of Different Phenolic Compounds. *Electrochim. Acta* **2006,** 52, 434-442.
169. Yamamura, S., Oxidation of Phenols. In *The Chemistry of Phenols*, 2nd ed.; Rappoport, Z., Ed. Wiley-Interscience: Hoboken, NJ, 2003; Vol. 2, pp 1315-1337.
170. DeSimone, R. E.; Drago, R. S., Magnetic Resonance Studies of Some Low-Spin d^5 Tris Diimine Complexes. *J. Am. Chem. Soc.* **1970,** 92, 2343-2352.
171. Andrieux, C. P.; Gonzalez, F.; Saveant, J.-M., Derivatization of Carbon Surfaces by Anodic Oxidation of Arylacetates. Electrochemical Manipulation of the Grafted Films. *J. Am. Chem. Soc.* **1997,** 119, 4292-4300.
172. Strickson, J. A.; Leigh, M., The Oxidation of Phenols with Chromyl Chloride II: 2,5-, 2,6- and 3,5- Dialkyl Phenols. *Tetrahedron* **1968,** 24, 5145-5149.
173. Brunschwig, B.; Sutin, N., Reactions of the excited states of substituted polypyridinechromium(III) complexes with oxygen, iron(II) ions, ruthenium(II) and -(III), and osmium(II) and -(III) complexes. *J. Am. Chem. Soc.* **1978,** 100, 7568-7577.
174. Strickson, J. A.; Brooks, C. A., The Oxidation of Phenols with Chromyl Chloride I: Phenol, Chlorophenols and Related Phenoxytrichlorosilanes. *Tetrahedron* **1967,** 23, 2817-2821.
175. Kanoufi, F.; Zu, Y.; Bard, A. J., Homogeneous Oxidation of Trialkylamines by Metal Complexes and Its Impact on Electrogenerated Chemiluminescence in the Trialkylamine/Ru(bpy)3 2+ System. *J. Phys. Chem. B* **2001,** 105, 210-216.
176. Saotome, M.; Takano, S.; Tokushima, A.; Ito, S.; Nakashima, S.; Nagasawa, Y.; Okada, T.; Miyasaka, H., Picosecond-Nanosecond Laser Photolysis Studies of a Photoacid Generator in Solutions: Transient Absorption Spectroscopy and Transient Grating Measurements. *Photochem. Photobiol. Sci.* **2005,** 4, 83-88.
177. Schreiber, E.; Steele, D., Advanced 1D NMR. In *VnmrJ Liquids NMR User Guide*, Steele, D., Ed. Varian Inc.: Palo Alto, California, 2003; pp 138-145.

178. Schreiber, E.; Carlisle, M., 1.5 Diffusion Experiments/DOSY. In *User Guide: Liquids NMR*, Steele, D., Ed. Varian, Inc.: Palo Alto, California, 2001; pp 40-67.

9.0 Appendix

9.1 Supporting Figures

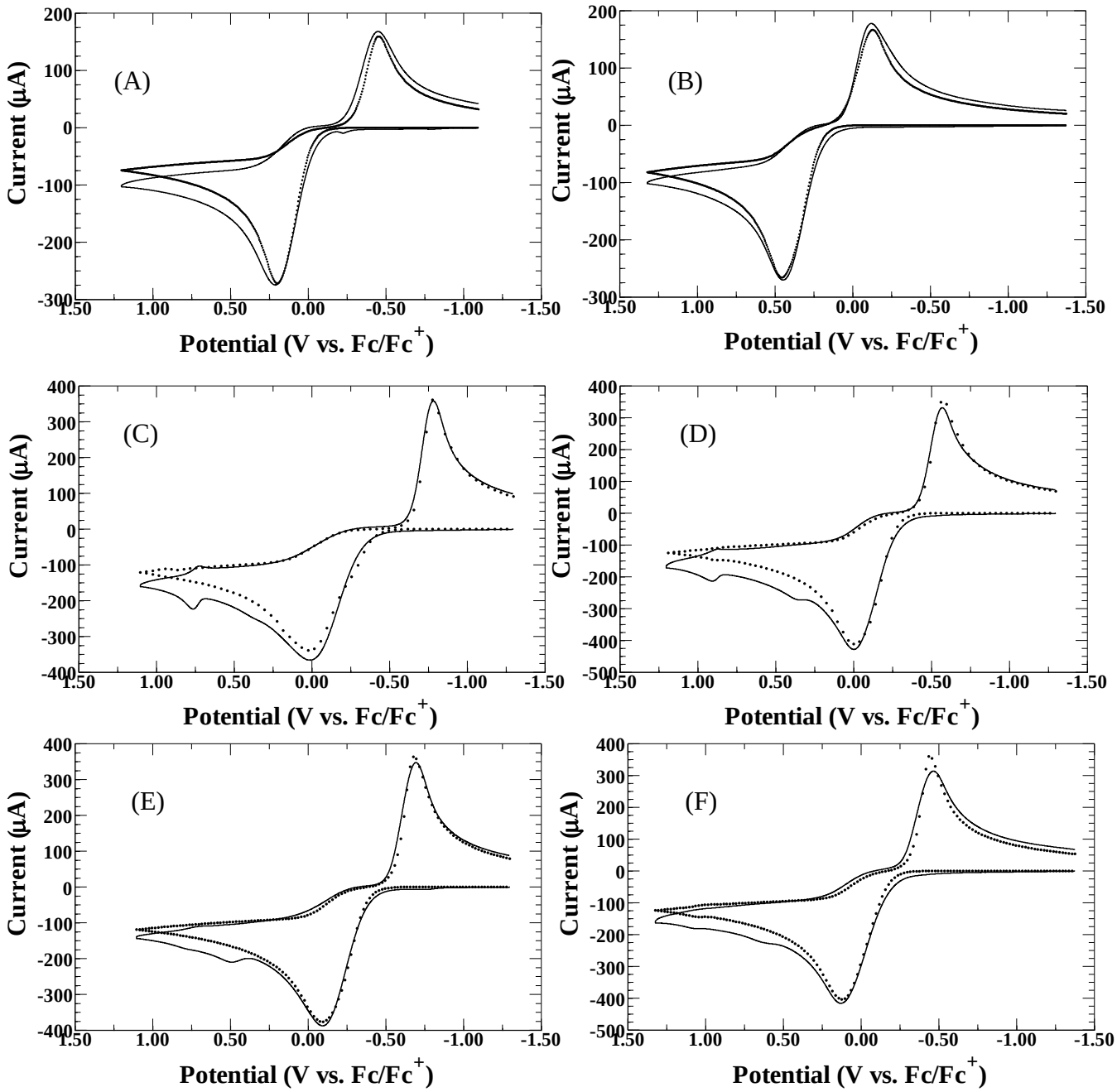

Figure A1. Voltammetry (line) and simulations (circles) of 5 mM 1,4-QH_2 with (A.) 10 mM pyridine at 0.2 V s^{-1}, (C.) 8.5 mM DIPEA 0.6 V s^{-1} and (E.) 8.3 mM TEA at 0.6 V s^{-1}. Voltammetry (line) and simulations (circles) of 5 mM 1,2-QH_2 with (B.) 10 mM pyridine at 0.2 V s^{-1}, (D.) 8.1 mM DIPEA at 0.6 V s^{-1} and (F.) 7.5 mM TEA at 0.6 V s^{-1}. All data shown here was recorded under argon at a glassy carbon electrode (0.06 cm^2) with 0.200 M $TBAPF_6$.

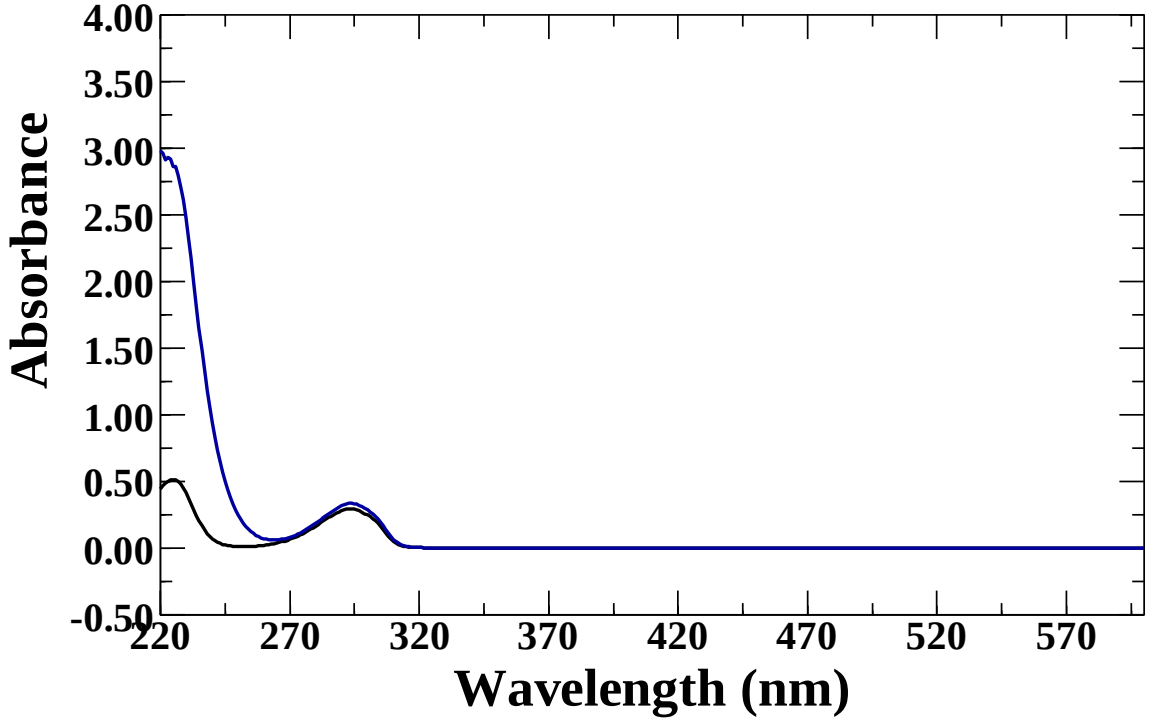

Figure A2. UV-vis spectra of HQ (1.00 mM) alone (black line) and with 22 equivalents of TEA (blue line).

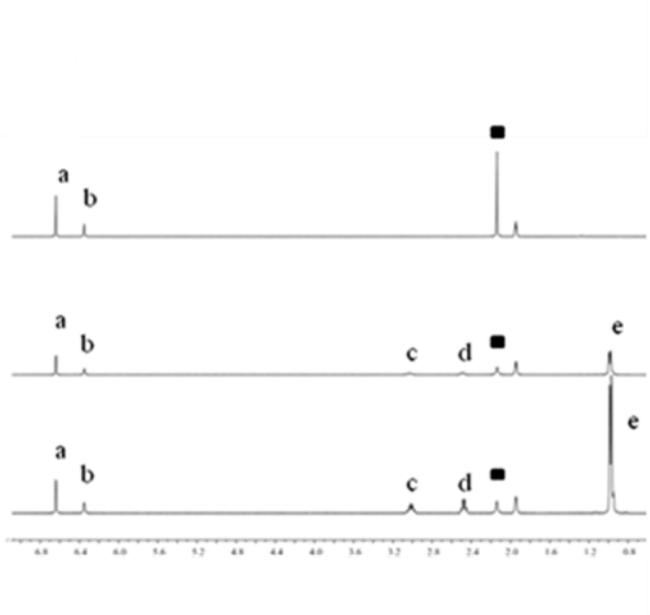

Figure A3. 5 mM 1,4-QH_2 with 0, 3 and 10 mM DIPEA. Peaks *a* and *b* are the aromatic and phenolic protons of 1,4-QH_2, while peaks *c*, *d* and *e* are the aryl protons of DIPEA. The black square is the HDO peak.

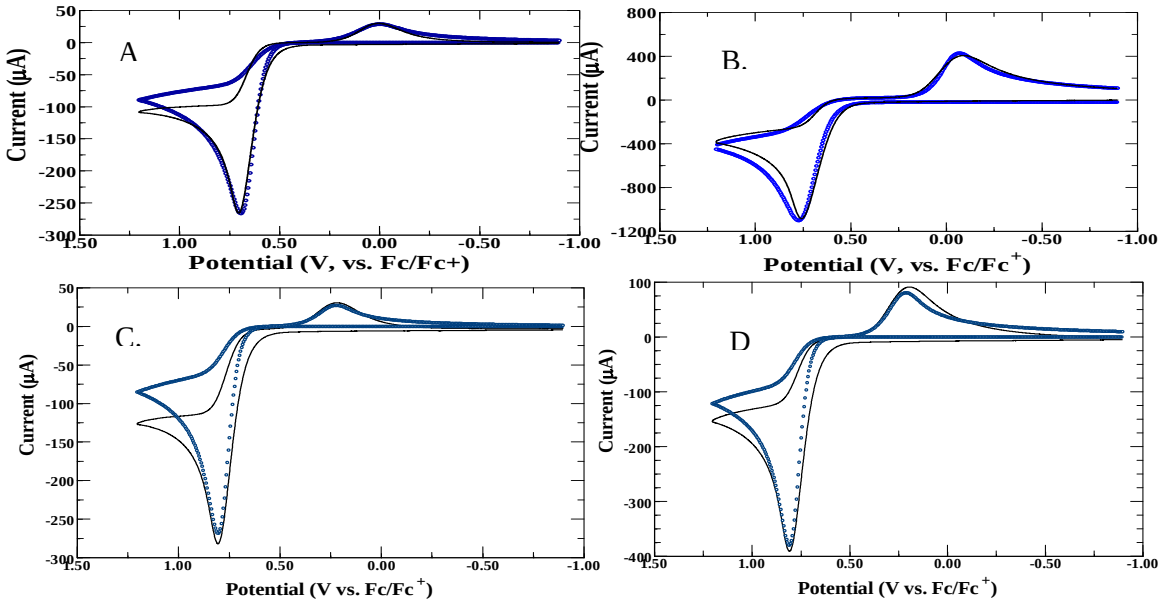

Figure A4. CV's (solid curves) and simulations (open circles) of 5.0 mM 1,4-QH_2 at scan rates of (A.) 0.1 V/s, (B.) 2 V/s. CV's and simulations of 5.0 mM 1,2-QH_2 are also displayed, at scan rates of (C.) 0.1 V/s and (D.) 0.2 V/s. CV's were recorded in anhydrous acetonitrile with 0.2 M $TBAPF_6$ as supporting electrolyte at a glassy carbon electrode (0.06 cm^2). Associated parameters given below.

(10) $QH_2 \rightleftharpoons QH_2^{\cdot +} + e^-$ $E^o_{10,\ 1,4\text{-}QH2}$ =0.357 V, $E^o_{10,\ 1,2\text{-}QH2}$ =0.754 V, $k_{s,\ 10,1,4\text{-}QH2}$ =(4.4 ± 1) x 10^{-5} $^{cm}/_{s}$, $k_{s,\ 10,1,2\text{-}QH2}$ =(1 ± 0.1) x 10^{-2} $^{cm}/_{s}$, $\alpha_{10,1,4\text{-}QH2}$ =0.5, $\alpha_{10,1,2\text{-}QH2}$ =0.4

(11) $QH_2^{\cdot +} \rightleftharpoons QH^{\cdot} + H^+$ $K_{equ,\ 11,\ 1,4\text{-}QH2}$ =4.1 x 10^{-3} M, $K_{equ,\ 11,\ 1,2\text{-}QH2}$ =6.5 x 10^8 M, $k_{f,11,\ 1,4\text{-}QH2}$ =1.2 x 10^3 s^{-1}, $k_{f,\ 11,\ 1,2\text{-}QH2}$ =2.6 x 10^6 s^{-1}, $k_{b,\ 11,\ 1,4\text{-}QH2}$ =2.9 x 10^5 M^{-1} s^{-1}, $k_{b,\ 11,\ 1,2\text{-}QH2}$ =4 x 10^3 M^{-1} s^{-1}

(12) $QH^{\cdot} \rightleftharpoons QH^+ + e^-$ $E^o_{12,\ 1,4\text{-}QH2}$ =0.357 V, $E^o_{12,\ 1,4\text{-}QH2}$ =0.494 V, $k_{s,12,\ 1,4\text{-}QH2}$ =(5.6 ± 1.5) x10^{-5} $^{cm}/_{s}$, $k_{s,12\ 1,2\text{-}QH2}$ =(1.1± 0.2) x 10^{-4} $^{cm}/_{s}$, $\alpha_{12,1,4\text{-}QH2}$ =0.5, $\alpha_{12,1,2\text{-}QH2}$ =0.47

(13) $QH^+ \rightleftharpoons Q + H^+$ $K_{equ,\ 13,\ 1,4\text{-}QH2}$ =0.65 M, $k_{f,\ 13,\ 1,4\text{-}QH2}$ =0.12 s^{-1}, $k_{b,\ 13,\ 1,4\text{-}QH2}$ =0.18 M^{-1} s^{-1}, $K_{equ,\ 13,\ 1,2\text{-}QH2}$ =1.3 x 10^3, $k_{f,\ 13,\ 1,2\text{-}QH2}$ =7 x 10^{-5}, $k_{b,\ 13,\ 1,2\text{-}QH2}$ =5.4 x 10^{-8}

(14) $QH^{\cdot} + QH^{\cdot} \overset{14a}{\rightleftharpoons}$ ***Hemiketal*** $\overset{14b}{\rightleftharpoons} Q + QH_2$ $K_{equ,\ 14a,\ 1,4\text{-}QH2}$ =5 x 10^7 M^{-1}, $k_{f,\ 14a,\ 1,4\text{-}QH2}$ =7.2 x 10^{-8} M^{-1} s^{-1}, $k_{b,\ 14a,\ 1,4\text{-}QH2}$ =1.4 x 10^{-15} s^{-1}; $K_{equ,\ 14b,\ 1,4\text{-}QH2}$ =3.2 x 10^{-6} M, $k_{f,\ 14b,\ 1,4\text{-}QH2}$ =8.9 x 10^{-5} s^{-1}, $k_{b,\ 14b,\ 1,4\text{-}QH2}$ =28 M^{-1} s^{-1}

Potentials given for each of the fittings is given vs. Fc/Fc^+. For the parameters displayed above, E^o represents the simulated value of the formal potential, k_s represents the heterogeneous kinetic constant, α is the transfer coefficient, K_{equ} is the homogeneous equilibrium constant, and k_f and k_b are the forward and backward rate constants for the indicated homogeneous reaction. For the above simulations, $D_{1,4\text{-}QH2}$ = 2.8 x 10^{-5} cm^2 s^{-1} and $D_{1,2\text{-}QH2}$ = 3.0 x 10^{-5} cm^2 s^{-1} (from Table 3 and 7).

Alternative Schemes for Fitting QH_2 with Amine Voltammetry

Below are some of the alternative Schemes used to fit the voltammetry of the QH_2's with the amines. A brief discussion involving each scheme is provided below.

Scheme A1

$QH_2 + B \rightleftharpoons QH^- + BH^+$ (15)

$QH^- \rightleftharpoons QH^{\cdot} + e^-$ (16)

$QH^{\cdot} + B \rightleftharpoons Q^{\cdot -} + BH^+$ (A1)

$Q^{\cdot -} \rightleftharpoons Q + e^-$ (A2)

$QH^{\cdot} + QH^{\cdot} \rightleftharpoons Q + QH_2$ (14)

Scheme A2

$QH_2 + B \rightleftharpoons QH^- + BH^+$ (15)

$QH^- + BH^+ \rightleftharpoons QH(BH)$ (A3)

$QH(BH) \rightleftharpoons QH^{\cdot}(BH) + e^-$ (A4)

$QH^{\cdot}(BH) \rightleftharpoons QH^+(BH) + e^-$ (A5)

$QH^+(BH) \rightleftharpoons QH^+ + BH^+$ (A6)

$QH^+ + B \rightleftharpoons Q + BH^+$ (18)

Scheme A3

$QH_2 + B \rightleftharpoons QH_2(B)$ (26)

$QH_2(B) \rightleftharpoons QH_2^{+\cdot}(B)$ (28)

$QH_2^{+\cdot}(B) \rightleftharpoons QH^{\cdot} + BH^+$ (30)

$QH^{\cdot} \rightleftharpoons QH^+ + e^-$ (12)

$QH^+ + B \rightleftharpoons Q + BH^+$ (18)

$QH^{\cdot} + QH^{\cdot} \rightleftharpoons Q + QH_2$ (14)

Scheme A1 never fit the reduction peak (peak II'), the reduction peak current was always too low. Scheme A2, the ion-pairing mechanism, like Scheme A1 never fit the reduction peak because the peak current was always too low. Though the PGE-^{1}H-NMR results did not show that there was a complexation between the amines and QH_2 this mechanism was attempted anyway. This mechanism was unable to fit the voltammetry because the only reasonable values for the equilibrium constant of equation 26, K_{26}, were low values ~ 10 – 30 M^{-1}, while the iterative fittings always involved large K_{26} values. This was reasoned due to the low values

found in other recent studies that document hydrogen bonding between quinone and acid/base species.[55, 57]

Some of the digital simulation fittings are provided above, Figure A1, while the kinetic values associated with those fittings are provided below, Table A1. Less than two equivalents of the alkylamines (DIPEA and TEA) were added to the QH_2's, typically ~8 mM, due to their oxidation at potentials noted in the text (Table 1). Oxidation of these bases would modify the surface of the electrode and significantly affect the electrochemistry displayed if cautious additions were not made.[175, 176] Because of this some of the original QH_2 electrochemical response (peak I and II) can still be noted at anodic potentials (such as in Figure A1, C. and D., ~0.8 V vs. Fc/Fc^+). However, Figure A1 D., E. and F. all show some oxidation of the added amine at potentials of ~0.5 V (vs. Fc/Fc^+). However, single experiments were conducted at 0.1 V s^{-1} on polished electrodes in which greater than 10 mM of the alkylamines was added to the QH_2 solutions. These experiments showed that there was not a significant impact on the oxidation peak of the QH_2.

(15) $QH_2 + B \rightleftharpoons QH^- + BH^+$ $K_{equ,\,15}$, $k_{f,\,15}$, $k_{b,\,15}$

(16) $QH^- \rightleftharpoons QH^{\cdot} + e^-$ E^o_{16}, $k_{s,\,16}$, α_{16}

(17) $QH^{\cdot} \rightleftharpoons QH^+ + e^-$ E^o_{17}, $k_{s,\,17}$, α_{17}

(18) $QH^+ + B \rightleftharpoons Q + BH^+$ $K_{equ,\,18}$, $k_{f,\,18}$, $k_{b,\,18}$

(14) $QH^{\cdot} + QH^{\cdot} \rightleftharpoons Q + QH_2$ $K_{equ,\,14}$, $k_{f,\,14}$, $k_{b,\,14}$

Table A1. Digital simulation fitting parameters used to fit the QH_2's with Brønsted bases added.

	TEA		DIPEA		Pyridine	
Parameter	**1,4-QH_2**	**1,2-QH_2**	**1,4-QH_2**	**1,2-QH_2**	**1,4-QH_2**	**1,2-QH_2**
$K_{equ,\ 15}$	5.6×10^{-5}	0.0027	5.6×10^{-5}	0.009	0.0069	0.006
$k_{f,\ 15}$ /M^{-1} s^{-1}	1×10^{9}	5×10^{6}	5×10^{8}	1×10^{7}	1×10^{7}	1×10^{7}
E^{o}_{16}/V[a]	-0.606	-0.096	-0.466	-0.166	0.094	0.304
$k_{s,\ 16}$ /cm s^{-1}	0.023 ± 0.003	0.031	0.05	0.0925 ± 0.004	0.1	0.029 ± 0.003
α_{16}	0.50	0.50	0.50	0.50	0.50	0.50
E^{o}_{17} /V[a]	-0.646	-0.376	-0.796	-0.596	-0.556	-0.056
$k_{s,\ 17}$ /cm s^{-1}	0.03	0.028	0.045 ± 0.007	0.046 ± 0.008	0.12	0.028
α_{17}	0.50	0.50	0.50	0.50	0.50	0.50
$K_{equ,\ 18}$	3.9×10^{24}	3.9×10^{24}	3.2×10^{24}	3.5×10^{24}	3.2×10^{20}	5.3×10^{20}
$k_{f,\ 18}$ /M^{-1} s^{-1}	4.9	9	0.8	5.5	4.5	5
$K_{equ,\ 14}$	3.30×10^{29}	7.8×10^{43}	2.16×10^{34}	7.19×10^{33}	3.04×10^{33}	1.07×10^{33}
$k_{f,\ 14}$ /M^{-1} s^{-1}	1.8×10^{4}	1.7×10^{4}	1.6×10^{4}	1×10^{4}	1.6×10^{4}	2.0×10^{4}
D_{QH2}[b] /cm^2 s^{-1}	2.8×10^{-5}	2.8×10^{-5}	2.8×10^{-5}	2.8×10^{-5}	2.8×10^{-5}	2.8×10^{-5}
D_B[b] /cm^2 s^{-1}	3.1×10^{-5}	3.1×10^{-5}	3.3×10^{-5}	3.3×10^{-5}	4.4×10^{-5}	4.4×10^{-5}
D_{BH+}[b] /cm^2 s^{-1}	2.1×10^{-5}	2.1×10^{-5}	2.3×10^{-5}	2.3×10^{-5}	2.6×10^{-5}	2.6×10^{-5}

[a.] Formal potentials are measured vs. Fc/Fc^{+}.
[b.] All QH_2 species used the given diffusion coefficients, regardless of protonation or redox state, protonated bases used their respective protonated D values.

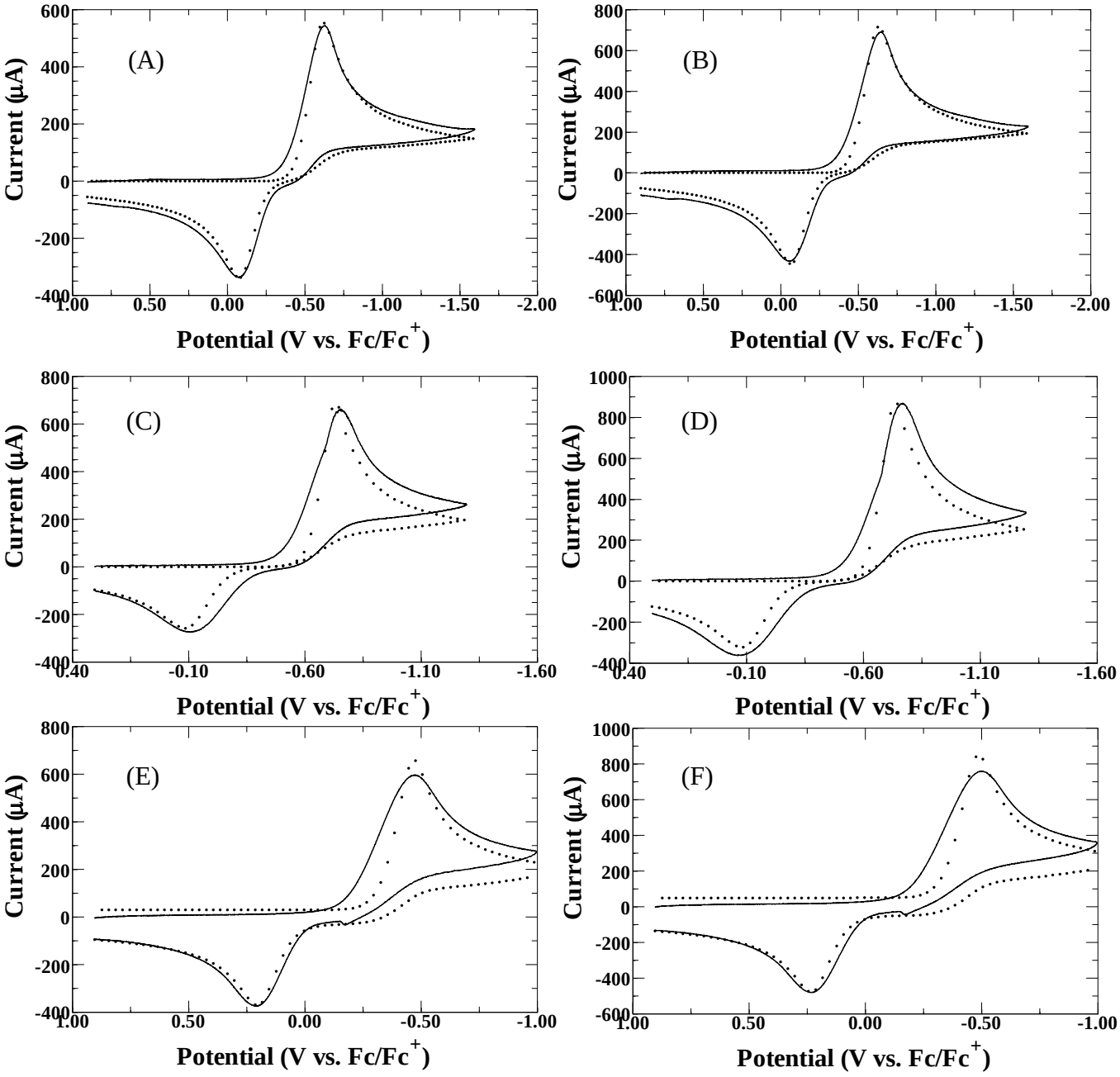

Figure A5. Volatammetry (lines) and simulations (circles) of 5.0 mM 1,4-Q with 114 mM acetic acid at (A) 0.6 and (B) 1 V s^{-1}, with 12 mM DIPEAH+ at (C) 0.6 and (D) 1 V s^{-1}, and with 13 mM pyridinium at (E) 0.6 and (F) 1 V s^{-1}. All voltammetry here was performed in dry acetonitrile under an argon environment at a glassy carbon electrode (0.060 cm^2).

(19) $Q + e^- \rightleftharpoons Q^{\cdot -}$ $E^o_{19}, k_{s,19}, \alpha_{19}$

(20) $Q^{\cdot -} + H^+ \rightleftharpoons QH^{\cdot}$ $K_{equ,20}, k_{f,20}, k_{b,20}$

(21) $QH^{\cdot} + e^- \rightleftharpoons QH^-$ $E^o_{21}, k_{s,21}, \alpha_{21}$

(22) $QH^- + H^+ \rightleftharpoons QH_2$ $K_{equ,22}, k_{f,22}, k_{b,22}$

(23) $Q + QH_2 \rightleftharpoons QH^{\cdot} + QH^{\cdot}$ $K_{equ,23}, k_{f,23}, k_{b,23}$

Table A2. Digital simulation fitting parameters used to fit 1,4-Q with Brønsted acids added.

Parameters	**1,4-Q with Acetic Acid**	**1,4-Q with DIPEAH$^+$**	**1,4-Q with Pyridinium**
E^o_{19}[a] /V	-0.646	-0.756	-0.356
$k_{s,19}$ /cm/s	0.078 ± 0.02	0.054 ± 0.01	(8.9 ± 0.8) x 10^{-3}
α_{19}	0.50	0.50	0.50
$K_{equ,20}$	1.6 x 10^9 (M^{-1})	8 x 10^8 (M^{-1})	1.6 x 10^{15} (M^{-1})
$k_{f,20}$	1.7 x10^8 (M^{-1} s^{-1})	3.4 x 10^8 (M^{-1} s^{-1})	1.7 x 10^7 (M^{-1} s^{-1})
E^o_{21}[a] /V	-0.474	-0.475	-0.124
$k_{s,21}$ /cm/s	(2.0 ± 0.008) x 10^{-4}	(2.2 ± 0.1) x 10^{-4}	(3.0 ± 0.8) x 10^{-4}
α_{21}	0.50	0.50	0.50
$K_{equ,22}$	5.5 x10^7 (M^{-1})	6.9 x 10^6 (M^{-1})	5.5 x 10^6 (M^{-1})
$k_{f,22}$	0.26 (M^{-1} s^{-1})	9 (M^{-1} s^{-1})	4 (M^{-1} s^{-1})
$K_{equ,23}$	0.19	1.4	0.19
$k_{f,23}$	3.6 x 10^7 (M^{-1} s^{-1})	2.8 x 10^5 (M^{-1} s^{-1})	3.6 x 10^7 (M^{-1} s^{-1})
$D_{1,4\text{-}Q}$[b] /cm^2 s^{-1}	3.5 x 10^{-5}	3.5 x 10^{-5}	3.5 x 10^{-5}
D_{H^+}[c] /cm^2 s^{-1}	6 x 10^{-5}	6 x 10^{-5}	6 x 10^{-5}

[a.] Formal potentials are measured vs. Fc/Fc^+.
[b.] All QH_2 species used the given diffusion coefficients, regardless of protonation or redox state, protonated bases used their respective

protonated D values.
[c] D value found for H_2O diffusion in d_3-ACN by PGE-NMR, also this value is similar to that from the literature.[176]

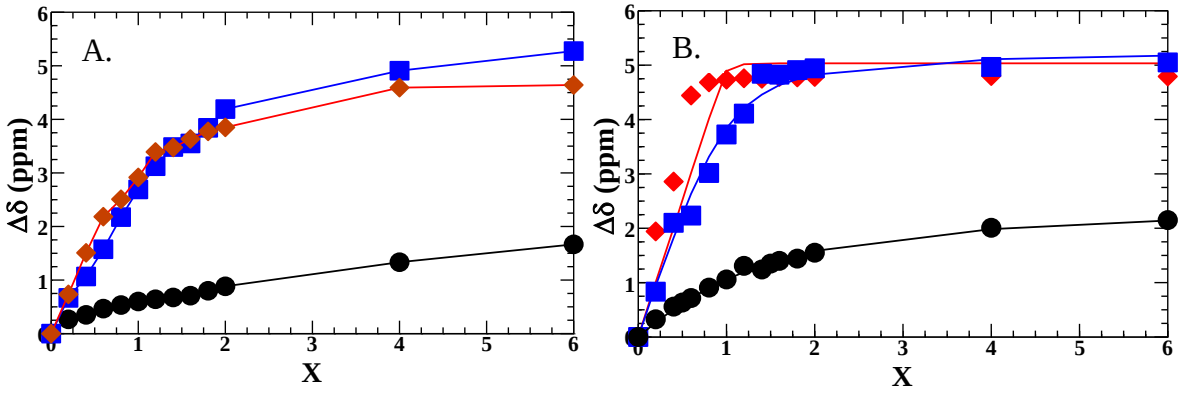

Figure A6. (A.) Molar ratio analyses for 5.0 mM 1,4-QH_2 with trifluoroacetate (black circles), acetate (blue squares) and benzoate (red diamonds) all at 5 °C. Molar ratio analyses for 5.0 mM 1,2-QH_2 with trifluoroacetate (black circles, at 25 °C), acetate (blue squares, at 5 °C) and benzoate (red diamonds, at 5 °C).

To determine the association constants for the QH_2's with acetate and benzoate at 25 °C, ^{1}H-NMR spectra were measured between 5°C and 15°C where the exchange peak for the QH_2 and acetate/benzoate complex is observed. Determination of the association constants at each temperature was completed by fitting to the 1:2 binding isotherm (equation 25). The kinetic constants and the associated error were fit to the van't Hoff equation, equation A7, which allowed for extrapolation of the association constants (K) at 25 °C. Missing data points were removed via the use of a q-test.

$$(\partial \ln K_a)/(\partial(1/T)) = -\Delta H^o/R \qquad \text{(A7)}$$

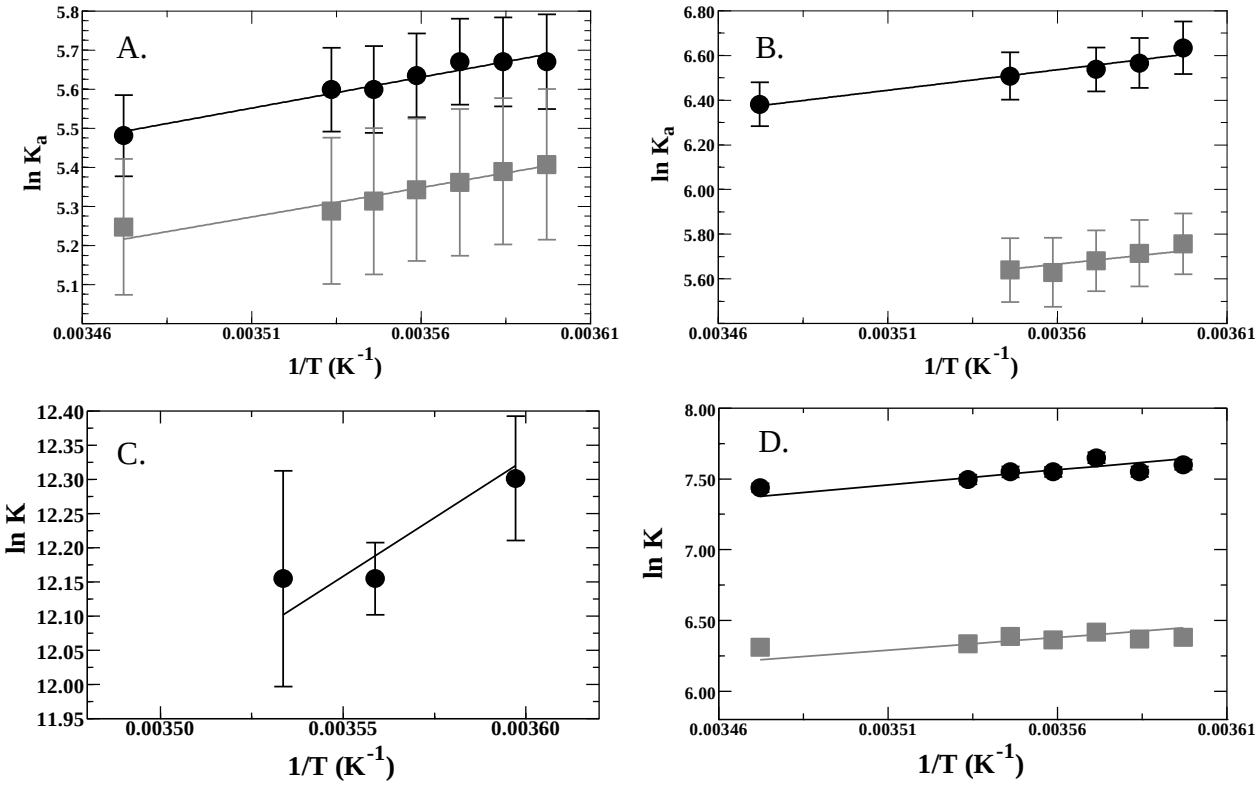

Figure A7. van't Hoff plots of 1,4-QH_2 with acetate (A.) and benzoate (B.) and 1,2-QH_2 with acetate (C.) and benzoate (D.). The values to determine K_1 are given by the black circles and line in each plot, while the values to determine K_2 are given by the gray squares and line in each plot. Lines represent the fitting of the van't Hoff equation to the data between 5 and 15 ^{o}C.

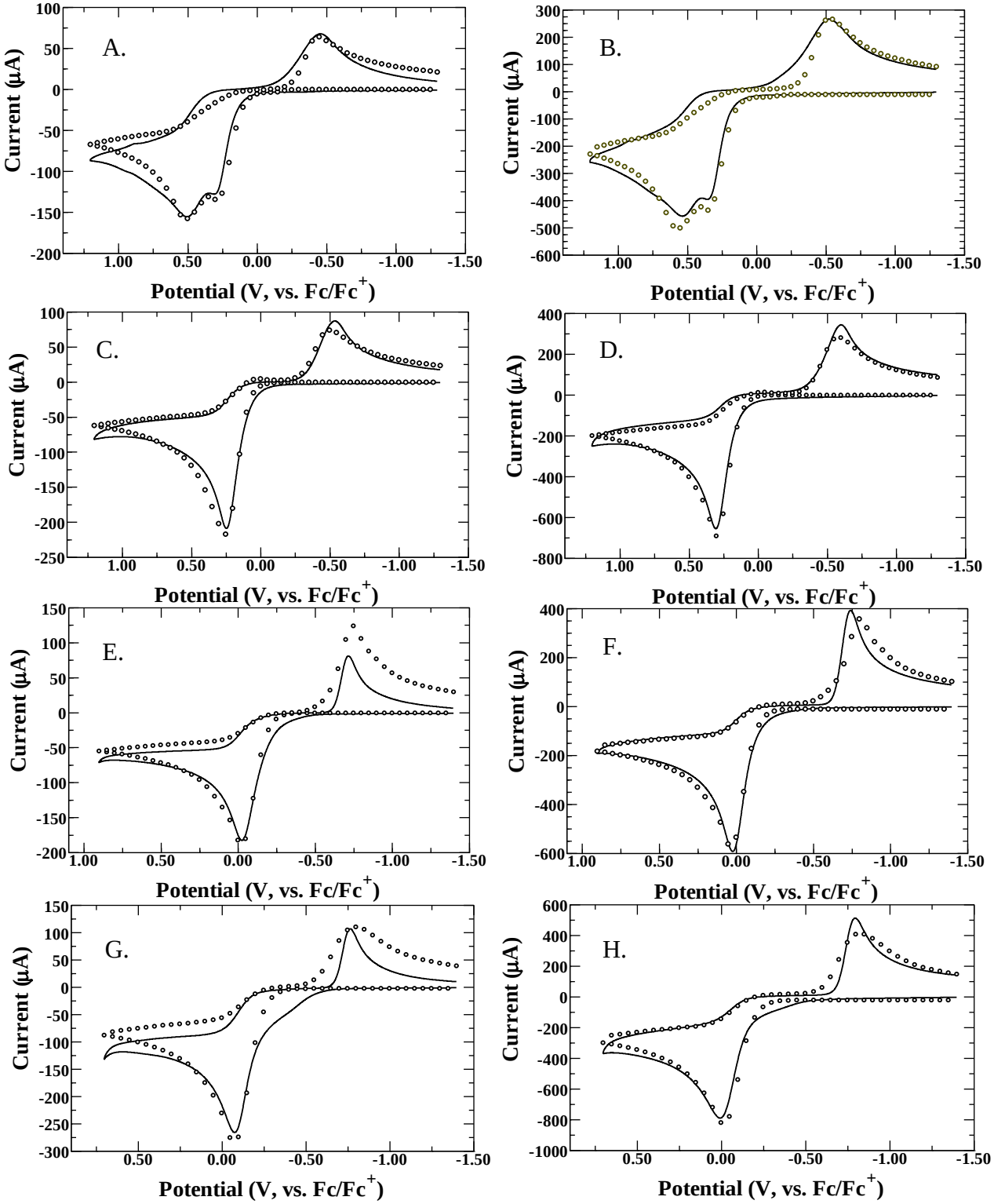

Figure A8. Voltammetry and simulations of 1,2-QH_2 with 10.0 trifluoroacetate at (A.) 0.1 and (B.) 1 V s^{-1}. Voltammetry and simulations of 1,2-QH_2 with 30.0 trifluoroacetate at (C.) 0.1 and (D.) 1 V s^{-1}. Voltammetry and simulations of 1,2-QH_2 with 20.0 benzoate at (E.) 0.1 and (F.) 1 V s^{-1}. Voltammetry and simulations of 1,2-QH_2 with 20.0 acetate at (A.) 0.1 and (B.) 1 V s^{-1}. All voltammetry recorded in 0.2 M $TBAPF_6$ in anhydrous acetonitrile under argon at a glassy carbon electrode (area range 0.06 to 0.073 cm^2).

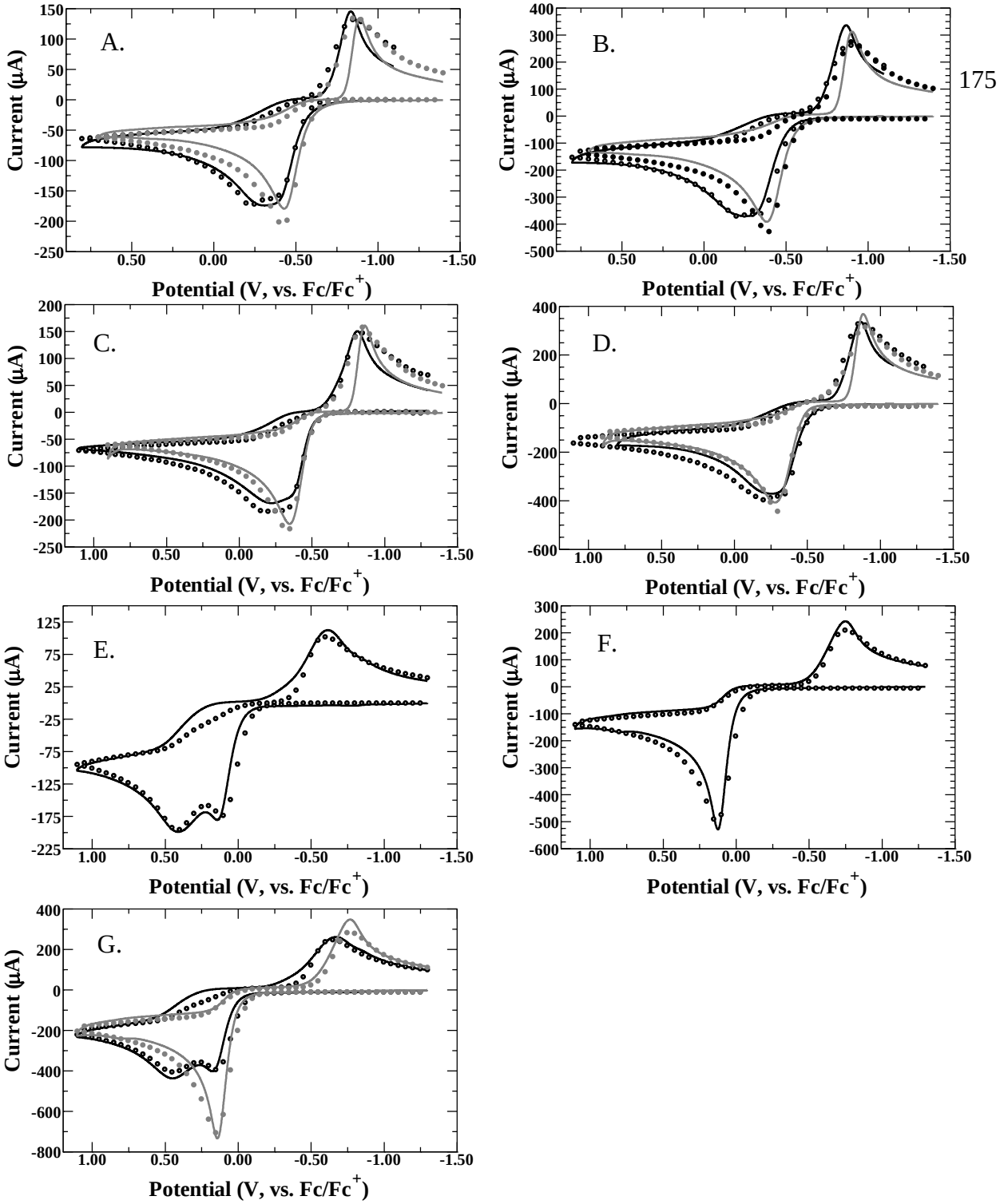

Figure A9. Voltammograms of 5.0 mM 1,4-QH_2 with 10.0 (black line) and 30.0 mM acetate (gray line) and simulations thereof (open black circles for 10.0 mM and closed gray circles at 30.0 mM) at 0.2 and 1 V s^{-1} (A.) and (B.), respectively. Voltammograms of 5.0 mM 1,4-QH_2 with 10.0 (black line) and 30.0 mM benzoate (gray line) and simulations thereof (open black circles for 10.0 mM and closed gray circles at 30.0 mM) at 0.2 and 1 V s^{-1} (C.) and (D.), respectively. Voltammogram of 5.0 mM 1,4-QH_2 with 10.0 mM trifluoroacetate (black line) and simulation thereof (black open circles) at 0.2 V s^{-1}, (E.). Voltammogram of 5.0 mM 1,4-QH_2 with 30.0 mM trifluoroacetate (black line) and simulation thereof (black open circles) at 0.5 V s^{-1}, (F.). Voltammograms of 5.0 mM 1,4-QH_2 with 10.0 (black line) and 30.0 mM trifluoroacetate (gray line) and simulations thereof (open black circles for 10.0 mM and closed gray circles at

30.0 mM) at 1 V s^{-1}, (G.). All voltammetry recorded in 0.2 M $TBAPF_6$ in anhydrous acetonitrile under argon at a glassy carbon electrode (area range 0.07 to 0.073 cm^2).

The parameters of Scheme 8 for the fitting of the above voltammograms can be found below. All formal potentials are reported as versus the ferrocene/ferrocenium couple in acetonitrile. The diffusion coefficients of all QH_2 species, no matter the state of oxidation, with the exception of 1,4-Q ($3.5x10^{-5}$ cm^2 s^{-1}, Table 3 and 7), were as reported in the text, Tables 3 and 7 . The diffusion coefficients of the base and conjugate acids are the same as those reported in the text and here, Tables 3 and 7, respectively. The diffusion coefficient of H^+, used in Scheme 8, was 6 x 10^{-5} cm^2 s^{-1}, found using the PGE-^{1}H-NMR technique on the HDO peak in acetonitrile.

Scheme 8A

(26) $QH_2 + B \rightleftharpoons QH_2(B)$

Fitting to CV of 1,4-QH_2/10 mM Acetate – K_{equ} = 200 M^{-1}, k_f = 1 x 10^8 M^{-1} s^{-1}, k_b = 5 x 10^5 s^{-1}
Fitting to CV of 1,4-QH_2/10 mM Benzoate – K_{equ} = 473 M^{-1}, k_f = 1 x 10^8 M^{-1} s^{-1}, k_b = 2.11 x 10^5 s^{-1}
Fitting to CV of 1,4-QH_2/10 mM Trifluoroacetate – K_{equ}=55 M^{-1}, k_f = 1 x 10^8 M^{-1} s^{-1}, k_b = 1.82 x10^6 s^{-1}

(27) $QH_2(B) + B^- \rightleftharpoons QH_2(B)_2$

Fitting to CV of 1,4-QH_2/10 mM Acetate – K_{equ} = 155 M^{-1}, k_f = 1 x 10^8 M^{-1} s^{-1}, k_b = 6.452 x 10^5 s^{-1}
Fitting to CV of 1,4-QH_2/10 mM Benzoate – K_{equ} = 200 M^{-1}, k_f = 1 x 10^8 M^{-1} s^{-1}, k_b = 5 x10^5 s^{-1}
Fitting to CV of 1,4-QH_2/10 mM Trifluoroacetate – K_{equ}= 5 M^{-1}, k_f = 1 x 10^8 M^{-1} s^{-1}, k_b = 2 x10^7 s^{-1}

(28) $QH_2(B) \rightleftharpoons QH_2^{+\cdot}(B) + e^-$

Fitting to CV of 1,4-QH_2/10 mM Acetate – E^o = -0.51 V, α = 0.5, k_s = 0.0005 cm s^{-1}
Fitting to CV of 1,4-QH_2/10 mM Benzoate – E^o = -0.45 V, α = 0.5, k_s = 0.0005 cm s^{-1}
Fitting to CV of 1,4-QH_2/10 mM Trifluoroacetate – E^o = -0.1 V, α = 0.5, k_s = 0.0001 cm s^{-1}

(29) $QH_2(B)_2 \rightleftharpoons QH_2^{+\cdot}(B)_2 + e^-$

Fitting to CV of 1,4-QH_2/10 mM Acetate – E^o = -0.53 V, α = 0.5, k_s = 0.0005 cm s^{-1}
Fitting to CV of 1,4-QH_2/10 mM Benzoate – E^o = -0.47 V, α = 0.5, k_s = 0.0005 cm s^{-1}
Fitting to CV of 1,4-QH_2/10 mM Trifluoroacetate – E^o = -0.12 V, α = 0.5, k_s = 0.0001 cm s^{-1}

(30) $QH_2^{+\cdot}(B) \rightleftharpoons QH^{\cdot} + HB$

Fitting to CV of 1,4-QH_2/10 mM Acetate – K_{eq} = 8 x 10^{-7} M, k_f = 1 x 10^4 s^{-1}, k_b = 1.25 x 10^{10} M^{-1} s^{-1}

Fitting to CV of 1,4-QH_2/10 mM Benzoate – K_{equ} = 2 x 10^{-8} M, k_f = 1 x 10^4 s^{-1}, k_b = 5 x 10^{11} $M^{-1}s^{-1}$
Fitting to CV of 1,4-QH_2/10 mM Trifluoroacetate – K_{equ}=1x10^{-9}, k_f=1x10^8 s^{-1}, $k_{\mathbf{b}}$ = 1x10^{17} M^{-1} s^{-1}

(31) $QH_2^{+\cdot}(B)_2 \rightleftharpoons QH^{\cdot} + HB_2$

Fitting to CV of 1,4-QH_2/10 mM Acetate – K_{eq} = 0.0001422 M, k_f = 1 x 10^8 s^{-1}, k_b = 7.032 x 10^{11} M^{-1} s^{-1}
Fitting to CV of 1,4-QH_2/10 mM Benzoate – K_{equ} = 1.837x10^{-6}, k_f=1x10^8 s^{-1}, $k_{\mathbf{b}}$ = 5.444x10^{13} M^{-1} s^{-1}
Fitting to CV of 1,4-QH_2/10 mM Trifluoroacetate – K_{equ}=6.98x10^{-6}, k_f=1x10^8 s^{-1}, $k_{\mathbf{b}}$ = 1.433x10^{13} M^{-1} s^{-1}

(32) $QH^{\cdot} \rightleftharpoons QH^+ + e^-$

Fitting to CV of 1,4-QH_2/10 mM Acetate – E^o = -0.37 V, α = 0.5, k_s = 0.005 cm s^{-1}
Fitting to CV of 1,4-QH_2/10 mM Benzoate – E^o = -0.42 V, α = 0.5, k_s = 0.002 cm s^{-1}
Fitting to CV of 1,4-QH_2/10 mM Trifluoroacetate – E^o -0.04 V, α = 0.5, k_s = 0.00005 cm s^{-1}

(33) $QH^+ + \mathbf{H}B_2 \rightleftharpoons$ 1,4-Q + H_2B_2

Fitting to CV of 1,4-QH_2/10 mM Acetate – K_{equ} = 385.28, k_f = 1 x 10^8 M^{-1} s^{-1}, k_b = 2.596 x 10^5 M^{-1} s^{-1}
Fitting to CV of 1,4-QH_2/10 mM Benzoate – K_{equ} = 200, k_f = 1 x 10^8 M^{-1} s^{-1}, k_b = 5 x 10^5 M^{-1} s^{-1}
Fitting to CV of 1,4-QH_2/10 mM Trifluoroacetate – K_{equ}=1000, k_f=1x10^8 M^{-1} s^{-1}, k_b = 1x10^5 M^{-1} s^{-1}

(14)$QH^{\cdot} + QH^{\cdot} \rightleftharpoons Q + QH_2$

Fitting to CV of 1,4-QH_2/10 mM Acetate – K_{equ} = 479.68, k_f = 1x10^8 M^{-1} s^{-1}, k_b = 2.085 x 10^5 M^{-1} s^{-1}
Fitting to CV of 1,4-QH_2/10 mM Benzoate – K_{equ} = 600, k_f = 1x10^5 M^{-1} s^{-1}, k_b = 166.67 M^{-1} s^{-1}
Fitting to CV of 1,4-QH_2/10 mM Trifluoroacetate - K_{equ} =25, k_f = 1000 M^{-1} s^{-1}, k_b =40 M^{-1} s^{-1}

(34) $HB \rightleftharpoons B + H^+$

Fitting to CV of 1,4-QH_2/10 mM Acetate – K_{equ} = 5.0 x 10^{-23} M, k_f = 1 x 10^5 s^{-1}, k_b = 2 x 10^{27} M^{-1} s^{-1}
Fitting to CV of 1,4-QH_2/10 mM Benzoate – K_{equ} = 2.0 x 10^{-21} M, k_f = 1 x10^5 s^{-1}, k_b = 5 x 10^{25} M^{-1} s^{-1}
Fitting to CV of 1,4-QH_2/10 mM Trifluoroacetate – K_{equ}=2.2x10^{-13} M, k_f = 6.78x10^4 s^{-1}, k_b=3.081x10^{17} M^{-1} s^{-1}

(35) $HB + B \rightleftharpoons HB_2$

Fitting to CV of 1,4-QH_2/10 mM Acetate – K_{equ} =6x10^4 M^{-1}, k_f = 1 x 10^5 M^{-1} s^{-1}, k_b = 1.6667 s^{-1}
Fitting to CV of 1,4-QH_2/10 mM Benzoate – K_{equ} = 4x10^4 M^{-1}, k_f = 1 x 10^5 M^{-1} s^{-1}, k_b = 2.5 s^{-1}
Fitting to CV of 1,4-QH_2/10 mM Trifluoroacetate – K_{equ}=7.6x10^4 M^{-1}, k_f = 1 x 10^8 M^{-1} s^{-1}, k_b = 1315.8 s^{-1}

(X) $H_2B_2 \rightleftharpoons HB + HB$

Fitting to CV of 1,4-QH_2/10 mM Acetate – K_{equ} =7.713x10^{-9} M, k_f = 141.18 s^{-1}, k_b=1.831x10^8 M^{-1} s^{-1}
Fitting to CV of 1,4-QH_2/10 mM Benzoate – K_{equ} =2.28x10^{-9} M, k_f = 5 s^{-1}, k_b=2.193x10^9 M^{-1} s^{-1}
Fitting to CV of 1,4-QH_2/10 mM Trifluoroacetate – K_{equ}=1.869x10^{-13} M, k_f = 100 s^{-1}, k_b=5.352x10^{14} M^{-1} s^{-1}

Scheme 8B

(26) $QH_2 + B \rightleftharpoons QH_2(B)$

Fitting to CV of 1,4-QH_2/30 mM Acetate - K_{equ} = 202 M^{-1}, k_f = 1 x 10^8 M^{-1} s^{-1}, k_b = 4.95 x 10^5 s^{-1}
Fitting to CV of 1,4-QH_2/30 mM Benzoate – K_{equ} = 473 M^{-1}, k_f = 1 x 10^8 M^{-1} s^{-1}, k_b = 2.11 x 10^5 s^{-1}
Fitting to CV of 1,4-QH_2/30 mM Trifluoroacetate - K_{equ}=55 M^{-1}, k_f = 1 x 10^8 M^{-1} s^{-1}, k_b = 1.82 x10^6 s^{-1}
Fitting to CV of 1,2-QH_2/10 & 30 mM Acetate - K_{equ} = 1250 M^{-1}, k_f = 1 x 10^8 M^{-1} s^{-1}, k_b = 8 x 10^4 s^{-1}
Fitting to CV of 1,2-QH_2/30 mM Trifluoroacetate - K_{equ}=270 M^{-1}, k_f = 1 x 10^8 M^{-1} s^{-1}, k_b = 3.704 x10^5 s^{-1}

(27) $QH_2(B) + B \rightleftharpoons QH_2(B)_2$

Fitting to CV of 1,4-QH_2/30 mM Acetate - K_{equ} = 155 M^{-1}, k_f = 1 x 10^8 M^{-1} s^{-1}, k_b = 6.45 x 10^5 s^{-1}
Fitting to CV of 1,4-QH_2/30 mM Benzoate – K_{equ} = 209 M^{-1}, k_f = 1 x 10^8 M^{-1} s^{-1}, k_b = 4.79 x 10^5 s^{-1}
Fitting to CV of 1,4-QH_2/30 mM Trifluoroacetate - K_{equ}=5 M^{-1}, k_f = 1 x 10^8 M^{-1} s^{-1}, k_b = 2 x10^7 s^{-1}
Fitting to CV of 1,2-QH_2/10 & 30 mM Acetate - K_{equ} = 400 M^{-1}, k_f = 5 x 10^4 M^{-1} s^{-1}, k_b = 125 s^{-1}
Fitting to CV of 1,2-QH_2/30 mM Trifluoroacetate - K_{equ}=82 M^{-1}, k_f = 1 x 10^8 M^{-1} s^{-1}, k_b = 1.22 x10^6 s^{-1}

(31) $QH_2(B)_2 \rightleftharpoons QH_2^{+\cdot}(B)_2 + e^-$

Fitting to CV of 1,4-QH_2/30 mM Acetate – E^o = -0.636 V, α = 0.5, k_s = 0.0005 cm s^{-1}
Fitting to CV of 1,4-QH_2/30 mM Benzoate – E^o = -0.516 V, α =0.5, k_s = 0.00078 cm s^{-1}

Fitting to CV of 1,4-QH_2/30 mM Trifluoroacetate – E^o = -0.134 V, α = 0.5, k_s = 0.003 cm s^{-1}
Fitting to CV of 1,2-QH_2/10 & 30 mM Acetate - E^o = -0.14 V, α = 0.5, k_s = 0.0012 cm s^{-1}
Fitting to CV of 1,2-QH_2/30 mM Trifluoroacetate – E^o = 0.22 V, α = 0.5, k_s = 0.002 cm s^{-1}

(36) $QH_2^{+\cdot}(B)_2 \rightleftharpoons QH^{\cdot}(B) + HB$

Fitting to CV of 1,4-QH_2/30 mM Acetate – K_{equ} = 1x 10^{-5}M, k_f = 1000 s^{-1}, k_b = 1x10^8 M^{-1} s^{-1}
Fitting to CV of 1,4-QH_2/30 mM Benzoate – K_{equ} = 1x10^{-5} M, k_f = 2000 s^{-1}, k_b = 2x10^8 M^{-1} s^{-1}
Fitting to CV of 1,4-QH_2/30 mM Trifluoroacetate – K_{equ} = 0.12 M, k_f = 1x10^4 s^{-1}, k_b = 8.33 x 10^4 M^{-1} s^{-1}
Fitting to CV of 1,2-QH_2/10 & 30 mM Acetate - K_{equ} = 15 M, k_f = 1x10^8 s^{-1}, k_b = 6.67 x 10^6 M^{-1} s^{-1}
Fitting to CV of 1,2-QH_2/30 mM Trifluoroacetate - K_{equ} = 3.9x10^{-5} M, k_f = 1x10^8 s^{-1}, k_b = 2.564 x 10^{12} M^{-1} s^{-1}

(37) $QH^{\cdot}(B) \rightleftharpoons QH^{+}(B) + e^{-}$

Fitting to CV of 1,4-QH_2/30 mM Acetate – E^o = -0.636 V, α = 0.5, k_s = 0.08 cm s^{-1}
Fitting to CV of 1,4-QH_2/30 mM Benzoate – E^o = -0.716 V, α = 0.5, k_s = 0.0025 cm s^{-1}
Fitting to CV of 1,4-QH_2/30 mM Trifluoroacetate – E^o = -0.436 V, α = 0.5, k_s = 0.003 cm s^{-1}
Fitting to CV of 1,2-QH_2/10 & 30 mM Acetate – E^o = -0.36 V, α = 0.5, k_s = 0.003 cm s^{-1}
Fitting to CV of 1,2-QH_2/30 mM Trifluoroacetate – E^o = 0.14 V, α = 0.5, k_s = 0.0019 cm s^{-1}

(38) $QH^{+}(B) \rightleftharpoons Q + HB$

Fitting to CV of 1,4-QH_2/30 mM Acetate – K_{equ} = 0.88 M, k_f = 1x10^8 s^{-1}, k_b = 1.14 x 10^8 M^{-1} s^{-1}
Fitting to CV of 1,4-QH_2/30 mM Benzoate – K_{equ} = 0.002 M, k_f = 1 x 10^8 s^{-1}, k_b = 5x10^{10} M^{-1} s^{-1}
Fitting to CV of 1,4-QH_2/30 mM Trifluoroacetate – K_{equ} = 0.1 M, k_f = 1x10^8 s^{-1}, k_b = 1x10^9 M^{-1} s^{-1}
Fitting to CV of 1,2-QH_2/10 & 30 mM Acetate – K_{equ} = 0.11 M, k_f = 1x10^8 s^{-1}, k_b = 9.091x10^8 M^{-1} s^{-1}
Fitting to CV of 1,2-QH_2/30 mM Trifluoroacetate - K_{equ} = 1000 M, k_f = 1x10^8 s^{-1}, k_b = 1x10^5 M^{-1} s^{-1}

(39) $QH^{\cdot}(B) + QH^{\cdot}(B) \rightleftharpoons Q + QH_2(B)_2$

Fitting to CV of 1,4-QH_2/30 mM Acetate – K_{equ} = 8.8 x 10^4, k_f = 0.0019 M^{-1} s^{-1}, k_b = 2.16 x 10^{-8} M^{-1} s^{-1}
Fitting to CV of 1,4-QH_2/30 mM Benzoate – K_{equ} = 4.8 x 10^5, k_f = 0.19 M^{-1} s^{-1}, k_b = 3.96 x 10^{-7} M^{-1} s^{-1}
Fitting to CV of 1,4-QH_2/30 mM Trifluoroacetate – K_{equ} = 9.79x10^4, k_f = 12 M^{-1} s^{-1}, k_b = 0.00012 M^{-1} s^{-1}
Fitting to CV of 1,2-QH_2/10 & 30 mM Acetate – K_{equ} = 38.317, k_f = 0.0002 s^{-1}, k_b = 5.22x10^{-6} M^{-1} s^{-1}
Fitting to CV of 1,2-QH_2/30 mM Trifluoroacetate – K_{equ} = 1.499x10^7, k_f = 1x10^4 s^{-1}, k_b = 0.0006669 M^{-1} s^{-1}

Scheme 8C

(26) $QH_2 + B \rightleftharpoons QH_2(B)$

Fitting to CV of 1,2-QH_2/30 mM Benzoate – $K_{equ} = 1.4x10^5\ M^{-1}$, $k_f = 1 \times 10^8\ M^{-1}\ s^{-1}$, $k_b = 714.29\ s^{-1}$

(28) $QH_2(B) \rightleftharpoons QH_2^{+\cdot}(B) + e^-$

Fitting to CV of 1,2-QH_2/30 mM Benzoate – $E^o = -0.2$ V, $\alpha = 0.5$, $k_s = 7x10^{-5}$ cm s^{-1}

(30) $QH_2^{+\cdot}(B) \rightleftharpoons QH^{\cdot} + HB$

Fitting to CV of 1,2-QH_2/30 mM Benzoate – $K_{equ} = 2x10^{-5}$ M, $k_f = 1x10^4\ s^{-1}$, $k_b = 5x10^8\ M^{-1}\ s^{-1}$

(40) $QH^{\cdot} + B \rightleftharpoons QH^{\cdot}(B)$

Fitting to CV of 1,2-QH_2/30 mM Benzoate – $K_{equ} = 1000\ M^{-1}$, $k_f = 1 \times 10^8\ M^{-1}\ s^{-1}$, $k_b = 1 \times 10^5\ s^{-1}$

(37) $QH^{\cdot}(B) \rightleftharpoons QH^{+}(B) + e^-$

Fitting to CV of 1,2-QH_2/30 mM Benzoate – $E^o = -0.39084$ V, $\alpha = 0.5$, $k_s = 9x10^{-5}$ cm s^{-1}

(38) $QH^{+}(B) \rightleftharpoons Q + HB$

Fitting to CV of 1,2-QH_2/30 mM Benzoate – $K_{equ} = 0.0002$ M, $k_f = 2500\ s^{-1}$, $k_b = 1.25x10^7\ M^{-1}\ s^{-1}$

(41) $QH^{\cdot} + QH^{\cdot}(B) \rightleftharpoons Q + QH_2(B)$

Fitting to CV of 1,2-QH_2/10 mM Benzoate – $K_{equ} = 120$, $k_f = 1x10^4\ M^{-1}\ s^{-1}$, $k_b = 83.333\ M^{-1}\ s^{-1}$

Scheme 8D

Parameters for this fitting found above in Table A1.

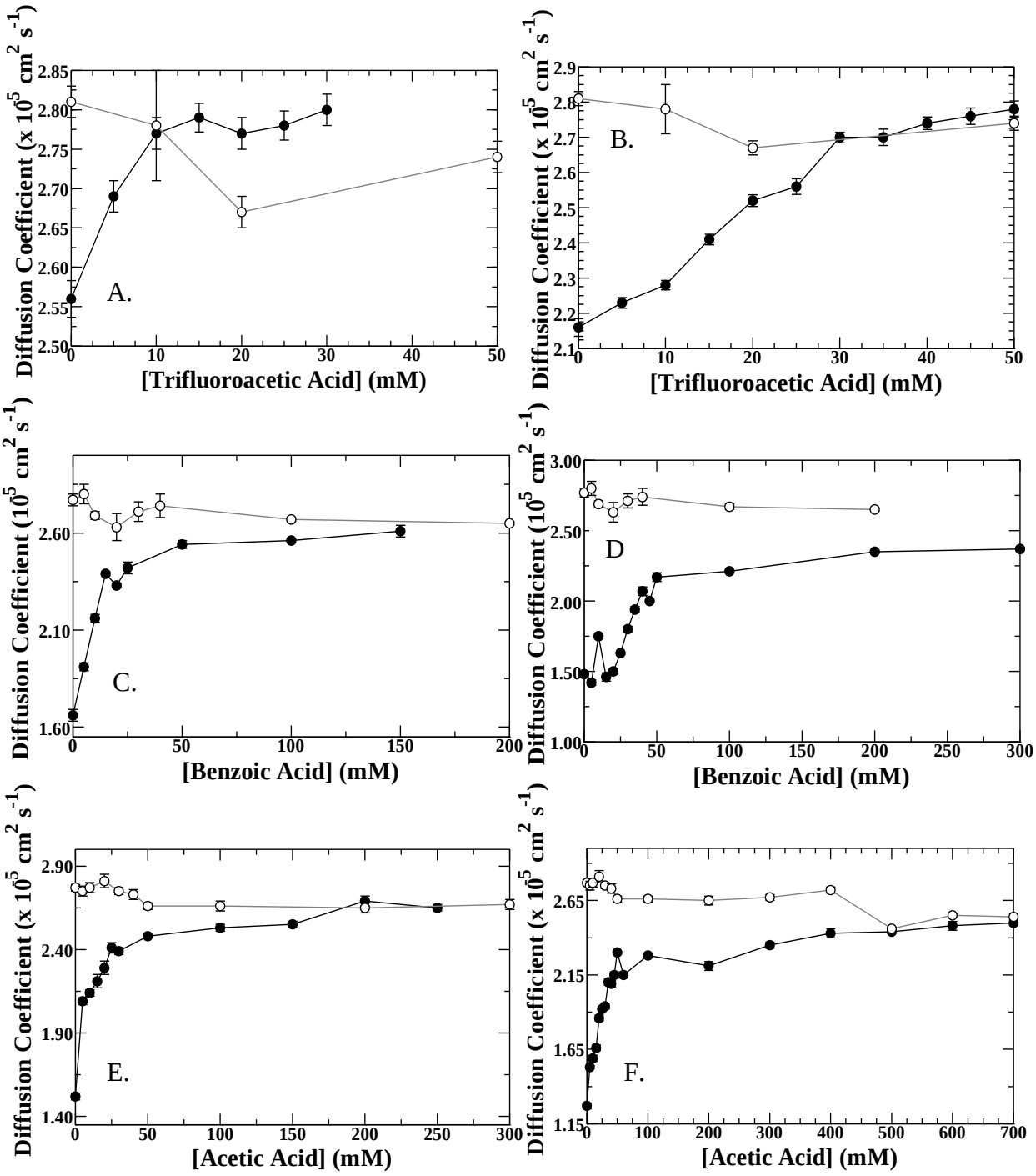

Figure A10. Change in the diffusion coefficient of 5.0 mM 1,4-QH_2 in the presence of A.) 10.0 and B.) 30.0 mM trifluoroacetate as trifluoroacetic acid is titrated. Change in the diffusion coefficient of 5.0 mM 1,4-QH_2 in the presence of C.) 10.0 and D.) 30.0 mM benzoate as benzoic acid is titrated. Change in the diffusion coefficient of 5.0 mM 1,4-QH_2 in the presence of E.) 10.0 and F.) 30.0 mM acetate as acetic acid is titrated. Solid lines do not represent fittings to the data. Filled circles represent the 1,4-QH_2 data with the indicated acetate and titrated conjugate acid, while the open circles and gray line represent the 1,4-QH_2 alone in solution with the titrated conjugate acid.

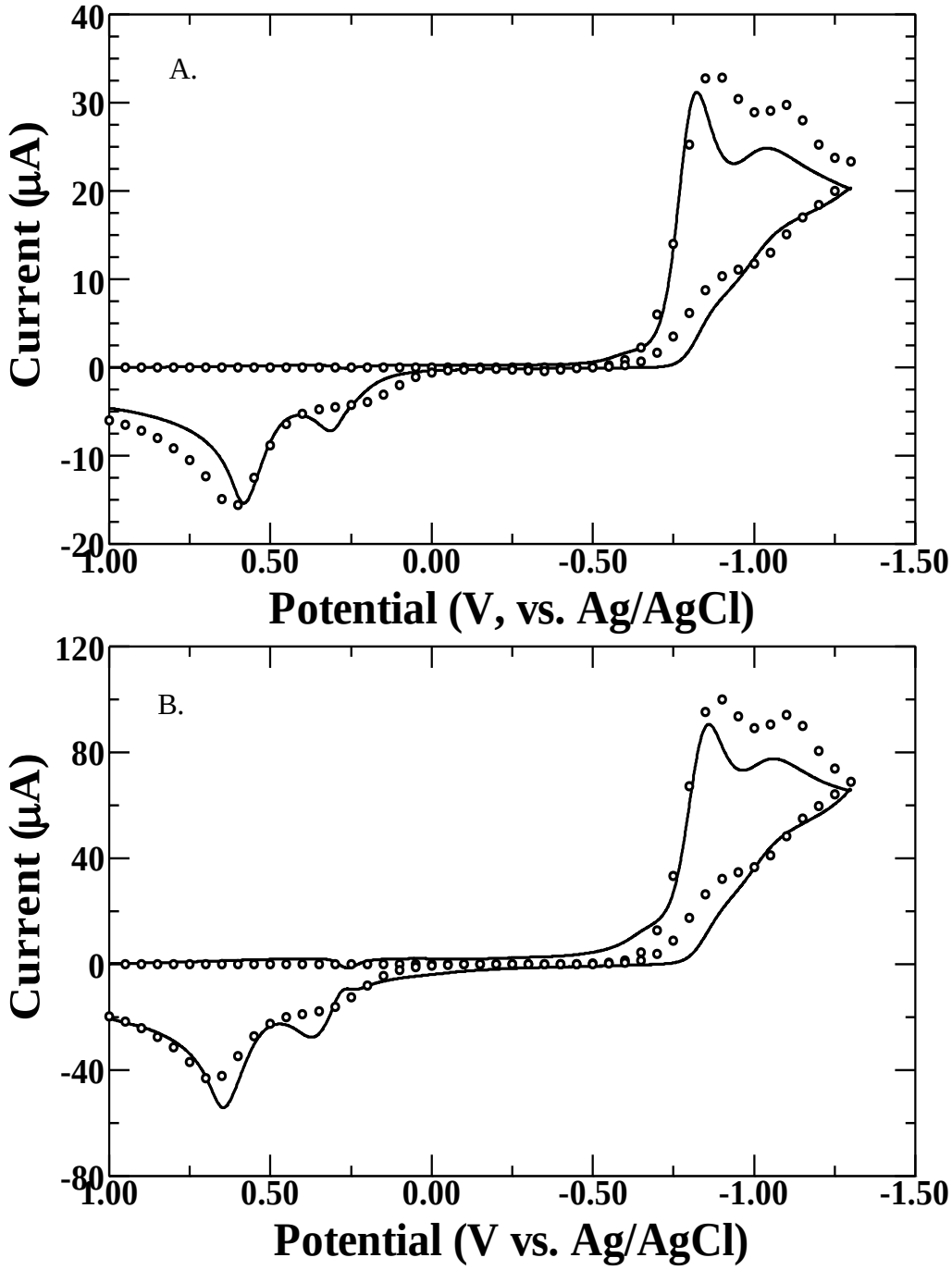

Figure A11. Voltammetry (solid lines) and simulations (open circles) of 2.0 mM PPC^+ in 0.1 M succinate buffer with KCl (I = 0.5) at pH 4. Experiments performed at a glassy carbon electrode (0.073 cm^2) at A.) 0.1 or B.) 1 V s^{-1} at 300 K.

Scheme A4. Equations and parameters used for fitting PPC^+ in 0.1 M Succinate pH 4.

$BH_2 + PPC^+ \rightleftharpoons HPPC^{2+} + BH^-$ (A8)

$K_{equ} = 0.010108$, $k_f = 9900\ M^{-1}\ s^{-1}$, $k_b = 9.794x10^5\ M^{-1}\ s^{-1}$

$BH^- + PPC^+ \rightleftharpoons HPPC^{2+} + B^{2-}$ (A9)

$K_{equ} = 0.00037555$, $k_f = 740\ M^{-1}\ s^{-1}$, $k_b = 1.97x10^6\ M^{-1}\ s^{-1}$

$PPC^+ + e^- \rightleftharpoons PPC^{\cdot}$ (A10)

$E^o = -0.522$ V, $\alpha = 0.6$, $k_s = 4.8x10^{-11}$ cm s^{-1}

$BH_2 + PPC^{\cdot} \rightleftharpoons HPPC^{+\cdot} + BH^-$ (A11)

$K_{equ} = 66.575$, $k_f = 2x10^{-5}\ M^{-1}\ s^{-1}$, $k_b = 3.755x10^{-7}\ M^{-1}\ s^{-1}$

$BH^- + PPC^{\cdot} \rightleftharpoons HPPC^{+\cdot} + B^{2-}$ (A12)

$K_{equ} = 2.4735$, $k_f = 0.0004\ M^{-1}\ s^{-1}$, $k_b = 0.00016171\ M^{-1}\ s^{-1}$

$PPC^{\cdot} + e^- \rightleftharpoons PPC^{o}$ (A13)

$E^o = -0.498$ V, $\alpha = 0.26$, $k_s = 0.00014$ cm s^{-1}

$HPPC^{2+} + e^- \rightleftharpoons HPPC^{+\cdot}$ (A14)

$E^o = -0.29605$ V, $\alpha = 0.5$, $k_s = 5.4x10^{-6}$ cm s^{-1}

$BH_2 + PPC^{o} \rightleftharpoons HPPC^{o} + BH^-$ (A15)

$K_{equ} = 4.393x10^5$, $k_f = 3.9x10^{-7}\ M^{-1}\ s^{-1}$, $k_b = 8.877x10^{-13}\ M^{-1}\ s^{-1}$

$BH^- + PPC^{o} \rightleftharpoons HPPC^{o} + BH^{2-}$ (A16)

$K_{equ} = 1.632x10^4$, $k_f = 0.026\ M^{-1}\ s^{-1}$, $k_b = 1.593x10^{-6}\ M^{-1}\ s^{-1}$

$HPPC^{+\cdot} + e^- \rightleftharpoons HPPC^{o}$ (A17)

$E^o = -0.29605$ V, $\alpha = 0.5$, $k_s = 5.4x10^{-6}$ cm s^{-1}

$HPPC^{2+} + HPPC^{o} \rightleftharpoons HPPC^{+\cdot} + HPPC^{+\cdot}$ (A18)

K_{equ} = 0.39223, k_f = 2x10^4 M^{-1} s^{-1}, k_b = 5.099x10^4 M^{-1} s^{-1}

9.2 Information Regarding Parameters in PGE-^{1}H-NMR Experiments, an Example of the Data Obtained and Control Experiments

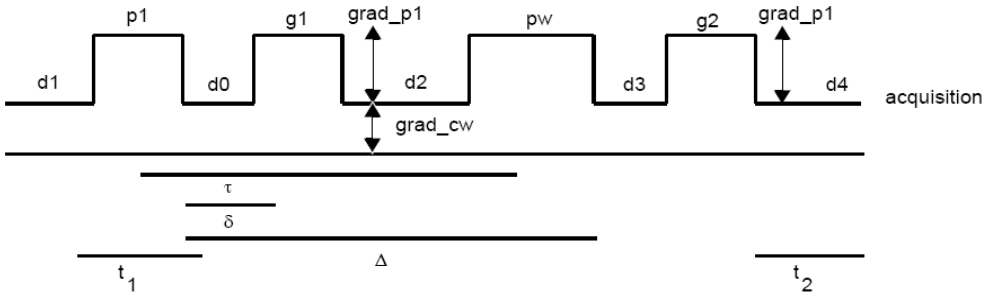

Figure A12. Pulse sequence of the PGE-^{1}H-NMR technique on a Varian NMR.[177, 178]

Values and important information regarding the PGE-NMR sequence can be found in Figure A12, were: δ = 1 ms, while Δ = varied depending on sample and pulse width (pw, 180°) value (generally ~73 ms), applied gradient range (*grad_p1* and *grad_p2*) was 20-30 G cm^{-1} in 10 steps.[77, 177, 178] The delay times were d1 = 2.000 s, d0 = d3 = 0.001 s, and d2 = d4 = 0.020 s. The parameter *grad_cw* was kept at 0 G cm^{-1}, as this parameter is typically used in DOSY experiments.[177, 178] Also, the parameter *tramp* (on Varian PGE-NMR) programs remained at 0 s throughout the collection of the PGE arrays. Furthermore, these experiments were not conducted in the *stimulated* mode (also known as, Pulsed Gradient Stimulated Echo (PGSE)), and therefore "*n*" was the input for this parameter,

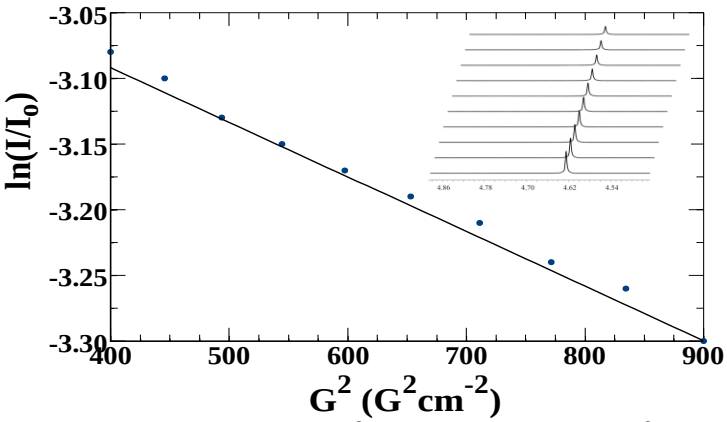

Figure A13. Example of graphical analysis of the PGE-^{1}H-NMR spectra of the HDO peak in D_2O. Inset, PGE-^{1}H-NMR spectra for HDO in D_2O.

indicating *no*.[177, 178] Figure A13 gives an example of the graphical analysis and PGE spectra obtained upon performing a PGE-^{1}H-NMR experiment on the HDO singlet peak in 100 % D_2O.

Before diffusion coefficients determined by NMR could be used in simulations or other analyses, it was necessary to apply a correction factor. The purpose of the correction factor was to correct the diffusion coefficients determined by ^{1}H-NMR (D_{NMR}) measured in isotopically enriched solvents without supporting electrolyte for those in isotopically unenriched solvents (D_C) with various supporting electrolytes. This difference in medium composition can be taken into account using the Stokes-Einstein equation, which establishes that the diffusion coefficient, D, is inversely proportional to the solvent or medium viscosity, η, that is

$$D = kT\eta^{-1}/(6\pi r_h) \quad \text{(A19)}$$

where r_h is the hydrodynamic radius of the diffusing species, *k* is Boltzmann's constant, and T is the absolute temperature. Assuming that the hydrodynamic radius and temperature remain constant, the following relation can be made,

$$D_1\eta_1 = D_2\eta_2 \quad \text{(A20)}$$

where the subscripts 1 and 2 represent the two medium compositions under investigation. Viscosities were measured at 25 ^oC by determining the flow times, *t*, of the solutions of different composition in an Ostwald capillary viscosimeter and their densities, ρ, using a calibrated balance and 1 mL of each solution. Thus, the solution viscosity can be determined using the relation,

$$\eta = B\rho t \quad \text{(A21)}$$

where *B* is a calibration constant. Once the viscosity ratio between the two solvents was known, often in this work between CD_3CN and 0.2 M $TBAPF_6$ in CH_3CN, was obtained, the D_{NMR} values can be corrected for differences in medium composition, giving the corrected diffusion

coefficients, D_C. The following relation allows for the determination of the D_c values in 0.2 M $TBAPF_6$ in CH_3CN.[79]

$$D_C = (1.04)D_{NMR} \quad \text{(A22)}$$

This correction factor, 1.04, was determined by Sun *et al*[79].

To determine whether ion pairing is responsible for the noted changes in diffusion NMR, experiments with 1,4-QH_2 with 10.0 mM and 0.2 mM $TBAPF_6$ (same as supporting electrolyte concentration) were performed. The diffusion coefficient (D) of 1,4-QH_2 in 10.0 mM $TBAPF_6$ was $2.83x10^{-5}$ cm^2 s^{-1} (+1.4% change), while the D of 1,4-QH_2 in 0.2 mM $TBAPF_6$ was $2.60x10^{-5}$ cm^2 s^{-1} (-6.8%). A similar experiment was also performed using 10.0 mM tetrabutylammonium perchlorate ($TBAClO_4$) was performed, which gave a D of 2.75 x 10^{-5} cm^2 s^{-1} (-1.4%). All of these values were corrected for changes in viscosity of light acetonitrile containing 0.2 mM of the indicated electrolyte in CD_3CN. However, a new correction factor for the diffusion experiment performed with 0.2 mM $TBAPF_6$ had to be made, by determining the viscosity of light and heavy acetonitrile containing 0.2 mM $TBAPF_6$. The correction factor was found to be 1.08, and was used for the above stated value for the D value of 1,4-QH_2 with 0.2 mM $TBAPF_6$.

Since D_{NMR} values were also determined for PPC^+ and $NMBC^+$ under both aqueous buffered and unbuffered conditions, correction factors were necessary to calculate their D_C values at various pH's and in various buffers. Table A3 gives the various correction factors for the indicated buffers or unbuffered solution under the indicated conditions. When the D_{NMR} values were determined the PGE-^{1}H-NMR measurements were made in 100 % D_2O.

Table A3. Correction factors used to correct the D_{NMR} values determined for $NMBC^+$ and PPC^+ under the given aqueous unbuffered and buffered conditions.

Solution and Conditions	Correction Factor
H_2O alone, pH = 1.01	1.21
H_2O with KCl (I=0.5), pH = 1.00	1.22
H_2O with KCl (I=0.5), pH = 3.53	1.23
H_2O with KCl (I=0.5), pH = 5.32	1.22
H_2O with KCl (I=0.5), pH = 8.84	1.26
H_2O with KCl (I=0.5), pH = 10.27	1.26
H_2O with KCl (I=0.5), pH = 12.53	1.26
0.1 M Phosphate with KCl (I = 0.5), pH = 1.00	1.20
0.1 M Phosphate with KCl (I = 0.5), pH = 2.00	1.21
0.1 M Phosphate with KCl (I = 0.5), pH = 3.00	1.22
0.1 M Phosphate with KCl (I = 0.5), pH = 4.00	1.21
0.1 M Phosphate with KCl (I = 0.5), pH = 5.00	1.21
0.1 M Phosphate with KCl (I = 0.5), pH = 6.00	1.20
0.1 M Phosphate with KCl (I = 0.5), pH = 7.00	1.21
0.1 M Phosphate with KCl (I = 0.5), pH = 8.00	1.24
0.1 M Phosphate with KCl (I = 0.5), pH = 9.00	1.21
0.1 M Phosphate with KCl (I = 0.5), pH = 10.00	1.23
0.1 M Phosphate with KCl (I = 0.5), pH = 11.00	1.25
0.1 M Phosphate with KCl (I = 0.5), pH = 12.00	1.26
0.01 M Phosphate with KCl (I = 0.5), pH = 1.00	1.22
0.01 M Phosphate with KCl (I = 0.5), pH = 2.00	1.24
0.01 M Phosphate with KCl (I = 0.5), pH = 3.00	1.24
0.01 M Phosphate with KCl (I = 0.5), pH = 4.00	1.25
0.01 M Phosphate with KCl (I = 0.5), pH = 5.00	1.22
0.01 M Phosphate with KCl (I = 0.5), pH = 6.00	1.23
0.01 M Phosphate with KCl (I = 0.5), pH = 7.00	1.25
0.01 M Phosphate with KCl (I = 0.5), pH = 8.00	1.25
0.01 M Phosphate with KCl (I = 0.5), pH = 9.00	1.23
0.01 M Phosphate with KCl (I = 0.5), pH = 10.00	1.23
0.01 M Phosphate with KCl (I = 0.5), pH = 11.00	1.27
0.01 M Phosphate with KCl (I = 0.5), pH = 12.00	1.27
0.1 M Phosphate with KCl (I = 0.5), pH = $pK_{a,1}$ = 2.15	1.22
0.1 M Malate with KCl (I = 0.5), pH = $pK_{a,1}$ 3.40	1.21
0.1 M Citrate with KCl (I = 0.5), pH = $pK_{a,1}$ = 3.13	1.20
0.1 M Borate with KCl (I = 0.5), pH = $pK_{a,1}$ = 9.23	1.21
0.1 M CAPS with KCl (I = 0.5), pH = $pK_{a,1}$ = 10.4	1.14
0.1 M Carbonate with KCl (I = 0.5), pH = $pK_{a,1}$ = 6.35	1.23
0.1 M TES with KCl (I = 0.5), pH = pK_a = 7.40	1.21
0.1 M THAM with KCl (I = 0.5), pH = pK_a = 8.06	1.21
0.1 M Glycine with KCl (I = 0.5), pH = $pK_{a,1}$ = 2.35	1.22
0.1 M Glycine with KCl (I = 0.5), pH = $pK_{a,2}$ = 9.78	1.21

0.1 M Phosphate with KCl (I = 0.5), pH = $pK_{a,2}$ = 7.20	1.20
0.1 M ACES with KCl (I = 0.5), pH = pK_a = 6.78	1.19
0.1 M Citrate with KCl (I = 0.5), pH = $pK_{a,2}$ = 6.40	1.15

10.0 Vita

Education

PhD, Analytical Chemistry, Virginia Commonwealth University, Richmond, VA
Advisor: Dr. Julio Alvarez

BS, Biochemistry; BA, Chemistry (cum laude), Virginia Polytechnic Institute and State University (Virginia Tech), Blacksburg, VA, May 2004

Dinwiddie County High School (Advanced Studies Diploma), Dinwiddie County, VA, June 2000

Honors/Affiliations

- The National Society of Collegiate Scholars, 2001 - Present
- Deans List (numerous times at Virginia Tech)
- Virginia Commonwealth University Graduate School Fellowship - August 2004 to August 2005
- American Chemical Society Member, 2005 - present
- AAAS Member 2007 - present
- Electrochemical Society Member 2007 - present
- Teaching Assistant of the Year - VCU Department of Chemistry - April 2006
- The R. Gerald and Susan Bass Scholarship - February 2007
- Philip Morris Graduate Research Award (Research Assistantship) - Spring 2008 to Fall 2008
- The James V. Quagliano Fellowship in Chemistry – February 2008
- *Who's Who Among Students in American Universities and Colleges* Member and Award – March 2008

Work Experience

Virginia Commonwealth University August 2004 – July 2010

"Mechanistic Studies on the Electrochemistry of Proton Coupled Electron Transfer and the Influence of Hydrogen Bonding"

Advisor: Dr. Julio Alvarez

Extracurricular

- Assisted with National Chemistry week demonstration for High School Students combined with discussions and a walk through tour around VCU Chemistry Department. – Oct. 2007
- Promotion Committee – Sept. 20 through Oct. 31, 2007
  Graduate Student Advocate – emailed past students about the teaching abilities of the faculty member up for promotion and sat in on promotion meetings.
- Worked with High School students in the lab, for the understanding and eventual publication on Streaming Potential measurements in microfluidic channels. – Spring 2005 - Fall 2006.
- Women In Science Girl Scout Science Fun/Science Careers Day – Medical Sciences Building, MCV. Answered questions and performed simple chemistry demonstrations. April 19, 2008, May 2, 2009 and May 8, 2010.
- Guest Speaker for Hope Parham's AP Chemistry class, Mills Godwin High School – Short Pump, VA, June 2, 2009 – gave a presentation of my work and answered questions involving graduate school, chemistry and my work.

- Hosted chemistry students from Jeremy Clark's Forensic Science class, Maggie Walker Governor's School – gave a tour and demonstration of NMR facility with the assistance of Dr. Qu.

Meetings

- Electrochemical Society 212th Meeting – Washington D. C. – October 9, 2007
  Presented Poster: "*Influencing the Kinetics and Thermodynamics of Quinones and Hydroquinones Through Strong Hydrogen Bonds"*
- Gordon Research Conference in Electrochemistry – Ventura Beach, CA – Jan. 6-11, 2008.
  Presented Poster: "*Influencing the Kinetics and Thermodynamics of Quinones and Hydroquinones Through Strong Hydrogen Bonds"*
- 11th Annual Graduate Research Symposium and Exhibit – VCU Student Commons – April 15, 2008. Presented Poster: "*Influencing the Kinetics and Thermodynamics of Quinones and Hydroquinones Through Strong Hydrogen Bonds"*
- 236th American Chemical Society National Meeting – Philadelphia, PA – August 17-22, 2008.
  Presented Talk:*"Kinetics and Thermodynamics of Quinones and Hydroquinones: Addition of Brønsted Acids and Bases and the Analysis of the Kinetic Isotope Effect."*
- 60th Pittsburgh Conference on Analytical Chemistry and Applied Spectroscopy (Pittcon '09) – Chicago, IL – March 8-13, 2009.Presented Talk: *"Investigations of Reaction Mechanisms of Quinones in Unbuffered Aqueous and Aqueous/Nonaqueous Mixed Media."*
- Gordon Research Seminar and Conference in Electrochemistry – Ventura, CA – Jan. 9-15, 2010. Presented Poster: *"Organic "One Electron-One Proton" Transfer in Buffered and Unbuffered Aqueous Solution."*

Publications

Luna Vera, F.; Pu, Q; Alligrant, T.; Alvarez, J.C.; Faulconer, E.; Farhi, J. Hurt, V. "Determination of Surface Charge in Microfluidic Channels Using Streaming Potential Measurements: An Experiment for High School Seniors and Undergraduate Students." *J. Chem. Ed.* **(To Be Submitted).**

Alligrant, T.M.; Hackett, J.C.; Alvarez, J.C. "Acid/Base Effects on the Coupled Proton-Electron Transfer of Quinones and Hydroquinones in Acetonitrile: Mechanistic Investigation by Voltammetry, ^{1}H-NMR, Electronic Spectra and Computation." *Electrochim. Acta* **(accepted).**

Alligrant, T. M.; Alvarez, J. C. "The Importance of the Hydrogen Bond in Proton-Coupled Electron Transfer: Interpretation of Electrochemical and NMR Evidence." *Chem. Eur. J.* **(To Be Submitted).**